Stony Brook University

Effects of a Changing Ocean on Marine Gel Particles and Implications for Aggregation Processes and POC export

A Dissertation Presented

by

Carolina Cisternas-Novoa

to

The Graduate School

in Partial Fulfillment of the

Requirements

for the Degree of

Doctor of Philosophy

in

Marine and Atmospheric Science

Stony Brook University

August 2015

Stony Brook University

The Graduate School

Carolina Cisternas-Novoa

We, the dissertation committee for the above candidate for the

Doctor of Philosophy degree, hereby recommend

acceptance of this dissertation.

Cindy Lee – Dissertation Advisor
Distinguished Professor, School of Marine and Atmospheric Science

Gordon T. Taylor - Chairperson of Defense
Professor, School of Marine and Atmospheric Science

Jackie Collier
Professor, School of Marine and Atmospheric Science

Anja Engel
Professor, GEOMAR Helmholtz Centre for Ocean Research Kiel
and School of Marine and Atmospheric Science

Xavier Mari
French Research Institute for Development (IRD), Marseille, France

This dissertation is accepted by the Graduate School

Charles Taber
Dean of the Graduate School

Abstract of the Dissertation

Effects of a Changing Ocean on Marine Gel Particles and Implications for Aggregation Processes and POC export

by

Carolina Cisternas-Novoa

Doctor of Philosophy

in

Marine and Atmospheric Science

Stony Brook University

2015

Marine gels are essential catalysts of aggregation and a significant component of the organic carbon pool. There is evidence showing that dissolved organic carbon (DOC) can self-assemble and form porous microgels that can reversibly exchange material with DOC and particulate organic carbon (POC). This abiotic self-assembly of materials results in particles that can sink and eventually sequester organic carbon into the deep ocean; the dissolution and remineralization of POM have important implications for ocean productivity and carbon cycling. Marine gels are hydrogels formed by a three-dimensional network of polymers and seawater. Operationally, transparent gel particles are defined as discrete particles, larger than 0.2 μm or 0.4 μm, that are present in seawater and phytoplankton cultures, and that can be visualized after staining with a specific dye. The origins of marine gel particles are diverse; however, a major source of gel particles is from exudates of phytoplankton and bacteria.

This research focuses on polysaccharide-rich gel particles called Transparent Exopolymeric Particles (TEP) and protein-rich gel particles called Coomassie Blue Stainable Particles (CSP). TEP and CSP are known to be abundant and ubiquitous in seawater and they contribute significantly to the formation of sinking aggregates; therefore, understanding the effect of elevated CO_2 and temperature on these particles is vital to predicting changes in the biological pump efficiency of the future ocean. This study investigates important uncertainties regarding gel particles from three different perspectives. First, a new technique for the semi-quantitative analysis of protein-rich CSP was developed. Using this new method to study TEP and CSP in parallel samples from the natural environment and from laboratory experiments, it was found that TEP and CSP are both produced during the phytoplankton bloom but that their maximum abundance occurs at different stages of growth; moreover TEP and CSP have different vertical distributions in the ocean. Second, the standard visualization technique using the FlowCAM and a new technique developed during this study indicated that TEP and CSP have different particle association behavior; that is, TEP were more abundant on aggregates formed by diatoms, while CSP were more abundant on aggregates dominated by cyanobacteria. Third, the effect of higher temperature and CO_2 was studied in indoor-mesocosm experiments with natural assemblages of coastal phytoplankton that were dominated by diatoms and in aggregation experiments using roller tanks. Photosynthesis and gel particle production were not significantly different between treatments in the mesocosm experiment. However, the roller tank experiments showed that aggregates formed at higher CO_2 were smaller and had lower sinking velocity than aggregates formed under present CO_2 conditions.

The results of this dissertation provide new information about differences in origin, particle association and distribution of gel particles in the ocean. This is especially novel for the

case of CSP, a protein-containing gel particle that has been seldom studied because of the lack of a semi-quantitative method. The method developed here provides an efficient tool to broaden the study of CSP in aquatic environments.

Dedication

To my parents Blanca and Raul for teach me that with work and perseverance I can always fulfill my dreams, and to my husband Jaime for been the best companion and the strongest supporter in this road.

Table of Contents

List of Figures

List of Tables

Acknowledgments

This dissertation is the result of several years of hard work and determination. I want to sincerely thank all the hands and minds that contributed to the development, execution, and interpretation of this work. Foremost, my advisor and mentor Dr. Cindy Lee for her generous and constant support and guidance in my development, not only as a scientist but as a caring person. It was a privilege to conduct my research with an advisor that walked me though the wonders of scientific research and at the same time supported me when things were not going as planned; Cindy helped me to look at the big picture and provided the perfect environment for me to develop knowledge, confidence and independence as a scientist. I hear that admiration is the first step for imitation, I really hope that is this true, and that I can keep with me some of Cindy's passion, talent and caring attitude. I am sure we will maintain our connection in the future as a mentor, role model and friend.

I want to thank all the members of my dissertation committee, Drs. Jackie Collier, Anja Engel, Gordon Taylor and Xavier Mari. I sincerely appreciate their time, guidance, valuable comments and ideas. I also want to thanks others faculty members at SoMAS, Drs. Mary Scranton and Bob Aller for discussions during class presentations that, without a doubt, helped me to improve my ability to communicate my research. I thank Drs. David Black and Kirk Cochran for sharing meaningful conversation about science and life during the BaRFlux cruises. Drs. Rob Armstrong, Qingzhi Zhu, Anne McElroy and Bruce Brownawell for their friendship, precise advise and appreciated company during those years.

Focus on my research would be a lot more difficult without the support of SoMAS staff members, particularly Dr. Christina Heilbrun, Stephen Abrams, David Hirschberg, and Shelagh Zegers, who very kindly assisted me with equipment, time, samples, and technical advice. In

addition, Eileen Goldsmith, Carol Dovi, Cristina Fink and Mark Lang, I appreciate their crucial assistance in administrative and informatics issues.

The past members of Lee's lab (or as we called it, the "pink lab") were also very important during this process. I thank Jenni Szlosek Chow for helping me start in the lab, and always having time to answer my questions or give a valuable advice, and also Tiantian Tang for sharing not only the office with me, but also experiences in the lab and during cruises.

I had the good fortune during my graduate school career to collaborate with outstanding colleagues. I spent two months with the research group of Dr. Anja Engel in Germany; there I meet colleagues and friend that I still maintain. I would like to thank the ADAGIO project team, especially Sonja Endres, Thea Dammrich and Roman De Jesus; my fellow grad-students and sailors in the BaRFlux project, Weilei Wang, Abel Guihou, Theresa King and Patrick Fitzgerald; my friends at SoMAS Liz Suter, Jungmin Lee, Claudia Hinrichs, Natasha Gownaris, Cassie Bauer, Christine O'Connell, and my dear friends Daniel and Elizabeth for understanding and love over those years at Stony Brook.

Funding for the first four years of my research came from a Fulbright-CONICYT scholarship provided by the Chilean government and the Fulbright commission. The next years where funded by the Chemical Oceanography Division of NSF through the ADAGIO and BarFlux projects. I thank the funding agencies and all the people involved for my support.

Finally, my sincere gratitude to my family; I would never have been able to complete this enterprise without the stronger motivation of your example, companion and love. My parents Blanca and Raul, my siblings Claudia and Raul, my nephew Martin and my nice Ema, were always with me, even when they were physically and literally at the end of the world. And last,

but always first, my husband Jaime for being the best partner in this adventure, for always being there… in all possible ways.

Chapter 1 :

Introduction and Background

Marine dissolved organic matter (DOM) can self-assemble and form porous microgels that can reversibly exchange material with DOM and particulate organic matter (POM) (Chin *et al*., 1998; Verdugo *et al.,* 2004). This abiotic self-assembly of materials forms particles that can sink and eventually sequester organic carbon into the deep ocean; dissolution and remineralization of this POM have important implications for ocean productivity and carbon cycling. Marine gels are a fundamental bridge in the DOM-POM continuum in the ocean (Verdugo *et al.,* 2004); they are hydrogels formed by a three-dimensional network of polymers and seawater. Operationally, transparent marine gels that form discrete particles larger than 0.2 μm or 0.4 μm in seawater and phytoplankton cultures, and that can be visualized after staining with a specific dye, have been termed Transparent Stainable Particles (TSP). TSP include polysaccharide-rich gel particles called Transparent Exopolymer Particles (TEP) and protein-rich gel particles called Coomassie Blue Stainable Particles (CSP).

Due to their transparency, gel particles have been visualized and studied only recently (Alldredge *et al.,* 1993; Long and Azam, 1996). Although TEP and CSP are known to be abundant in seawater, and their importance in the DOM-POM continuum has been recognized, only for the last two decades has research been focused on their significance to aggregation and sedimentation (Engel, 2000; Passow *et al.,* 2001; Beauvais *et al.,* 2006; Kahl *et al.,* 2008) and to POC vertical flux (Mari, 1999; Engel and Passow, 2001; Mari *et al.,* 2001), as well as to the effect that the changing ocean has on their distribution and behavior (Engel *et al.,* 2004b; Riebesell *et al.,* 2007; Mari 2008). There are still important questions regarding marine gel particles, especially about CSP and the significance of gel particles in future ocean processes. Marine gel particles are a heterogeneous group; their exact chemical composition and whether or not TEP and CSP represent polysaccharide and protein rich subunits of the same particles or of

separate particles have remained uncertain. In addition, the effect of warming and acidification on the production and fate of gel particles is thought to be an important control on the aggregation and POC flux in the ocean (Arrigo, 2007; Wohlers et al., 2009). Most of our knowledge about gel particles comes from the study of TEP; our lesser knowledge of CSP is at least partly due to the lack of an effective method to measure CSP.

1. Determination of Marine Gel Particle Concentrations

Since TEP were first described (Alldredge *et al.*, 1993), numerous studies have shown their ubiquity and significance in biogeochemical cycling of carbon (e.g., Mari 1999; Engel and Passow 2001), food web structure (Mari *et al.*, 2004; Grossart and Simon 2007), nutrients and trace metal availability (Alvarado-Quiroz *et al.*, 2006), as well as their role in aggregation and POC flux (Beauvais *et al.*, 2006; Kahl *et al.*, 2008; Engel et al., 2009a, 2009b; Gärdes et al.**,** 2011). To date most of the knowledge that we have about gel particles comes from these studies of TEP.

Gel particles are made of large organic polymers (MW> 1 kDa) and are considered stable macrogels (Verdugo, 2012). TEP are discrete exopolymers that consist predominantly of surface active acidic polysaccharides and that are stainable with Alcian Blue (Alldredge *et al.,* 1993, Mopper *et al.*, 1995; Zhou *et al.,* 1998), a cationic copper phthalocyanine dye that reacts with the carboxyl (COO^-) and sulfate half ester (OSO_3^-) functional groups of acid mucopolysaccharides and glycosaminoglycans. (Parker and Diboll, 1966; Decho, 1990).

TEP have been analyzed by microscopic and spectrophotometric methods after staining with Alcian Blue. The microscopic method allows visual determination of the number and size

of the gel particles (Alldredge *et al.*, 1993), while the spectrophotometric method is semi-quantitative and measures absorbance of dye that can be acid-extracted from stained particles. The amount of TEP that is bound to the dye is standardized using the exopolymer Xanthan gum (XG eq.L^{-1}) (Passow and Alldredge, 1995); xanthan gum is a microbially-produced heteropolysaccharide that contains D-glucoronic acid and that reacts with Alcian Blue.

CSP are protein-containing particles that are stainable with Coomassie Brilliant Blue (CBB) (Long and Azam, 1996); CBB is a disulfonated triphenylmethane dye that binds to proteins and longer peptides (Chial and Splittgerber, 1993). Until now, the only available method for CSP determination was a qualitative microscopic method developed by Long and Azam (1996). Microscopic measurements are complicated and difficult to standardize due the heterogeneous nature of TEP and CSP. Comparison between TEP and CSP concentrations in aquatic systems was thus limited to qualitative descriptions due to the lack of a semi-quantitative method for CSP determination analogous to the spectrophotometric method existing for TEP.

Concentrations of TEP vary from 100 to 300 µg XG eq.L^{-1} in coastal areas (Passow, 2002a) and from 28 to 140 µg XG eq.L^{-1} in the open ocean (*e.g.*, Ramaihah *et al.*, 2001; Engel, 2004). During a phytoplankton (especially diatom) bloom, TEP concentrations can be much higher, close to 1000 µg XG eq.l^{-1} (Passow, 2002a). High concentrations of CSP have also been associated with diatom blooms (Long and Azam, 1996), although the highest estimated number of CSP particles in that study was during a *Gonyaulax polyedra* dinoflagellate bloom off Scripps Pier, 10^4 particles ml^{-1}, and the cumulative area (the sum of surface areas of the different size classes) ranged from 10^3 to 10^4 mm^2 L^{-1} (Long and Azam, 1996). Berman and Viner-Mozzini (2001) compared the concentration of TEP and CSP in fresh water using microscopy and image analysis, finding that TEP and CSP were ubiquitous all year in Lake Kinneret; they also

estimated the projected spherical encased volume and the surface area. TEP abundance ranged from 440-25,000 particles mL^{-1}, and CSP ranged from 140-12,000 particles mL^{-1}; the projected spherical encased volume ranged from 80-5503 $mm^3\ L^{-1}$ for TEP and from 8-5199 $mm^3\ L^{-1}$ for CSP; and surface area varied between 897-15,073 $mm^2\ L^{-1}$ for TEP and between 200-14,514 $mm^2\ L^{-1}$ for CSP.

Concentrations of both TEP and CSP are highest in the upper 30 to 100 meters of the oceanic water column, decreasing with depth (Passow, 2002a; Long and Azam, 1996), and show enrichment in the surface microlayer (Kuznetsova *et al.*, 2005; Galgani and Engel 2013). The relative abundance of TEP vs. CSP in fresh water is dependent on the dominant phytoplankton species, which varies with depth and time of year, and the TSP turnover times (Berman and Viner-Mozzini, 2001). Higher abundances of CSP than TEP have been reported in the Arabian Sea (Long and Azam, 1996). Few studies have compared concentrations of TEP and CSP in parallel samples using microscopy in fresh water (Berman and Viner-Mozzini 2001), coastal areas (Long and Azam 1996), diatom cultures (Grossart and Simon., 2007; Bhaskar *et al.*, 2005), and the surface microlayer Kuztnetsova et al., 2005; Galgani and Engel 2013). The development of a semi-quantitative spectrophotometric method to determine CSP concentration will provide an effective way to study TEP and CSP in parallel samples, from different environments.

2. Origin of Marine Gel Particles

Marine gel particles are a chemically and physically diverse group; they are in principle made of exopolymeric substances (EPS) that are chemically rich in high molecular weight organic macromolecules (10 to 30 kDa), and are released external to the biomembrane by

phytoplankton or bacteria (Decho, 1990; Wotton, 2004). EPS from marine phytoplankton are composed mostly of polysaccharide-rich anionic colloidal polymers and amphiphilic proteins (Alvarado-Quiroz, 2006; Ding *et al.*, 2009). The predominant sugars in EPS, fucose, rhamnose, and arabinose, are also present in TEP (Myklestad and Haug 1972; Zhou *et al.*, 1998). The polysaccharide compositions of EPS and TEP closely resemble that of bulk DOM (Aluwihare *et al.*, 1997; Aluwihare and Repeta, 1999). EPS may comprise between 10 and 40% of DOM (Guo and Santschi, 1997); however, not all EPS can assemble to form discrete particles such as TEP or CSP (Passow, 2002a). Gel particle formation leads to a size continuum of marine gels in the ocean (Fig. 1-1); it is thought that organic molecules exuded by marine organisms align, form tangled webs, and stabilize to produce colloids that aggregate and form gel particles like TEP and CSP (Verdugo *et al.*, 2004). This process represents an important link between colloids, which belong to the DOC pool (Wells and Goldberg, 1991), and POC in the ocean.

The chemical composition of TEP precursors varies as a function of nutrient availability (Obernosterer and Herndl, 1995; Staats *et al.*, 1999, Underwood *et al.*, 2004), light (Smith and Underwood, 2000), species, and physiological stage (Claquin *et al.*, 2008). Dissolved precursors may be released as overflow carbon when cells are able to photosynthesize but not to divide, for instance, under silicate limitation (Engel, 2000; Kahl *et al.*, 2008). In natural seawater from different locations the carbon content of TEP ranges from 10 to 800 μg C L^{-1} (Engel and Passow, 2001; Mari, 1999) and C: N varies between 20 (Mari, 1999) and 26 (Engel and Passow, 2001). The average C: N of TEP is similar to that of the high molecular weight DOC produced by marine phytoplankton (Biddanda and Benner, 1997), supporting the idea that TEP is formed mainly from colloidal precursors exuded by phytoplankton that can spontaneously assemble into microscopic polymers (Chin et al., 1998).

Three mechanisms have been suggested for the formation of gel particles: a) aggregation of polymer fibrils and colloids by physical processes according to coagulation theory (Jackson, 1995; Burd and Jackson, 2009), b) spontaneous assembly of DOM to form larger polymer gels (Chin et al., 1998; Verdugo *et al.*, 2004; Ding *et al.*, 2009), and c) biotic release of particulate exudates from phytoplankton (Kiørboe and Hansen, 1993) or cell lysis (Long and Azam 1996). According to coagulation theory, aggregation depends on the abundance, size and stickiness (α, the probability of two particles adhesion upon collision) of colloidal particles, as well as the intensity of the physical processes bringing them together, such as Brownian motion, laminar and turbulent shear, differential settling, surface coagulation, diffusive capture, filtration and motility, in the case of living particles (Jackson, 1990; Kepkay, 1994; Burd and Jackson, 2009). The second mechanism, spontaneous assembly, examines DOC assembly from a physicochemical perspective, and involves the spontaneous or induced assembly of polymer chains that form the matrix of polymer gels. This assembly is not thought to be caused by collision or explained by stickiness, but is a chemical (covalent) or a physical (e.g., electrostatic, hydrogen bonding, van der Waals forces, and hydrophilic/hydrophobic bond) process that occurs when the molecules are close enough to interact (Doi and Edwards, 1986). The third mechanism for gel particle formation is based on the idea that phytoplankton cells exude not only TEP precursors, but also TEP and particulate mucus that promotes cell aggregation (Kiørboe and Hansen, 1993). The origin of CSP is unclear; they might form by the same process as TEP or originate from cell lysis and adsorption of protein into non-proteinaceous material (Long and Azam 1996). Recently described extracellular vesicles produced by ocean microbes (Billar et al., 2014) may also be a source of CSP.

Two types of chemical bonding have been proposed to explain how gel particles hold together. First, divalent cations (Ca^{2+}, Mg^{2+}) and half-ester sulfates (OSO_3^-) bind acidic monomers to form TEP (e.g., Engel, 2009), similar to the cation bridging mechanism that forms colloids in freshwater (Leppard et al., 1977; Massalski and Leppard, 1979). Diatom aggregates that contain TEP break apart in the presence of EDTA, a powerful chelating agent that binds with divalent cations and disrupts their attachment to polysaccharides (Decho, 1990; Alldredge *et al.,* 1993). Bacteria and algae release hydrocolloid polymers that contain predominantly water and can form gels in the presence of cations like K^+ and Ca^{2+} (Verdugo *et al.,* 2004); the Ca^{2+} cross linking follows second-order kinetics (Ding *et al.,* 2008). Second , POC and bacterial aggregates could be bound together by EPS through hydrophobic interactions (Stoderegger and Herndl, 2004). Empirical studies show that EPS from marine phytoplankton can self-assemble in Ca^{2+}-free seawater, implying that phytoplankton EPS may be held together by hydrophobic bonding (Ding *et al.,* 2009) in a first-order reaction (Ding *et al.,* 2008). The actual polymeric interactions responsible for the formation of gel particles are unknown. More experiments are required to clearly understand the kinetics and binding forces involved in TEP and CSP formation.

TEP, and potentially CSP, can form from dissolved exopolymeric exudate release by phytoplankton that are actively growing (Bhaskar et al., 2005). This abiotic assembly is promoted by bubble adsorption (Mopper *et al*., 1995; Mari and Burd, 1998; Zhou *et al.,* 1998; Mari, 1999) and laminar or turbulent shear (Passow and Alldredge, 1994; Passow, 2000; Engel and Passow, 2001). How these gel particles reach their final equilibrium size is not totally understood (Verdugo, 2012); it has been suggested that it is a several step process in which fibrillar TEP-precursors form large colloids, and ultimately macrogels and TEP (Passow, 2002a),

in the same way that small fibrillar polymers assemble to form nanogels that then form large colloids by annealing and aggregation (Chin et al., 1998) (Fig. 1-1).

3. Marine Gel Particles: Role in Aggregation and POC Flux

Flocculation and subsequent sedimentation of blooms is one of the largest carbon sinks in the ocean (Smetacek, 1985; Fowler and Knauer, 1986). Gel particles are thought to be involved in aggregation and sedimentation of some species of phytoplankton (e.g., Alldredge *et al.,* 1993; Logan *et al.*, 1995). Phytoplankton aggregation can be described by coagulation theory (Kiørboe and Jackson, 2001), and it has been hypothesized that formation and sinking of phytoplankton aggregates are responsible for ending diatom blooms (Jackson, 1990; Riebesell, 1991; Kiørboe et al., 1994). However, aggregate formation and sedimentation do not occur at the end of every diatom bloom, suggesting that factors like diatom species, production and concentration of gel particles, and environmental factors also play a role in post-bloom aggregation.

Two mechanisms have been proposed for the formation and sinking of aggregates. First, according to the coagulation model, cell-cell phytoplankton collisions and subsequent adhesion due to stickiness can produce large aggregates under bloom situations (Jackson, 1990). This model is based on the postulate that the abundance of phytoplankton cells is limited by a critical concentration value, and that above this concentration the removal of phytoplankton by aggregation occurs. This model further predicts the coagulation of phytoplankton in some environments (Kiørboe *et al.,* 1994), but more usually overestimates the amount of aggregate formation (Riebesell, 1991; Hill, 1992). Experimental evidence also suggests that changes in particle size distribution (Jackson, 1995) and the significance of TEP to aggregation (Passow and

Alldredge, 1995; Dam and Drapeau, 1995, Logan et al., 1995) can be explained by coagulation theory (Alldredge and Jackson, 1995).

Second, it has been proposed that aggregation of phytoplankton cells can be assisted by the abundance of highly sticky TEP (Alldredge et al., 1993), and presumably CSP, although it has been suggested that CSP would have less impact on the formation of marine aggregates than TEP, since no correlation has been found between CSP and aggregate abundance (Prieto et al., 2002). TEP could enhance aggregate formation in two different ways: 1) TEP are abundant in aquatic systems, especially during phytoplankton blooms (Alldredge *et al.,* 1995; Schuster and Herndl, 1995; Mari and Burd, 1998),which increases particle concentration and thus collision frequency, and 2) TEP stickiness is high and variable (between 0.1 and 0.8), (Dam and Drapeau, 1995, Engel, 2000; Mari and Robert, 2008), in part due to polymer bridging (Mopper *et al.*, 1995) and also possibly because of steric and entropic effects (Burd and Jackson, 2009); higher stickiness increases the coagulation efficiency (Engel, 2000).

The role of phytoplankton-derived TEP in the formation of large sedimenting aggregates has been investigated for diatoms (Passow *et al*., 1994; Passow and Alldredge, 1995; Kiørboe *et al.*, 1996; Passow *et al.*, 2001; Martin *et al.*, 2011; Gärdes *et al.*, 2011), cocolithophores (e.g., Engel et al., 2004a; Engel et al., 2004b) dinoflagellates (Alldredge *et al.*, 1998) and cyanobacteria (Grossart and Simon, 1997). It has been suggested that changes in stickiness and production of TEP and presumably CSP, could affect the efficiency of aggregation, sedimentation and ultimately the biological pump (Jackson, 1995; Logan *et al.*, 1995, Engel, 2000; Mari *et al.*, 2007). Passow et al. (2001) showed that sedimentation is the main process removing TEP from the euphotic zone (Fig. 1-2), and that the sedimentation of diatoms, biogenic silica and lithogenic silica is directly related to TEP abundance, suggesting that large TEP-rich

aggregates are crucial in the sedimentation of small biogenic particles and clays. For example, diatoms embedded in aggregates have higher sinking velocities, between 50 and 200 m d^{-1} (Asper, 1987; Alldredge and Gotschalk, 1988), than single cells, between <1 and 10 m d^{-1} (Culver and Smith, 1989).

Aggregate sinking velocity is determined by size, dry weight, porosity, excess density, variations in water density, differences between average aggregate density and surrounding water density (Crocker and Passow, 1995; Alldredge and Gotschalk, 1988; Burd and Jackson, 2009), and turbulence of the surrounding seawater (Shanks, 2002). Aggregate density is affected by the presence of trapped gas (Riesebell, 1992), the density of embedded solid particles (Asper, 1987) and the TEP: solid particle ratio (Engel and Schartau, 1999; Azetsu-Scott and Passow, 2004). Earlier it was proposed that mucus material included in an aggregate has a density similar to that of the water in which they formed (Alldredge and Crocker, 1995), However, latterly, it has been shown that particle-free TEP has lower density than seawater, usually between 0.7 and 0.84 g cm^{-3} (Azetsu-Scott and Passow, 2004). Particle-free TEP is buoyant and ascends and accumulates at the surface (Azetsu-Scott and Passow, 2004). There is evidence that aggregates with high TEP: solid particle ratios have lower sinking velocities (or are even positively buoyant) (Azetsu-Scott and Passow, 2004), and they have lower excess density (Engel and Schartau, 1999). This suggests that even though gel particles like TEP and CSP are fundamental for the aggregation process, the fraction of gel particles required for an aggregate to sink is variable, as is the direction and velocity of the vertical flux (Azetsu-Scott and Passow, 2004; Mari *et al.*, 2007). There are no empirical measurements of how the content of CSP may affect the vertical flux of aggregates.

4. Effect of Future Changes in Temperature and pCO_2 on Marine Gel Particles

Anthropogenically-induced climate change is driving rapid alterations that are affecting the world's oceans. Rising atmospheric CO_2 has led to increases in global temperature and ocean acidification. Future elevated temperature and CO_2 conditions will affect key phytoplankton processes, such as primary production (Rost *et al.,* 2008; Egge *et al.,* 2009), growth rate (Feng *et al.*, 2008), calcification (Gattuso *et al.,* 1998; Riebesell *et al.,* 2000; Langdon, 2003; Delille, 2005; Rost *et al.,* 2008), nitrogen fixation (Rost et al., 2008), and production of extracellular material (Engel, 2002; Engel *et al.,* 2004b). Additionally, changes in stratification, nutrient inputs, and oxygen concentrations are affecting biological productivity, the biological pump and the role of the ocean in biogeochemical cycles and as a climate regulator (Doney, 2010). Climate change is impacting biological community composition and physiological responses, as well as the vertical export of POC from the photic zone to the deep ocean (Passow and Carlson 2012) . Responses of plankton species to increases in CO_2 concentration, rising temperature, and alteration of nutrient inputs have been analyzed in manipulative experiments during the last two decades; however a limited number of studies has addressed the synergistic effect of multiple stressors on phytoplankton (e.g., Borchard *et al.,* 2011; Cai *et al*., 2011), organic matter composition (Chen *et al*., 2015), and aggregation (Seebah *et al.,* 2014).

The rapid increase in atmospheric CO_2 from preindustrial levels of approximately 280 ppm to the present 400 ppm has caused a decrease in ocean pH by 0.1 unit. pH is expected to fall another 0.3 - 0.4 units by the year 2100 if the burning of fossil fuels continues at current rates (Caldeira and Wickett, 2003), causing increases in aqueous CO_2 and total inorganic carbon concentrations, carbonate ion concentration and calcium carbonate saturation (Doney *et al*.,

2009). Ocean acidification may affect the sinking velocity of marine aggregates, and the efficiency of export due to a decrease in the ballast component (Armstrong *et al.,* 2002; Klaas and Archer, 2002), leading to less sinking of aggregates or slower sinking velocities. On the other hand, it has been hypothesized that because the CO_2 uptake by phytoplankton will increase under elevated CO_2 conditions (Arrigo, 2007; Riebesell *et al.*, 2007), exudation and therefore the production of gel particles, like TEP, will also increase (Fig. 1-3). Under elevated concentrations of CO_2, carbon overconsumption (relative to N) has been hypothesized to increase extracellular release of TEP precursors, and also TEP formation and consequent loss of POC as sinking aggregates from the surface layer (Engel, 2005; Riebesell et al., 2007). However, there is no concrete evidence to demonstrate that this will occur.

Mesocosm experiments have shown that under elevated CO_2 concentrations (i.e., 750 to 1000 ppm of CO_2), TEP normalized to cell abundance increases, suggesting increased formation and sinking of TEP-enriched aggregates (Engel, 2005). In these experiments, there was a strong relationship between TEP and POC after nutrient depletion, but no correlation between TEP and PON concentrations, supporting the idea of Engel and Passow (2001) that TEP do not contain nitrogen as a fundamental component. There is no similar data on the concentration of CSP or its relationship with POC or PON.. Phytoplankton under elevated CO_2 conditions consumes carbon and nitrogen in a stoichiometric C: N ratio of 8, exceeding the Redfield ratio of 6.6. (Riebesell *et al*., 2007). Recent studies show inconclusive evidence regarding the increase of TEP production under elevated CO_2 conditions. Engel *et al.* (2014) found higher concentration of TEP at higher CO_2, while other studies did not show a direct relationship between elevated CO_2 and increased TEP concentration (Egge *et al.,* 2009). In any case, higher TEP concentration with CO_2 may not always lead to an enhancement in aggregation and particle sinking (e.g., Seebah et al., 2014).

Mari (2008) found that TEP formed under low pH conditions (pH=7.36) are larger in size, but more positively buoyant, than those formed at higher pH (pH=8.16), and this increased buoyancy resulted in an upward flux of TEP-latex bead aggregates. He suggested that the excess of organic matter produced at high CO_2 conditions could accumulate in the surface microlayer instead of sinking, assuming that phytoplankton cells interact with TEP in the same way as latex beads. However, Passow (2012) suggested that these results show changes in TEP size and concentration due to changes in total alkalinity (TA), rather than ocean acidification, since the acidification method used by Mari (2008) involves addition of strong acid, which alters pH and TA without modifying DIC (Passow, 2012). She found that elevated CO_2 conditions do not affect abiotic formation of TEP. Effects of elevated CO_2 on CSP concentration, transparent gel particle production by phytoplankton, or gel particle properties like stickiness have not been studied.

Acidification is only one of the alterations expected in the future ocean; higher sea surface temperature, stronger stratification and changes in nutrient input and light could also modify the dynamics of gel particles, aggregation and ultimately vertical flux of carbon. The increase in the global mean surface temperature is expected to be 1.8 - 4.0°C at the end of the 21st century depending on the emission scenario (Solomon et al., 2007). Such warming resulted in a sea level rise rate of about 2.5 mm/year in the 1993-2003 decade based on satellite altimetry (Cazenave et al., 2008), increased stratification, decreased sea-ice cover in the Arctic (Polyakov *et al.*, 2010), Antarctic (Stammerjohn *et al.*, 2008), and changes in circulation patterns, precipitation, and fresh water input. A strengthened vertical stratification is expected to change light availability because of reduced mixing and a reduction in nutrient upwelling, thus decreasing new production (Doney, 2010).

Experimental evidence reveals that the responses to elevated temperature in terms of photosynthesis, TEP production, and acclimation ability, varies significantly between phytoplankton species; for instance Claquin et al. (2008) showed that temperature affects TEP production in three species of diatoms, but not in *Emiliania huxleyi* and *Lepidodinium chlorophorum*. Chemostat experiments with both elevated CO_2 and temperature show reduction in the growth rate of *Emiliania huxleyi*, enhanced DOC exudation, and the formation of TEP, aggregates, and an increase of POC (Borchard *et al.*, 2011). The combined effect of elevated CO_2 and temperature on the origin and fate of marine gel particles is a key component to predicting the efficiency of the biological pump and the implications for vertical export of POC in the water column under future ocean scenarios.

This dissertation research will focus on: 1) developing a new technique for the quantitative analysis of protein-rich particles, 2) differences in the origins and vertical distributions of TEP and CSP in the ocean, and 3) effects of higher temperature and CO_2 on gel particle formation, aggregation, and POC flux.

References

Aluwihare, L.I., Repeta, D.J., 1999. A comparison of the chemical characteristics of oceanic DOM and extracellular DOM produced by marine algae. Mar. Ecol. Progr. Ser., 186: 105-117.

Aluwihare, L.I., Repeta, D.J., Chen, R.F., 1997. A major biopolymeric component to dissolved organic carbon in surface sea water. Nature, 387: 166-169.

Alvarado Quiroz, N.G., Hung, C.-C., Santschi, P.H., 2006. Binding of thorium (IV) to carboxylate, phosphate and sulfate functional groups from marine exopolymeric substances (EPS). Mar. Chem., 100(3–4): 337-353.

Alldredge, A.L., Passow, U., Haddock, H.D., 1998. The characteristics and transparent exopolymer particle (TEP) content of marine snow formed from thecate dinoflagellates. J. Plankton Res., 20(3): 393-406

Alldredge, A.L., Crocker, K.M., 1995. Why do sinking mucilage aggregates accumulate in the water column? Sci. Total Environ., 165(1–3): 15-22.

Alldredge, A.L., Jackson, G.A., 1995. Preface: Aggregation in marine system. Deep Sea Res. Part II, 42(1): 1-7.

Alldredge, A.L., Gotschalk, C., Passow, U. and Riebesell, U., 1995. Mass aggregation of diatom blooms: Insights from a mesocosm study. Deep Sea Res. Part II, 42(1): 9-27.

Alldredge, A.L., Passow, U., Logan, B.E., 1993. The abundance and significance of a class of large, transparent organic particles in the ocean. Deep-Sea Res. Part I, 40(6): 1131-1140.

Alldredge, A.L., Gotschalk, C., 1988. In situ settling behavior of marine snow. Limnol. Oceanogr., 33(3): 339-351.

Arrigo, K.R., 2007. Carbon cycle: Marine manipulations. Nature, 450(7169): 491-492.

Armstrong, R., Lee, C., Hedges, J., Honjo, S., Wakeham, S., 2002. A new, mechanistic model for organic carbon fluxes in the ocean based on the quantitative association of POC with ballast minerals. Deep-Sea Res. Part II, 49: 219.

Asper, V.L., 1987. Measuring the flux and sinking speed of marine snow aggregates. Deep Sea Res. Part I, 34(1): 1-17.

Azetsu-Scott, K., Passow, U., 2004. Ascending marine particles: significance of transparent exopolymer particles (TEP) in the upper ocean. Limnol. Oceanogr., 49(3): 741-748.

Beauvais, S., Pedrotti, M.L., Egge, J., Iversen, K., Marrasé, C., 2006. Effects of turbulence on TEP dynamics under contrasting nutrient conditions: implications for aggregation and sedimentation processes. Mar. Ecol. Progr. Ser., 323: 47-57.

Berman, T., Viner-Mozzini, Y., 2001. Abundance and characteristics of polysaccharide and proteinaceous particles in Lake Kinneret. Aquat. Microb. Ecol., 24(3): 255-264.

Bhaskar, P.V., Grossart, H.-P., Bhosle, N.B., Simon, M., 2005. Production of macroaggregates from dissolved exopolymeric substances (EPS) of bacterial and diatom origin. FEMS Microbiol. Ecol., 53(2): 255-264.

Biddanda, B., Benner, R., 1997. Major contribution from mesopelagic plankton to heterotrophic metabolism in the upper ocean. Deep-Sea Res. Part I, 44(12): 2069-2085.

Biller, S.J., Schubotz, F., Roggensack, S.E., Thompson, A.W., Summons, R.E., Chisholm, S.W., 2014. Bacterial vesicles in marine ecosystems. Science, 343(6167): 183-186.

Borchard, C., Borges, A.V., Händel, N., Engel, A., 2011. Biogeochemical response *of Emiliania huxleyi* (PML B92/11) to elevated CO2 and temperature under phosphorous limitation: A chemostat study. J. Exp. Mar. Biol. Ecol., 410(0): 61-71.

Burd, A.B., Jackson, G.A., 2009. Particle aggregation. Ann. Rev. Mar. Sci., pp. 65-90.

Cai, W.-J. et al., 2011. Acidification of subsurface coastal waters enhanced by eutrophication. Nature Geosci, 4(11): 766-770.

Caldeira, K., Wickett, M.E., 2003. Anthropogenic carbon and ocean pH. Nature, 425: 365.

Cazenave, A., Lombard, A., Llovel, W., 2008. Present-day sea level rise: A synthesis. C. R. Geosci., 340(11): 761-770.

Chen, C.-S., Anaya, J.M., Chen, E.Y.T., Farr, E. and Chin, W.-C., 2015. Ocean warming–acidification synergism undermines dissolved organic matter assembly. PLoS ONE, 10(2): e0118300.

Chial, H., Splittgerber, A., 1993. A comparison of the binding of Coomassie brilliant blue to proteins at low and neutral pH. Anal Biochem. , 213(2): 362-9.

Chin, W.-C., Orellana, M.V., Verdugo, P., 1998. Spontaneous assembly of marine dissolved organic matter into polymer gels. Nature, 391(6667): 568-572.

Claquin, P., Probert, I., Lefebvre, S., Veron, B., 2008. Effects of temperature on photosynthetic parameters and TEP production in eight species of marine microalgae. Aquat. Microb. Ecol., 51(1): 1-11.

Crocker, K.M., Passow, U., 1995. Differential aggregation of diatoms. Mar. Ecol. Progr. Ser., 117: 249-257.

Culver, M.E., Smith, W.O., 1989. Effects of environmental variation on sinking rates of marine phytoplankton1. J. Phycol., 25(2): 262-270.

Dam, H.G., Drapeau, D.T., 1995. Coagulation efficiency, organic-matter glues and the dynamics of particles during a phytoplankton bloom in a mesocosm study. Deep-Sea Res. Part II, 42(1): 111-123.

Decho, A.W., 1990. Microbial exopolymer secretions in ocean environments: Their role(s) in food web and marine processes. Oceanogr. Mar. Biol. Annu. Rev., 28: 73–153.

Delille, B., 2005. Response of primary production and calcification to changes of naturem during experimental blooms of the coccolithophorid *Emiliania huxleyi*. Glob. Biogeochem. Cycles, 19: GB2023.

Ding, Y.-X., Hung, C.-C., Santschi, P.H., Verdugo, P., Chin, W.-C., 2009. Spontaneous assembly of exopolymers from phytoplankton. Terr. Atmos. Ocean. Sci., 20(5): 741-745.

Ding, Y.-X. et al., 2008. Amphiphilic exopolymers from *Sagittula stellata* induce DOM self-assembly and formation of marine microgels. Mar. Chem., 112(1–2): 11-19.

Doi, M., Edwards, S.F., 1986. The Theory of Polymer Dynamics. Oxford University Press, 408 pp.

Doney, S.C., Fabry, V.J., Feely, R.A., Kleypas, J.A., 2009. Ocean Acidification: The Other CO_2 Problem. Ann. Rev. Mar. Sci., 1(1): 169-192.

Doney, S.C., 2010. The growing human footprint on coastal and open-ocean biogeochemistry. Science, 328(5985): 1512-1516.

Egge, J., Thingstad, T.F., Larsen, A., Engel, A., Wohlers, J., Bellerby, R.G.J., and U. Riebesell., 2009. Primary production during nutrient-induced blooms at elevated CO_2 concentrations. Biogeosciences, 6: 877-885.

Engel, A., Piontek, J., Grossart, H., Riebesell, U., Schulz, KG., and M. Sperling., 2014. Impact of CO_2 enrichment on organic matter dynamics during nutrient induced coastal phytoplankton blooms. J. Plankton Res., 36(3): 641-657.

Engel, A., 2009. Determination of marine gel particles. In: O. Wurl (Editor), Practical Guidelines for the Analysis of Seawater. CRC Press, Boca Raton.

Engel, A., 2005. Testing the direct effect of CO_2 concentration on a bloom of the coccolithophorid *Emiliania huxleyi* in mesocosm experiments. Limnol. Oceanogr., 50: 493-504.

Engel, A., Thoms, S., Riebesell, U., Rochelle-Newall, E., Zondervan, I., 2004a. Polysaccharide aggregation as a potential sink of marine dissolved organic carbon. Nature, 428: 929-932.

Engel, A. Delille, B., Jacquet, S., Riebesell, U., Rochelle-Newall, E., Terbrüggen, A., and I. Zondervan, 2004b. Transparent exopolymer particles and dissolved organic carbon production by Emiliania huxleyi exposed to different CO2 concentrations: a mesocosm experiment. Aquat. Microb. Ecol., 34(1): 93-104.Engel, A., 2002. Direct relationship between CO_2 uptake and transparent exopolymer particles production in natural phytoplankton. J. Plankton Res., 24(1): 49-53.

Engel, A., Passow, U., 2001. Carbon and nitrogen content of transparent exopolymer particles (TEP) in relation to their Alcian Blue adsorption. Mar. Ecol. Progr. Ser., 219: 1-10.

Engel, A., 2000. The role of transparent exopolymer particles (TEP) in the increase in apparent particle stickiness α during the decline of a diatom bloom. J. Plankton Res., 22(3): 485-497.

Engel, A., Schartau, M., 1999. Influence of transparent exopolymer particles (TEP) on sinking velocity of *Nitzschia closterium* aggregates. Mar. Ecol. Progr. Ser., 182: 69-76.

Feng, Y., Warner, M. E., Zhang, Y., Sun, J., Fu, F.X., Rose, J. M.,and D.A. Hutchins., 2008. Interactive effects of increased pCO2, temperature and irradiance on the marine coccolithophore *Emiliania huxleyi* (Prymnesiophyceae). Eur. J. Phycol., 43(1): 87-98..

Fowler, S.W., Knauer, G.A., 1986. Role of large particles in the transport of elements and organic compounds through the oceanic water column. Progr. Oceanogr., 16(3): 147-194.

Gattuso, J.P., Frankignoulle, M., Bourge, I., Romaine, S., Buddemeier, R.W., 1998. Effect of calcium carbonate saturation of seawater on coral calcification. Glob. Planet. Change, 18: 37-46.

Gärdes, A., Iversen, M.H., Grossart, H.-P., Passow, U., Ullrich, M.S., 2011. Diatom-associated bacteria are required for aggregation of *Thalassiosira weissflogii.* ISME J., 5: 436-445.

Grossart, H.-P. and Simon, M., 2007. Interactions of planktonic algae and bacteria: effects on algal growth and organic matter dynamics. Aquat. Microb. Ecol., 47(2): 163-176.

Grossart HP, Simon, M., 1997. Formation of macroscopic organic aggregates (lake snow) in a large lake: the significance of transparent exopolymer particles, phytoplankton, and zooplankton. Limnol Oceanogr, 42: 1651-1659.

Guo, L., Santschi, P.H., 1997. Composition and cycling of colloids in marine environments. Rev. Geophys., 35: 17-40.

Hill, P.S., 1992. Reconciling aggregation theory with observed vertical fluxes following phytoplankton blooms. J. Geophys. Res., 97(C2): 2295-2308.

Jackson, G.A., 1995. TEP and coagulation during a mesocosm experiment. Deep-Sea Res. Part II, 42(1): 215-222.

Jackson, G.A., 1990. A model of the formation of marine algal flocs by physical coagulation processes. Deep-Sea Res. Part I, 37(8): 1197-1211.

Kahl, L., Vardi, A., Schofield, O., 2008. Effects of phytoplankton physiology on export flux. Mar. Ecol. Progr. Ser., 354: 3-19.

Kepkay, P.E., 1994. Particle aggregation and the biological reactivity of colloids. Mar. Ecol. Prog. Ser., 109: 293-304.

Kiørboe, T., Jackson, G.A., 2001. Marine snow, organic solute plumes, and optimal chemosensory behavior of bacteria. Limnol. Oceanogr, 46(6): 1309-1318.

Kiørboe, T., Saiz, E., Viitasalo, M., 1996. Prey switching behavior in the planktonic copepod Acartia tonsa. Mar. Ecol. Progr. Ser., 143: 65-75.

Kiørboe, T., Lundsgaard, C., Olesen, M., Hansen, J.L.S., 1994. Aggregation and sedimentation processes during a spring phytoplankton bloom: A field experiment to test coagulation theory. J. Mar. Res.,52(2): 297-323.

Kiørboe, T., Hansen, J.L.S., 1993. Phytoplankton aggregate formation: observations of patterns and mechanisms of cell sticking and the significance of exopolymeric material. J. Plankton Res., 15(9): 993-1018.

Klaas, C., Archer, D.E., 2002. Association of sinking organic matter with various types of mineral ballast in the deep sea: Implications for the rain ratio. Global Biogeochem. Cycles, 16(4): 1116.

Kuznetsova, M., Lee, C., Aller, J., 2005. Characterization of the proteinaceous matter in marine aerosols. Mar. Chem., 96(3-4): 359-377.

Langdon, C., 2003. Effect of elevated CO_2 on the community metabolism of an experimental coral reef. Glob. Biogeochem. Cycles, 17: 1011.

Leppard, G.G., Massalski, A., Lean, D.R.S., 1977. Electron-opaque microscopic fibrils in lakes: Their demonstration, their biological derivation and their potential significance in the redistribution of cations. Protoplasma, 92: 289-310.

Logan, B.E., Passow, U., Alldredge, A.L., Grossartt, H.-P., Simont, M., 1995. Rapid formation and sedimentation of large aggregates is predictable from coagulation rates (half-lives) of transparent exopolymer particles (TEP). Deep Sea Res. Part II, 42(1): 203-214.

Long, R., Azam, F., 1996. Abundant protein-containing particles in the sea. Aquat. Microb. Ecol., 10(3): 213-221.

Mari, X., 2008. Does ocean acidification induce an upward flux of marine aggregates? Biogeosciences, 5(4): 1023-1031.

Mari, X., Robert, M., 2008. Metal induced variations of TEP sticking properties in the southwestern lagoon of New Caledonia. Mar. Chem., 110(1–2): 98-108.

Mari, X., Rochelle-Newall, E., Torréton, J. P.,Pringault, O., Jouon, A., and C. Migon, 2007. Water residence time: a regulatory factor of the DOM to POM transfer efficiency. Limnol. Oceanogr., 52(2): 808-819.

Mari, X., Beauvais, S., Lemée, R., Pedrotti, M.L., 2001. Non-Redfield C : N Ratio of Transparent Exopolymeric Particles in the Northwestern Mediterranean Sea. Limnol. Oceanogr., 46(7): 1831-1836

Mari, X., 1999. Carbon content and C:N ratio of transparent exopolymeric particles (TEP) produced by bubbling exudates of diatoms. Mar. Ecol. Progr. Ser., 183: 59-71.

Mari, X., Burd, A.B., 1998. Seasonal size spectra of transparent exopolymeric particles (TEP) in a coastal sea and comparison with those predicted using coagulation theory. Mar. Ecol. Progr. Ser., 163: 63-76.

Massalski, A., Leppard, G.G., 1979. Morphological examination of fibrillar colloids associated with algae and bacteria in lakes. J. Fish. Res. Board Can., 36(8): 922-938.

Martin, P., Lampitt, R. S, Jane P. M., Sanders, R., Lee, C., and E. D'Asar, 2011. Export and mesopelagic particle flux during a North Atlantic spring diatom bloom. Deep Sea Res. Part I, 58(4): 338-349.

Mopper, K. Zhou, J., Sri Ramana, K., Passow, U., Dam, H. G., and D.T. DrapeaU., 1995. The role of surface-active carbohydrates in the flocculation of a diatom bloom in a mesocosm. Deep-Sea Res. Part II, 42(1): 47-73.

Myklestad, S., Haug, A., 1972. Production of carbohydrates by the marine diatom *Chaetoceros affin*is var. willei (Gran) Hustedt. I. Effect of the concentration of nutrients in the culture medium. J. Exp. Ma. Biol. Ecol., 9(2): 125-136.

Obernosterer, I., Herndl, G.J., 1995. Phytoplankton extracellular release and bacterial growth: dependence on the inorganic N:P ratio. Mar. Ecol. Progr. Ser., 116: 247-257.

Parker, B.C., Diboll, A.G., 1966. Alcian stains for histochemical localization of acid and sulfated polysaccharides in algae. Phycologia, 6(1): 37-46.

Passow, U., 2012. The abiotic formation of TEP under different ocean acidification scenarios. Mar. Chem., 128–129(0): 72-80.

Passow, U. and Carlson, C., 2012. The biological pump in a high CO_2 world. Mar. Ecol. Prog. Ser., 470: 249–271.

Passow, U., 2002a. Transparent exopolymer particles (TEP) in aquatic environments. Progr. Oceanogr., 55(3-4): 287-333.

Passow, U. Shipe, R. F., Murray, A., Pak, D. K, Brzezinski, M. A, and A. L Alldredge, 2001. The origin of transparent exopolymer particles (TEP) and their role in the sedimentation of particulate matter. Cont. Shelf Res., 21(4): 327-346.

Passow, U., 2000. Formation of transparent exopolymer particles, TEP, from dissolved precursor material. Mar. Ecol.-Progr. Ser., 192: 1-11.

Passow, U., Alldredge, A.L., 1995. A dye-binding assay for the spectrophotometric measurement of transparent exopolymer particles (TEP). Limnol. Oceanogr. 40(7): 1326-1335.

Passow, U., Alldredge, A., 1994. Distribution, size and bacterial colonization of transparent exopolymer particles (TEP) in the ocean Mar. Ecol.Progr. Ser., 113(1-2): 185-194.

Passow, U., Alldredge, A.L., Logan, B.E., 1994. The role of particulate carbohydrate exudates in the flocculation of diatom blooms Deep-Sea Res. Part I, 41(2): 335-357.

Polyakov, I.V., Timokhov, L.A., Alexeev, V.A., Bacon, S., Dmitrenko, I.A., 2010. Arctic Ocean warming contributes to reduced polar ice cap. J. Phys. Oceanogr., 40: 2743.

Prieto, L. et al., 2002. Scales and processes in the aggregation of diatom blooms: high time resolution and wide size range records in a mesocosm study. Deep-Sea Res. Part I, 49(7): 1233-1253.

Ramaihah, N., Yoshikawa, T., Furuya, K., 2001. Temporal variations in transparent exopolymer particles (TEP) associated with a diatom spring bloom in a subarctic ria in Japan. Mar. Ecol. Progr. Ser., 212: 79-88.

Riebesell, U., Schulz, K. G., Bellerby, R. G. J., Botros, M., Fritsche, P., Meyerhofer, M., Neill, C., Nondal, G., Oschlies, A., Wohlers, J., and E. Zollner., 2007. Enhanced biological carbon consumption in a high CO_2 ocean. Nature, 450(7169): 545-548.

Riebesell, U., Zondervan, I., Rost, B., Tortell, P. D., Zeebe, R. E., and F.M. M. Morel., 2000. Reduced calcification of marine plankton in response to increased atmospheric CO_2. Nature, 407(6802): 364-367.

Riebesell, U., 1992. The formation of large marine snow and its sustained residence in surface waters. Limnol. Oceanogr., 37: 63-76.

Riebesell, U., 1991. Particle aggregation during a diatom bloom. I. Physical aspects Mar. Ecol. Progr. Ser., 69: 273-280.

Rost, B., Zondervan, I., Wolf-Gladrow, D., 2008. Sensitivity of phytoplankton to future changes in ocean carbonate chemistry: current knowledge, contradictions and research directions. Mar. Ecol. Progr. Ser., 373: 227-237.

Seebah, S., Fairfield, C., Ullrich, M.S. and Passow, U., 2014. Aggregation and sedimentation of *Thalassiosira weissflogii* (diatom) in a warmer and more acidified future ocean. PLoS ONE, 9(11): e112379.

Shanks, A.L., 2002. The abundance, vertical flux, and still-water and apparent sinking rates of marine snow in a shallow coastal water column. Cont. Shelf Res., 22(14): 2045-2064.

Schuster, S., Herndl, G., 1995. Formation and significance of transparent exopolymeric particles in the northern Adriatic Sea. Mar. Ecol. Progr. Ser., 124: 227-236.

Smetacek, V.S., 1985. Role of sinking in diatom life-history cycles: ecological, evolutionary and geological significance Mar. Biol., 84: 239-251.

Smith, D.J., Underwood, G.J.C., 2000. The production of extracellular carbohydrates by estuarine benthic diatoms: the effects of growth phase and light and dark treatment. J. Phycol., 36(2): 321-333.

Solomon, S., Qin, D., Manning, M., Chen, Z., Marquis, M., 2007. Climate change 2007: the physical science basis: contribution of working group I to the fourth assessment report of the Intergovernmental Panel on Climate Change.

Staats, N., De Winder, B., Stal, L.J., Mur, L.R., 1999. Isolation and characterization of extracellular polysaccharides from the epipelic diatoms *Cylindrotheca closterium* and *Navicula salinarum*. Eur. J. Phycol., 34(2): 161-169.

Stammerjohn, S.E., Martinson, D.G., Smith, R.C., Yuan, X., Rind, D., 2008. Trends in Antarctic annual sea ice retreat and advance and their relation to El Niño–Southern Oscillation and Southern Annular Mode variability. J. Geophys. Res., 113(C3): C03S90.

Stoderegger, K.E., Herndl, G.J., 2004. Dynamics in bacterial cell surface properties assessed by fluorescent stains and confocal laser scanning microscopy. Aquat. Microb. Ecol. 36(1): 29-40.

Underwood, G.J.C., Boulcott, M., Raines, C.A., Waldron, K., 2004. Environmental effects on exopolymer production by marine benthic diatoms: dynamics, changes in composition, and pathways of production1. J. Phycol., 40(2): 293-304.

Verdugo, P. et al., 2004. The oceanic gel phase: a bridge in the DOM–POM continuum. Mar. Chem., 92(1–4): 67-85.

Verdugo, P., 2012. Marine Microgels. Ann. Rev. Mar. Sci., 4(1): 375-400.

Wells, M.L., Goldberg, E.D., 1991. Occurrence of small colloids in sea water. Nature, 353(6342): 342-344.

Wohlers, J. et al., 2009. Changes in biogenic carbon flow in response to sea surface warming. PNAS, 106(17): 7067-7072.

Wotton, R., 2004. The essential role of exopolymers (EPS) in aquatic systems, Oceanogr. Mar. Biol. Annu. Rev., pp. 57-94.

Zhou, J., Mopper, K., Passow, U., 1998. The role of surface-active carbohydrates in the formation of transparent exopolymer particles by bubble adsorption of seawater. Limnol. Oceanogr., 43(8): 1860-1871.

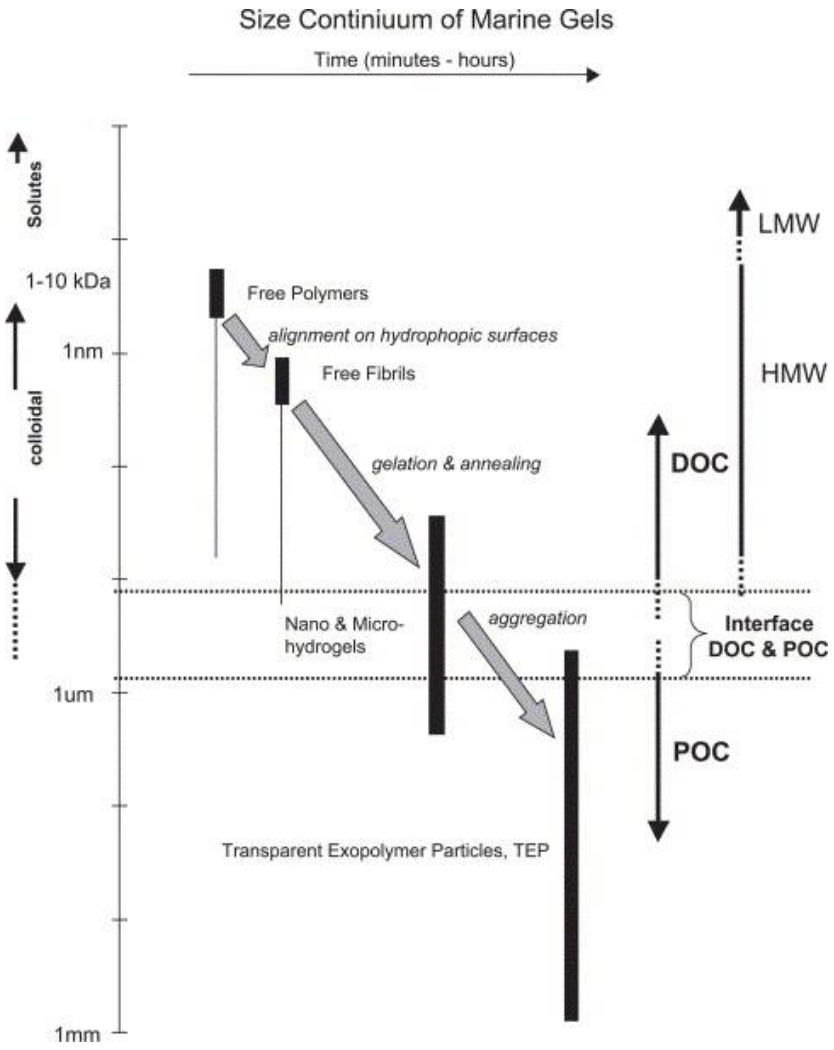

Figure 1-1. Size continuum of marine gel particles and the mechanisms of gel formation; first the free polymers align into free fibrils, and then the fibrils assemble to form nanogels; nanogels then anneal to form POC size microaggregates linking the DOC and the POC pools (from Verdugo *et al.*, 2004)

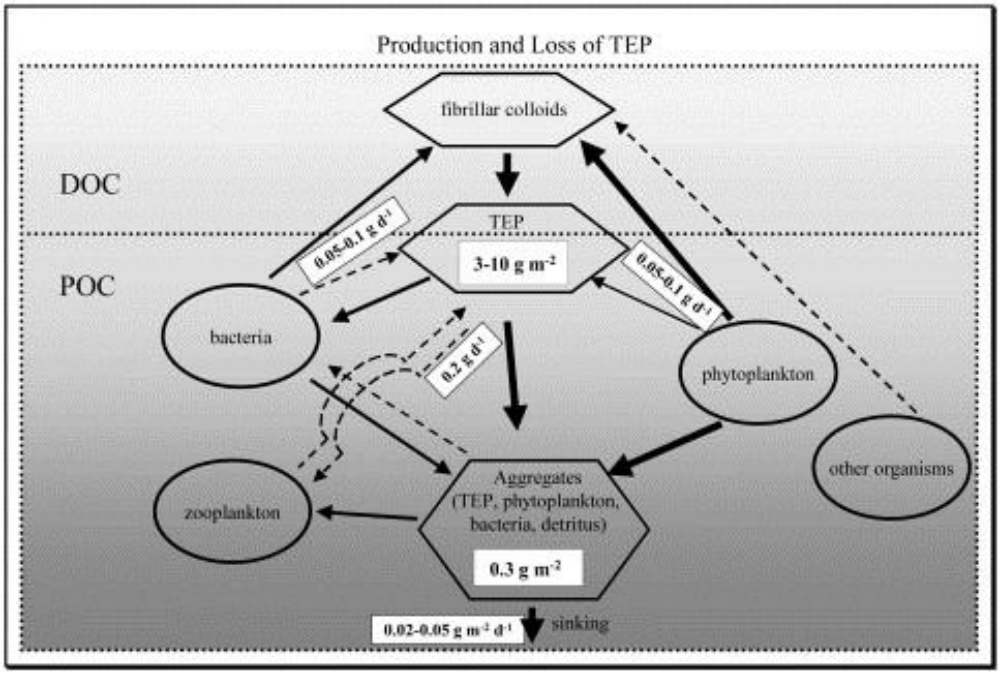

Figure 1-2. Production and loss of TEP from the pelagic zone. TEP exists in the dissolved and particulate organic carbon pools; due their flexibility and size range a significant fraction of TEP is not retained on a 0.4 μm filter. TEP and dissolved TEP precursors are released by bacteria and phytoplankton. TEP may be degraded by bacteria or grazed by zooplankton; TEP can also form aggregates that may be grazed by zooplankton or sink out the euphotic zone. Solid, fat arrows represent processes that are generally important, solid thin arrows represent local processes, and dashed lines represent poorly studied processes (from Passow, 2002a).

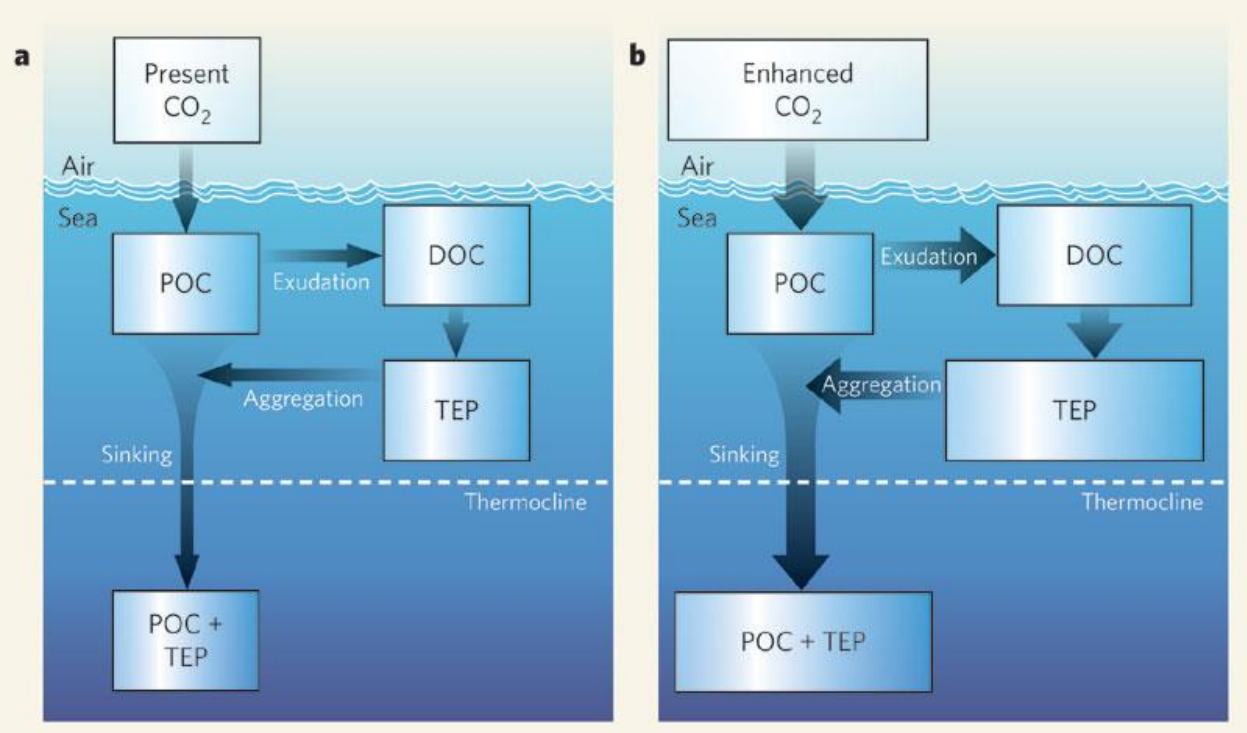

Figure 1-3. Relative size and flux magnitude of the organic carbon pools at a) present CO_2 conditions and b) elevated CO_2 conditions. Under elevated CO_2, the fixation of DIC increases over current conditions, which enhances photosynthesis and the production of DOC. The increase of TEP precursors and consequently TEP formation will increase aggregation and increase the flux of POC sinking below the thermocline (from Arrigo, 2007). The POC pool above the thermocline is in steady state

Chapter 2 :

A semi-quantitative spectrophotometric, dye-binding assay for determination of Coomassie Blue stainable particles

(Published in Limnology and Oceanography Methods, November 2014)

Abstract

Coomassie stainable particles (CSP) are protein-containing transparent particles that can be stained with Coomassie brilliant blue (CBB) and are found abundantly in aquatic systems; however, their distribution and role remain poorly known, in part due to the lack of an efficient method to study them. We developed a new, simple and low cost, semi-quantitative spectrophotometric method for determination of CSP in aquatic systems. The method is analogous to that used to quantify polysaccharide-rich gel particles called transparent exopolymeric particles (TEP). CSP concentration is determined relative to bovine serum albumin (BSA) standard aggregates (in a manner similar to how TEP is quantified relative to xanthan gum). The method is based on the linear relationship between CSP concentration and the absorbance of the eluted dye from a CBB-protein complex, which has an absorbance maximum (λmax) at 615 nm. The limit of detection and the precision (%RSD) for the proposed method are 6 μg BSA equivalent and 11% respectively. The new spectrophotometric method was validated with the existing microscopic method. This new method to quantify CSP is simple, enables rapid measurements, and allows a more efficient comparison with TEP concentrations than the present microscopic method. The spectrophotometric analyses will further the investigation of the abundance, distribution and role of CSP in the biogeochemistry of the ocean.

1. Introduction

In 1963, Riley identified marine gel particles as a significant component of the organic carbon pool. More than 40 years later there is considerable evidence showing that dissolved organic carbon (DOC) can self-assemble and form porous, transparent, microgels that can reversibly exchange material with DOC and particulate organic carbon (POC) (e.g., Chin et al. 1998; Engel et al. 2004, Verdugo et al. 2004). This abiotic self-assembly of materials forms particles that can sink and eventually sequester organic carbon into the deep ocean; dissolution and remineralization of particulate organic matter (POM) have important implications for ocean productivity and carbon cycling. Marine gel particles, of which transparent stainable particles (TSP) are part, are a fundamental bridge in the DOM-POM continuum in the ocean; they are hydrogels formed by a three-dimensional network of organic compounds, inorganic cations, and water. TSP such as Transparent Exopolymeric Particles (TEP; Alldredge et al. 1993) and Coomassie Stainable Particles (CSP; Long and Azam 1996) are made of large organic polymers and are considered stable macrogels (Verdugo 2012). TEP are visualized by staining with Alcian Blue (Alldredge et al. 1993, Mopper et al. 1995; Zhou et al. 1998), a cationic copper phthalocyanine dye that reacts with the carboxyl (COO^-) and sulfate half ester (OSO_3^-) functional groups of acid mucopolysaccharides and glycosaminoglycans (Parker and Diboll 1966; Decho 1990). CSP are protein-containing particles that are stainable with Coomassie Brilliant Blue (CBB) (Long and Azam 1996); CBB is a disulfonated triphenylmethane dye that binds to proteins and longer peptides (Chial and Splittgerber 1993).

Since TEP were first described (Alldredge et al. 1993), numerous studies have shown their ubiquity and significance in biogeochemical cycling of carbon (e.g., Mari 1999; Engel and Passow 2001), food web structure (Mari et al. 2004; Grossart and Simon 2007), nutrients and

trace metal availability (Alvarado-Quiroz et al. 2006), their role in aggregation and POC flux (Beauvais et al. 2006; Kahl et al. 2008; Gärdes et al. 2011), and the impact that ocean acidification might have on them (Engel 2002; Mari 2008; Passow 2012). TEP have been analyzed by microscopic and spectrophotometric methods after staining with Alcian Blue dye. The microscopic method allows visual determination of the number and size of the gel particles (Alldredge et al. 1993), while the spectrophotometric method is semi-quantitative and measures absorbance of dye that can be acid-extracted from a stained particle; the amount of TEP that is bound to the dye is standardized using the polymer Xanthan gum (XG eq. L^{-1}) (Passow and Alldredge 1995). There is more known about TEP than other stainable particles, in part due to the availability of a spectrophotometric method to measure them efficiently.

CSP were first visualized by Long and Azam (1996) using the protein stain Coomassie brilliant blue in anionic form (pH 7.4). There is evidence that CSP are abundant in seawater (Long and Azam 1996; Kuznetsova et al. 2005), fresh water (Berman and Viner-Mozzini 2001), and phytoplankton cultures (Prieto et al. 2002; Galgani and Engel 2013); however, the composition, distribution and function of CSP are not well known. Currently, the only available method for CSP identification is the microscopic method developed by Long and Azam (1996).

Few studies have compared concentrations and distributions of TEP and CSP in parallel samples. Berman and Viner-Mozzini (2001) compared the concentration of TEP and CSP in fresh water using microscopy and image analysis, finding that TEP and CSP were ubiquitous all year in Lake Kinneret. Concentrations of both TEP and CSP are highest in the upper 30 to 100 m of the oceanic water column, decreasing with depth (Passow 2002; Long and Azam 1996), and show enrichment in the surface microlayer (Kuznetsova et al. 2005; Galgani and Engel 2013). Berman and Viner-Mozzini (2001) suggested that the relative abundances of TEP and CSP in

fresh water are dependent on the dominant phytoplankton species and the TSP turnover times. There is limited data on CSP abundance and dynamics in marine environments, and their formation mechanisms and role remain largely unknown. Microscopic measurements provide valuable information about particle size and shape; however, the fact that microscopy is the only available technique to analyze CSP is limiting the study of these particles, because microscopy is labor-intensive, time-consuming, and inefficient for large field surveys. Microscopic measurements may be difficult to compare if not measured by the same person. Typically the threshold for what is and what is not a particle needs to be visually defined by the researcher, for example when particles are quantified and sized directly by microscopy or if the software used needs visual adjustment of the threshold for identifying pixels that belong to a particle (e.g., WCIF Image J). Moreover, microscopic measurements do not allow us to determine the natural variations in chemical composition between discrete particles. Are TEP and CSP the same particle, or are they different? We can investigate this question by measuring the relative polysaccharide and protein composition using analyses such as described here.

In this paper, we propose a semi-quantitative spectrophotometric method, analogous to the TEP colorimetric method (Passow and Alldredge 1995), to measure CSP concentration relative to a standard. We also identify a useful standard that allows comparison between samples. The new method is based on the linear relationship between CSP concentration and the absorbance of the eluted dye from the CBB-protein complex that is formed. It provides an effective way to determine TEP and CSP concentration in parallel samples both in the field and in laboratory experiments. This will increase our understanding of abundances, distribution and role of CSP in aquatic systems, and will allow a direct comparison between TEP and CSP

dynamics, adding to our knowledge about the relationship between these gel particles and whether or not they are different chemical subunits of the same particle or are discrete particles.

2. Materials and procedures

2.1 Equipment and apparatus

A filtration unit that allows vacuum release and has a 25-mm filter holder with a PTFE-coated screen support (Sartorius Company, model 16315) was used for stained sample filtration; the filter support screen is an important detail; it should not be made of glass, because glass adsorbs the stain causing a variable error to the measurement.

A Shimadzu Spectrophotometer model UV-1800 UV-Vis was used in all spectrophotometric measurements. Nuclepore filters used for calibration were weighed using a Sartorius ME5 micro analytical balance equipped with an ionization system (HAUG Corp., Germany).

2.2 Reagents and solutions

All reagents were of analytical reagent grade or HPLC-UV grade, and all solutions were prepared with ultrapure water from a Millipore (Bedford, MA) Milli-Q UV Plus Ultra-Low Organic Water system.

A 1 mg ml^{-1} bovine serum albumin (Sigma, St. Louis, MO, USA) stock solution was prepared in ultrapure water. After homogenizing the BSA stock solution by stirring it for 30 minutes it was placed in a heating thermostatted bath at 85°C to form gel aggregate particles; then the mixture was immediately cooled in a water bath at 25 °C, and refrigerated overnight at 4°C. Next, the BSA sol-gel was sonicated for 30 seconds to break apart excessively large

aggregates. A set of five calibration standards of increasing concentration was prepared by diluting the BSA stock with ultrapure water.

The stock solution of Coomassie Brilliant Blue (CBB-G 250; Serva) was prepared according to Long and Azam (1996). One gram of CBB was dissolved in 100 ml of ultrapure water. A working solution was prepared fresh before each use from the 1% CBB stock solution; it was diluted with 0.2-μm filtered seawater in a ratio of 1:25 (vol:vol), giving a working preparation of 0.04% CBB at pH 7.4. The working solution was filtered through 0.2-μm disposable syringe filters before use to remove dye particles that might form spontaneously. The stain extraction solution was prepared by dissolving 30 g of sodium dodecyl sulfate (SDS; BIO-RAD 161-0302) into a mixture of 500 ml of isopropyl alcohol (PHARMCO-AAPER) and 500 ml of ultrapure water, giving an extraction solution of 3% SDS in 50% isopropyl alcohol.

2.3 Sample collection

Samples for this study came from a) *Thalassiosira weissflogii* batch cultures, b) a mesocosm experiment, and c) a station in the North Atlantic Ocean. Batch cultures of *T. weissflogii* were grown in f/2 medium (Guillard and Ryther 1962) in 3.5-L culture vessels. Temperature was maintained at 17 ºC, and light at 190 μmol photons m^{-2} s^{-2} with a light: dark cycle of 14:10. Samples for CSP determination were taken from the cultures during both exponential and stationary phases. A mesocosm experiment was conducted during August, 2011. Tanks (~1 m^3) were filled with coastal seawater from Stony Brook Harbor that had been filtered through a 200-μm size mesh to remove large detritus and zooplankton. A light source was suspended above each tank, providing a surface irradiance of 90 μmol photons m^{-2} s^{-2} with a light: dark cycle of 14:10. Irradiance was set at the beginning of each experiment with a LICOR Model LI-2100 light meter. Tanks were kept at 16°C by circulating cold water (4°C) through

silicone tubes installed inside the tanks. Nutrients were added, and the resulting phytoplankton bloom was monitored for 14 days. Samples were collected at various times throughout the bloom. Open ocean samples were taken on a cruise to the Bermuda Rise (33.68°N, 57.6°W). A vertical profile of the water column was sampled with a CTD/ Niskin-bottle rosette and water from each depth was transferred to a 10-L container for analysis. Subsamples were stained immediately with Alcian Blue for TEP determination and with Coomassie Brilliant Blue for CSP determination and stored frozen until analysis as described below. Concentrations of TEP were determined by the spectrophotometric method of Passow and Alldredge (1995). Microscopic examination of CSP was conducted following the method of Long and Azam (1996). In addition, CSP concentrations were determined by the spectrometric method we introduce here.

2.4 Reference microscopic method

CSP were visualized using the microscopic method of Long and Azam (1996), and surface area determined from the equivalent spherical diameter, using the method for image analysis of Engel (2009). CytoClear slides (Sterlitech Corporation) were prepared by filtering the sample (1 or 2 ml from the cultures and mesocosm, and 10 ml from open ocean seawater) at low, constant vacuum (<200 mmHg) onto 0.4-μm Nuclepore filters and staining them with 0.04% CBB-G 250 dye at pH 7.4 for 30 seconds. The filters were rinsed with Milli-Q water to remove the excess dye and placed on a CytoClear slide with a drop of 0.2-μm filtered immersion oil underneath and on top of the filter, then covered with a glass cover slide. Slides were examined and photographed with an inverted microscope (Olympus CK2) equipped with a digital camera (Moticam 2500) at 200x magnification. Thirty pictures were taken for each filter, fifteen along the vertical axis and fifteen along the horizontal axis. Particles were automatically counted and sized using MATLAB (Version 7.1, The MathWorks, USA). MATLAB code similar to Image J

was written specifically for particle quantification (see Appendix). The use of MATLAB code is an alternative to using Image J software, which is typically used to analyze TEP particles. Using the code has the advantage that is faster and can be automatized. The user can modify the threshold in the code for each set of pictures based on visual comparison with the original photo (similarly to image J), then the threshold can be fixed and particles automatically identified and sized. The results generated by the program are in pixels, but can be transformed to μm according to the magnification used, the size and resolution of the picture, etc. The minimum area for CSP determination was 0.2 μm^2; the parameters measured by the program were area of the particle (A_P), diameter, and the minimum and maximum axis. The equivalent spherical diameter (ESD) was calculated from the area of the particle using the equation:

$$ESD = \sqrt{\frac{A_P}{\pi}} \times 2$$

The total area of the total number (N) of CSP per liter was calculated according to Engel (2009):

$$Total\ area\ (L^{-1}) = \frac{A_F \times A_P}{b \times M \times V}$$

where A_F is the effective filter area (mm^2) stained with CBB solution, A_p is the area of gel particles sized in total, b is the number of frames analyzed, M is the area of one frame (mm^2), and V is the volume of sample filtered (L). The total number of particles per liter ($N\ L^{-1}$) is calculated by replacing A_p by the total number of particles counted in the equation above. For comparison of the spectrophotometric and the microscopic method, the total area of particles per liter is preferred in this study because is more representative of the amount of stainable material in the filter.

2.5 Spectrophotometric determination of TEP

For TEP determination the colorimetric method of Passow and Alldredge (1995) was used. Samples (50 ml from cultures and the mesocosm and 250 ml from open ocean seawater) were filtered at low, constant vacuum (<200 mm Hg) onto 0.4-μm Nuclepore filters; the filters were stained with 500 μl of 0.02% Alcian Blue working solution (pH of ~ 2.5) for 5 seconds. The Alcian Blue working solution is prepared by diluting a stock solution (1% Alcian Blue and 3% acetic acid) by 50 times with ultrapure water, adjusting the pH to 2.5 if it is necessary, and pre-filtering with a 0.2-μm filter before each use. After staining, while filters were still in the filtration system, they were rinsed with 1 ml of Milli-Q water 3 times to remove excess dye; rinsing does not wash off TSP. Filters were stored frozen until analysis (no more than 2 months after collection). Filters were transferred to 15-ml polypropylene tubes. An aliquot of 6 ml 80% sulfuric acid was added and the filters were incubated for 2 h. The tubes were gently agitated two or three times during this period. After incubation, absorbance of the Alcian Blue in solution was measured spectrophotometrically at 787 nm in a 1-cm cell. Samples were prepared in duplicate, and blanks were prepared from Milli-Q water or 0.2-μm filtered seawater for each set of samples.

The concentration of TEP is referred to the standard xanthan gum and it is expressed in micrograms of xanthan gum equivalents per liter (μg XG eq.L^{-1}) as calculated by the equation:

$$TEP\ (\mu g\ XGeq.L^{-1}) = \frac{(A_{787} - C_{787})}{V_F} \times F_{(X)}$$

where A_{787} is the absorbance of the sample, C_{787} is the absorbance of the blank at 787 nm, V_F is the filtered volume in liters, and $F_{(x)}$ is the calibration factor in μg. The calibration factor is

calculated by relating the dry weight of the standard polysaccharide xanthan gum retained in the filter to its staining capability, *i.e.,* it is the slope of the regression of weight in micrograms versus absorbance. Values for $F_{(x)}$ typically range from 50 to 300 μg (Engel 2009)

2.6 Spectrophotometric determination of CSP

This method is analogous to the colorimetric method for TEP determination in many ways. For spectrophotometric determination of CSP, variable volumes of sample are filtered depending of the gel particle concentration. In general about 50-300 ml of seawater or 5-20 ml of culture are filtered onto 25-mm 0.2 or 0.4-μm pore size polycarbonate filters (e.g., Nuclepore, Whatman) at low, constant vacuum (< 200 mm Hg). The vacuum is released and the filter, still in the holder, is stained with 1 ml of 0.04 % Coomassie Brilliant Blue (CBB-G 250) dye at pH 7.4 for 30-60 seconds. After staining, the vacuum is resumed and the filter rinsed with 1 ml ultrapure water at least three times to remove the excess dye; rinsing does not wash CSP off the filter. For best reproducibility, all the samples should to be rinsed the same number of times. Then the filter is transferred to a 15-ml polypropylene tube (BD Falcon) (filters can be stored frozen at this point as in the TEP colorimetric method). To elute the dye, 4 ml of extraction solution (3% SDS in 50% isopropyl alcohol; Ball 1986) are added to the tube containing the stained filter, and the tube sonicated in a water bath (50-60 kHz) for 2 hours at 37 °C. In this manner the dye that is bound to protein is extracted from the filter into the extraction solution. The absorption maximum of the eluted dye is 615 nm (Fig. 2-1); the absorbance is determined spectrophotometrically in a 1-cm cell against ultrapure water. For each set of samples, blanks are prepared from seawater pre-filtered twice though 0.2-μm pore size filters and from ultrapure Milli-Q water. There was no significant difference between the absorbance of the seawater and freshwater blanks (absorbance values for the blanks were between 0.032-0.058 for the

experiments reported here). However, to decrease the absorbance and variability of the blanks, they were rinsed with 5 to 10 ml of Milli-Q water after staining. Volume of rinsing did not affect the absorbance of the samples, after a minimum of 3 ml rinse was used.

2.7 Sample preservation and storage

After the samples are stained, they can be frozen until analysis. For microscopic analysis of CSP, using the same dye as the proposed method, samples slides can be frozen for 2 to 3 months before analysis (Engel 2009). We compared samples that were stained and immediately analyzed, with samples than were stained, frozen and then analyzed two days later; there were no significant differences between absorbances of the fresh and frozen samples.

Samples do, however, need to be filtered and stained immediately after collection. We compared Bermuda Rise samples that were stained immediately after collection and samples that were preserved with 1% formaldehyde and stored for two weeks before staining and analysis as described above; the absorbance in formaldehyde-preserved samples was different than in freshly stained samples. These differences in absorbance were not consistent; sometimes the absorbance in preserved samples was larger and other times smaller than in the unpreserved samples. The formaldehyde may disrupt cells creating more Coomassie stainable material (in which case the amount of CSP would be overestimated), or may break up CSP and make them smaller and unable to be retained on the filter (the amount of CSP would be underestimated).

3. Assessment

3.1 Standard selection and optimization

We evaluated several proteins for their usefulness as a standard to calibrate the staining capacity of Coomassie Brilliant Blue dye. Such a standard needs to be soluble in water but also

able to form small gel-like particles, similar in shape and size to CSP. The gel particles formed have to be large enough to be retained on a 0.4-μm polycarbonate filter, abundant enough to allow dry weight determination, and have a high enough staining capacity to be detected. We tested bovine serum albumin, bovine gamma globulin, casein and RuBisCO as potential standards (Table 2-1); results from comparisons of these compounds are provided in Appendix (Table 2-4 (A1)).

Bovine serum albumin (BSA) was chosen because it forms gel-like particles by thermal aggregation that have a size distribution similar to that of CSP. BSA gel-like particles are retained on a 0.4 μm filter and can be used as standard to generate a calibration curve that linearly relates mass of particles retained on the filter and absorbance of CBB eluted from the particles after staining. BSA forms fractal aggregates when heated in solution (Hagiwara et al. 1998), and its thermal aggregation capability is frequently used in the food industry (Totosaus et al. 2002). The mechanism of thermal aggregation of protein molecules is denaturation followed by adhesion due to hydrophobic interactions and disulphide bond formation (Clark and Lee-Tuffnell 1986). An aggregate's fractal dimension is related to the number of particles that form an aggregate. Fractal dimensions for BSA aggregates heated at 95º C for 90 min have been determined previously by light scattering, and were 1.5 and 2.1 at pH 5 and 7, respectively (Hagiwara et al. 1996). Logan and Wilkinson (1990) calculated the three-dimensional fractal dimension for general marine snow, 1.39±0.06, for marine snow formed predominantly of diatoms, 1.52±0.19, and for microbial aggregates of *Zoogloea ramigera,* 1.8 ±0.19 (Logan and Wilkinson 1990). Therefore structural properties of aggregates formed by thermal aggregation of BSA are comparable to those of natural particles in the ocean. Optimal BSA concentration, temperature of aggregation, and length of heating were determined as described in Table 2- 2.

Briefly, the BSA stock we used to form adequate gel particles for the calibration standards had a concentration of 1 mg ml^{-1}, was heated for 2 hours at 85ºC, placed in the refrigerator overnight, and sonicated for 30 s. The optimal conditions for BSA preparation were determined by examining microscopically the aggregates formed, and assessing the linearity of the calibration curve. Results for all the comparisons are given in Appendix (Table 2-5(A2) and 2-6 (A3)).

We prepared the BSA standard in Milli-Q water rather than seawater for the calibration of staining capability of CBB dye; the xanthan gum standard used to calibrate Alcian Blue for the colorimetric determination of TEP is also prepared in pure water. BSA aggregation is affected by the ionic strength of the water used (Bagger et al. 2007).

We observed that at the low concentrations of BSA required for the CSP calibration, BSA aggregate particles formed in seawater were too small to be retained on the filter (i.e., <0.4 μm). Thus there was not a linear relationship between the filtered volume of BSA standard and the absorbance. However, the linearity of the relationship between absorbance and amount of CSP material in seawater was confirmed by measuring CSP in increasing volumes of *T. weissflogii* culture and by measuring increasing volumes of natural seawater sample (Appendix, Table 2-7 (A4)).

3.2 Preparation, optimization, and calibration of CBB G-250 staining solution

Coomassie Brilliant Blue (CBB) exists in three ionic forms: cationic (red), neutral (green), and anionic (blue) (Bradford 1976; Compton and Jones 1985). The anionic and the neutral species bind to proteins (Georgiou et al. 2008), shifting the absorption peaks from 590 nm to 615 nm and from 650 nm to 615 nm, respectively. At pH > 1.3 the blue anionic species is present. CBB is frequently used in molecular biology and biochemistry to stain proteins at low

pH due to the high color intensity and good linear relationship between absorbance and protein concentration.

CSP were first stained by Long and Azam (1996) using a CBB solution at pH 7.4; this pH was chosen to prevent lysis of organisms that can artificially create CSP; however lysis was not demonstrated nor tested. To determine the most appropriate staining solution, we tested three different preparations of Coomassie Brilliant Blue Serva G-250 with different compositions and pH values. Table 2-3 describes the concentration and pH of the tested staining solutions, as well as their linearity, sensitivity, stability and calibration; detailed results of testing dye solutions using a diatom culture or a BSA standard are provided in Appendix; Tables 2-7 (A4) and 2-8 (A5), respectively. The staining solution proposed by Long and Azam (1996) exhibited the best linear relation between concentration and absorbance for the BSA standard, and even though this staining solution was designed to be prepared daily, by diluting the stock solution with 0.2-μm pre-filtered seawater and pre-filtering before use, the calibration factor $F_{(x)}$ was fairly constant in calibration curves prepared on different days using the same stock solution and the same 0.2-μm pre-filtered seawater. The best contrast between the chemical blank and the samples and BSA standard was obtained by staining samples with 1 ml of 0.04% CBB solution for 30 s or 1 min (Fig. 2-2); 30 s was chosen for the work shown here.

To calibrate Coomassie Brilliant Blue dye, a standard stock solution of 1 mg ml^{-1} BSA in ultrapure Milli-Q water was prepared. The stock solution was stirred for 30 min to dissolve it completely, and then placed in a water bath at 85°C for 2 h to generate aggregates. The mixture was refrigerated for ~12 hours, and then sonicated for 30 s to break up larger particles and generate a standard with particle size spectrum similar to that of CSP. Size frequency distribution was calculated according to Engel (2009). BSA aggregates were compared with CSP from

mesocosm experiments, from a *T. weissflogii* culture, and from natural seawater from the Bermuda Rise (Fig. 2-3). The stock solution was diluted with ultrapure water to obtain five calibration standards of increasing concentration, 2, 4, 8, 20, 50 μg ml^{-1}. Seven replicates (4 ml) of each diluted BSA standard were filtered onto 0.4-μm polycarbonate filters (Nuclepore, Whatman), resulting in a target mass of BSA aggregates on the filters of 8, 16, 32, 80 and 200 μg, respectively. The retention of BSA aggregates on the filters was not 100%, and decreased with increasing standard concentration from 82 ±11% when a low concentration standard (2 $\mu g ml^{-1}$) was filtered to 18 ± 1% when a high concentration standard (50 $\mu g ml^{-1}$) was filtered (Appendix Table 2-9 (A6)). However, this is not a problem because the calibration curve used the actual measured mass retained on the filters, and the relation between actual mass on the filter that can be stained with CBB and the absorbance measured is linear. The mass is determined from 4 of the 7 replicates by pre-weighing the filters, filtering the standard, drying the filters overnight at 40°C and reweighing them. The 3 remaining replicates were stained with CBB and absorbance measured on the extracted stain as described above.

Three different preparations of the CBB-staining solution were calibrated against BSA standard aggregates to test the sensitivity and linearity of CBB absorption (Table 2-3). All staining solutions contained 0.04% CBB 250-G, but in different solvents. The CBB solution prepared according to Long and Azam 1996 was chosen. Ultrapure water blanks were treated in the same way as the BSA calibration standards. The absorbance of the blanks was between 0.032 and 0.058, while the absorbance of the standard ranged from 0.12 to 0.49. Once blanks were subtracted from sample absorbances, a comparison of net absorbance versus mass of stained gel particles resulted in a calibration curve that was linear between 0 and 36 μg of BSA (Fig. 2-4).

The slope of this curve with intercept zero represents the calibration factor, F(x). The calibration factor for Coomassie Brilliant Blue, using BSA as a standard, was between 102 and 156. This value is within the range reported for the calibration factor for TEP analysis (usually 50 - 300 μg; Engel 2009). The limit of detection and the precision, calculated as percentage standard deviation (%RSD), of this method are 6 μg BSA equivalents and 11% respectively.

The content of CSP relative to BSA concentration is reported in units of μg BSA equivalents per unit volume, using the following equation:

$$CSP\ (\mu g\ BSA\ eq.L^{-1}) = \frac{(A_{615-}C_{615})}{V_F} \times F_{(X)}$$

where A_{615} is the absorbance of the sample and C_{615} is the absorbance of the blank at 615 nm, V_F is the filtered volume in liters, and $F_{(x)}$ is the calibration factor in μg. The calibration factor is calculated by relating the dry weight of the standard BSA retained on the filter to the CBB absorbance. The slope of the regression of weight in micrograms (W) versus absorbance (ABS) is the calibration factor $F_{(x)}$.

4. Discussion

4.1 Comparison of microscopic and spectrophotometric methods

Currently the reference microscopic method of Long and Azam (1996), as described above, allows an indirect estimate of the equivalent spherical diameter of CSP; this is calculated from the area of the particle measured from images captured under a light microscope. For comparison and validation of the spectroscopic method introduced here, the amount of CSP was determined by both the reference microscopic method and the spectrophotometric method in parallel samples.

Using different aqueous concentrations of BSA standard aggregates, the total area of CSP ($\mu m^2 L^{-1}$), obtained directly from image analysis of pictures taken under the microscope (200x), was linearly well correlated ($r^2 = 0.95$) with the spectrophotometric measure of CSP (Fig. 2-5), suggesting that these two completely independent methods are measuring the same aggregate particles. We also compared the two CSP methods using samples from different stages of bloom development of a *T. weissflogii* culture grown in the lab (Fig. 2- 6A), and field samples collected from different depths in the oligotrophic Bermuda Rise area (Fig. 2-6B). The linear relationship between total area and μg of BSA equivalents was also found in the culture ($r^2 = 0.81$) and natural seawater ($r^2 = 0.88$) samples, although variability was higher than for the BSA standard aggregates. As in the TEP colorimetric method, it is important to filter a sample volume small enough to avoid clogging the filter, which causes the relation between absorbance and the amount of stainable material in the filter to be non-linear. The concentration of CSP in the culture was about two orders of magnitude higher than concentrations found at the Bermuda Rise site, but the relation between the two methods was still robust. The Bermuda site in the Sargasso Sea has low surface nutrients and low productivity, so that our preliminary analyses suggest a relationship between phytoplankton production and CSP concentration, as found with TEP (Fig. 2- 7). A vertical depth profile of CSP concentration shows the similarity between the relative distributions of CSP using the two methods, even though the methods are not directly comparable quantitatively (Fig. 2-7). Using both methods, CSP particles decreased with depth. Using the spectrophotometric method concentrations were between 23.5 μg BSA $eq.L^{-1}$ at 50 m to 11.3 μg BSA $eq.L^{-1}$ at 300 m; the microscopic method gave total areas of CSP particles as 9×10^7 $\mu m^2 L^{-1}$at 50 m and 2×10^7 $\mu m^2 L^{-1}$ at 300 m. Previously, Long and Azam 1996 reported total areas between 2×10^8 $\mu m^2 L^{-1}$ and 1.4×10^{10} $\mu m^2 L^{-1}$ for larger particles in coastal waters off

Scripps Pier. The values of total areas reported here are one order of magnitude smaller, which is not surprising given the oligotrophic origin of our samples. The spectroscopic method also appears to be more sensitive than the microscopic method; in some samples with lower concentrations, the microscopic images did not have enough contrast to be quantified and sized by the software, whereas the spectrophotometric method easily measured the amount of CSP.

4.2 Vertical distribution of TEP and CSP

We measured the vertical distribution of TEP and CSP at a North Atlantic Bermuda Rise station (Fig. 2- 8) by staining parallel samples with Alcian Blue and Coomassie Brilliant Blue respectively, during three research cruises in February, May and November, 2012. Even though TEP concentration is reported as μg xanthan gum equivalents per liter (μg XG eq L^{-1}), and CSP concentration is reported as μg bovine serum albumin equivalents per liter (μg BSA eqL^{-1}), we can compare their relative vertical distribution.

TEP concentration at the Bermuda Rise ranged from 23.3±3.1 to 53.4±2.0 μg XG eq L^{-1}, and in general decreased gradually with depth. TEP were more abundant during February and showed more variability with depth then compared to May and November. CSP concentration ranged from 2.1± 1.5 to 23.5±4.2 μg BSA eqL^{-1}. CSP values in deep waters were always very low; sometimes the reagent blank, prepared with water from the same station but a different depth, was higher than the sample value leading to a negative result; thus, for the spectrophotometric determination of CSP in Bermuda Rise samples, we used the lowest absorbance in the water column as a blank, so that the perceived larger range in concentration compared to TEP is not necessarily true. The method was sensitive enough to distinguish higher concentration of CSP in the upper 200 m relative to the rest of the water column in February and May (Fig. 8). The highest concentrations of CSP were detected in February as was the case with

TEP; however, in other ways, the CSP and TEP profiles are quite different, with the CSP max being somewhat below the TEP max. These differences in vertical distribution again suggest that the two particle types have different behavior. Proteins are a valuable carbon and nitrogen source for marine bacteria. Thus, CSP may be more labile than TEP, being colonized and consumed by bacteria faster, while TEP remain longer in the water column. TEP and CSP could both be produced at the same depth, but TEP may ascend to the surface (Azetsu-Scott and Passow 2004) due to the combination of its buoyancy, and a presumably high TEP to solid particle ratio found due to the low productivity at the Bermuda Rise site.

5. Comments and recommendations

There are several drawbacks to the CSP spectroscopic method introduced here that are similar to those of the TEP method. TEP and CSP are heteropolymeric particles of diverse origin and composition; their exact chemical composition is unknown and it possibly changes with the age of the particle. As a consequence, the amount of dye that binds to specific monomers within the gel particles will depend on their origin and composition. This particle heterogeneity limits the application of TEP and CSP staining techniques and thus gel particle measurements are semi-quantitative and relative to a standard.

One problem with the spectrophotometric determination of both TEP and CSP is that the methods do not differentiate between gel material attached to phytoplankton cells, and free TEP or CSP. Samples are not usually pre-filtered, so Coomassie Blue stainable material attached to a cell is also stained (in the same way that acidic polysaccharides on cells are stained by Alcian Blue in the spectrophotometric determination of TEP). One way to obtain free CSP concentrations is to normalize CSP to the cell number or Chl-*a* content. Present methods for TEP

and CSP determination do not allow distinction of the origin or age of the stained gel material, *i.e.,* between particles attached to the phytoplankton cell that is freshly exuded and gel particles that attach or reattach to phytoplankton cells due their stickiness. This latter idea has been proposed for TEP particles (e.g., Passow and Alldredge 1999), but whether CSP are as highly sticky as TEP remains unknown.

CBB stains all proteins and polypeptides. A specific limitation of quantifying CSP using CBB is that there is significant variation in protein-dye complex formation that depends on protein composition; the dye stains basic amino acids more efficiently than acidic amino acids (Ball 1986; Tanoue 1992). However, bovine serum albumin is intermediate in its efficiency to form a dye-protein complex (Chial and Splittgerber 1993), and has been widely used as a standard for protein determination using CBB. This specificity will only be a problem if the ratio between acidic and basic amino acids in aquatic proteins varies greatly with environment. Therefore, as in the colorimetric method for TEP determination, the amount of CSP in the method introduced here is referred to a standard. The fact that the standards for TEP and CSP are different does not allow an absolute quantitative comparison of these two types of particles. However, the proposed spectrophotometric method represents a practical and efficient tool to measure CSP in lab experiments and field samples and allows a comparison in relative terms of the concentration of TEP and CSP in parallel samples so that temporal and spatial variations can be compared. The use of the colorimetric method for CSP determination will allow routine measurement of CSP, facilitating the study of their composition in terms of nitrogen, carbon and amino acid content. The proposed spectrophotometric method uses the same dye as the microscopic method to stain CSP, so that the spectrophotometric method will probably work for fresh water samples in the same way that the microscopic method does. Moreover, the

calibration curve was generated from a BSA standard prepared in Milli-Q water, so the same process of standardization of the dye presented here should be suitable for freshwater samples.

The microscopic method for CSP determination allows the determination of the number and size of particles, but could underestimate the amount of CSP because it is a two-dimensional method, or could overestimate the area of the particles if they flatten during filtration. The spectrophotometric method stains all the material on the filters, is faster and allows the processing of more samples. The microscopic and the spectrophotometric methods are complementary, and the choice of method will depend on the focus of a particular study. For instance, if the goal is to determine changes in the size frequency distribution, the shape, or the extent of bacterial colonization of CSP, the microscopic method may be a better choice, but if the goal is to study how CSP is related to TEP, nutrients or other variables in different environments or at different times, the spectrophotometric method will allow more information to be gathered more efficiently. We expect that in the same way that the spectrophotometric method for TEP determination has been an essential tool to increase our understanding about the abundance, distribution and role of TEP in aquatic processes, the development of the CSP spectrophotometric method will facilitate the study and understanding of CSP in the ocean.

References

Alldredge, A.L., U. Passow, and B.E. Logan 1993. The abundance and significance of a class of large, transparent organic particles in the ocean. Deep-Sea Res. I 40: 1131-1140. [doi: 10.1016/0967-0637(93)90129-Q]

Alvarado Quiroz, N.G., C.-C. Hung, and P. H. Santschi. 2006. Binding of thorium (IV) to carboxylate, phosphate and sulfate functional groups from marine exopolymeric substances (EPS). Mar. Chem. 100**:** 337-353. [doi: 10.1016/j.marchem.2005.10.023]

Azetsu-Scott, K., and U. Passow. 2004. Ascending marine particles: significance of transparent exopolymer particles (TEP) in the upper ocean. Limnol. Oceanogr. 49: 741-748.

Ball, E.H., 1986. Quantitation of proteins by elution of Coomassie brilliant blue R from stained bands after sodium dodecyl sulfate-polyacrylamide gel electrophoresis. Anal. Biochem. 155: 23-27. [doi: 10.1016/0003-2697(86)90218-6]

Beauvais, S., M.L. Pedrotti, J. Egge, K. Iversen, and C. Marrasé. 2006. Effects of turbulence on TEP dynamics under contrasting nutrient conditions: implications for aggregation and sedimentation processes. Mar. Ecol. Prog. Ser. 323: 47-57. [doi: 10.3354/meps323047]

Bagger, H. L., L. H. Øgendal, and P. Westh. 2007. Solute effects on the irreversible aggregation of serum albumin. Biophys Chem 130**:** 9-9. [doi: 10.1016/j.bpc.2007.06.014]

Berman, T., and Y. Viner-Mozzini. 2001. Abundance and characteristics of polysaccharide and proteinaceous particles in Lake Kinneret. Aquat. Microb. Ecol., 24: 255-264. [doi: 10.3354/ame024255]

Bradford, M.M. 1976. A rapid and sensitive method for the quantitation of microgram quantities of protein utilizing the principle of protein-dye binding. Anal. Biochem.72: 248-254. [doi: 10.1016/0003-2697(76)90527-3]

Chial, H., and A. Splittgerber. 1993. A comparison of the binding of Coomassie brilliant blue to proteins at low and neutral pH. Anal. Biochem. 213: 362-9. [doi: 10.1006/abio.1993.1433]

Chin, W.-C., M.V. Orellana, and P. Verdugo. 1998. Spontaneous assembly of marine dissolved organic matter into polymer gels. Nature, 391: 568-572. [doi: 10.1038/35345]

Clark, A. H., and C. D. Lee-Tuffnell. 1986. Gelation of globular proteins, p. 203–272. *In* J. R. Mitchell and D. A. Ledward [eds.], Functional properties of food macromolecules. Elsevier Applied Science.

Compton, S. J., and C. G. Jones. 1985. Mechanism of dye response and interference in the Bradford protein assay. Anal. Biochem. 151**:** 369-374. [doi: 10.1016/0003-2697(85)90190-3]

Decho, A. W. 1990. Microbial exopolymer secretions in ocean environments: Their role(s) in food web and marine processes. Ocean. Mar. Biol. 28: 73–153.

Engel, A., and U. Passow. 2001. Carbon and nitrogen content of transparent exopolymer particles (TEP) in relation to their Alcian Blue adsorption. Mar. Ecol. Prog. Ser. 219: 1-10. [doi: 10.3354/meps219001]

Engel, A. 2002. Direct relationship between CO_2 uptake and transparent exopolymer particles production in natural phytoplankton. J. Plankton Res. 24: 49-53. [doi: 10.1093/plankt/24.1.49]

Engel, A., S. Thoms, U. Riebesell, E. Rochelle-Newall, and I. Zondervan. 2004. Polysaccharide aggregation as a potential sink of marine dissolved organic carbon. Nature 428: 929-932. [doi:10.1038/nature02453]

Engel, A. 2009. Determination of marine gel particles. practical guidelines for the analysis of seawater. CRC Press. [doi:10.1201/9781420073072.ch7]

Galgani, L., and A. Engel. 2013. Accumulation of gel particles in the sea-surface microlayer during an experimental study with the diatom *Thalassiosira weissflogii*. Int. J. Geosci. 4**:** 129-145.[doi: 10.4236/ijg.2013.41013.

Gärdes, A., M. H. Iversen, H.-P. Grossart, U. Passow, and M. S. Ullrich. 2011. Diatom-associated bacteria are required for aggregation of *Thalassiosira weissflogii*. The ISME Journal 5**:** 436-445. [doi: 10.1038/ismej.2010.145]

Georgiou, C. D., K. Grintzalis, G. Zervoudakis, and I. Papapostolou. 2008 Mechanism of Coomassie brilliant blue G-250 binding to proteins: a hydrophobic assay for nanogram quantities of proteins. Anal. Bioanal. Chem. 391**:** 391-403. [doi: 10.1007/s00216-008-1996-x]

Grossart, H.-P., and M. Simon. 2007. Interactions of planktonic algae and bacteria: effects on algal growth and organic matter dynamics. Aquat. Microb. Ecol. 47**:** 163-176. [doi: 10.3354/ame047163]

Guillard, R. R. L., and J. H. Ryther. 1962. Studies of marine planktonic diatoms. I. *Cyclotella nana* Hustedt, and *Detonula confervaceae* (Cleve) Gran. Can. J. Microbiol. 8: 229–239. [doi: 10.1139/m62-029]

Hagiwara, T., H. Kumagai, and K. Nakamura. 1996. Fractal analysis of aggregates formed by heating dilute BSA solutions using light scattering methods. Biosci Biotechnol Biochem 60**:** 1757-1763.

Hagiwara, T., H. Kumagai, and K. Nakamura. 1998. Fractal analysis of aggregates in heat-induced BSA gels. Food Hydrocoll. 12: 29-36. [doi: 10.1016/S0268-005X(98)00043-5]

Kahl, L., A. Vardi, and O. Schofield. 2008. Effects of phytoplankton physiology on export flux. Mar. Ecol. Prog. Ser. 354**:** 3-19. [doi: 10.3354/meps07333]

Kuznetsova, M., C. Lee, and J. Aller. 2005. Characterization of the proteinaceous matter in marine aerosols. Mar. Chem. 96: 359-377. [doi: 10.1016/j.marchem.2005.03.007]

Logan, B. E., and D. B. Wilkinson. 1990. Fractal geometry of marine snow and other biological aggregates. Limnol. Oceanogr. 35**:** 130-136. [doi: 10.2307/2837345]

Long, R.A., and F. Azam. 1996. Abundant protein-containing particles in the sea. Aquat. Microbial. Ecol. 10: 213-221. [doi: 10.3354/ame010213]

Mari, X., 1999. Carbon content and C:N ratio of transparent exopolymeric particles (TEP) produced by bubbling exudates of diatoms. Mar. Ecol. Progr. Ser. 183: 59-71. [doi: 10.3354/meps183059]

Mari, X., and F. Rassoulzadegan. 2004. Role of TEP in the microbial food web structure. I. Grazing behavior of a bacterivorous pelagic ciliate. Mar. Ecol. Progr. Ser. 279: 13-22.

Mari, X. 2008. Does ocean acidification induce an upward flux of marine aggregates? Biogeosciences 5: 1023-1031. [doi: 10.5194/bg-5-1023-2008]

Mayer, L. M., L. L. Schick, and F. W. Stetchell. 1986. Measurement of protein in nearshore marine sediments. Mar. Ecol. Progr. Ser. 30: 159-165.

Mopper, K., J. Zhou, K. Sri Ramana, U. Passow, H. G. Dam, and D. T. Drapeau. 1995. The role of surface-active carbohydrates in the flocculation of a diatom bloom in a mesocosm. Deep-Sea Res. II 42**:** 47-73. [doi: 10.1016/0967-0645(95)00004-A]

Parker, B. C., and A. G. Diboll. 1966. Alcian stains for histochemical localization of acid and sulfated polysaccharides in algae. Phycologia 6: 37-46.

Passow, U., and A. L. Alldredge. 1995. A dye-binding assay for the spectrophotometric measurement of transparent exopolymer particles (TEP). Limnol. Oceanogr. 40: 1326-1335. [doi: 10.4319/lo.1995.40.7.1326]

Passow, U., and A. L. Alldredge. 1999. Do transparent exopolymer particles (TEP) inhibit grazing by the euphausiid *Euphausia pacifica*? J. Plankton Res. 21**:** 2203-2217. [doi: 10.1093/plankt/21.11.2203]

Passow, U. 2002. Transparent exopolymer particles (TEP) in aquatic environments. Prog. Oceanogr. 55: 287-333.

Passow, U. 2012. The abiotic formation of TEP under different ocean acidification scenarios. Mar. Chem. 128–129**:** 72-80. [doi: 10.1016/j.marchem.2011.10.004]

Prieto, L., J. Ruiz, F. Echevarria, C.M. Garcia, A. Bartual. J.A. Galvez, A. Corzo, and D. Macas. 2002. Scales and processes in the aggregation of diatom blooms: high time resolution and wide size range records in a mesocosm study. Deep-Sea Res. I 49**:** 1233-1253. [doi: 10.1016/s0967-0637(02)00024-9]

Riley, G. 1963. Organic aggregates in sea water and the dynamics of their formation and utilization. Limnol. Oceanogr. 8: 372-381.

Tanoue, E. 1992. Occurrence and characterization of particulate proteins in the Pacific Ocean. Deep-Sea Res. 39: 743-761.[doi: 10.1016/0198-0149(92)90118-D]

Totosaus, A., J. G. Montejano, J. A. Salazar, and I. Guerrero. 2002. A review of physical and chemical protein-gel induction. Int. J. Food Sci. Tech.37: 589-601. [doi: 10.1046/j.1365-2621.2002.00623.x]

Verdugo, P., A. L. Alldredge, F. Azam, D. L. Kirchman, U. Passow, and P. H. Santschi. 2004. The oceanic gel phase: a bridge in the DOM–POM continuum. Mar. Chem. 92**:** 67-85, [doi:10.1016/ j.marchem.2004.06.017]

Verdugo, P. 2012. Marine microgels. Ann. Rev. Mar. Sci. 4: 9.1–9.25,[doi: 10.1146/annurev-marine-120709-142759]

Zhou, J., K. Mopper, and U. Passow. 1998. The role of surface-active carbohydrates in the formation of transparent exopolymer particles by bubble adsorption of seawater. Limnol. Oceanogr. 43**:** 1860-1871.

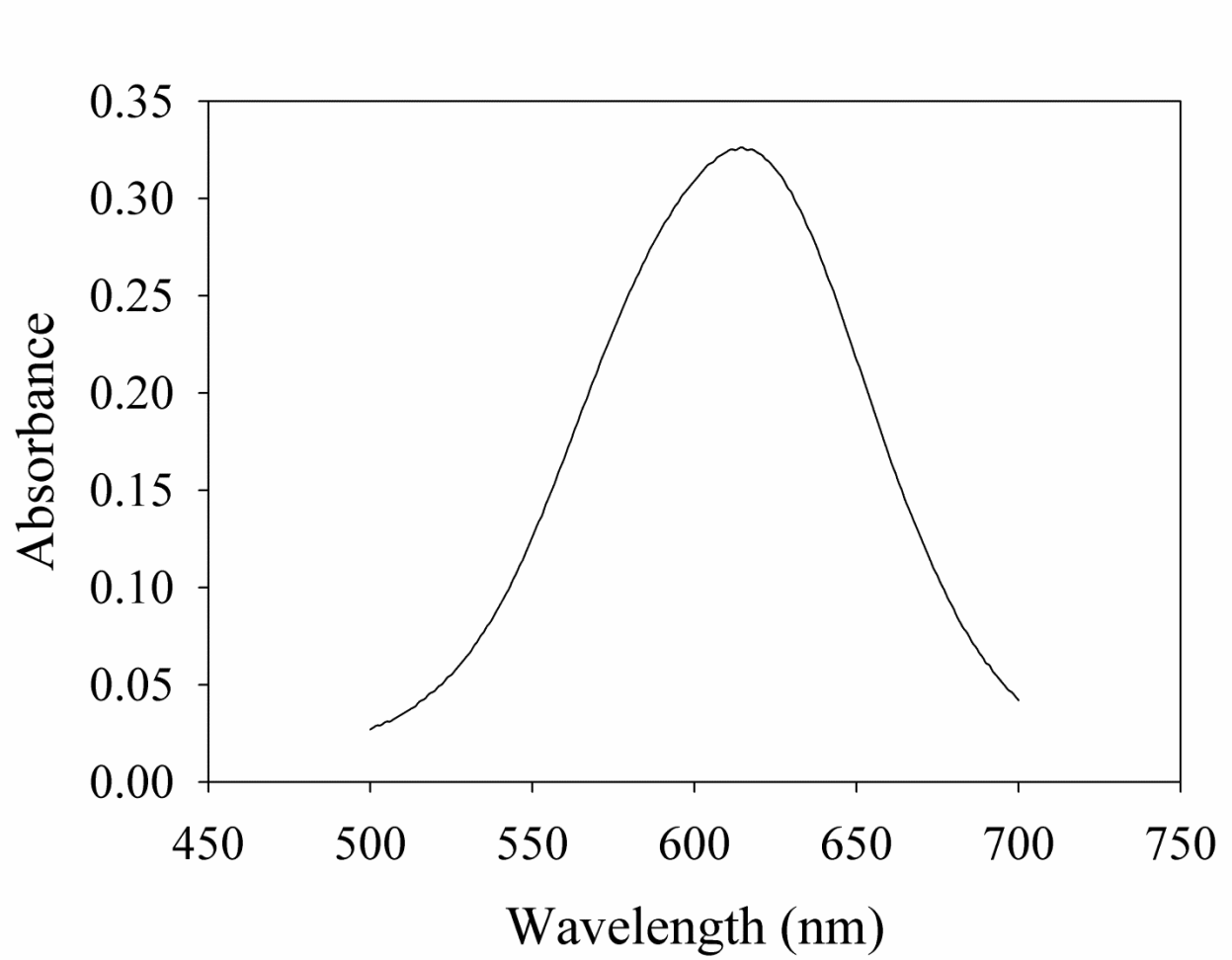

Figure 2-1. The continuous absorption spectrum of Coomassie Brilliant Blue in 3% SDS extraction solution. The absorption maximum lies at 615 nm.

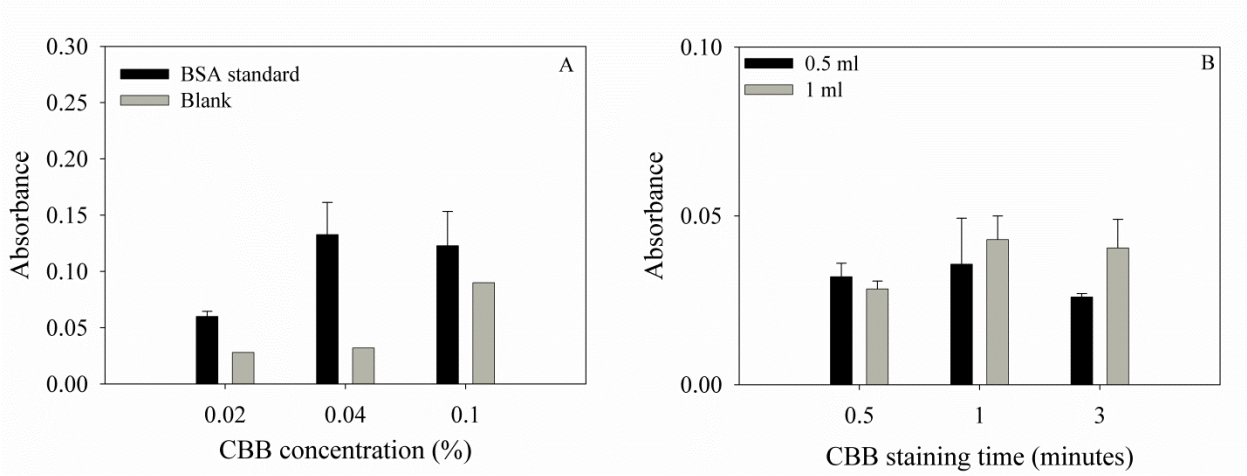

Figure 2-2 . Optimization of the staining procedure. (A) Absorbance of the working CBB staining solution as a function of concentration. Black columns correspond to BSA standard and gray columns to the blank; the error bars for the BSA standard values correspond to the range of the measurements (n = 4). A concentration of 0.04% showed the best contrast between the standard and the blank. (B) Absorbance of the working CBB staining solution as a function of staining time. The error bars correspond to the range of the measurements (n = 3 for 0.5 and 1 min, and n = 2 for 3 min). One milliliter of dye for only 30 s gave the least variability; staining the sample for less time is also preferable when multiple samples are being processed.

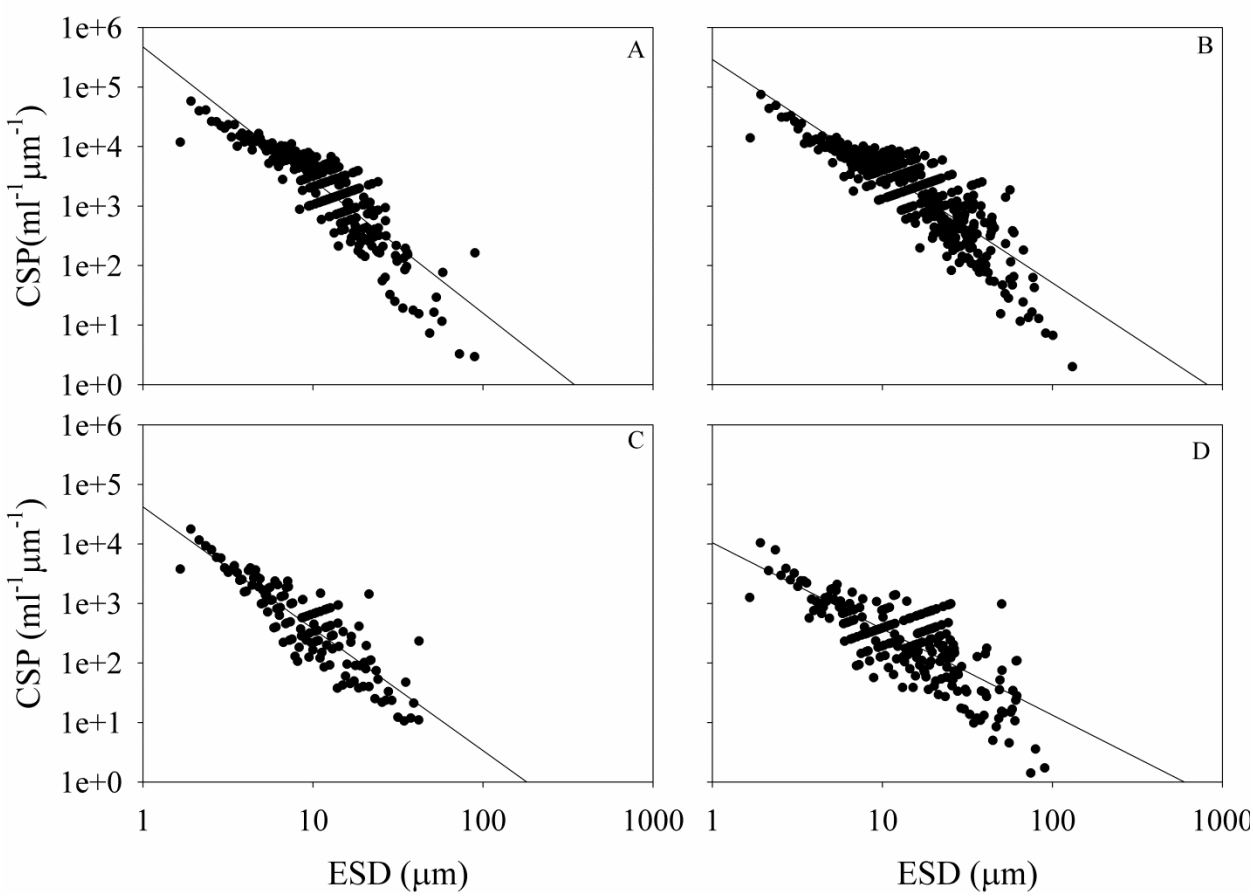

Figure 2-3. Size spectrum of CSP measured in (A) BSA standard (50 µg mL–1), (B) mesocosm experiment, (C) Thalassiosira weissflogii culture, and (D) natural seawater from the Bermuda Rise (100 m). The CSP were analyze by compound light microscope, using the image analysis software ImageJ. The CSP were produced from the BSA standard have a similar size distribution to that produced by diatoms inthe mesocosm experiment, in the cultures, and in open ocean samples. In all cases, the abundance of CSP decreased quickly with the increment in size.

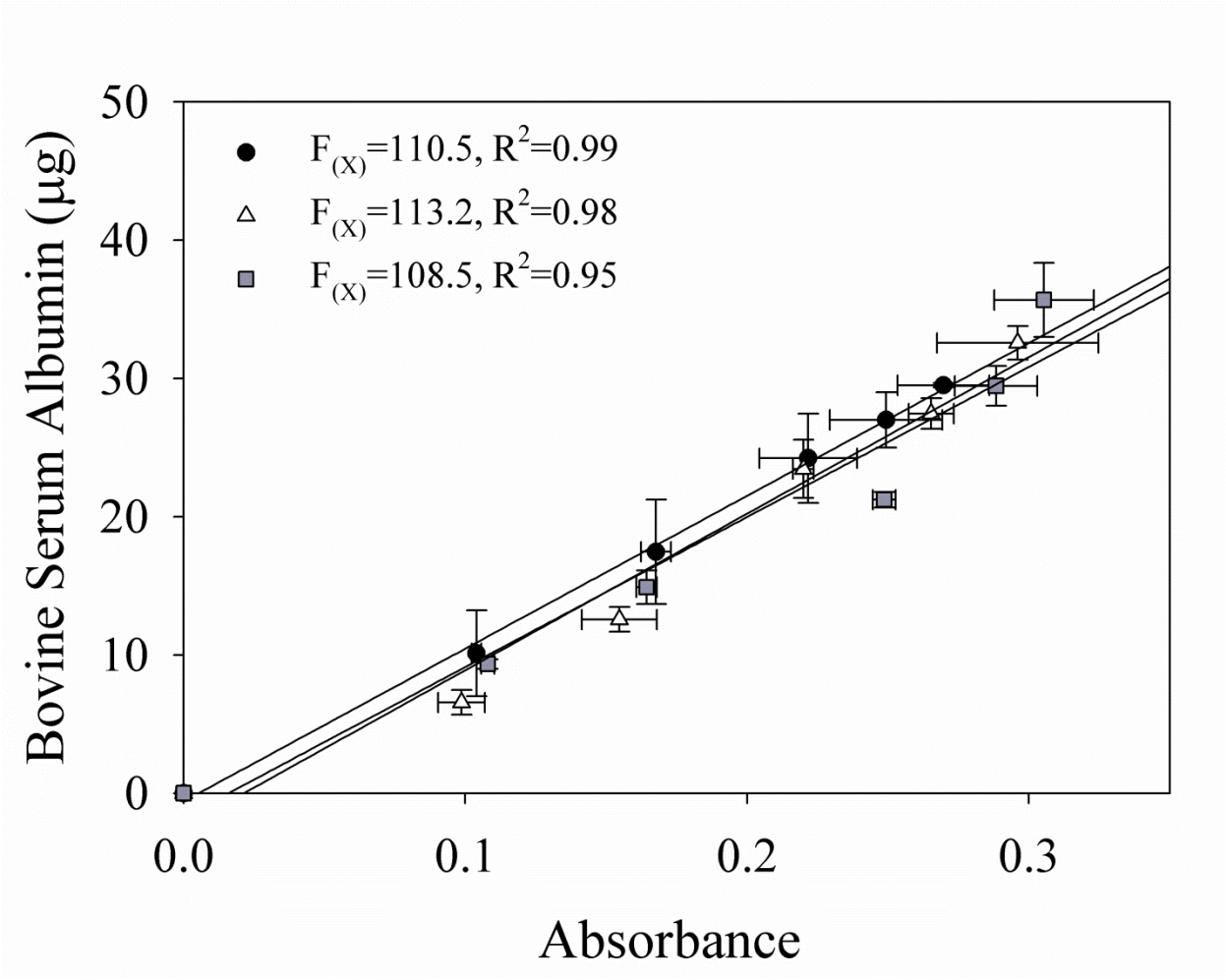

Figure 2-4. Calibration curve showing the coefficient of determination (R^2) between the means of absorbance (blank subtracted) and weight of the BSA standard. Three different curves were made using fresh standard and fresh dye each time. The slope of the regression gives the conversion factor F(x), used to calculate the µg BSA equivalent of CSP from the measured absorbance in a sample. The conversion factor varies slightly for different batches of CBB. The error bars correspond to the range of the measured values (n = 3).

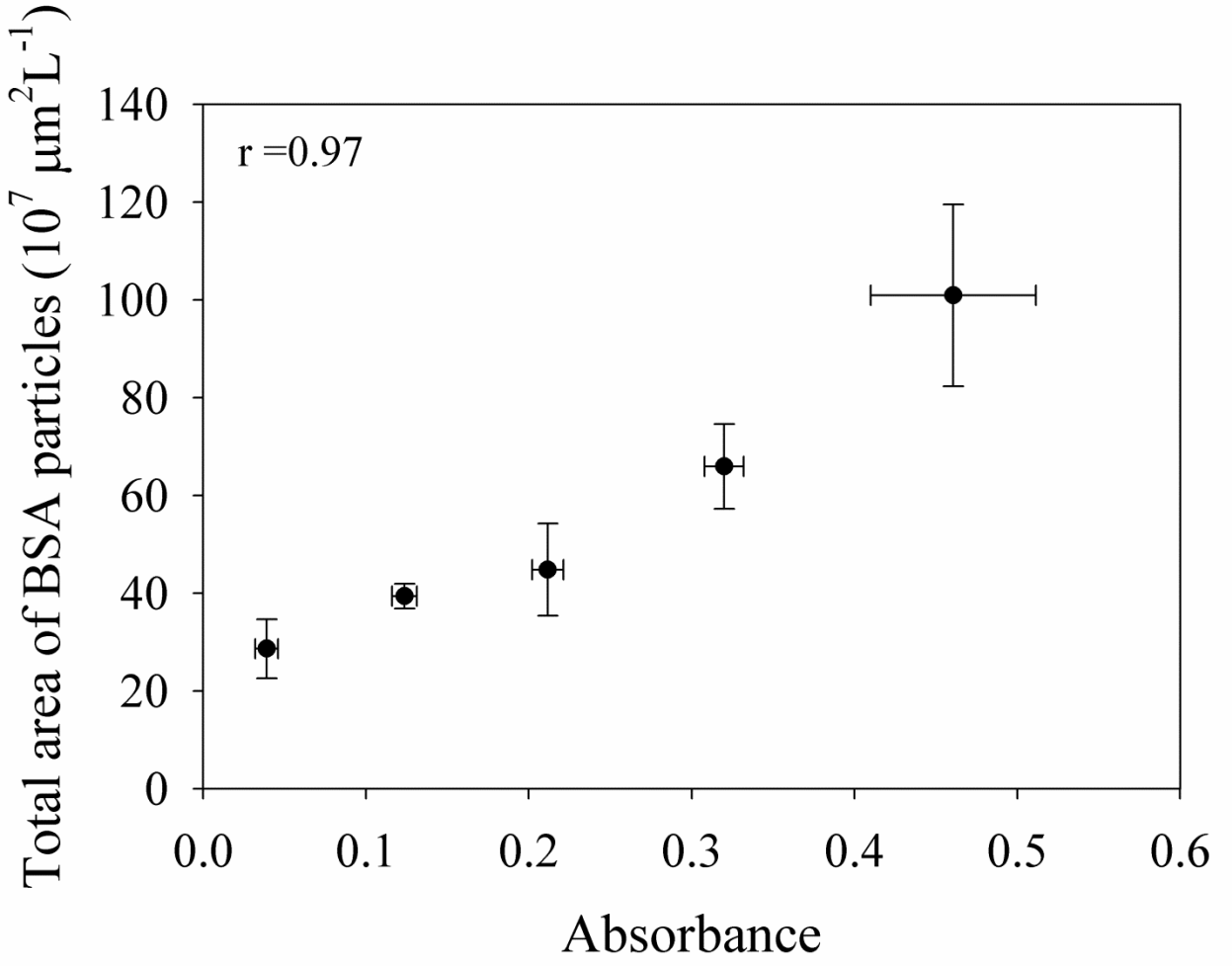

Figure 2-5. Correlation between total area of BSA aggregate particles (microscopic method) and the absorbance of the dye extracted from staining BSA particles (spectrophotometric method); the Pearson's product moment correlation (r) is 0.97. The error bars around the means correspond to the range of the measured values (n = 3).

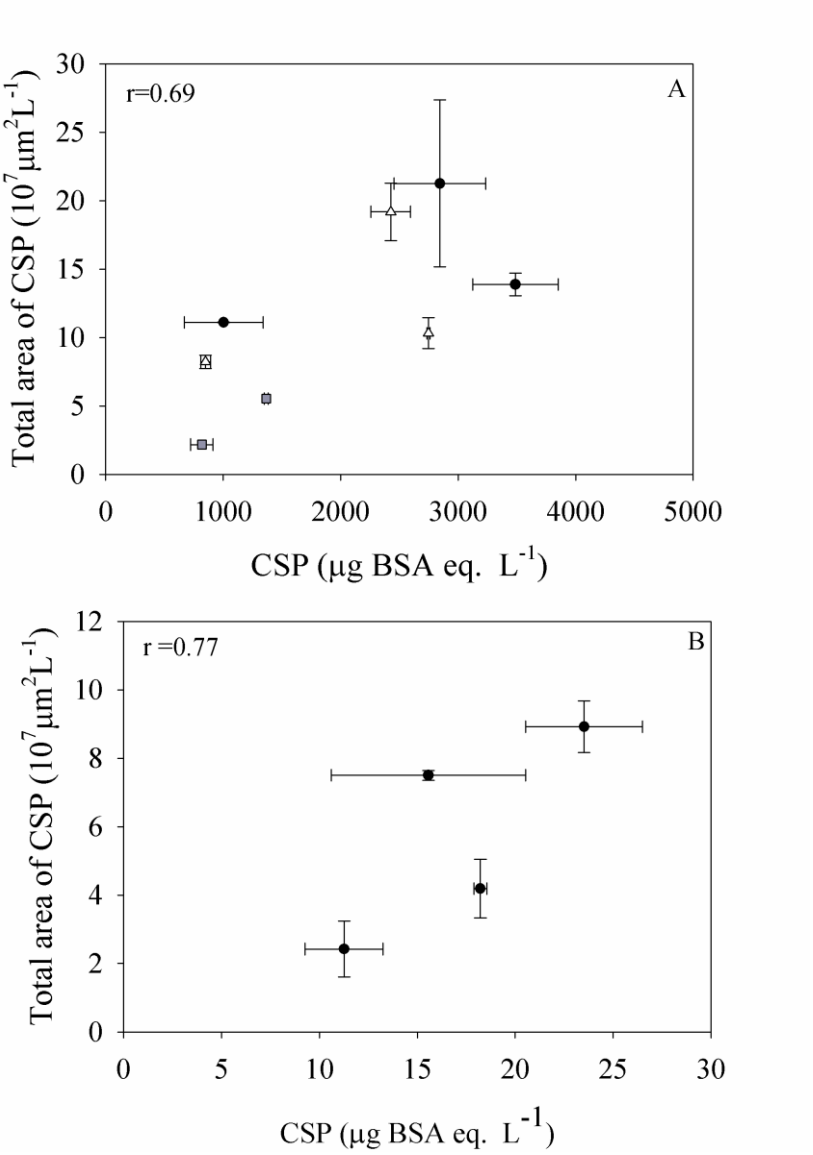

Figure 2-6. Comparison of CSP total area using the microscopic method with CSP concentrations in BSA equivalents using the spectrophotometric method. Measurements were made in (A) a growing culture of *T. weissflogii*, where 2 mL (black circles), 4 mL (white triangles), and 10 mL (gray squares) samples were taken at three different times during the growth phase; and (B) a natural seawater sample collected from the Bermuda Rise in February 2012. The Pearson's product-moment correlation (r) is shown in each figure. The error bars around the means correspond to the range of the measurement values (n = 2).

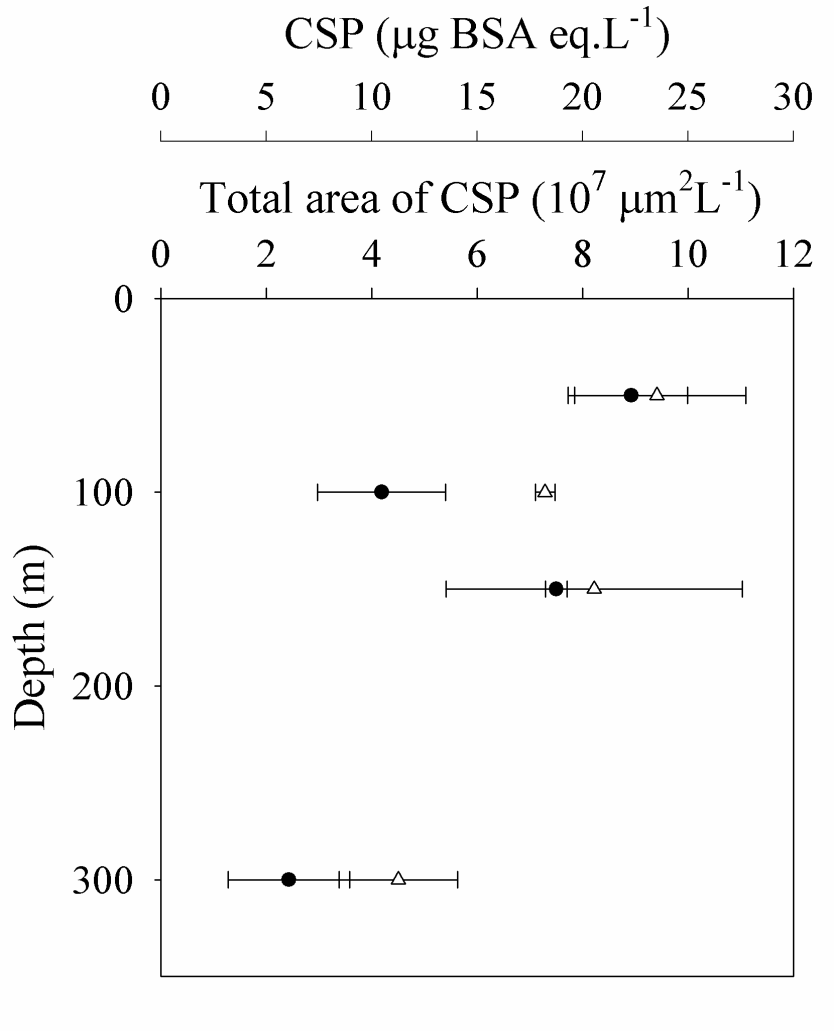

Figure 2-7. Depth profiles of total area of CSP (black circles), determined by the microscopic method, and concentration of CSP as μg BSA equivalents L^{-1} (open triangles), determined spectrophotometrically, in samples collected near the Bermuda Rise in February 2012. The error bars around the means correspond to the range of the measured (n = 2).

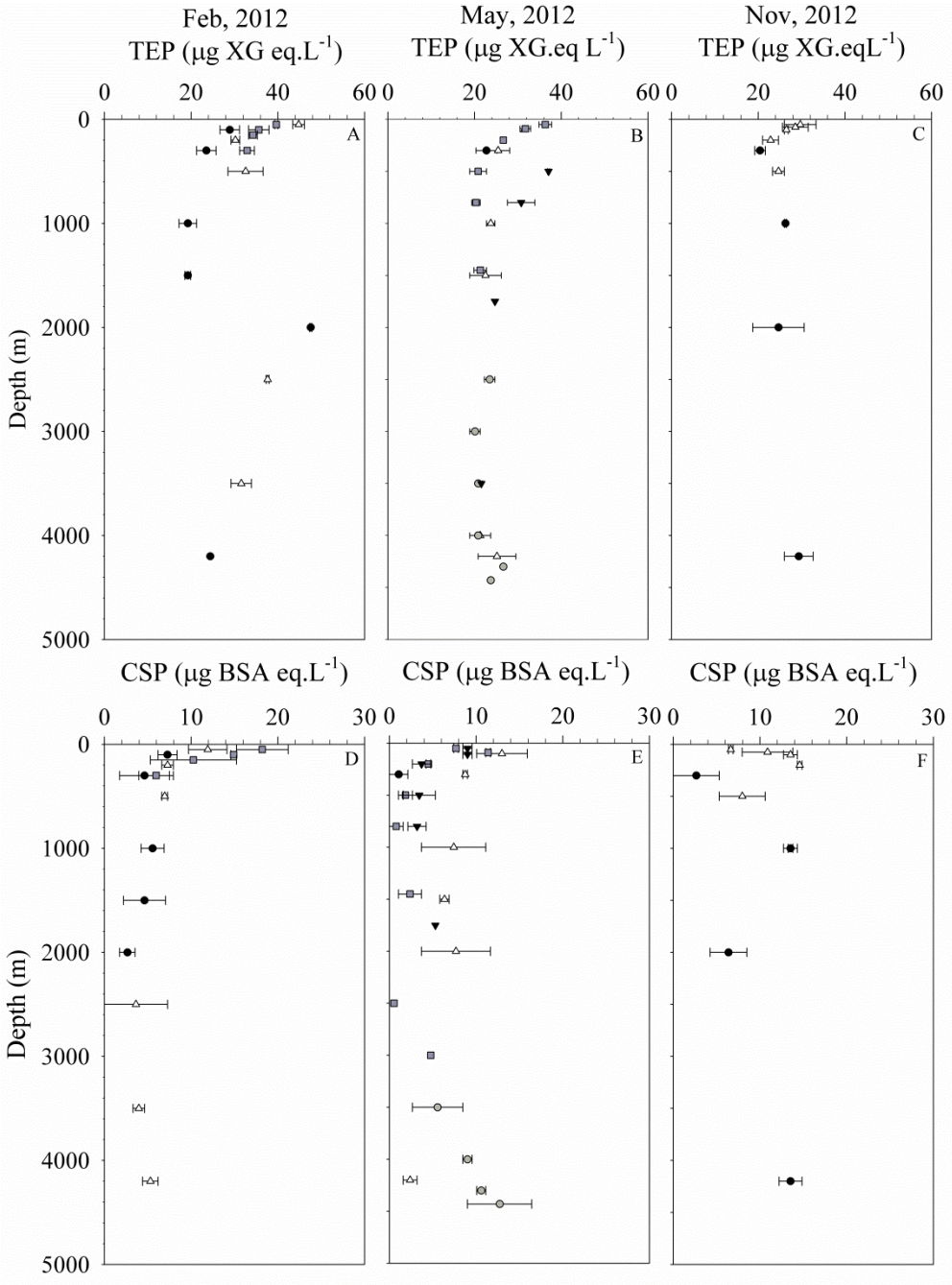

Figure 2-8. Depth profiles of total area of CSP (black circles), determined by the microscopic method, and concentration of CSP as µg BSA equivalents L–1 (open triangles), determined spectrophotometrically, in samples collected near the Bermuda Rise in February 2012. The error bars around the means correspond to the range of the measured (n = 2).

Table 2-1: Proteins tested as a potential standard for the CSP spectrophotometric method. Percentage of material retained on the filter (%), linearity of the calibration curve (LCC), calibration factor ($F_{(x)}$), maximum absorbance (ABS_{max}), minimum absorbance after blank subtraction (ABS_{max}-blk)

Potential Standard	%	LCC	$F_{(x)}$	ABS_{max}	ABS_{max}-blk
Bovine Serum Albumin (BSA)	18-82 %	(0 -35 μg) r^2= 0.94-0.97	102- 156	0.36	0.30
Bovine Gama Globulin (BGG)	10-20%	(0 to 20 μg) r^2= 0.97	213	0.164	0.099
Casein-NaOH	3-27%	(0 to 26 μg) r^2= 0.96	199	0.119	0.052
RUBISCO	10-20%	(0 to 26 μg) r^2= 0.96	785	0.55	0.015

Table 2-2: Parameters tested during optimization of the BSA standard calibration

Parameter	Conclusion	Comments
Physical properties and absorbance of various potential standards (Bovine Serum Albumin, Casein, Bovine Gamma Globulin, Rubisco).	Bovine Serum Albumin (BSA)	BSA was chosen as the standard because it forms fractal gel aggregates that are comparable with CSP in shape and size. Other substances did not form aggregates easily and the absorbance after staining was lower than that of BSA.
Temperature of thermal aggregation of BSA (60°C, 85°C, and 95°C)	85°C	BSA heated at 85°C for 2 h had higher absorbance after staining with CBB than when heated for longer periods.
Time of thermal aggregation of BSA (10 min, 30 min, 1 h, 2 h)	2 hour	
Process of making BSA aggregate particles comparable to CSP in size (sonicator vs. Tissue grinder)	Sonication or grinder	Sonication or grinding the heated BSA solution made particles comparable to CSP in samples. Tissue grinding made particles of more homogeneous size, while the replicability of sonicated samples was better.

Table 2-3: Coomassie Brilliant Blue staining solution tested for the colorimetric method for CSP determination.

Staining solution description	Composition	pH	Conclusion
CBB staining **solution 1:** modified from Mayer *et al.*, 1986	0.04% CBB 250-G, 10% ethanol, pH adjusted with phosphoric acid. Pre-filtered (0.2-μm) before use	2.1, 4.9, 7.4	High blank absorption. Low sensitivity
CBB staining **solution 2:** modified from Tanoue, 1992	0.04% CBB 250-G, 25% isopropanol, 10% glacial acetic acid	2	Linear relationship between the standard mass and the extracted dye (r^2 =0.93). Good sensitivity, but high blank adsorption. This problem can be overcome using an extra dye destaining step. Calibration factor between 192 and 292 μg
CBB staining **solution 3:** according to Long and Azam, 1996	Working solution is made daily diluting a stock solution 1% CBB to 0.04% CBB in 0.2-μm pre-filtered seawater	7.4	Linear relationship between the standard mass and the extracted dye (r^2 between0.90 and 0.94). Good sensitivity. There is no need for extra destaining step. Calibration factor is 123μg

Appendix:

Image processing MATLAB code:

1. Main function, CSPprosample.m:

Although the MATLAB code needed for each study will vary, we thought it useful to include that used in the study described here. Basically, it works similarly to Image J, identifying blue particles on the red channel, but the threshold is fixed once for the entire set of samples based on the difference in color intensity between pixels in the background and pixels that are particles. In this way the subjectivity of particle identification is lessened. This first code is for reading the image files from the working folder and calls subroutines (CSPpropic.m and CSPthresh.m, see below) to calculate the properties of the images analyzed, and then concatenates the image properties for the entire set of pictures in the sample. The results generated by the program can be transformed to μm according to the magnification used, the size and resolution of the picture, etc. This version of the code does not do that automatically, but the next version will do that.

```
function [area,diameter,mal,mil,nu]= CSPprosample
% last modification 08/16/2013
Foldername =pwd;
if ~isdir(Foldername)
  errorMessage = sprintf('Error:folder does not exist:\n%s', Foldername);
  uiwait(warndlg(errorMessage));
  return;
end
filelist = fullfile(Foldername, '*.tif');
% replace '*.tif' by '*.newformatextension' e.g '*.jpg'
Imfiles = dir(filelist);
Commname = Imfiles(1).name;
Entirename = fullfile(Foldername, Commname);
fprintf(1, 'reading %s\n', Entirename);
im=imread(Entirename);
[area,diameter,mal,mil,p]= CSPpropic(im(:,:,1));
if (p~=0)
    u=1;
end
for k = 2:length(Imfiles)
  Commname = Imfiles(k).name;
```

```
  Entirename = fullfile(Foldername, Commname);
  fprintf(1, 'Now reading %s\n', Entirename);
  im=imread(Entirename);
  [area2,diameter2,mal2,mil2,p]= CSPpropic(im(:,:,1));
   if (p==1)
      if (area~=NaN)
        area=cat(1,area,area2);
        diameter=cat(1,diameter,diameter2);
        mal=cat(1,mal,mal2);
        mil=cat(1,mil,mil2);

      else
        area=area2;
      end
      u=1;
    end
end
if (u==0)
    area=NaN;
end
```

2. Subroutine CSPpropic. m:

This subroutine calculates particle properties for each image analyzed.

```
function [areas,diameter,mal,mil,p]=CSPpropic(x)
% x is a unit8 var
x=double(x);
[a,b,c]=size(x);

p=1;
nu=1;
% background correction
[z,s]=meshgrid(1:a,1:b);
z=reshape(z,a*b,1);
s=reshape(s,a*b,1);
q=reshape(x,a*b,1);
fc=fit([z,s],q,'poly13');
f2=feval(fc,z,s);f2=reshape(f2,a,b);
f3=x-f2;
% enhancing contrast for peaks
c=log(1/1000)/(max(f3(:))-min(f3(:)));
k=power(1000,(max(f3(:))/(max(f3(:))-min(f3(:)))));
f4=k*exp((f3.*c));

% detecting threshhold
thr=CSPthresh(f4);
% generating binary image
f5=(f4>thr);
figure;image(f5,'CDataMapping','scaled')

% properties
```

```
[L,num]=bwlabeln(f5);
dat=regionprops(L,'all');
[gh,gj]=size(dat);
if (gh~=0)
 for i=1:gh
areas(i,1)=dat(i).Area;
diameter(i,1)=dat(i).EquivDiameter;
mal(i,1)=dat(i).MajorAxisLength;
mil(i,1)=dat(i).MinorAxisLength;
 end
else
areas=NaN;
diameter=NaN;
p=0;
end
```

3. Subroutine CSPthresh.m:

This subroutine calculates the threshold value to define the CSP boundaries.

```
function [bck]=CSPthresh(y)
% y is the red channel (double)after background correction and contrast
% enhancement.

[a,b]=size(y);
c=1;d=3;
for i=1:200:a-200
    for j=1:200:b-200
        t=y(i:i+200,j:j+200);
        u1(c)=mean(t(:));
        c=c+1;
    end
end
bck=d*mean(u1(:));
% d is an empirical correction factor related to differences
% in color intensity between particles and background.

% for-end loops where used instead of internal functions as nlfilter or
% colfilt for faster response.
```

Supplementary tables:

Table 2-4 (A1): Proteins tested as a possible standard for the colorimetric determination of CSP. Target mass on the filter, μg (TMF), actual mass on the filter, μg (AMF), percentage of material retained on the filter (%), absorbance of the material retained in the filter (ABS), absorbance of the material retained on the filter after blank subtraction (ABS-b), calibration curve values (CCV), squared correlation coefficient (R^2), calibration factor (F_x). BSA was chosen as the standard because the thermal aggregates formed by this substance are retained on the filter in an amount sufficient enough for the absorbance of the blank to be low compared with the

Protein	TMF	AMF	%	ABS	ABS-b	CCV	
						R^2	$F_{(x)}$
Bovine serum albumin (BSA)	0	0.0 ± 0.5		0.056 ± 0.003	0.000 ± 0.003	0.96	104
	8	6.8 ± 1.5	84.7	0.160 ± 0.002	0.104 ± 0.002		
	16	15.1 ± 1.2	94.4	0.223 ± 0.005	0.168 ± 0.005		
	32	23.6 ± 1.8	73.6	0.277 ± 0.016	0.222 ± 0.016		
	48	26.7 ± 1.3	55.6	0.305 ± 0.022	0.249 ± 0.022		
	72	30.1 ± 0.3	41.8	0.325 ± 0.015	0.270 ± 0.015		
Bovine gamma globulin (BGG)	0	0.0 ± 1.3		0.065 ± 0.005	0.000 ± 0.005	0.97	213
	20	11.1 ± 1.0	55.6	0.125 ± 0.004	0.060 ± 0.004		
	40	17.2 ± 1.2	43.1	0.144 ± 0.002	0.079 ± 0.002		
	60	19.4 ± 1.3	32.4	0.146 ± 0.005	0.082 ± 0.005		
	80	20.3 ± 1.1	25.4	0.164 ± 0.017	0.099 ± 0.017		
Casein-NaOH	0	0.0 ± 2.4		0.067	0.000	0.77	199
	20	0.3 ± 2.0	1.7	0.090	0.023		
	40	10.8 ± 10.8	26.9	0.100	0.033		
	60	11.9 ± 3.9	19.8	0.119	0.052		
	80	14.2 ± 2.0	17.8	0.146	0.079		
RuBisCO	0	0.0 ± 1.2		0.040	0.000	0.42	785
	20	4.0 ± 2.1	20.0	0.040	0.000		
	40	6.3 ± 0.6	15.8	0.045	0.005		
	60	11.3 ± 2.5	18.9	0.050	0.010		
	80	8.7 ± 1.2	10.8	0.055	0.015		

absorbance of the calibration standard. In addition, the concentration range over which the absorbance was linear, was larger than for any other tested substance.

Table 2-5 (A2): Results of different procedures used to prepare the bovine serum albumin (BSA) standard (1 mg ml^{-1}). Target mass of BSA on the filter, μg (TMF), actual mass of BSA on the filter, μg (AMF), percentage of material retained on the filter (%), linear regression (LR), target mass of BSA on the filter vs. actual mass of BSA retained on the filter), square correlation coefficient (R^2), slope (α). Heating the BSA solution forms gel-like aggregates; sonication or grinding made aggregates comparable in size to CSP observed in samples. Sonication of the heated BSA solution was preferred because it was easier to standardize the procedure.

Treatment	TMF	AMF	%	LR	
				R^2	α
1. BSA dissolved in	0	0		0.48	0.036
Milli-Q water (stirred	20	7.1	35%		
for 30 min)	40	10.7	27%		
	60	10.4	17%		
	100	10.7	11%		
2. BSA heated	0	0		0.63	0.139
(dissolved and placed	20	15.1	75%		
in a hot bath, 85ºC, for	40	21.1	53%		
2 hours)	60	28.4	47%		
	100	26.4	26%		
3. BSA heated and	0	0		0.79	0.173
sonicated (for 30 s)	20	18.1	90%		
	40	20.4	54%		
	60	24.4	41%		
	100	30.4	30%		

4. BSA heated and ground (4 times with a tissue grinder)	0	0		0.99	0.153
	20	17.1	85%		
	40	25.1	63%		
	60	30.4	51%		
	100	31.8	32%		

Table 2-6 (A3): Absorbance, measured at 615 nm, when heating temperature and heating time were varied to optimize thermal aggregation of the bovine serum albumin standard. The absorbance of the blank was 0.049, and it was not subtracted from the data in the table. Heating the BSA solution at temperatures higher than 60ºC forms gel-like particles. Heating at 85 ºC for two hours was chosen because these conditions gave higher absorbance and higher reproducibility.

	Absorbance (615 nm)	
Heating time (min)	60 °C	85°C
20	0.111 ± 0.021	0.113 ± 0.020
60	0.129 ± 0.019	0.125 ± 0.019
120	0.094 ± 0.004	0.107 ± 0.007

Table 2-7 (A4): Absorbance of different dilutions of *Thalassiosira weissflogii* culture with 0.2 μm filtered seawater, staining with Coomassie brilliant blue solution 1, 2 and 3 at different pH. CBB solution 1 at pH 7.4 was chosen because it gave a reasonable relationship between the filtered culture volume and the absorbance of the material in the filter. This pH ensured that the cells were not lysed and intracellular material was not stained. This staining solution is the same one used by the microscopic method and thus allows more direct comparison between the particles detected by the two methods.

	PH	Percentage of T. weissflogii culture diluted in 0.2 μm filtered seawater			Linear regression (T. weissflogii culture percentage vs. absorbance)	
		25%	50%	100%	R^2	Slope
CBB staining **solution 1:** modified from Mayer *et al.*, 1986	0.6	0.047	0.057	0.059	0.72	$1x10^{-4}$
	2.1	0.045	0.086	0.059	0.02	$8x10^{-5}$
	4.9	0.053	0.079	0.096	0.91	$5x10^{-4}$
	7.4	0.059	0.068	0.065	0.93	$2x10^{-4}$
CBB staining **solution 2:** modified from Tanoue, 1992	0.6	0.019	0.031	0.027	0.25	$8x10^{-5}$
	2.1	0.086	0.082	0.091	0.49	$8x10^{-5}$
	4.9	0.119	0.117	0.105	0.96	$-2x10^{-4}$
	7.4	0.99	0.11	0.112	0.71	$2x10^{-4}$
CBB staining **solution 3:** according to Long and Azam, 1996	0.6	0.029	0.034	0.038	0.94	$1x10^{-4}$
	2.1	0.021	0.043	0.066	0.97	$6x10^{-4}$
	4.9	0.019	0.042	0.05	0.80	$4x10^{-4}$
	7.4	0.02	0.034	0.037	0.73	$2x10^{-4}$

Table 2-8 (A5): Example of calibration curve using BSA as the standard and different preparations of Coomassie Brilliant Blue staining. The BSA curve stained with CBB solution 3 was linear, and the slope of the curve that represents the calibration factor is in the same range as the calibration factor for Alcian Blue in the colorimetric method for TEP determination.

	pH	BSA retained in the filter (μg)	Absorbance of standard curve CBB staining	Linear regression (absorbance vs. retained BSA, μg)	
				R^2	slope
CBB staining **solution 1:** modified from Mayer *et al.,* 1986	2.1	0.0 ± 0.5	0.062 ± 0.007	0.98	90.7
		8.2 ± 0.2	0.213 ± 0.016		
		28.8 ± 0.7	0.366 ± 0.004		
		30.3 ± 1.9	0.430 ± 0.002		
		41.0 ± 0	0.518 ± 0.025		
	4.9	0.0 ± 0.5	0.053 ± 0.004	0.99	129.7
		8.2 ± 0.2	0.139 ± 0.002		
		28.8 ± 0.7	0.250 ± 0.013		
		30.3 ± 1.9	0.276 ± 0.008		
		41.0 ± 0	0.382 ± 0.045		
	7.4	0.0 ± 0.5	0.043 ± 0.002	0.91	484.1
		8.2 ± 0.2	0.075 ± 0.008		
		28.8 ± 0.7	0.105 ± 0.002		
		30.3 ± 1.9	0.118 ± 0.006		
		41.0 ± 0	0.118 ± 0.005		
CBB staining **solution 2:** modified from Tanoue, 1992	2.1	0.0 ± 1.6	0.025 ± 0.006	0.84	529.9
		8.0 ± 1.3	0.072 ± 0.005		
		22.4 ± 2.9	0.106 ± 0.017		
		49.6 ± 0.9	0.112 ± 0.004		
		60.9 ± 1.5	0.145 ± 0.006		
CBB staining **solution 3:** according to Long and Azam, 1996	7.4	0.0 ± 1.6	0.039 ± 0.010	0.97	156.4
		8.0 ± 1.3	0.124 ± 0.008		
		22.4 ± 2.9	0.212 ± 0.009		
		49.6 ± 0.9	0.320 ± 0.010		
		60.9 ± 1.5	0.461 ± 0.045		

Table 2-9 (A6): Target mass of BSA filtered (µg) (TMF), and retention percentage of BSA standard (%) filtered to generate three calibration curves for three different batches of BSA. The retention of BSA aggregates decreased with increasing standard concentration. The calibration of the CBB solution uses the actual mass retained on the filter, and the relationship between absorbance of stained particles and µg of BSA retained in the filter is linear.

TMF	%			
	Curve A	Curve B	Curve C	Average
0	79 ± 6	82± 5	80 ± 1	82 ± 11
8	92 ± 3	78 ± 8	88 ± 4	87 ± 9
16	72 ± 5	73 ± 4	66 ± 2	70 ± 5
32	55± 1			
48				
64		43± 1		
72	41 ±0			
80			37 ± 2	
120		27 ± 1		
200			18 ± 2	

Chapter 3 :

Transparent exopolymer particles (TEP) and Coomassie stainable particles (CSP): Differences between their origin and vertical distributions in the ocean

(Published in Marine Chemistry, May, 2015)

Abstract

The discovery of ubiquitous, abundant and transparent gel-like particles, such as the polysaccharide-containing Transparent Exopolymer Particles (TEP) and protein-containing Coomassie Stainable Particles (CSP) has changed our conception of particle- organism interaction and created new questions about the origin, composition, and role of these particles in aquatic systems. Using both standard and novel staining methods, we studied these gel-like particles to determine whether CSP and TEP are sub-units of the same particle, are distinct particles with different characteristics and behaviors, or are both. Our seawater mesocosm results show that phytoplankton produce both TEP and CSP; however, their highest abundances occur at differences phases in the phytoplankton bloom. We developed a new technique for visualizing stained transparent material in unfiltered aqueous samples with the FlowCAM; this technique allows in-situ visualization and imaging of TEP and CSP in parallel stained samples. Visual examination of stained and unstained TEP and CSP from seawater microcosms, marine algal cultures, and freshwater showed that TEP and CSP have different shape, size and particle-association behavior. In a diatom-dominated microcosm, TEP concentrations were higher than CSP concentrations and unlike CSP, TEP were usually associated with diatom cells or aggregates. The cyanobacteria culture, however, showed higher CSP than TEP concentrations and aggregates of those cells appeared to be CSP-rich. Vertical and seasonal distributions of TEP and CSP in the Sargasso Sea were different. Even though both types of particles were most abundant in the upper 100 m of the water column, CSP closely followed fluorescence and total particle concentration, while the highest TEP concentration was always in the shallowest sample collected. Thus, we conclude that TEP and CSP are different particles, produced by different

species at different growth phases and rates. They have different roles and are affected by different processes according to the community composition and environmental conditions.

1. Introduction

Marine gel particles are stable macrogels that include large organic polymers and are part of the particulate organic carbon (POC) pool (Verdugo, 2012). Operationally, marine gel particles are defined as discrete transparent particles that are larger than 0.2- 0.4μm and visible only after staining with specific dyes. Transparent exopolymer particles (TEP) are discrete exopolymers that consist predominantly of surface-active acidic polysaccharides and that are stainable with Alcian Blue (AB) (Alldredge et al., 1993). Coomassie stainable particles (CSP) are transparent protein-containing particles that are stainable with the dye Coomassie Brilliant Blue (CBB) (Long and Azam, 1996).

Most of what we know about the origin, formation mechanisms, and role in the ocean of transparent gel particles comes from the study of TEP; information about CSP characteristics and behaviors is very limited. TEP are thought to abiotically assemble from exopolymeric substances (EPS) that are released external to cell biomembranes by phytoplankton or bacteria (Decho, 1990; Mopper et al., 1995; Passow 2000; Wotton, 2004). The monosaccharide composition of EPS released by marine diatoms is dominated by the deoxy sugars fucose and rhamnose, as well as arabinose (Myklestad et al., 1972); similarly, surface-active polysaccharides and TEP formed by bubble coagulation are also enriched in fucose and rhamnose (Mopper et al., 1995 and Zhou et al., 1998). These sugars are also major constituents of phytoplankton exudates studied in the laboratory, and of naturally occurring high molecular weight dissolved organic carbon (DOC) (Aluwihare et al., 1997; Aluwihare and Repeta, 1999). EPS may comprise between 10 and40%

of dissolved organic matter (DOM) (Guo and Santschi, 1997); however, not all EPS can assemble to form discrete particles such as TEP or CSP (Passow, 2002a). Gel particle formation leads to a size continuum of marine gels in the ocean; organic molecules exuded by marine organisms align, form tangled webs, and stabilize to produce colloids that aggregate and form gel particles like TEP (Passow 2000; Verdugo et al., 2004; Verdugo 2012). This process represents an important link between colloids, which belong to the DOC pool (Wells and Goldberg, 1991), and gels that are part of the POC in the ocean.

Three mechanisms have been suggested for the production of gel particles: a) aggregation of polymer fibrils and colloids by physical processes according to coagulation theory (Jackson, 1995; Mari and Burd, 1998; Engel et al. 2004., Burd and Jackson, 2009), b) spontaneous assembly of DOM to form larger polymer gels (Chin et al., 1998; Verdugo et al., 2004; Ding et al., 2009), and c) biotic release of readily assembled particulate exudates from phytoplankton and bacteria that can promote cell aggregation (Kiørboe and Hansen, 1993). TEP and their precursors may be released as overflow carbon when cells are able to photosynthesize but not to divide, e.g., under silicate limitation (Engel, 2000; Khal et al., 2008). TEP and CSP are ubiquitous in the ocean; TEP abundances are generally around 10^6 L^{-1}, and higher abundances (10^8 L^{-1}) have been reported during phytoplankton blooms. Similarly, CSP can range between 10^6 and 10^8 L^{-1} in coastal waters (Long and Azam, 1996). TEP concentrations relative to a xanthan gum standard are on the order of 10^3 μg XG eq L^{-1} during phytoplankton blooms, and in general, the highest abundance of TEP coincides with the decline of the bloom. Unlike TEP, there is limited information about the changes in CSP concentration during the development of a phytoplankton bloom or about the potential effect that nutrient limitation may have on CSP production and degradation.

Phytoplankton-derived TEP have a significant role in the formation of large sedimenting aggregates; this has been investigated for diatoms (Passow et al., 1994; Passow and Alldredge, 1995a; Kiørboe et al., 1996; Passow et al., 2001; Martin et al., 2011; Gärdes et al., 2011), dinoflagellates (Alldredge et al., 1998) and cyanobacteria (Grossart et al., 1997). It has been suggested that changes in stickiness and production of TEP can affect the efficiency of aggregation, sedimentation and ultimately the biological carbon pump (Jackson, 1995; Logan et al., 1995, Engel, 2000; Mari et al., 2007); it is not clear whether CSP affects aggregation or if CSP are as sticky as TEP. Passow et al. (2001) showed that sedimentation is the main process removing TEP from the euphotic zone, and that the sedimentation of diatoms, biogenic silica and lithogenic silica is directly related to TEP abundance, suggesting that large TEP-rich aggregates are crucial in the sedimentation of small biogenic particles and clays. There are no measurements of how CSP may affect the vertical flux of aggregates in the ocean, but Prieto et al. (2002) investigated the role of TEP and CSP in the aggregation of a diatom-dominated bloom in a mesocosm experiment. They concluded that CSP would have less impact on the formation of marine aggregates than TEP since they found a better correlation between TEP and total aggregate volume than between CSP and total aggregate volume.

The abundance of marine gel particles, and subsequently their role in POC flux, exhibits temporal and spatial variability. Higher concentrations of TEP are usually found in the euphotic zone and in coastal areas (Passow and Alldredge, 1994; Engel and Passow, 2001) and are apparently related to phytoplankton biomass (Passow, 2002b). However, the relatively high contribution of TEP to the POC pool, normalized to phytoplankton biomass, is not exclusive to coastal areas, but can also appear in low nutrient areas like the open ocean (Engel et al., 2004). Moreover, it has been hypothesized that exopolymers may be crucial for survival of bacteria in

oligotrophic environments with low nutrients (Ding et al., 2008). There is little data available about the distribution of CSP in the water column for comparison with TEP.

In seawater from different locations, the carbon content of TEP ranges from 10 to 800 μg C L^{-1} (Engel and Passow, 2001; Mari, 1999) and C:N varies between 20 (Mari, 1999) and 26 (Engel and Passow, 2001). The average C:N of TEP is similar to that of the high molecular weight DOC produced by marine phytoplankton (Biddanda and Benner, 1997), supporting the idea that TEP are formed mainly from colloidal precursors exuded by phytoplankton (Jackson, 1995; Chin et al., 1998; Mari and Burd, 1998). This high C:N ratio has led to the hypothesis that the N present in TEP could have been adsorbed to the sticky gel particles rather than be an integral part of the TEP itself (Engel and Passow, 2001). However, there is no conclusive evidence for this, and whether or not TEP and CSP are subunits of the same particle is still an intriguing question, i.e., are they are formed and produced by the same processes, or are they independent particles with different origins, behaviors and roles in the ocean.

In the present study, we sought to determine whether protein-rich CSP and polysaccharide-rich TEP are the same type of particle, or whether they are discrete units with different characteristics and behaviors. We studied gel particles using three different approaches; first, using standard spectrophotometric techniques in a mesocosm experiment we measured and compared the net production of TEP and CSP, and the relationship between these gel particles and biogeochemical parameters like chlorophyll *a* (Chl *a*) and POC. Second, using a novel particle imaging system (FlowCAM) technique, we visually examined images of TEP and CSP, from freshwater, seawater microcosm experiments and batch cultures of cyanobacteria and diatoms, to compare their general physical appearance, their particle association behavior, and differences in TEP and CSP production by different phytoplankton species. Finally, we studied

vertical and seasonal distributions of TEP and CSP in a natural oligotrophic oceanic environment at a site on the Bermuda Rise during 2012 -2013.

2. Methods

A list of abbreviations is given in Table 3-1.

2.1. *Sample collection*

2.1.1 Laboratory

Mesocosm, microcosm, and culture experiments were conducted in the laboratory to compare the net production of TEP and CSP by phytoplankton over time.

2.1.1.1 *Mesocosm experiment*

Marine gel particles were measured over a complete growing cycle during a phytoplankton bloom in an experimental mesocosm facility. The mesocosm experiment was conducted at the Flax Pond Marine Laboratory of Stony Brook University during July 2011 to study the effect of ocean acidification and increased temperature on phytoplankton, TEP and CSP production, and aggregation processes. Six mesocosms were manipulated to simulate a future ocean: CO_2 concentration (750 ppm) was altered by the addition of high-CO_2 seawater and temperatures were held at 16°C and 20°C. Control mesocosms were maintained at present CO_2 concentration (380 ppm) and temperature (16°C). Effects of ocean acidification and increased temperature during these experiments will be discussed elsewhere. There was in fact no significant difference in Chl *a*, TEP and CSP net production between treatments with different CO_2 and temperature. Thus in this study, we will present data from the six mesocosm tanks without distinction. Briefly, the mesocosms were created by filling six tanks (~1 m^3) with coastal seawater from Stony Brook Harbor that had been passed through a 200-μm mesh to remove large

detritus and zooplankton. As a light source, pairs of fluorescent lights (F40T12, full spectrum) were suspended above each tank, providing a surface irradiance of 190 μmol photons m^{-2} s^{-1} with a light: dark cycle of 14: 10. Irradiance was set at the beginning of each experiment with a LICOR Model LI-2100 light meter. All mesocosms were slowly stirred by mechanically controlled paddles. After 5 days of stabilization, nutrients (20 μM nitrate, 20 μM silicate and 1.5 μM phosphate) were added to the tanks to initiate a diatom-dominated phytoplankton bloom; the dominant species were chain-forming diatoms such as *Skeletonema* spp. and *Chaetoceros* spp., and solitary diatoms like *Rhizosolenia* sp. and *Ditylum* sp. The bloom was monitored for 21 days; during this period the tanks were sampled four times.

2.1.1.2 *Microcosm experiment*

Separate microcosm experiments were conducted with water from Stony Brook Harbor that was filtered through a 153-μm mesh to remove large zooplankton and detritus. The incubations were conducted in 10-L clear culture vessels at 17 ºC, with light at 190 μmol photons m^{-2} s^{-1} and a light: dark cycle of 14:10. Nutrients, vitamins and minerals were added according to f/2 medium (Guillard and Ryther 1962) to initiate a bloom. The resulting bloom was dominated by diatoms such as *Chaetoceros* spp., *Skeletonema costatum, Asterionella glacialis* and *Thalassionema nitzschioides*. Samples were collected every day for 12 days for total particle concentration measurements and every other day for spectrophotometric measurement of TEP and CSP. Additionally, these particles were analyzed by FlowCAM as described below, during the exponential phase, day=6, and during the stationary phase, day=11.

2.1.1.3 Batch cultures

Batch cultures of *Thalassiosira weissflogii* (CCMP 1336); and *Synechococcus bacillaris* (CCMP 1333), were grown in f/2 medium (Guillard and Ryther 1962) in 3.5-L culture vessels.

To obtain cultures with different bacteria abundances, we prepared the f/2 media in two different ways. First, natural seawater from the Sargasso Sea was 0.2-μm filtered, and nutrients and trace metals were added. This medium was autoclaved to reduce bacterial concentrations (LB= low bacteria). A second medium was prepared in the same manner, but was not autoclaved (HB= high bacteria). This resulted in a 4-fold difference in bacterial abundance in LB ($8.5\pm2.3\times10^5$ cells mL^{-1}) and HB ($3.2\pm1.7\times10^6$ cells mL^{-1}) *T. weissflogii* cultures and 2-fold (LB: $1.1\pm0.46\times10^6$ cells mL^{-1}; HB: $2.6\pm1.2\times10^6$ cells mL^{-1}) for *S. bacillaris* cultures on day 4 of the experiment. Controlling bacteria concentrations while maintaining healthy algal growth is challenging; previous studies have concluded that interactions between *T. weissflogii* and diatom attaching-bacteria were required for TEP formation and aggregation (Gärdes et al., 2011), thus a completely sterile culture is undesirable in gel particle experiments. Even though we had expected a larger difference in bacteria concentrations, we used these HB and LB cultures in our experiments to investigate whether bacteria influenced the concentration of TEP and CSP over time. However, future degradation experiments are required to obtain more robust evidence of bacterial effects. The cultures were maintained at room temperature (20 ºC), with light at 190 μmol photons m^{-2} s^{-1} and a light: dark cycle of 14:10. Cells were quantified and sized every day using the FlowCAM, and TEP and CSP were measured spectrophotometrically every other day for 30 days. Gel particles were visualized using a FlowCAM, as described below, in the stationary phase, day=19.

The chelating agent Na_2EDTA (sodium ethylenediaminetetraacetate) was used to study whether or not TEP and CSP produced by cultures of *S. bacillaris* and *T. weissflogii* are bound by divalent cations (Ca^{2+}, Mg^{2+}). The concentration of TEP and CSP was measured spectrophotometrically before and after the addition of Na_2EDTA to a final concentration of 100

mM. Alcian Blue (AB) and Coomassie Brilliant Blue (CBB) were also added directly to samples to visualize the effect of the removal of the divalent cations on the concentration, shape, and size of TEP and CSP in *S. bacillaris* and *T. weissflogii* culture, and specifically in aggregates; images were captured by the FlowCAM (as described below).

2.1.2. *Natural samples from the Sargasso Sea*

Open ocean samples were collected as part of the BarFlux project during five cruises to the Bermuda Rise (33.68°N, 57.6°W). Sampling dates were in February, May, August and November 2012 as well as June 2013. Vertical profiles of the water column were sampled with a CTD (Sea-Bird Electronics)/ Niskin-bottle rosette; relative concentration of Chl *a* was measured with a flow-through fluorometer (WET Labs WETStar) associated to the CTD. Seawater was transferred from each Niskin-bottle to a 10-L container and subsamples were filtered for analysis of TEP and CSP; total particle concentration was measured with the FlowCAM on board. Subsamples for gel particle analysis were stained immediately with AB for TEP determination and with CBB for CSP determination and stored frozen until analysis. Vertical distribution profiles for TEP and CSP were used to investigate the relationship between TEP and CSP and seasonal changes in Chlorophyll-*a*.

2.2. *Analyses*

2.2.1. *Transparent gel particles: TEP and CSP*

TEP and CSP were analyzed spectrophotometrically after staining with a solution of 0.02% AB (Alcian blue 8X, Sigma Aldrich) at pH 2.5 and a solution of 0.04% CBB (Coomassie brilliant blue G-250, SERVA electrophoresis) at pH 7.4, according to Passow and Alldredge (1995b) and Cisternas-Novoa et al. (2014), respectively. Briefly, 10 -20 mL for culture, 20 -50 mL for microcosm and mesocosm experiments, or 200 -500 mL for natural samples from

Sargasso Sea were filtered using low, constant vacuum (< 200 mbar) onto 0.4-μm Nuclepore filters (25 mm). Parallel samples were stained for TEP and CSP determination. TEP filters were stained with 1 mL AB for 5 s and CSP filters with 1 mL of CBB for 30 s. Excess dye was removed by rinsing with Milli-Q water. All filters were prepared in duplicate and stored frozen at -20 °C until analysis; for TEP determination, stained filters were placed in 15-mL polypropylene tubes and 6 mL of extraction solution (80% H_2SO_4) was added; tubes were incubated with gentle shaking for 2 h. Absorbance of the AB in solution was measured spectrophotometrically at 787 nm in a 1-cm cell. Blanks were prepared from Milli-Q water or 0.2-μm filtered seawater for each set of samples. Concentrations of TEP are reported relative to a xanthan gum standard and expressed in micrograms of xanthan gum equivalents per liter (μg XG eq L^{-1}) after Passow and Alldredge (1995b).

For CSP measurements, stained filters were transferred to 15-mL polypropylene tubes (filters can be stored frozen at this point as in the TEP colorimetric method), and 4 mL of extraction solution (3% SDS in 50% isopropyl alcohol; Ball 1986) was added. Tubes were sonicated in a water bath (50 -60 kHz) for 2 h at 37°C. After the incubation, the absorbance of the extraction solution was determined spectrophotometrically. The absorption maximum of the eluted CBB is 615 nm. Blanks were treated in the same way as for TEP determination. Concentrations of CSP are reported relative to a bovine serum albumin standard and expressed in micrograms of bovine serum albumin equivalents per liter (μg BSA eq L^{-1}) after Cisternas-Novoa et al. (2014).

2.2.2. *Chlorophyll* a and *particulate organic carbon*

Concentrations of chlorophyll *a* (Chl *a*) were determined by ion-pairing reverse-phase high-pressure liquid chromatography (HPLC) (Mantoura and Llewellyn, 1983; Bidigare et al., 1987; Sun et al., 1991). Briefly, between 20 and 50-mL samples were filtered onto combusted GF/F filters in duplicate and frozen until analysis. Chl *a* was extracted from filters by sonicating in HPLC-grade 100% acetone; two successive 5-mL extracts were combined and filtered through a 0.2-µm Zetapor membrane. Samples were covered with aluminum foil to protect them from light during handling and analysis. Chl *a* was separated from other chloropigments by HPLC on a 5-µm Adsorbosphere C-18 column (Sun et al., 1991). Chl *a* was detected by fluorescence (excitation λ=440 nm, emission λ=660 nm) and was identified and quantified using an authentic standard (Sigma-Aldrich).

Particulate organic carbon (POC) contents were quantified using a Carlo Erba EA-1112 CNS analyzer (uncertainty ±2% for C and ±5% for N analysis). Samples of 20 -50 mL were filtered onto combusted GF/F filters in duplicate. The presence of particulate calcite was assessed by measuring carbon before and after treatment with 10% HCl to remove particulate inorganic carbon (PIC). For mesocosm samples, PIC was not removed because preliminary analysis showed negligible differences between HCl-treated and non-treated samples. The mesocosm experiment was dominated by diatoms, with a minimum presence of PIC.

2.2.3. *FlowCAM measurements*

Total concentration and size of cells, individual particles, and aggregates in cultures and in natural samples were determined with a portable FlowCAM system (Fluid Imaging Inc.). The FlowCAM enables microscopic particle measurements and imaging in two dimensions using a regular microscope objective lens as the sample passes through a glass chamber in a continuous

flow (Sieracki et al., 1998). The FlowCAM automatically counts and sizes the particles, and obtains individual pictures of each particle. All the measurements in this study were made using the automatic imaging mode and an objective lens of 10 X, leading to an overall magnification of 100 X. A 300-μm-deep flow cell allowed measurement of particle sizes between approximately 2 and 300 μm. It is possible to see smaller particles, but without morphological information, i.e., only for relative comparison of particle abundance. It is also possible to see larger particles (up to 1 mm) if a long, skinny particle is located along the flow cell. A sample volume of 0.5 mL was analyzed, with a flow rate between 0.1 and 0.4 mL min^{-1} and a camera rate of 7.0 frames s^{-1}. Between samples, the system was flushed with Milli-Q water for 5 to 10 min at a flow rate of 0.5 mL min^{-1}, and a visual inspection of the flow cell was performed between samples to ensure cleanliness. During each run, samples were gently mixed by a small stirring bar to prevent particle sedimentation, and were pumped through the flow cell using a peristaltic pump. Samples from cultures and experiments were diluted with artificial seawater when needed. Natural seawater samples did not require dilution. Results were analyzed using VisualSpreadsheet software version 3.1.10 (Fluid Imaging Inc.).

In addition, the FlowCAM flow-imaging microscope was used to visualize *in-situ* particles after the direct addition of 0.2 μm prefiltered AB or CBB to aqueous samples. The addition of AB and CBB allows polysaccharide-rich and protein-rich material that was transparent before dye addition to be visualized, and automatically photographed by the FlowCAM. This method allows the characterization of unfiltered gel particles by eye in the raw image when the sample is flowing through the FlowCAM, as well as in images that are collected and stored. Measured parameters such as shape, size and transparency allow the evaluation of differences between types of particles such as TEP, CSP, cells, individual detrital particles, and

aggregates. By definition TEP and CSP are discrete particles larger than 0.4 μm that are stainable with AB, which stains acidic polysaccharides, or CBB, which stains proteins. It is important to consider that the FlowCAM method proposed here, like other alternative methods to measure TEP (e.g., Thornton et al., 2007; Claquin et al., 2008), measures discrete particles >0.4 μm but also acidic polysaccharides <0.4 μm attached to particles. This method, like the spectrophotometric methods for TEP and CSP determination, will measure proteins and polysaccharides without distinguishing if they are free or attached to cells.

The method was evaluated in samples from a freshwater pond, from the seawater microcosm experiment, and from *T. weissflogii* and *S. bacillaris* cultures, using Milli-Q water and double 0.2-μm-filtered artificial seawater as a blank. For all the analyses, 4 mL of AB and 2 mL of CBB were added directly to 20 mL of sample, the dye was allowed to act for 2 min, and then samples were analyzed using FlowCAM. The freshwater sample, collected in March 2014 from a local pond, was dominated by small cells, a few chain-forming diatoms, and detrital material; the sample was analyzed within 2 h of collection. The microcosm experiment was sampled during the exponential phase (day 6 after nutrient addition) and the stationary phase (day 11). Cultures of *T. weissflogii* and *S. bacillaris* were sampled during the stationary phase (day 19).

Since salts present in seawater interfere with the direct staining of marine samples (Hayat 2000; Passow and Alldredge 1995b), the FlowCAM method where AB and CBB were added directly to the unfiltered seawater samples was only qualitative. Even though the data discussed in this paper is qualitative, a dialysis step to desalt marine samples before the addition of the dye could be included for quantitative applications. Dialysis has been used previously to purify

diatom EPS (Underwood et al., 2004) and to quantify acidic polysaccharides (Thornton et al., 2007). We dialyzed samples according to Thornton et al. (2007) to eliminate artifacts; this would allow the quantification of TEP and CSP in seawater samples. Briefly, we used regenerated cellulose dialysis tubing with molecular weight cut-off (MWCO) 4000 -6000 Da (Spectra/Por, Spectrum Laboratories). The dialysis tubing was stored in 0.05% sodium azide, and soaked in Milli-Q water for 30 min to remove the preservative before using it. We tested the effect of dialysis on gel particles in a microcosm experiment similar to that described above, and on a culture of *S. bacillaris*. Samples from the microcosm experiment were taken and dialyzed 6 days (ME2, d6) and 8 days (ME2, d8) after nutrient addition; the *S. bacillaris* culture was sampled and dialyzed two months after nutrient addition. Between 20 and 50 mL of sample was loaded into dialysis tubing, sealed with closures (Spectrum Laboratories), and placed in a large (4L) stirred bath of Milli-Q water for approximately 20 h, changing the water bath once after 8 to 10 h. A few drops of chloroform were added to the water bath to prevent microbial activity (Underwood et al., 2004). The salinity of the sample was measured before and after the dialysis with a hand-held refractometer. In addition to FlowCAM analysis; TEP and CSP concentration of the sample was measured spectrophotometrically before and after the dialysis procedure to evaluate the effect of dialysis on gel particles concentration.

3. Results and Discussion

3. 1 Net production of gel particles in mesocosm

Nutrient-induced phytoplankton blooms in the experimental mesocosms started approximately 24 h after nutrient addition, and the highest Chl-*a* concentration was reached between 12 and 16 days (Fig. 3-1A). Nutrients declined to below detection limits after 16 days.

Spectrophotometric measurements of TEP and CSP concentrations during the growing cycle of phytoplankton in the mesocosms indicate that the highest abundance of those particles was reached at different times. Production of TEP increased gradually during the phytoplankton bloom, and the highest concentration of TEP was observed on the last sampling day, when the bloom was senescing (Fig. 3-1B). On the other hand, the maximum net production rate of CSP was highest during the exponential growth phase of the phytoplankton. The highest concentration of CSP coincided with the Chl-*a* maximum (Fig. 3-1C); after that the production rate of CSP decreased drastically, similarly to the Chl-a concentration.

Consistently, there was a closer relationship between CSP and Chl *a* than between TEP and Chl *a*, suggesting that CSP abundance is more related to phytoplankton biomass than that of TEP. CSP showed a significant relationship with Chl *a* with a Pearson product-moment correlation coefficient of r= 0.81 (n=36, p-value < 0.0001; Fig. 3-2a), while the correlation between TEP concentration and Chl *a* was lower, r= 0.37 (n=36, p-value < 0.05; Fig.3-2b). In contrast, there was no correlation between CSP and POC, r=0.17 (n=35, p-value > 0.05; Fig.3-2c), while TEP concentration was more closely related to POC concentration, r=0.57 (n=35, p-value < 0.0001; Fig. 2-2d).

TEP has been shown to form from precursors produced during diatom-dominated phytoplankton blooms (Passow, 2000; Passow 2002; Pedrotti et al., 2010), and the significance of TEP in aggregate formation and bloom termination has been demonstrated (Passow and Alldredge 1995a; Thornton and Thake 1998; Engel 2000; Pedrotti et al., 2010). In our mesocosm experiments, both TEP and CSP formed when the phytoplankton bloomed, but the highest concentration of those two types of gel-like particles occurred at different phases of the bloom. TEP concentration increased with time and was highest at the end of the experiment, during the

senescent phase of the bloom; those results are consistent with previous experiments and *in-situ* measurements (e.g., Passow 2002, Engel et al. 2014).

The fact that TEP concentration correlates so well with POC concentration supports the idea of the formation of gel particles like TEP being a bridge between DOC exuded by phytoplankton and POC (Alldredge et al., 1993; Chin et al., 1998; Engel et al., 2004). Our mesocosm observations are also consistent with previous results of Prieto et al. (2002) that showed a concomitant increment of TEP and aggregates, but a decrease in CSP when aggregate formation began. CSP, on the other hand, increased consistently with Chl-*a* concentration and reached their highest concentration at the same time as Chl *a*. This agrees with CSP being actively produced by phytoplankton during the exponential phase when they still have nutrients available. We cannot be certain that the decrease in concentration of CSP after the Chl-*a* maximum was due to a decrease in production, as CSP might also decrease due to an increase in consumption by bacteria after nutrient depletion; particle-associated bacteria have been found to increase in the post bloom phase (Riemann et al., 2000). However, the difference in TEP and CSP abundance patterns with time indicates that they behave differently and/or may interact differently with the microbial community; CSP might be more labile and might be used as a source of nitrogen by bacteria after nutrient depletion.

3.2 Evaluation of FlowCAM technique to visualize unfiltered TEP and CSP

To use the dyes directly with the FlowCAM, we had to determine whether the tendency of AB to precipitate in seawater would preclude its use in this application. First, we measured absorption of an AB-stained blank of artificial seawater that had been double 0.2-μm-filtered; the concentration of AB-stainable particles, determined with the FlowCAM, was significantly less in

this filtered blank than in samples from microcosms and cultures (Fig. 3-3a); and the maximum equivalent spherical diameter (ESD-max) in the blank was in general smaller than the ESD-max observed in samples (Fig. 3-3b). Second, when Milli-Q water was stained with AB and CBB, the concentration and ESD of particles was negligible. Third, visual examination of images captured by the FlowCAM in 0.2 μm pre-filtered artificial seawater (ASW) used as a blank, and in freshwater used as a reference (Fig. 3- 4), showed that TEP associated with cells and aggregates in samples (Fig. 3-5a, c and e) looked distinctly different from the precipitate formed in the blank (Fig. 3-4a). CBB also formed small, very distinctive particles in the blank (Fig.3- 4b), but again they were visually different from the CSP observed in samples (Fig. 3-5b, d and f). Fourth, we stained a freshwater pond sample because neither AB nor CBB precipitates in freshwater, and particles identified as TEP (Fig. 3-4c) have the same appearance, cloud-like shape, and association with cells and aggregates as TEP has in seawater (Fig. 3-5a,c and e).

Although we can visually distinguish precipitated particles from particles originally in the sample, the FlowCAM cannot automatically distinguish them when calculating total particle concentration and particle size spectra. This precludes the automatic quantification of particles by this technique. When TEP concentration is low we can manually delete artifacts (e.g., from Fig. 3-5e), and recalculate particle size and concentration; however, we did not do that for this study because when TEP concentration is very high (e.g., Fig. 3-5a and 3-5c), it is not always possible to capture artifact images. When images of artifacts are captured, it is easy to recognize them because they have a distinctive shape and sharp edges, compared with artifacts found in AB-stained artificial seawater (Fig. 3-4a). Therefore we use this technique to identify TEP and compare them to CSP in a qualitative way.

One issue complicates comparison of total numbers of stained and unstained particles. In unstained and CBB-stained samples (these samples looked similar because CBB did not significantly stain cells or detrital particles in these samples) from the freshwater pond, the FlowCAM captured pictures of individual cells, cell-clusters and small detrital particles and counted each particle as an individual (Fig. 3-6a). However in the AB-stained sample the FlowCAM counted not only individual cells and detrital material, but also larger aggregates with small detrital particles, individual cells, and cell-clusters embedded in the stained acidic polysaccharide TEP matrix, which was newly visible (Fig. 3-6b). The AB stain in fact revealed TEP and larger aggregates composed of individual cells and acidic polysaccharide, that were present before the AB staining but not visible to the FlowCAM due to the transparency of the acidic polysaccharides, thus changing the size distribution from many smaller cells to fewer larger cells. Since FlowCAM counts the total number of particles, histograms of ESD versus particle frequency showed that the most frequent diameter was the same in CBB-stained (Fig. 3-6c) and AB-stained samples (Fig. 3-6d). However, the number of smaller particles increased in the AB-stained sample due to the newly visualized smaller TEP. There were also more larger particles, especially >285 μm in ESD, in the AB-stained sample (Fig. 3-6d) due to the visualization of a single aggregate with acidic polysaccharides containing embedded particles.

To address the issue of salts interfering with AB staining and to evaluate future applications of FlowCAM to quantify gel particles, a simple dialysis step was added before the addition of the AB and CBB dyes to desalt marine samples taken from a microcosm experiment (ME2) and for a *S. bacillaris* culture. After 16 h of dialysis the salinity of the samples was zero. Visual examination of the FlowCAM capture windows when particles in the fluid sample were passing through the flow cell showed that the small background particles in the AB-stained

sample were not formed in the dialyzed AB-stained microcosm sample. . Particle concentration, measured with the FlowCAM, in unstained samples from the microcosm was similar pre- and post-dialysis, but decreased by 53% between pre- and post-dialysis samples from the *S. bacillaris* culture (Fig. 3-7a). AB-stained particle concentrations measured with the FlowCAM were 81%, 87% and 57% lower after dialysis in samples from microcosm days 6 (ME2, d6) and 8 (ME2, d8) and the *S. bacillaris* culture, respectively (Fig. 3-7b). CBB-stained particle concentrations measured with the FlowCAM did not change significantly between the pre and post-dialysis samples from microcosm day 6, but were 30% and 70% lower after dialysis in microcosm day 8 and *S. bacillaris* culture samples, respectively. The average ESD was around 7 μm for the microcosm experiment and around 1.2 μm for *S. bacillaris*; the average did not change significantly after the dialysis and the standard deviation was high. A useful way to analyze changes in size is by comparing the maximum ESD of particles. ESD-max of unstained particles was larger before dialysis in samples from ME2, d6 (29%) and ME2, d8 (5%), but in the *S. bacillaris* culture, the ESD-max was higher (16%) after dialysis (Fig. 3-7d). The ESD-max of AB-stained particles was lower after dialysis in samples from ME2, d6 (19%) and the *S. bacillaris* culture (26%); however, the ESD-max for ME2, d8 was 135% larger after dialysis than before (Fig. 3-7e). For CBB-stained particles the ESD-max was higher after dialysis for all three samples (Fig. 3-7f).

Analysis of FlowCAM images from microcosm experiment samples before and after dialysis showed that there was no clear visual difference in unstained samples before (Fig. 3-8a) and after dialysis (Fig. 3-8d). AB-stained particles in seawater and in desalted samples had different shapes and were associated differently with the diatom aggregates. In seawater, AB-stained particles surrounded the aggregates and cells, and were similar in shape to TEP (Fig. 3-

8b). In dialyzed samples, AB seemed to stain detrital material and cells within the aggregate itself, thus the aggregates looked more compact (Fig. 3-8e). The amount of AB-stained particles was significantly greater before dialysis; this difference was at least partially due to the elimination of background particles that formed as an artifact of adding AB to seawater, but also presumably because of some loss in TEP as well. In the case of CBB-stained particles, visual examination showed that before dialysis (Fig. 3-8c), not all diatom aggregates had CSP and when CSP was present they looked like discrete particles. Dialyzed aggregates (Fig. 3-8f) showed more CBB-staining and also more staining internally; the fact that more material was CBB-stained after dialysis and that the appearance of AB and CBB material was similar (more internal staining within the aggregate) after dialysis might suggest that gel particles or their precursors leaked from cells lysed by the desalting procedure. Particles from the *S. bacillaris* culture were too small to visually differentiate in this way.

To further test the effect of dialysis on TEP and CSP particle concentrations, these gel particles were measured spectrophotometrically before and after dialysis. Results demonstrate that TEP concentration, measured as μg xanthan gum equivalents L^{-1}, was 33% lower after dialysis in a sample from microcosm day 8, and was 54% lower in a dialyzed sample from the *S. bacillaris* culture (Fig. 3-9a). On the other hand, CSP concentration measured as μg bovine serum albumin equivalents L^{-1}, was 66% and 87% higher in dialyzed samples from microcosm day 8, and in *S. bacillaris* culture, respectively (Fig 3-9b). The CSP/TEP ratio after dialysis was twice the ratio before dialysis in both samples. Higher protein/carbohydrate ratios can indicate protein leakage from lysed cells (Comte et al., 2006). The lower concentrations of TEP in dialyzed samples may be due in part to loss of TEP and TEP precursors during dialysis using 4000 -6000 Da MWCO. Passow (2000) reported loss of TEP precursors using tubing with 8,000

Da MWCO. This may be prevented to some degree by using smaller MWCO dialysis tubing; for instance, Thornton et al. (2007) used 1000 Da. Another possible cause of loss of TEP during dialysis is the loss of calcium and magnesium ions by the desalting process. TEP are stabilized by divalent cations, and exclusion of these cations by chelation or dialysis can cause microgel dispersion and size reduction (Chin et al., 1998). If dialysis compromises cell integrity and allows leakage of intracellular fluid, this may also cause overestimation of CSP in samples, since this technique measures CSP, and all free and cell-associated protein.

In general, dialysis eliminated artifacts created by the interactions of AB and seawater and allowed *in-situ* visualization, identification and quantification of particles in directly-stained samples passing through the FlowCAM. However, our tests suggest that dialysis may disrupt cells and cause an overestimation of CSP, but cause an underestimate of TEP due to loss of TEP precursors. Therefore, further experimentation with smaller MWCO dialysis tubing and shorter dialysis time is suggested to achieve more accurate values of TEP and CSP using this technique quantitatively. Nevertheless, even without dialysis, the FlowCAM technique described in this paper is still a valuable tool for comparative studies, for example in experiments in which relative quantities of TEP and CSP are sufficient to answer a scientific question. Moreover, the qualitative data presented here on the visual differentiation of shape and particle association of TEP and CSP in unfiltered marine samples using the FlowCAM, did not require dialysis.

3.3 *Differentiation of TEP and CSP in microcosms and algal cultures using FlowCAM*

Using our new method of analyzing stained samples with the FlowCAM, seawater microcosm experiments dominated by diatoms were analyzed during the exponential phase, i.e., day 6 after nutrient addition (ME, d=6), and again at the end of the stationary phase, day 11 (ME,

d=11). Total particle concentrations, measured as particles per liter by FlowCAM, increased significantly after the addition of AB (96% on d=6 and 89% on d=11, Fig. 3-3a) in both samples, suggesting the presence of TEP. After the addition of CBB (to other samples from the microcosms), however, total particle concentration was 63% higher in the exponential phase and 9% lower during senescence at the end of the stationary phase (Fig. 3-3a). The ESD-max calculated using all particles in the sample was larger in AB-stained samples (Fig. 3-3b) than in the non-stained or CBB-stained samples.

In the whole microcosm sample stained with AB and CBB, visual examination of the sample flowing through the FlowCAM, as well as images automatically captured, showed that during the exponential phase of growth, the spines of diatoms were stained with AB indicating the presence of TEP (Fig. 3-5a). We cannot determine whether TEP on the spines were produced by the diatoms, or if they were produced elsewhere and attached to the spines later. The CBB-stained sample did not show any stain on diatom or diatom spines (Fig. 3-5b). At the end of the stationary phase, aggregates were observed. Aggregates are defined here as particles that were visible to the naked eye, and which appear under the microscope as a collection of cells, gel-like particles and unidentified detrital material gathered together forming a larger unit. The surfaces of AB-stained aggregates were coated with TEP (Fig. 3-5c), and the aggregates were occasionally surrounded by even larger cloud-like TEP that were not captured in images, but visible while the sample was flowing through the FlowCAM; this was consistent with the larger ESD-max measurement, that showed larger ESD-max for AB-stained samples (Fig. 3-3b), and with the idea that TEP can act as an organic glue holding together aggregates formed by diatoms and detritus. Even though aggregates were visible in the CBB-stained sample, they did not adsorb the stain (Fig. 3-5d).

Cultures of *T. weissflogii* and *S. bacillaris* were examined by FlowCAM before and after staining them with AB and CBB. Total particle concentrations of the stained sample from the stationary phase (day 19) of *T. weissflogii* cultures showed a pattern similar to that of the microcosm experiment; higher particle concentrations in AB-stained samples than in unstained samples or CBB-stained samples (Fig. 3-3a). However, the ESD-max was larger in both stained samples (Fig. 3-3b). Particle concentrations in the *S. bacillaris* culture were different, with CBB-stained samples having more particles than AB-stained and unstained samples (Fig. 3-3a). The ESD-max was similar in the stained and unstained samples (Fig. 3-3b).

Visual examination by the FlowCAM of cells and aggregates in the diatom-dominated microcosm bloom, *T. weissflogii* culture, and pond water samples suggested that AB and CBB stained different particles. AB-stained particle concentrations were higher than the concentration of CBB-stained particles in all these samples. On the other hand, concentrations of CBB-stained particles were higher in the *S. bacillaris* culture. TEP and CSP concentrations determined spectrophotometrically in cultures were consistent with total particle concentrations and visual observations. Total particle concentration of *T. weissflogii* and *S. bacillaris* (Fig. 3-10a) showed that the cultures reached the stationary phase approximately on day 19. The value of TEP concentration (mg XG eq L^{-1}) was higher than CSP concentration (mg BSA eq L^{-1}) in the *T. weissflogii* culture (12.2 -27.9 mg XG eq L^{-1} vs. 3.0 -8.5 mg BSA eq L^{-1}), while the reverse was found in the *S. bacillaris* culture (2.2 - 5.7 mg XG eq L^{-1} vs. 2.3 - 14.3 mg BSA eq L^{-1}) (Fig. 3-10 b, c). Even though TEP and CSP are measured in different units and therefore not directly comparable, the fact that the concentration of TEP was higher in the diatom culture while CSP concentration was higher in the cyanobacteria culture suggests that the production and significance of TEP and CSP may be directly affected by the phytoplankton composition. During

the stationary phase, aggregates that formed in the *S. bacillaris* cultures were visible before the dye addition and were clearly stained blue after CBB addition (Fig. 3-5f), but not after AB addition (Fig. 3-5e), indicating that they were probably more enriched in proteins.

It is important to consider that the microcosm experiment as well as the pond sample contained natural bacteria. To study the effect of bacteria on the concentration of TEP and CSP, we compared these gel particles in low bacteria (LB) and high bacteria (HB) cultures of *T. weissflogii* and *S. bacillaris* (Fig. 3-10a). TEP concentration was slightly higher in the LB cultures, while the concentration of CSP was significantly higher in the LB cultures (Fig. 3-10b), suggesting that CSP may be more prone to bacterial degradation and have a shorter turnover time. The turnover time of TEP depends on their age and chemical composition (Passow, 2002b). Previous studies have shown that diatom-produced aggregates and TEP were not degraded even after 11 days of observation (Piontek et al., 2009), while bacteria themselves may produce refractory TEP (Stoderegger and Herndl, 1999). Nevertheless, due to the small differences in bacteria concentration in our LB and HB cultures, our results can only suggest that CSP may be more labile to bacterial degradation than TEP. Further degradation experiments are required to make a robust conclusion about their relative degradation rates.

Aggregates that formed during the stationary phase in the microcosm experiment and the *T. weissflogii* culture were visible in unstained samples, but they appeared bigger and surrounded by cloud-like TEP when stained with AB (Fig. 3-5c). The measured ESD-max (Fig. 3-3b) of the AB-stained aggregates was larger, because the blue cloud-like TEP increased the aggregate's apparent size. The AB-stained freshwater pond sample also showed cloud-like TEP around the aggregates (Fig. 3-4c). The fact that similar cloud-like TEP associated with aggregates are observed in freshwater and in seawater, and that those cloud-like particles are different from the

precipitates observed in the blank (ASW), further suggests that the visualized particles were not precipitated dye. As in the CBB-stained seawater sample, there were only a few CBB-stained particles in the freshwater sample (Fig. 3-4d), and most of these particles were not associated with cells or cell colonies. The ESD-max was considerably larger in the AB-stained microcosm, diatom culture, and freshwater samples (Fig. 3-3b) due to the FlowCAM imaging a single large stained particle instead of individual smaller particles as described in the previous section.

Aggregates in *S. bacillaris* cultures behaved differently than those in *T. weissflogii* cultures; they were stained with CBB but not with AB (Fig. 3-5e, f). Visually those aggregates appeared more compact and solid than the diatom aggregates observed in the microcosm, pond and *T. weissflogii* culture samples. The difference in TEP and CSP content of aggregates from different origins suggests that the role of gel particles in aggregate formation and POC export is complex, and varies between species and therefore will have different effects on different environmental and ecological conditions. These findings agree with conclusions made by Berman and Viner-Mozzini (2001) that the relative abundances of TEP and CSP in freshwater depend on the dominant phytoplankton and the gel particle turnover times.

3.4 Ionic bonding of TEP and CSP

The concentration of TEP and CSP measured spectrophotometrically decreased after the addition of Na_2EDTA in both *T. weissflogii* and *S. bacillaris* cultures (Fig. 3-12). TEP (μg XG eq L^{-1}) decreased by 33% in *T. weissflogii* culture and by 30% in *S. bacillaris* culture. CSP (μg BSA eq L^{-1}) decreased by 32% in *T. weissflogii* culture and by 95% in *S. bacillaris* culture.

Visual examination of FlowCAM images indicated that the addition of Na_2EDTA disrupted *S. bacillaris* aggregates, possibly due to removal of a cross-linking divalent cation.

This was seen when unstained aggregates in the AB-stained sample (Fig. 3-11a), and blue aggregates in the CBB-stained sample (Fig. 3-11b), disappeared after Na_2EDTA addition. String-like blue particles, similar to ones found in the artificial seawater blank (Fig. 4a-b) were the predominant particles found in samples after Na_2EDTA addition. This suggests that CSP present in aggregates of *S. bacillaris* are bound together by divalent cations in the same way as TEP (Alldredge et al., 1993; Thorton and Thake, 1998).

Disruption of aggregates and decreases in TEP and CSP after the addition of Na_2EDTA, as seen visually by FlowCAM and as measured spectrophotometrically (Fig. 3-12), indicate that there may be crosslinking between divalent cations (especially Ca^{2+}) and acidic polysaccharides forming TEP, and proteins forming CSP. Thus Ca^{2+} bonding may be involved not only in TEP formation as suggested previously (Alldredge et al., 1993; Thornton & Thake, 1998; Thornton, 2004), but also in CSP formation. This suggests that similar to TEP, CSP can be formed abiotically from protein-rich dissolved precursors linked by ionic bonding; however, we did not directly test this here.

3.5 Vertical and seasonal distribution of gel particles in Sargasso Sea.

Transparent gel particles, TEP and CSP, were most abundant in the upper 100 m of the Sargasso Sea water column. TEP concentrations ranged from 21.5±1.9 to 56.7±3.4 μg XG eq L^{-1} in the upper 100 m of the water column, and decreased with depth to a minimum of 16.6±1.9 μg XG eq L^{-1} (Fig. 3-13). The highest TEP concentration was always found in the shallowest sample taken, usually 50 m (Fig. 3-14). TEP concentrations were uniformly low, below 100 m, except in February 2012 when a secondary maximum was present at 2000 m. TEP concentrations varied slightly over the year, being lowest during May (2012) and June (2013) (Fig. 3-13).

CSP concentration ranged between 3.2±0.7 to 22.4±0.4 μg BSA eq L^{-1} in the upper 100 m. Maximum CSP concentrations were between 70 and 100 m (Fig. 3-13), which coincided with the Chl *a* fluorescence maximum (Fig. 3-15) and with the highest concentration of total particles measured with the FlowCAM (Fig. 3-13). CSP concentrations, as well as total number of particles, increased near the seafloor, which coincided with the presence of a strong nepheloid layer observed below 4000 m, during May, 2012 and June, 2013 cruises (Fig. 3-13). Recent studies have suggested that aggregation of picoplankton may contribute largely to the transport of organic carbon from the surface to the deep ocean (e.g., Richardson and Jackson 2007; Lomas and Moran 2011); aggregation and transport by fecal pellets have been proposed as possible mechanisms. Our results from *S. bacillaris* cultures show that aggregates of these cyanobacteria are enriched in CSP. This suggests that CSP may be transported to the deep ocean in association with particles, for example, as aggregates of CSP-enriched *Synechococcu*s. The concentrations of TEP and CSP were constant throughout the year and were always detectable, suggesting, as was proposed by Ding et al. (2008), that gel particles could be a source of carbon and nitrogen for bacterioplankton in oligotrophic systems.

Concentrations of TEP and CSP were quantified using semi-quantitative methods that were relative to different standards; therefore direct comparisons of the magnitude of their abundances cannot be made. However, comparisons on relative terms can be useful to study differences in their seasonal and vertical distributions. As far as we know, this is the first study that shows the vertical and seasonal distributions of CSP and compares this in parallel with TEP for open ocean samples. With that in mind, vertical distribution profiles of CSP and TEP measured in the Sargasso Sea were different from each other. CSP maximum concentrations always coincided with the Chl *a* fluorescence maximum, and for most cruises it was slightly

below the maximum TEP concentration. This supports the idea that TEP and CSP are different types of particles, and their abundances are dominated by different processes. As noted previously, there is no definitive method to know if the particles we observed are exclusively TEP or CSP or both (Long and Azam 1996; Engel and Passow 2001). Because of TEP's stickiness, it has been suggested that TEP can adsorb proteins (Engel and Passow 2001), thus it is possible that some gel-particles contain both polysaccharides and proteins. Nevertheless, our results indicate that in general, TEP and CSP may have similar origins; for instance, they might both be formed from precursors exuded by phytoplankton, but after particle formation follow different pathways.

It is also possible that the exudation of various precursors depends on environmental conditions and the type of dominant phytoplankton. Observations of the pure culture of *S. bacillaris* showed that this cyanobacteria formed aggregates enriched in CSP (Fig. 3-5f). *Synechococcus* spp. are major contributors to total primary productivity in the Sargasso Sea (Goericke and Welschmeyer, 1993). In oligotrophic oceans like the Sargasso Sea where cyanobacteria are an important contributor to primary productivity, CSP could be a source of nitrogen for microorganisms and even higher trophic levels. For example, Motwani and Goroknova (2013) demonstrated mesozooplankton grazing on *Synechococcus* spp. in the Baltic Sea. The formation of CSP-rich aggregates of *Synechococcus* may be a mechanism that allows higher trophic levels to feed on cyanobacteria. Thus we speculate that a possible cause for the different depth profiles of TEP and CSP may be that CSP are produced by cyanobacteria like S*ynechococcus* spp, while TEP may be formed by other phytoplankton, such as diatoms, dinoflagellates or cocolithophores. There is evidence that aggregates with high TEP: solid particle ratios have lower sinking velocities (or are even positively buoyant) (Azetsu-Scott and

Passow, 2004), and have lower excess density (Engel and Schartau, 1999). This could explain why TEP are always more abundant in shallower samples, i.e., the low concentrations of solid particles like large diatoms or ballast minerals in the Sargasso Sea could affect the direction and velocity of the vertical flux of TEP (Azetsu-Scott and Passow, 2004; Mari et al., 2007) allowing TEP accumulation in the surface of the ocean (Wurl et al., 2011).

4. Conclusions

This study investigated TEP and CSP from several different perspectives with the aim of learning if they are polysaccharide and proteinaceous sub-units of the same type of particle, or if they are different particles with distinct characteristics and behaviors. We have shown that TEP and CSP behaved like different particles in a diatom-dominated bloom during a mesocosm experiment, in microcosm experiments, marine algal cultures, and in samples from Sargasso Sea and a freshwater pond. The highest abundance of TEP and CSP occurred at different phases in the phytoplankton bloom. The highest TEP concentration was during the senescent phase, while the highest CSP concentration co-occurred with that of Chl *a*. Although we did not directly test if this timing difference was due to differences in production or degradation, our measurements of gel particle concentrations under both low and high bacteria concentrations in cultures of the diatom *T. weissflogii* and the cyanobacteria *S. bacillaris*, taken together with previous reports of higher bacteria densities associated with CSP than with TEP (Berman and Viner-Mozzini, 2001), suggest that higher bacteria concentrations might have caused a larger decrease in CSP than in TEP concentration. CSP might be more prone to bacterial degradation, possibly due to use of CSP as a nitrogen source after nutrient depletion.

The proposed technique for visualizing stained transparent material in unfiltered aqueous samples with the FlowCAM is a useful tool for qualitative study of acidic polysaccharides stained with Alcian Blue and for comparison with particles stained with Coomassie Brilliant Blue. Moreover, the FlowCAM method allows quantification of particles in freshwater, and a dialysis step added to the procedure may be useful in developing a quantitative method in the future for seawater samples. The visualization and imaging of TEP and CSP directly in parallel unfiltered water samples using FlowCAM led to new insights into the role of TEP and CSP in the aggregation of different phytoplankton species. Studying gel particles directly in water allows the visualization of particles without alterations to their shape and size as may occur with filtering techniques. Moreover, this method allows visualizing gel particles that may pass through a 0.2- 0.4 μm pore size filter due their flexibility, even though their apparent size is larger. Visual examination of TEP and CSP from diatom-dominated microcosms, diatom cultures, and freshwater samples showed that diatom aggregates are enriched in TEP. On the other hand, *S. bacillaris* cultures formed dense and compact aggregates that were stained with CBB, but not with AB, indicating that they were protein-rich, but depleted in acidic polysaccharides. Formation of CSP-rich aggregates by *Synechococcus* can be an important mechanism making cyanobacteria available to higher trophic levels and transporting CSP to the deep ocean in oligotrophic systems like the Sargasso Sea.

Vertical distributions of TEP and CSP were different in the Sargasso Sea. Both types of particles were more abundant in the upper 100 m of the water column, suggesting a common origin from phytoplankton precursors. However, higher abundances of TEP were always found in the shallowest sample collected, while the maximum concentration of CSP coincided with maximum Chl *a* fluorescence and total particle concentration. The difference in TEP and CSP

profile shapes and their relation with the total particle concentration indicates that after formation these particles follow different pathways and undergo different degradation and aggregation processes. The concentrations of gel particles, although relatively low, were constant throughout the year and always detectable, suggesting that gel particles might be a source of carbon and nitrogen for bacterioplankton in oligotrophic systems.

Overall, our results of net production, visual examination, and natural distribution of gel particles in the open ocean support the concept that TEP and CSP are different types of particles. We showed that they are formed by precursors exuded by phytoplankton, but did not reject the possibility that in the ocean they have a complex and diverse origin. We demonstrated that CSP, as well as TEP, are linked by cations; however, the role of hydrophobic interactions remains to be studied. Our results indicate that TEP and CSP interactions with phytoplankton and bacterioplankton communities can be much more complex in the field than in the laboratory, especially compared to a single species in culture. Future research that addresses the composition and role of these particles in specific ecosystems is needed to determine their real significance particularly in aquatic systems.

References

Alldredge, A.L., Passow, U., Logan, B., 1993. The abundance and significance of a class of large, transparent organic particles in the ocean. Deep-Sea Res. Part I 40(6), 1131-1140.

Alldredge, A.L., Passow, U., Haddock, H.D., 1998. The characteristics and transparent exopolymer particle (TEP) content of marine snow formed from thecate dinoflagellates. J. Plankton Res. 20(3), 393-406.

Aluwihare, L.I., Repeta, D.J., Chen, R.F., 1997. A major biopolymeric component to dissolved organic carbon in surface sea water. Nature 387, 166-169.

Aluwihare, L.I., Repeta, D.J., 1999. A comparison of the chemical characteristics of oceanic DOM and extracellular DOM produced by marine algae. Mar. Ecol. Prog. Ser. 186, 105-117.

Azetsu-Scott, K., Passow, U., 2004. Ascending marine particles: Significance of transparent exopolymer particles (TEP) in the upper ocean. Limnol. Oceanogr. 49(3), 741-748.

Berman, T., Viner-Mozzini, Y., 2001. Abundance and characteristics of polysaccharide and proteinaceous particles in Lake Kinneret. Aquat. Microb. Ecol. 24(3), 255-264.

Bidigare, R.R., Smith, R.C., Baker, K.S., Marra, J., 1987. Oceanic primary production estimates from measurements of spectral irradiance and pigment concentrations. Global Biogeoch. Cy. 1(3), 171-186.

Biddanda, B., Benner, R., 1997. Major contribution from mesopelagic plankton to heterotrophic metabolism in the upper ocean. Deep-Sea Res. Part I 44(12), 2069-2085.

Burd, A.B., Jackson, G.A., 2009. Particle aggregation. Annu. Rev. Mar. Sci. 1: 65.

Cisternas-Novoa, C., Lee, C., Engel, A., 2014. A semi-quantitative spectrophotometric, dye-binding assay for determination of Coomassie Blue stainable particles. Limnol. Oceanogr. Methods 12, 604-616.

Chin, W.-C., Orellana, M.V., Verdugo, P., 1998. Spontaneous assembly of marine dissolved organic matter into polymer gels. Nature 391, 568-572.

Comte, S., Guibaud, G., Baudu, M., 2006. Relations between extraction protocols for activated sludge extracellular polymeric substances (EPS) and EPS complexation properties: Part I. Comparison of the efficiency of eight EPS extraction methods. Enzyme Microb. Technol. 38(1–2): 237-245.

Decho, A.W., 1990. Microbial exopolymer secretions in ocean environments: Their role(s) in food web and marine processes. Oceanogr. Mar. Biol. Annu. Rev. 28, 73–153.

Ding, Y.-X. et al., 2008. Amphiphilic exopolymers from *Sagittula stellata* induce DOM self-assembly and formation of marine microgels. Mar. Chem. 112(1–2), 11-19.

Ding, Y.-X., Hung, C.-C., Santschi, P.H., Verdugo, P., Chin, W.-C., 2009. Spontaneous assembly of exopolymers from phytoplankton. Terr. Atmos. Ocean. Sci. 20(5), 741-745.

Engel, A., Schartau, M., 1999. Influence of transparent exopolymer particles (TEP) on sinking velocity of *Nitzschia closterium* aggregates. Mar. Ecol. Prog. Ser. 182, 69-76.

Engel, A., 2000. The role of transparent exopolymer particles (TEP) in the increase in apparent particles stickiness ([alpha]) during the decline of a diatom bloom. J. Plankton Res. 22, 485-497.

Engel, A., Passow, U., 2001. Carbon and nitrogen content of transparent exopolymer particles (TEP) in relation to their Alcian Blue adsorption. Mar. Ecol. Prog. Ser. 219, 1-10.

Engel, A., Thoms, S., Riebesell, U., Rochelle-Newall, E., Zondervan, I., 2004. Polysaccharide aggregation as a potential sink of marine dissolved organic carbon. Nature 428, 929-932.

Engel, A., Piontek, J., Grossart, H. P., Riebesell, U., Schulz, K. G., Sperling, M., 2014. Impact of CO_2 enrichment on organic matter dynamics during nutrient induced coastal phytoplankton blooms. J. Plankton Res. 36, 641-657.

Gärdes, A., Iversen, M.H., Grossart, H.-P., Passow, U.,Ullrich, M.S., 2011. Diatom-associated bacteria are required for aggregation of *Thalassiosira weissflogii*. ISME J. 5, 436-445.

Goericke, R.,Welschmeyer, N.A., 1998. Response of Sargasso Sea phytoplankton biomass, growth rates and primary production to seasonally varying physical forcing. J. Plankton Res. 20, 2223-2249.

Grossart, H.P., Simon, M., Logan, B., 1997. Formation of macroscopic organic aggregates (lake snow) in a large lake: the significance of transparent exopolymer particles, phytoplankton, and zooplankton. Limnol. Oceanogr. 42, 1651-1659.

Guillard, R.R.L. and Ryther, J.H., 1962. Studies on marine planktonic diatoms I. *Cyclotella nana* Hustedt and *Denotula confervaceae* (Cleve) Gran. . Can. J. Microbiol., 8: 229-239.

Guo, L., Santschi, P.H., 1997. Composition and cycling of colloids in marine environments. Rev. Geophys. 35, 17-40.

Hayat, M.A., 2000. Positive staining. In: M.A. Hayat (Editor), Principles and Techniques of Electron Microscopy: Biological Applications. Cambridge Univ. Press.

Jackson, G.A., 1995. TEP and coagulation during a mesocosm experiment. Deep-Sea Res. Part II 42(1), 215-222.

Kahl, L., Vardi, A., Schofield, O., 2008. Effects of phytoplankton physiology on export flux. Mar. Ecol. Prog. Ser. 354, 3-19.

Kiørboe, T., Hansen, J.L.S., 1993. Phytoplankton aggregate formation: observations of patterns and mechanisms of cell sticking and the significance of exopolymeric material. J. Plankton Res. 15(9), 993-1018.

Kiørboe, T., Saiz, E., Viitasalo, M., 1996. Prey switching behavior in the planktonic copepod *Acartia tonsa*. Mar. Ecol. Prog. Ser. 143, 65-75.

Logan, B.E., Passow, U., Alldredge, A.L., Grossart, H.-P. ,Simon, M., 1995. Rapid formation and sedimentation of large aggregates is predictable from coagulation rates (half-lives) of transparent exopolymer particles (TEP). Deep-Sea Res. Part II 42(1), 203-214.

Lomas, M.W., Moran, S.B., 2011. Evidence for aggregation and export of cyanobacteria and nano-eukaryotes from the Sargasso Sea euphotic zone. Biogeosciences 8(1): 203-216.R

Long, R., Azam, F., 1996. Abundant protein-containing particles in the sea. Aquat. Microb. Ecol. 10(3), 213-221.

Mantoura, R.F.C., Llewellyn, C.A., 1983. The rapid determination of algal chlorophyll and carotenoid pigments and their breakdown products in natural waters by reverse-phase high-performance liquid chromatography. Anal. Chim. Acta 151(0), 297-314.

Mari, X., Burd, A.B., 1998. Seasonal size spectra of transparent exopolymeric particles (TEP) in a coastal sea and comparison with those predicted using coagulation theory. Mar. Ecol. Prog. Ser. 163, 63-76.

Mari, X., 1999. Carbon content and C,N ratio of transparent exopolymeric particles (TEP) produced by bubbling exudates of diatoms. Mar. Ecol. Prog. Ser. 183, 59-71.

Mari, X. et al., 2007. Water residence time: A regulatory factor of the DOM to POM transfer efficiency. Limnol. Oceanogr. 52(2), 808-819.

Martin, P. et al., 2011. Export and mesopelagic particle flux during a North Atlantic spring diatom bloom. Deep Sea Res. Part I 58(4), 338-349.

Motwani, N.H., Gorokhova, E., 2013. Mesozooplankton grazing on picocyanobacteria in the Baltic Sea as inferred from molecular diet analysis. PLOS ONE 8(11), e79230.

Passow, U., Alldredge, A., 1994. Distribution, size and bacterial colonization of transparent exopolymer particles (TEP) in the ocean. Mar. Ecol. Prog. Ser. 113(1-2), 185-194.

Passow, U., Alldredge, A.L., Logan, B.E., 1994. The role of particulate carbohydrate exudates in the flocculation of diatom blooms. Deep Sea Res. Part I 41(2), 335-357.

Passow, U., Alldredge, A.L., 1995a. Aggregation of a diatom bloom in a mesocosm: The role of transparent exopolymer particles (TEP). Deep Sea Res. Part II 42(1), 99-109.

Passow, U. and Alldredge, A.L., 1995b. A dye-binding assay for the spectrophotometric measurement of transparent exopolymer particles (TEP). Limnol. Oceanogr. 40(7), 1326-1335.

Passow, U., 2000. Formation of transparent exopolymer particles, TEP, from dissolved precursor material. Mar. Ecol. Prog. Ser. 192, 1-11.

Passow, U., et al., 2001. The origin of transparent exopolymer particles (TEP) and their role in the sedimentation of particulate matter. Cont. Shelf. Res. 21(4), 327-346.

Passow, U., 2002a. Production of transparent exopolymer particles (TEP) by phyto- and bacterioplankton. Mar. Ecol. Prog. Ser. 236, 1-12.

Passow, U., 2002b. Transparent exopolymer particles (TEP) in aquatic environments. Prog. Oceanogr. 55(3-4), 287-333.

Pedrotti, M. et al., 2010. Effects of nutrients and turbulence on the production of transparent exopolymer particles: a mesocosm study. Mar. Ecol. Prog. Ser. 419, 57-69.

Piontek, J. et al., 2009. Effects of rising temperature on the formation and microbial degradation of marine diatom aggregates. Aquat. Microb. Ecol. 54(3): 305-318.

Prieto, L. et al., 2002. Scales and processes in the aggregation of diatom blooms: high time resolution and wide size range records in a mesocosm study. Deep Sea Res. Part I 49(7), 1233-1253.

Richardson, T.L., Jackson, G.A., 2007. Small phytoplankton and carbon export from the surface ocean. Science 315(5813): 838-840.

Riemann, L., Steward, G.F., Azam, F., 2000. Dynamics of bacterial community composition and activity during a mesocosm diatom bloom. Appl. Environ. Microbiol. 66(2): 578-587.

Stoderegger, K.E., Herndl, G.J., 1999. Production of exopolymer particles by marine bacterioplankton under contrasting turbulence conditions. Mar. Ecol. Prog. Ser. 189, 9-16.

Sieracki, C.K., Sieracki, M.E., Yentsch, C.S., 1998. An imaging-in-flow system for automated analysis of marine microplankton. Mar. Ecol. Progr. Ser. 168, 285-296.

Sun, M., Aller, R.C., Lee, C., 1991. Early diagenesis of chlorophyll-a in Long Island Sound sediments: A measure of carbon flux and particle reworking. J. Mar. Res. 49, 1-23.

Thornton, D.C.O., Thake, B., 1998. Effect of temperature on the aggregation of *Skeletonema costatum* (Bacillariophyceae) and the implication for carbon flux in coastal waters. Mar. Ecol. Prog. Ser. 174, 223-231.

Thornton, D.C.O., 2004. Formation of transparent exopolymeric particles (TEP) from macroalgal detritus. Mar. Ecol. Prog. Ser. 282, 1-12.

Thornton, D.C.O., Fejes, E.M., DiMarco, S.F., Clancy, K.M., 2007. Measurement of acid polysaccharides in marine and freshwater samples using alcian blue. Limnol. Oceanogr. Methods 5: 73-87.

Underwood, G.J.C., Boulcott, M., Raines, C.A., Waldron, K., 2004. Environmental effects on exopolymer production by marine benthic diatoms: dynamics, changes in composition, and pathways of production. J. Phycol. 40(2), 293-304.

Verdugo, P. et al., 2004. The oceanic gel phase: a bridge in the DOM–POM continuum. Mar. Chem. 92(1–4), 67-85.

Verdugo, P., 2012. Marine microgels. Ann. Rev. Mar. Sci. 4(1), 375-400.

Wells, M.L., Goldberg, E.D., 1991. Occurrence of small colloids in sea water. Nature 353(6342), 342-344.

Wotton, R., 2004. The Essential Role of Exopolymers (EPS) in Aquatic Systems. Oceanogr. Mar. Biol. Annu. Rev. 42, 57-94.

Wurl, O., Miller, L., Vagle, S., 2011. Production and fate of transparent exopolymer particles in the ocean. J. Geophys. Res. 116: C00H13.

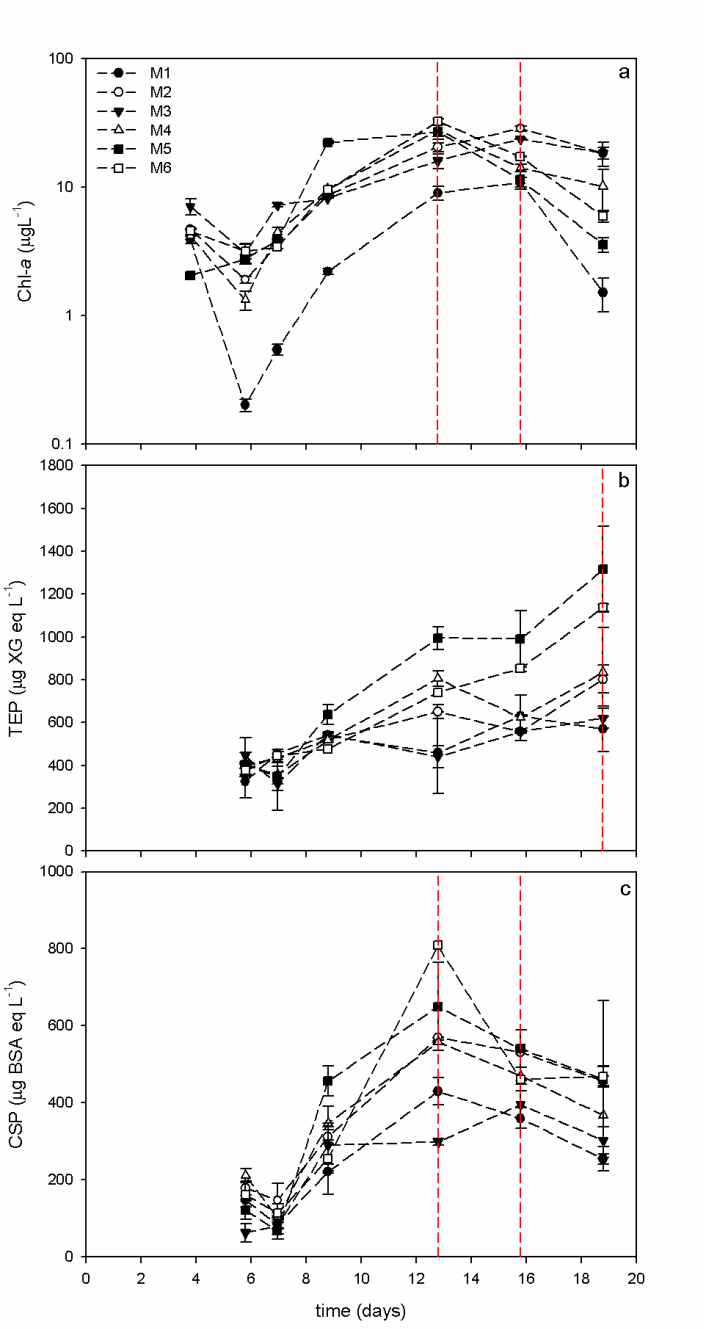

Figure 3-1. Chl a (a), TEP (b), and CSP (c) concentrations during the development of the nutrient-induced phytoplankton bloom in six mesocosm tanks (M1 to M6). Red lines indicate the highest concentration. The error bars around the means correspond to the range of the measured values (n = 2).

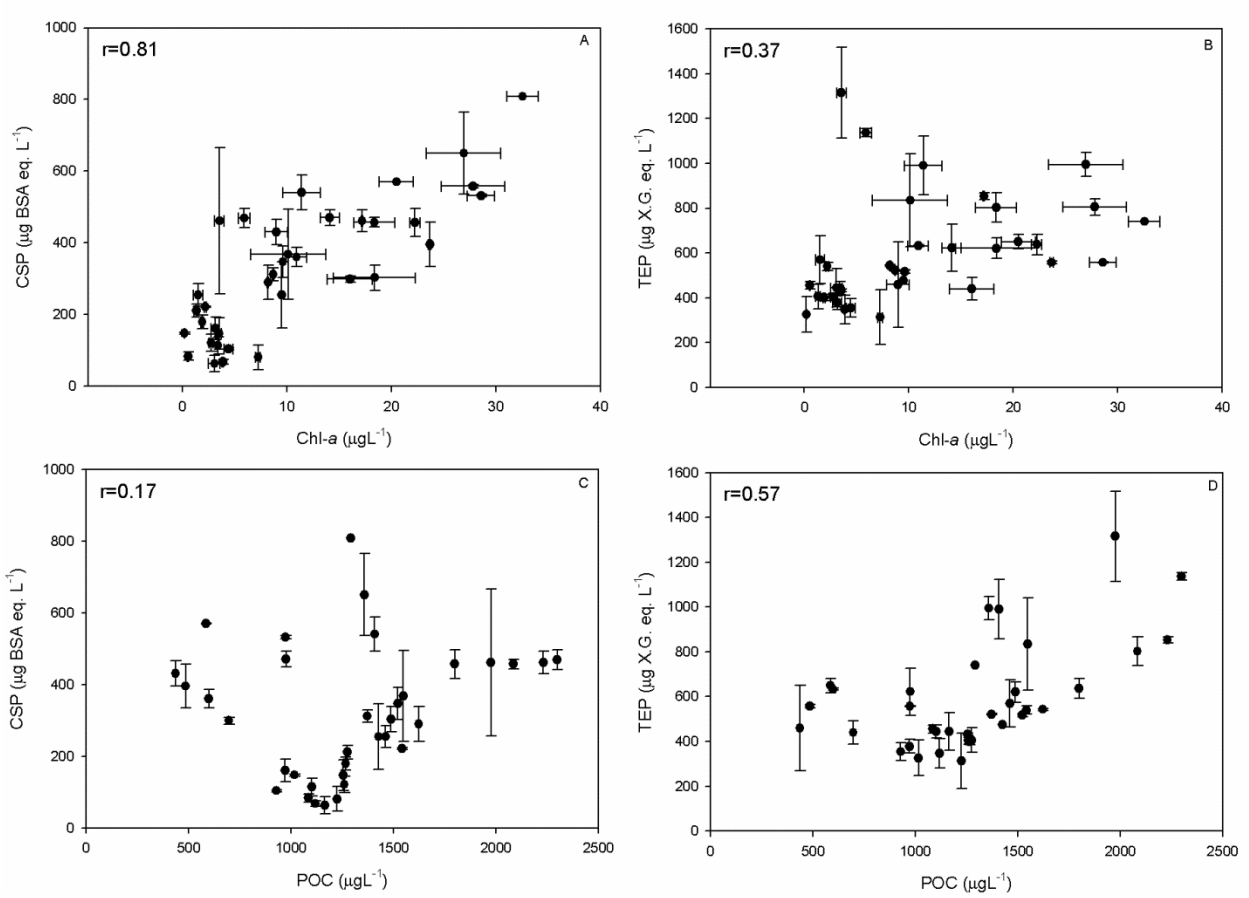

Figure 3-2. Relationship of gel particles with potential drivers of their distribution. (a) CSP versus Chl *a*; (b) TEP versus Chl *a*; (c) CSP versus POC; (d) TEP versus POC. The error bars around the means correspond to the range of the measured values (n = 2).

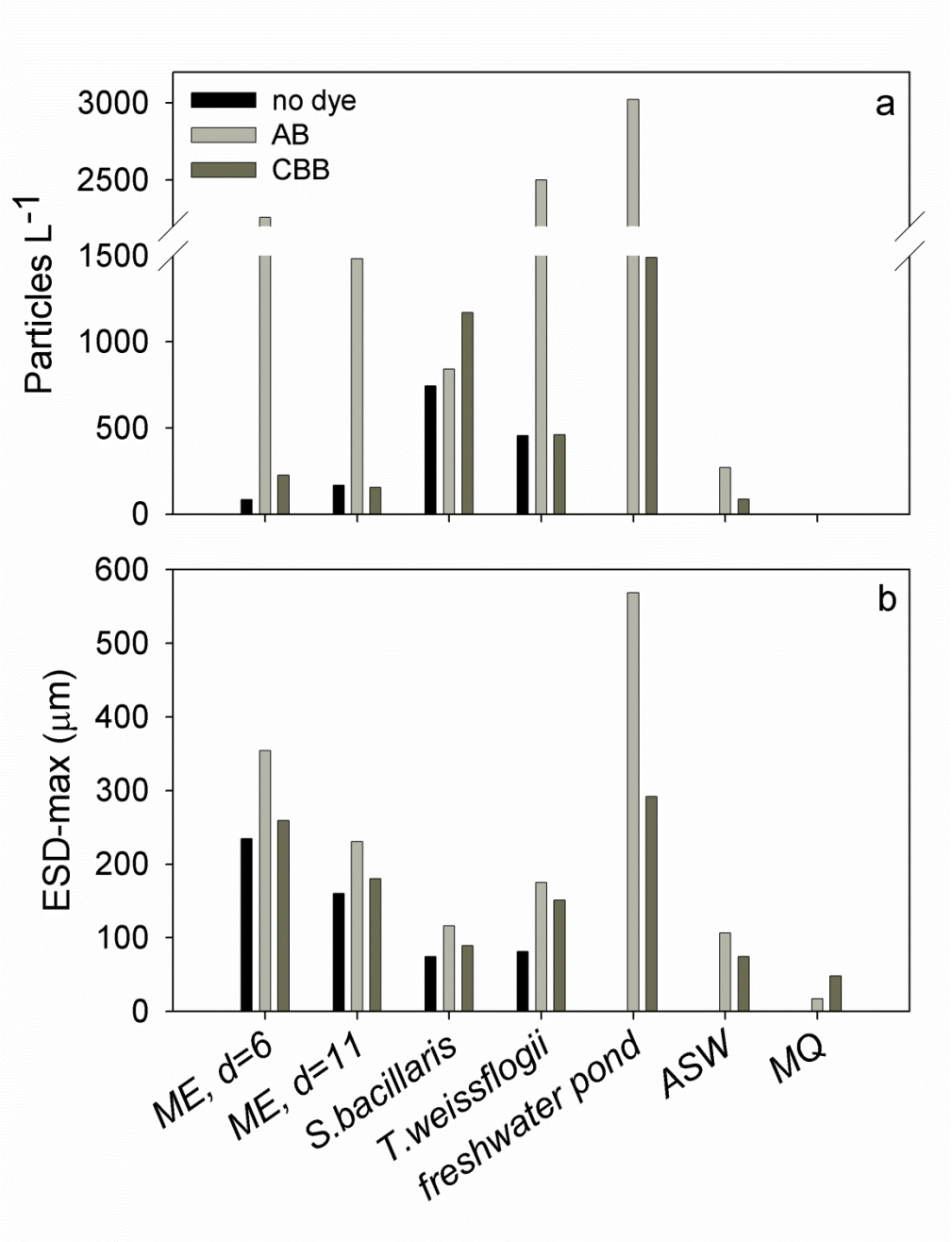

Figure 3-3. Particle concentration (a) and maximum equivalent spherical diameter (ESD-max) (b), determined by FlowCAM in samples from a microcosm experiment during the exponential phase of a diatom dominated bloom (ME, d=6), during the stationary phase, (ME, d=11); cultures of *T.weissflogii* and *S. bacillaris* with low bacteria (LB) concentrations; a freshwater pond, and 0.2 μm pre-filtered artificial seawater (ASW).

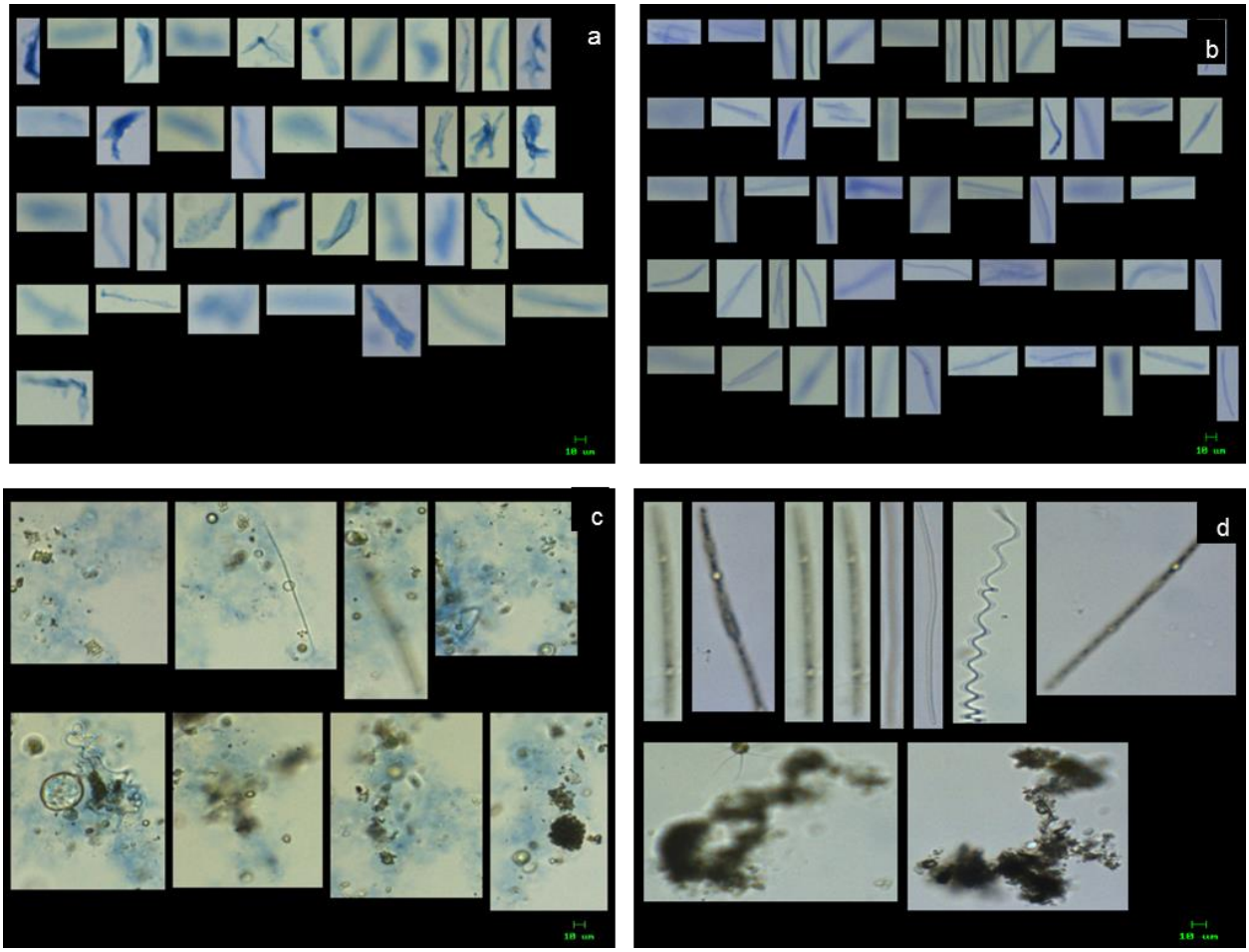

Figure 3-4. Images captured by the FlowCAM and sorted by equivalent spherical diameter to show the size range of particles and aggregates in artificial seawater (ASW, a-b) and freshwater (c-d). Samples were stained with Alcian Blue (AB) and Coomassie Brilliant Blue (CBB) to visualize TEP and CSP, respectively. (a) AB-stained 0.2 μm pre-filtered ASW. (b) CBB-stained ASW. (c) AB-stained freshwater from a pond. (d) CBB-stained freshwater from a pond.

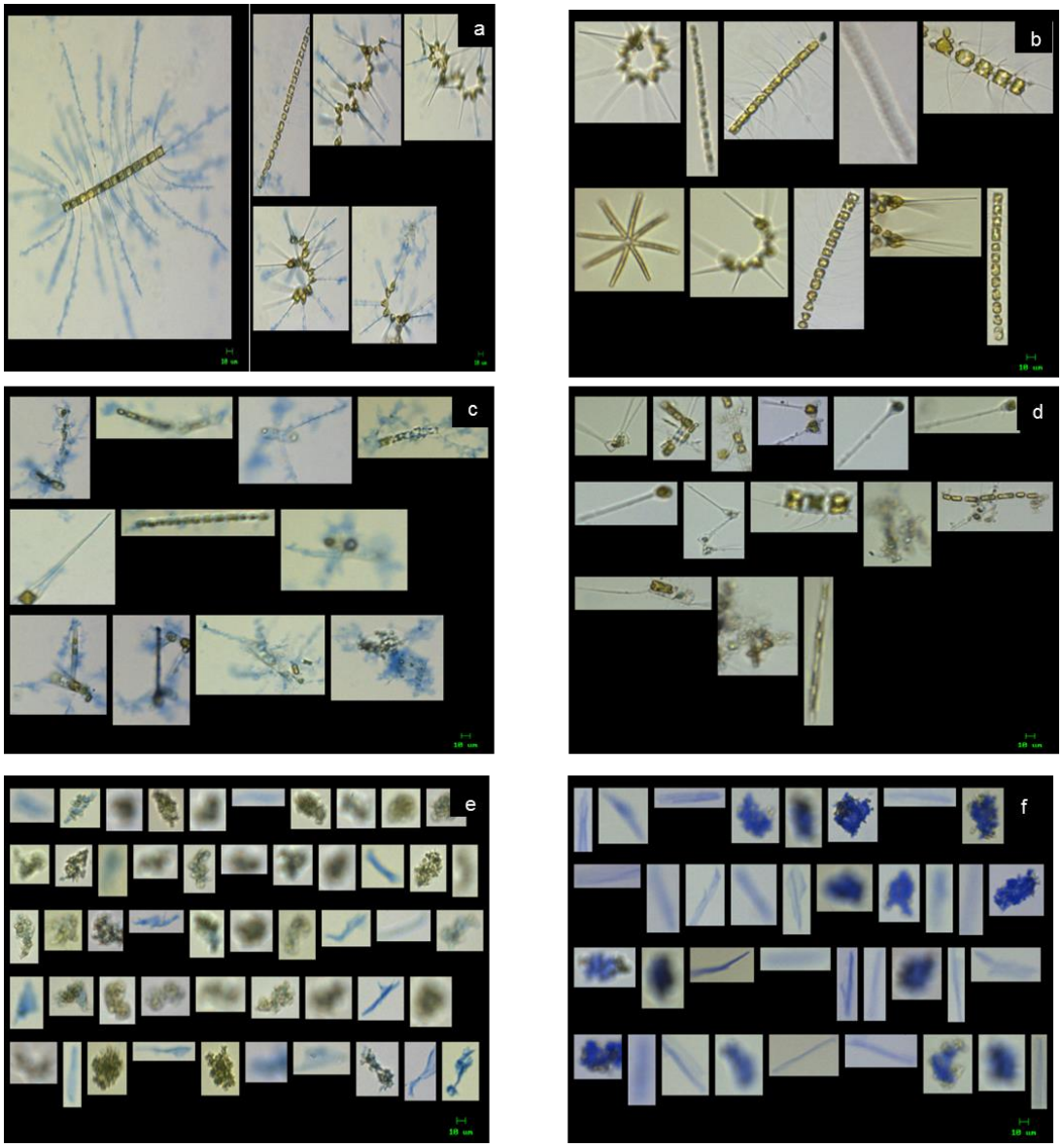

Figure 3-5. Images captured by the FlowCAM and sorted by equivalent spherical diameter to show largest particles and aggregates. Samples were stained with Alcian blue (AB) and Coomassie brilliant blue (CBB) to visualize TEP and CSP respectively. (a) AB-stained sample from the microcosm experiment (ME, d=6). (b) CBB-stained sample from ME, d=6; (c) AB-stained sample from the stationary phase of the microcosm experiment (ME, d=11). (d) CBB-stained sample from ME, d=11; (e) AB-stained sample from cultures of *S. bacillaris* with low bacteria (LB) concentration. (f) CBB-stained sample from LB cultures of *S. bacillaris*.

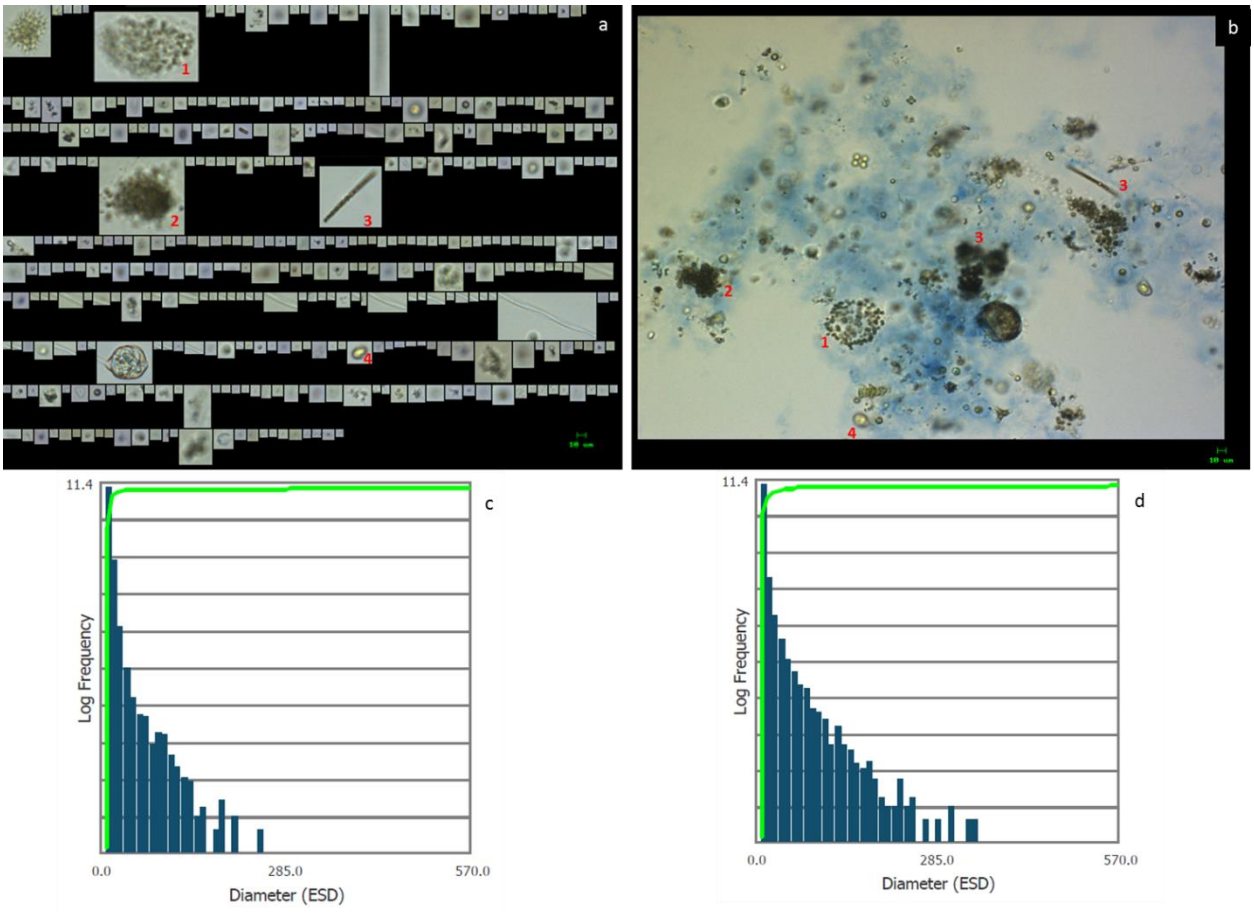

Figure 3-6. Freshwater pond collage of images captured by FlowCAM showing how staining changes the size distribution of particles. (a) CBB-stained sample (which looks the same like the unstained for this sample); images of individual cells and smaller detrital particles are observed; (b) AB-stained sample: a single larger aggregate is shown, although the scale is the same (green bar: 10μm) as in (a). Red numbers represent cells and smaller particles that were photographed and counted as individual particles before staining (a) and after AB-staining (b) when they (or similar particles) appear embedded in TEP and are recognized by the FlowCAM as a single particle. Histogram of equivalent spherical diameter (ESD) in μm versus particle frequency in (c) the CBB-stained sample, and (d) the AB-stained sample.

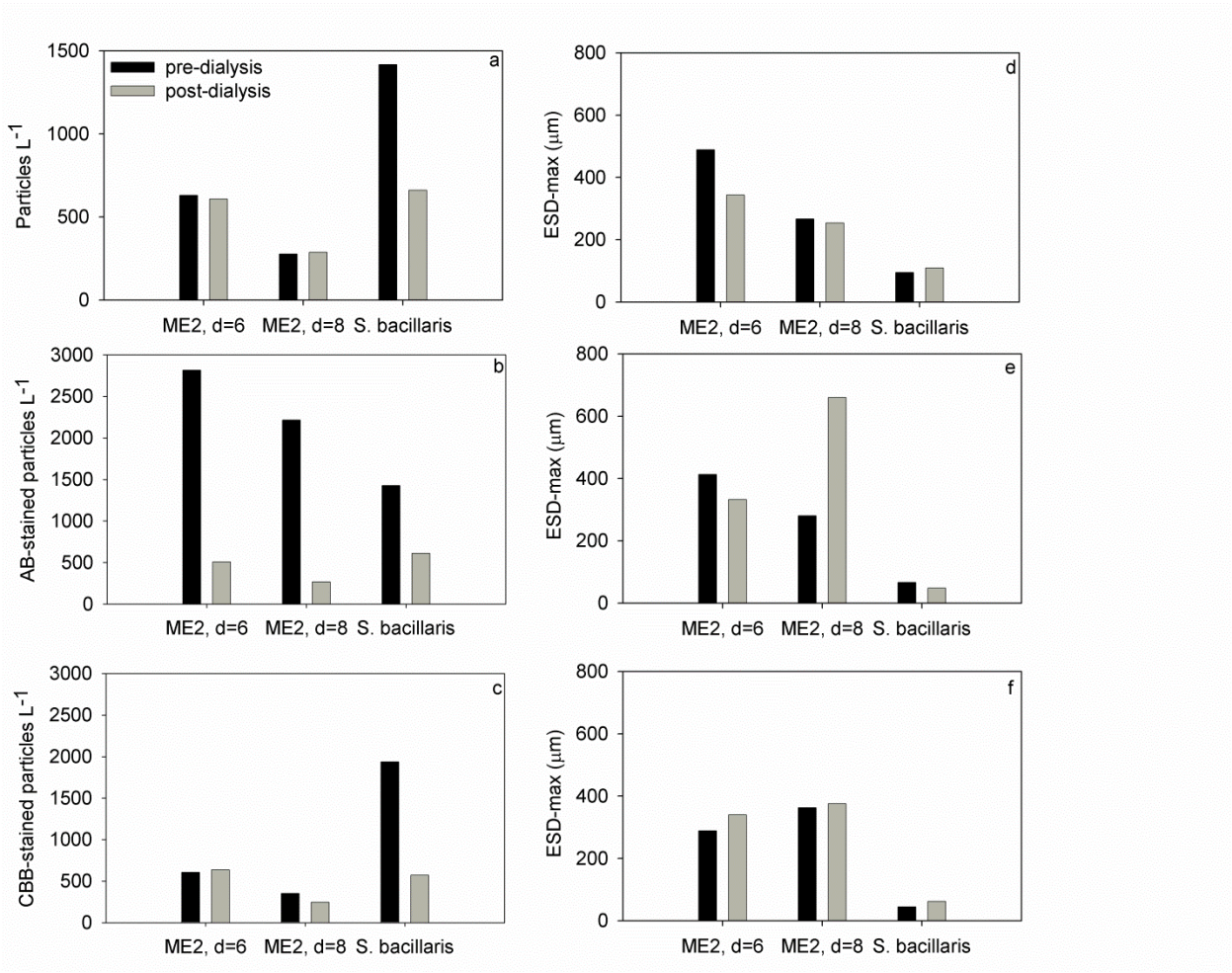

Figure 3-7. Particle concentration and maximum equivalent spherical diameter (ESD-max), determined by FlowCAM in samples pre- and post- dialysis from a microcosm experiment during day 6 (ME2, d6), and day 8 (ME2, d8) and from a *S. bacillaris* culture. (a) Particle concentration in unstained samples; (b) AB-stained particle concentration; (c) CBB-stained particle concentration; (d) ESD-max in unstained samples; (e) ESD-max in AB-stained sample and (f) ESD-max in CBB-stained sample.

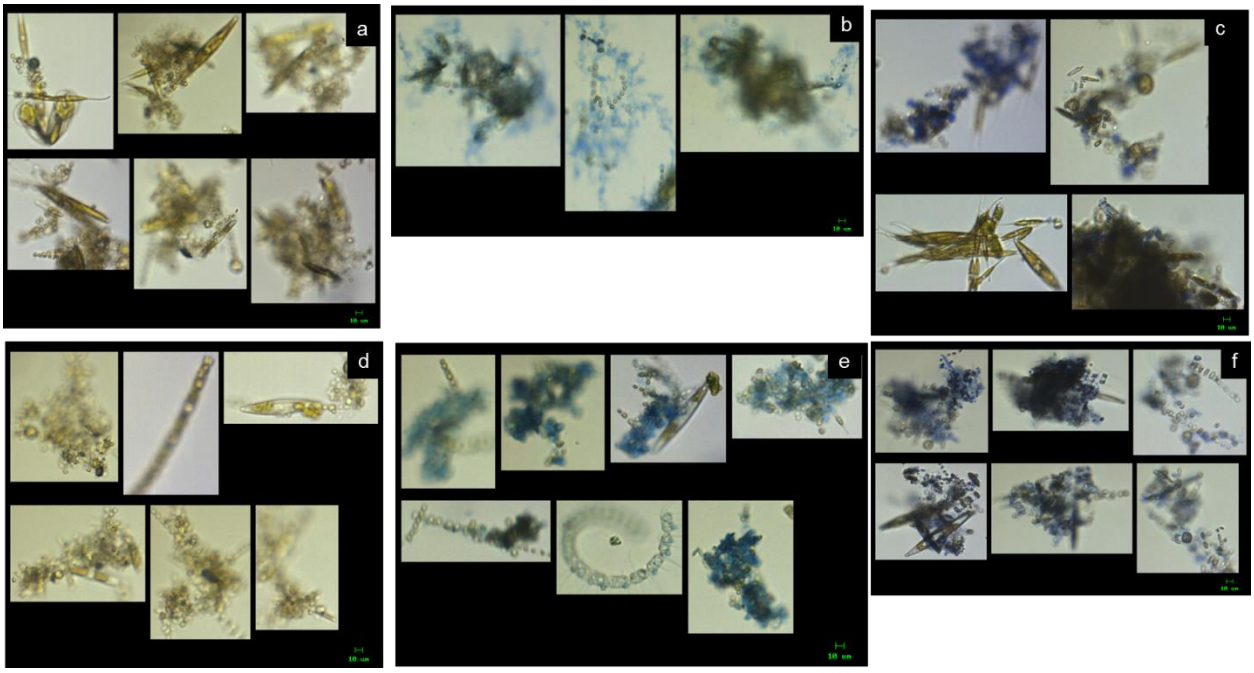

Figure 3-8. Images captured by the FlowCAM and sorted by equivalent spherical diameter (ESD) to show largest particles and aggregates before and after dialysis in samples from a microcosm experiment day 8 (ME2, d8). (a) Unstained sample, pre-dialysis; (b) AB-stained sample pre-dialysis; (c) CBB-stained sample pre-dialysis; (d) unstained sample, post-dialysis; (e) AB-stained sample post-dialysis and (f) CBB-stained sample post-dialysis.

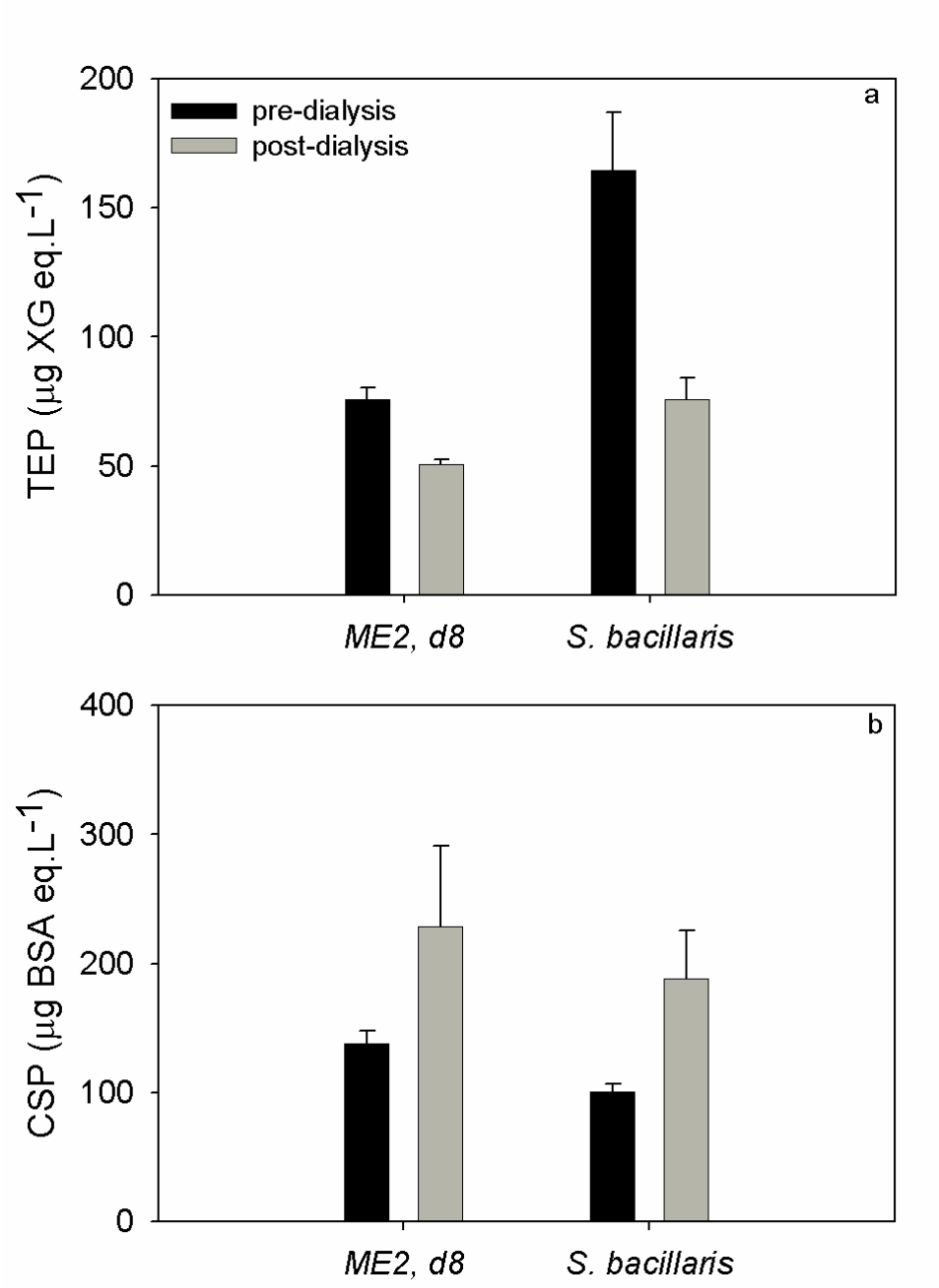

Figure 3-9. Concentration of TEP (a) and CSP (b) on microcosm experiment day 8 (ME2, d8), and in the *S. bacillaris* culture before (black) and after (gray) dialysis. The error bars around the means correspond to the range of the measured values (n = 2).

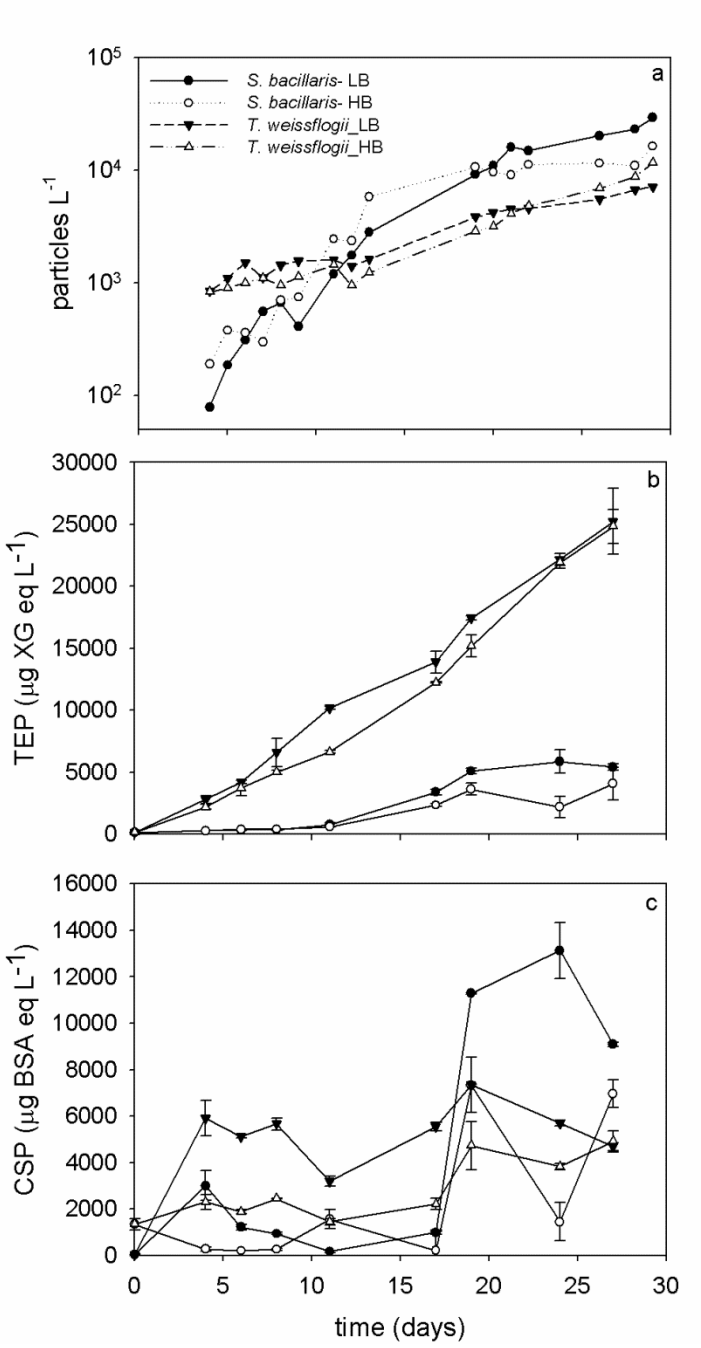

Figure 3-10. (a) Total particle concentration, (b) concentration of TEP and (c) CSP with low bacteria (LB; black symbols) and high bacteria (HB; white symbols) concentration for cultures of *T. weissflogii* (triangles) and *S. bacillaris* (circles).

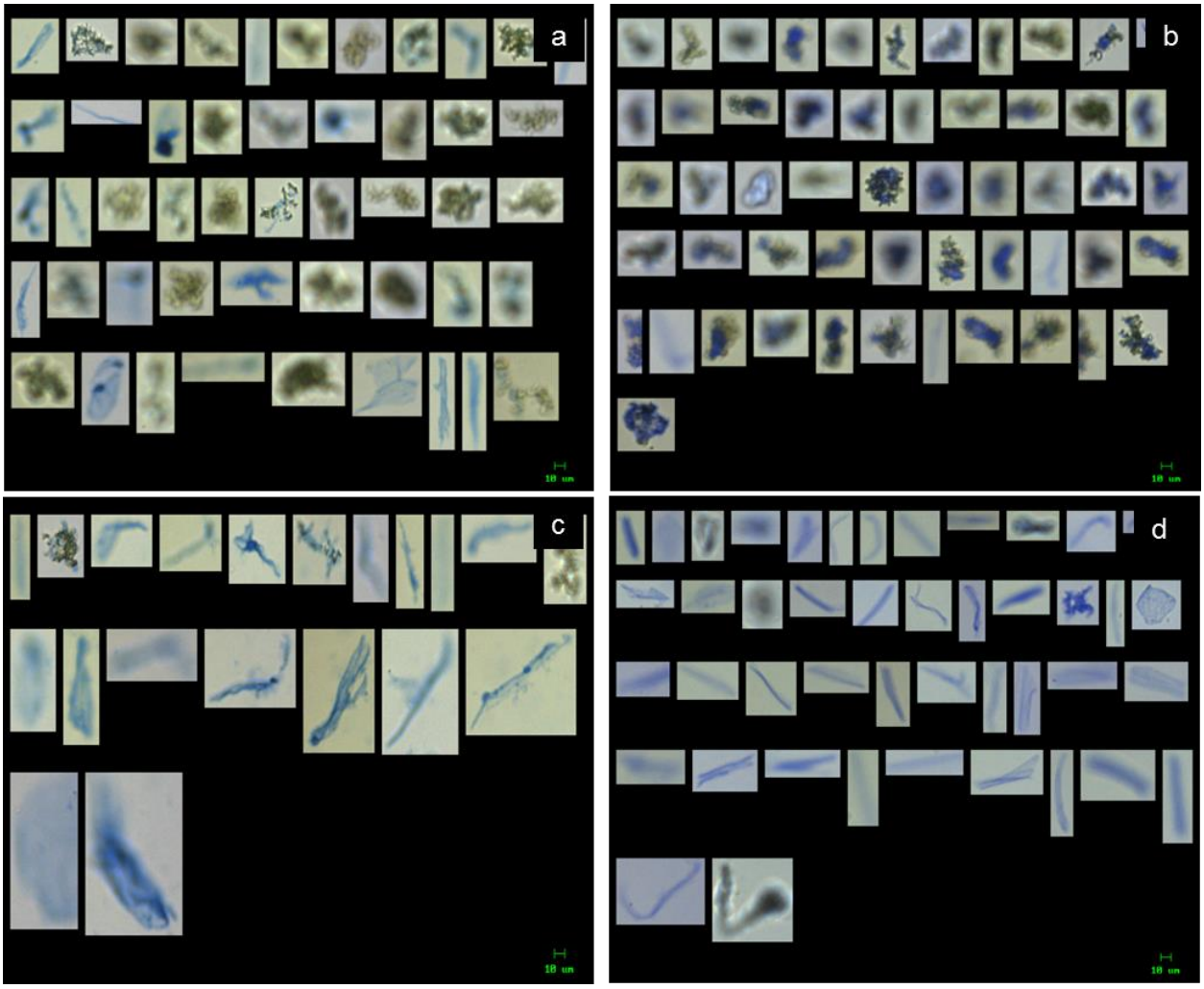

Figure 3-11. Images from a *S. bacillaris* culture, captured by the FlowCAM and sorted by equivalent spherical diameter (ESD) to show aggregates. (a) AB-stained aggregates of *S. bacillaris;* (b) CBB-stained aggregates of *S. bacillaris;* (c) AB-stained aggregates of *S. bacillaris* previously treated with the chelating agent Na_2EDTA; (d) CBB-stained aggregates of *S. bacillaris* previously treated with Na_2EDTA.

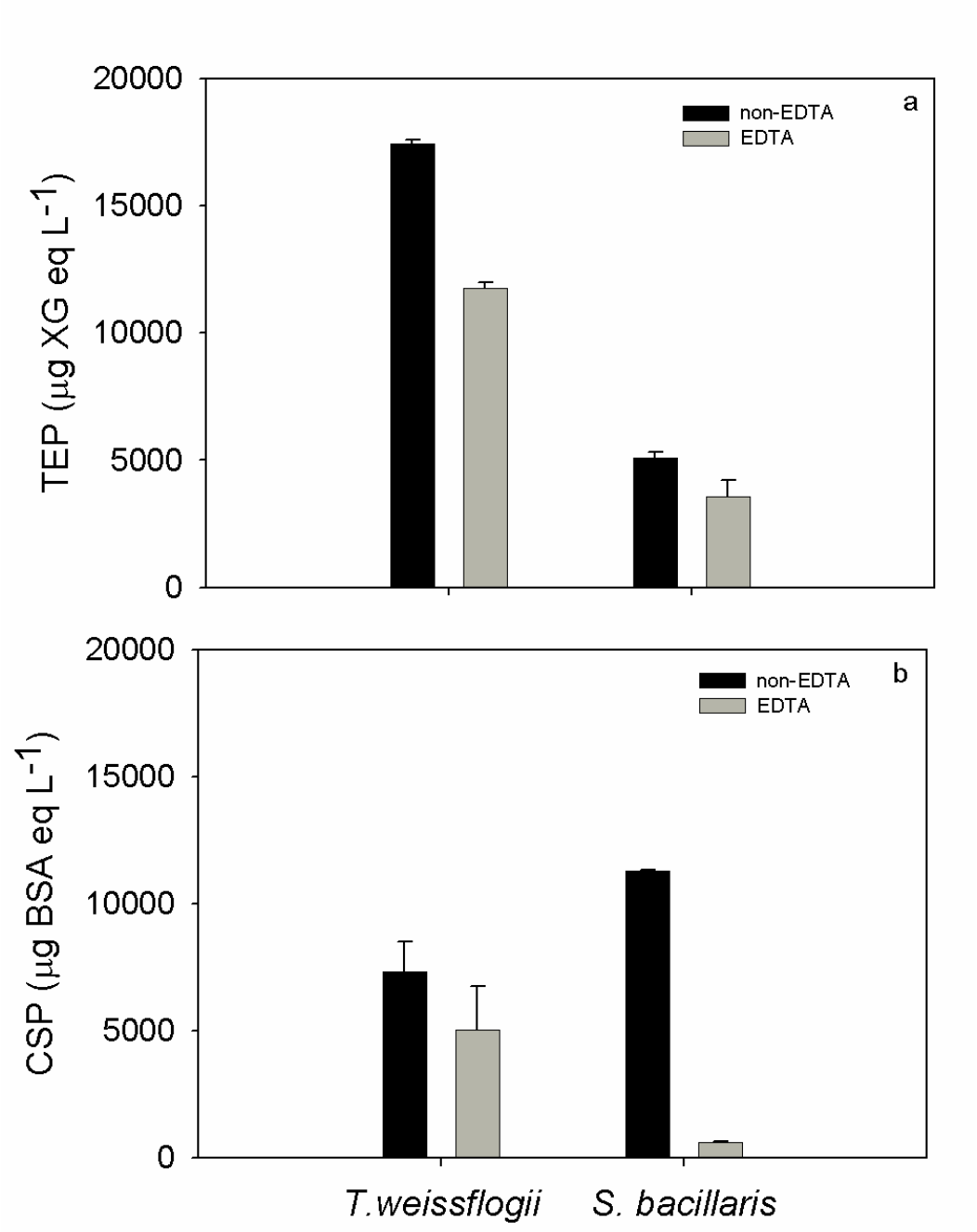

Figure 3-12. Concentration of TEP (a) and CSP (b) in cultures of *T. weissflogii* and *S. bacillaris* with low bacteria (LB) concentrations before (black) and after (gray) Na_2EDTA addition. The error bars around the means correspond to the range of the measured values (n=2).

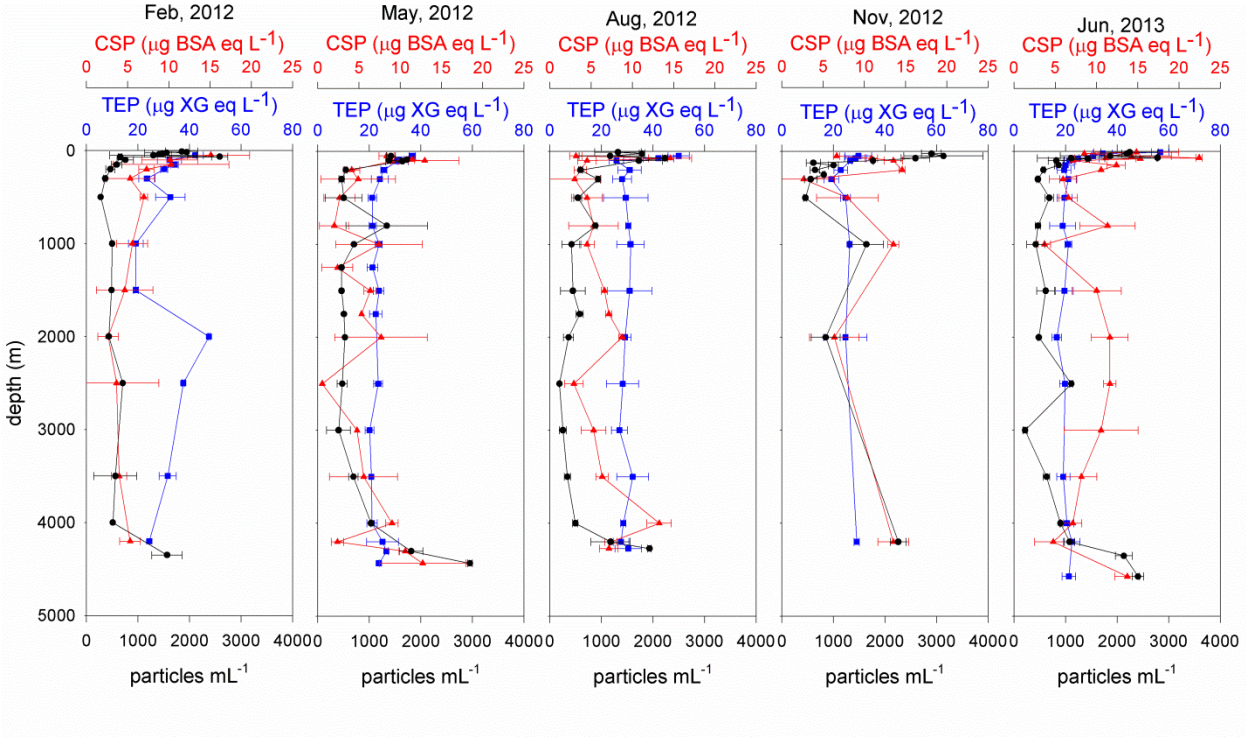

Figure 3-13. Vertical and temporal distribution of TEP (blue-square), CSP (red-triangle), and particles determined by FlowCAM (black-circle) at a site on the Bermuda Rise during five research cruises in 2012-2013.

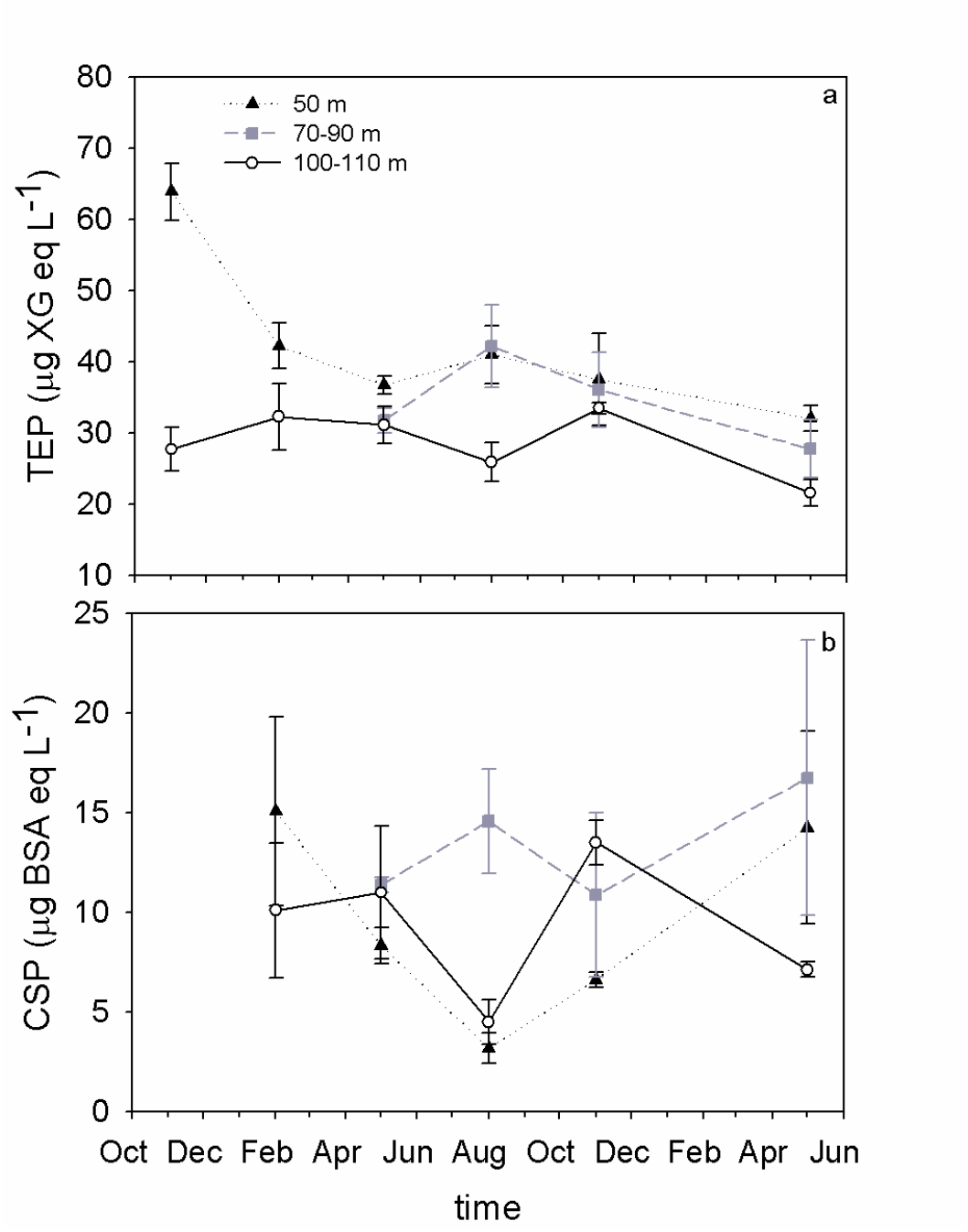

Figure 3-14. Distribution of TEP (a) and CSP (b) from February 2012 to June 2013 at 50 m (black-triangle), 70-90 m (gray-square) and 100-110 m (white-circle) at the Bermuda Rise site. The error bars around the means correspond to the standard deviation of the measured values (n=2 or n=4).

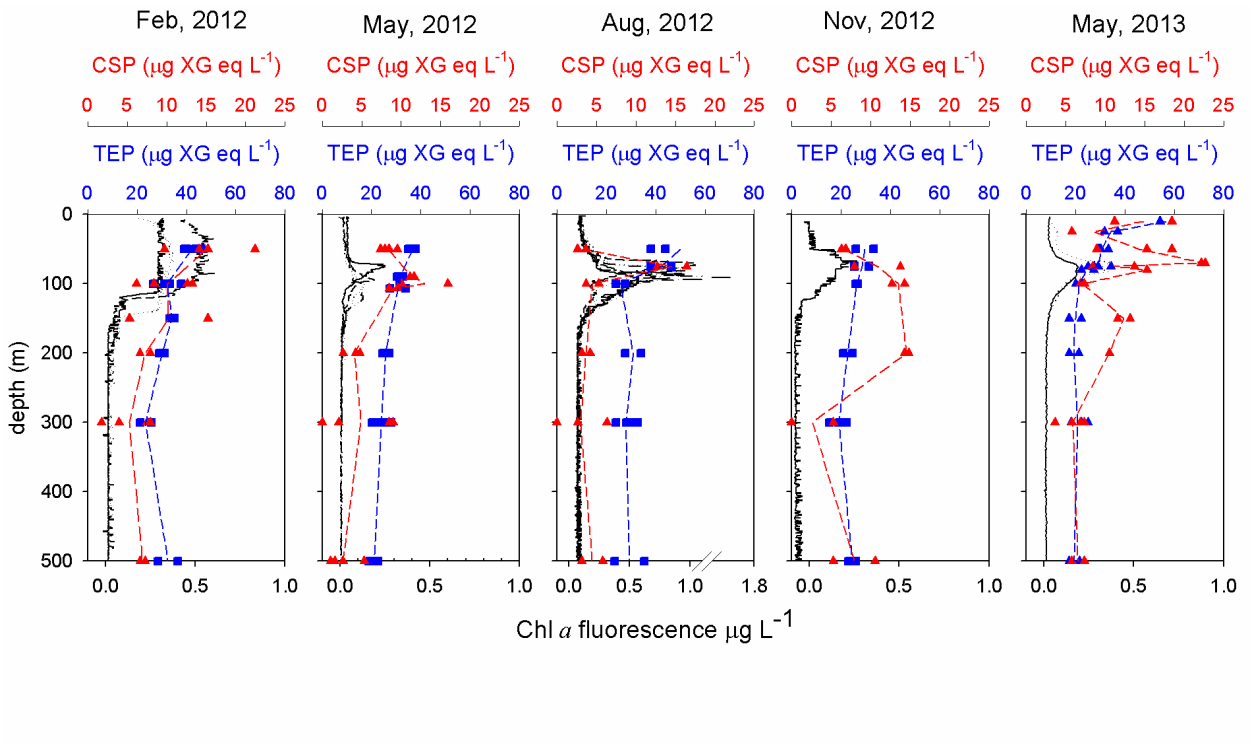

Figure 3-15. Vertical and temporal distributions of CTD/Chl *a* fluorescence (black-line), TEP (blue-square), and CSP (red-triangle) at a site on the Bermuda Rise during five research cruises in 2012-2013.

Table 3-1: Abbreviations

AB	Alcian blue
BSA	Bovine serum albumin
CBB	Coomassie brilliant blue
Chl *a*	Chlorophyll *a*
CSP	Coomassie stainable particles
DOC	Dissolved organic carbon
DOM	Dissolved organic matter
EPS	Exopolymeric Substances
ESD	Equivalent spherical diameter
HB	High bacteria concentration
HPLC	High-pressure liquid chromatography
LB	Low bacteria concentration
MWCO	Molecular weight cut-off
TEP	Transparent exopolymeric particles
PIC	Particulate inorganic carbon
POC	Particulate organic carbon
XG	Xanthan gum

Chapter 4 :

Effects of Higher CO_2 and Temperature on Gel Particle Composition and Physical Properties of Diatom Aggregates: Results from Mesocosm and Aggregation Experiments

Abstract

The effects of elevated CO_2 concentration and temperature were studied in nutrient-induced phytoplankton blooms in indoor mesocosms with surface seawater collected from Stony Brook Harbor, NY. At various times during the blooms, aggregation experiments in roller tanks were conducted using seawater from the differently-treated mesocosms. We measured phytoplankton biomass, particulate organic carbon and nitrogen production, and gel particle concentrations in the mesocosms. We measured sinking velocity, size, excess density and gel particle (TEP and CSP) content of aggregates formed in the roller tanks. No significant differences between treatments were observed in overall nutrient uptake, Chl-*a* concentration, gel particle concentration or aggregate formation, abundance or composition. However, the roller tank experiments showed that aggregates formed during the bloom peak at higher CO_2 and the present temperature were smaller and had lower sinking velocity than aggregates formed under present CO_2 conditions. We suggest that the effect of CO_2 on aggregate properties may vary at different stages of the phytoplankton bloom and that these variations should be considered in making conclusions about effects of the future ocean on the biological pump. The absence of a clear CO_2 effect during these mesocosm experiments may be more representative of coastal environments, which naturally have a wide range of temperature and CO_2 conditions and are dominated by diatoms that have low sensitivity to high CO_2 and temperature, and might not be directly applicable to open ocean environments.

1. Introduction

Rising atmospheric CO_2 has led to increases in global temperature and ocean acidification. Future elevated temperature and CO_2 conditions will affect rates of key phytoplankton processes, such as primary production (Rost et al., 2008; Egge et al., 2009), growth (Feng et al., 2008), calcification (Gattuso et al., 1998; Riebesell et al., 2000; Langdon, 2003; Delille, 2005; Rost et al., 2008), nitrogen fixation (Rost et al., 2008), and production of extracellular material (Engel, 2002; Kim et al., 2011; Engel et al., 2014). Responses of plankton species to increases in CO_2 concentration and temperature have been analyzed in manipulative experiments over the last two decades; however fewer studies have addressed the synergistic effects of warming and acidification on phytoplankton (e.g., Borchard et al., 2011), organic matter (Borchard and Engel 2012; Kim et al., 2011; Chen et al., 2015) and aggregation (Seebah et al., 2014).

Sinking particles, such as marine snow and aggregates of marine detritus and phytoplankton, are the main mechanisms for vertical transport and sequestration of carbon (e.g., Alldredge and Jackson 1995; Honjo, 2008; Turner 2002, 2015). Aggregation of phytoplankton cells can be assisted by the presence of highly sticky transparent exopolymeric particles, TEP (Alldredge et al., 1993), and presumably Coomassie stainable particles, CSP (Long and Azam 1996), although it has been suggested that CSP would have less impact on the formation of marine aggregates than TEP (Prieto et al., 2002).

In the last 250 years, ocean pH has fallen by 0.1 unit and is expected to fall another 0.3 - 0.4 units by the year 2100 if the burning of fossil fuels continues at current rates (Caldeira and Wickett, 2003), causing increases in aqueous CO_2 and total inorganic carbon concentrations and decreases in pH, carbonate ion concentration and calcium carbonate saturation (Doney et al.,

2009). Lower $CaCO_3$ saturation levels may affect the sinking velocity of marine aggregates, and the efficiency of export due to a decrease in the ballast component (Armstrong et al., 2002; Klaas and Archer, 2002), leading to less sinking of aggregates. On the other hand, it has been hypothesized that under elevated CO_2 conditions, both CO_2 uptake and DOC exudation by phytoplankton will increase, leading to higher concentrations of gel particles since they originate from dissolved precursors (Verdugo 2012). Higher abundances of gel particles, such as TEP and CSP, might enhance aggregation and the POC flux into the deep ocean (Arrigo, 2007).

Mesocosm experiments using natural seawater have shown that under elevated CO_2 concentrations (i.e., 750 to 1000 ppm of CO_2), the consumption of DIC by phytoplankton increases, and the net production of POC and PON related to the consumption of DIC and nitrate decreases (Engel, 2005; Riebesell et al., 2007). This lower net production of POC and PON under elevated concentrations of CO_2 may be due to carbon overconsumption (relative to N) that results in an increase in the release of carbon-rich TEP precursors and thus TEP formation, with the consequent loss of both POC and PON as sinking aggregates from the surface layer (Engel, 2005; Riebesell et al., 2007). Recent studies have in fact shown higher TEP concentrations under elevated CO_2 conditions (Engel et al., 2014). However, not all experiments show a direct relationship between elevated CO_2 levels and higher TEP production (Egge et al., 2009), or between higher TEP and greater aggregation and particle sinking (Seebah et al., 2014).

Mari (2008) found that TEP formed under low pH conditions are larger in size, but more positively buoyant, than those formed at higher pH, and this increased buoyancy resulted in an upward flux of TEP-latex bead aggregates; he suggested that the excess of organic matter produced at high CO_2 conditions might accumulate in the surface microlayer instead of sinking. However, Passow (2012) suggested that these changes in TEP size and concentration were due to

changes in total alkalinity (TA), rather than to ocean acidification, since the acidification method used was addition of strong acid, which alters pH and TA without modifying DIC; she argued that if TA is not altered, elevated CO_2 conditions do not directly affect abiotic formation of TEP. There is no information on how acidification may affect CSP concentration and stickiness or on the relationship between CSP and POC or PON.

The increase in the global mean sea surface temperature is expected to be 1.8 - 4.0°C for the 21st century depending on the emission scenario (Solomon et al., 2007). Experimental evidence reveals that responses to elevated temperature and acclimation ability vary significantly between phytoplankton species (Claquin et al., 2008); temperature affects TEP production in three species of diatoms (*Thalassiosira pseudonana*, *Skeletonema marinoi,* and *Pseudo-nitzschia fraudulenta*) and in two species of *Isochrysis*, but not in in *Emiliania huxleyi* and *Lepidodinium chlorophorum*. Additionally, incubation experiments in the Southern Ocean show that extracellular dissolved photosynthate production increases by 54% when temperature is increased from ambient (-1.4 to 0.4°C) to 2°C (Moran et al., 2006). Chemostat experiments with both elevated CO_2 and temperature show reduction in the growth rate of *Emiliania huxleyi*, but enhanced DOC exudation and formation of TEP, aggregates, and POC (Borchard et al., 2011). The effect of temperature on CSP production remains unknown.

Not all experimental evidence agrees on how higher CO_2 and temperature will affect aggregate formation and the efficiency of the biological pump. Mesocosm experiments, investigating effects of warming, or acidification and warming together, show an enhancement of the DOC: POC production ratio, but a decrease in the sinking and sequestration of organic carbon into the deep ocean (Wohlers et al., 2009; Kim et al., 2011). However, Piontek et al. (2009) showed that elevated temperature increased not only aggregation, probably due to higher

TEP concentrations, but also bacterial activity and remineralization. The effect of ocean acidification and warming on aggregation and carbon export varies depending on the dominant phytoplankton groups. On one hand, the effect of elevated CO_2 on aggregation has been found to be negligible in the absence of changes in biologically produced particle concentration in diatom-dominated environments (Passow et al., 2014); on the other hand aggregates produced by calcifiers like *Emiliania huxleyi* showed low excess density in high CO_2 treatments due to the reduction of the ballasting calcite (Biermann and Engel; 2010).

We studied the effects of ocean acidification and warming in nutrient-induced phytoplankton blooms in three indoor mesocosm experiments with surface water collected from Stony Brook Harbor, NY. Aggregation experiments were conducted using phytoplankton growing at different temperature and CO_2 conditions in the mesocosms. We measured phytoplankton biomass, organic carbon production, and gel particle concentrations in the mesocosms, as well as sinking velocity, size, excess density and gel particle (TEP and CSP) content of aggregates in the aggregation experiments, to determine the impact that warming and acidification together will have on aggregates formed during a natural coastal phytoplankton bloom dominated by diatoms.

2. Methods

2.1 Experimental Set-up

2.1.1 Mesocosm experiments

Three controlled mesocosm experiments were conducted to study the effect of ocean acidification and increased temperature, together and separately, on phytoplankton growth, community structure, gel particle concentration (Transparent Exopolymer Particles, TEP, and Coomassie Stainable Particles, CSP), and aggregation (Fig.1).

During the first mesocosm experiment (ME1), conducted at the Flax Pond Marine Laboratory of Stony Brook University during July 2011, nine tanks (~1 m^3) were filled simultaneously with coastal seawater from Stony Brook Harbor after filtration through a 200-μm size mesh to remove large detritus and zooplankton. Two sets of triplicate mesocosms were manipulated to simulate a future ocean: CO_2 concentration 750 ppm, and 16°C (acidified-cooler temperature, AC); CO_2 concentration 750 ppm, and 20°C (acidified-warmer temperature, AW); and control mesocosms in triplicate with CO_2 concentration 390 ppm, and 16°C (present CO_2-cooler temperature, PC). Triplicate mesocosms are designated A, B, and C (e.g., AC-A, AC-B, AC-C). The desired future CO_2 concentration (750 ppm) was achieved by addition of high-CO_2 seawater, rather than by bubbling, to avoid the formation of gel particles due to bubbling. The pH corresponding to 750 ppm was calculated using the program CO2SYS (Lewis and Wallace et al., 1998); pH was monitored once a day to determine the amount of high-CO_2 seawater added (between 1 and 2 L every 24 h). Room temperature was controlled and relatively constant at 20°C; the tanks at 16°C were cooled by circulating cold water (4°C) through silicone tubes installed inside the tanks. As a light source, pairs of fluorescent lights (F40T12, full spectrum) were suspended above each tank, providing a surface irradiance of 190 μmol photons m^{-2} s^{-1} with a light: dark cycle of 14: 10. Irradiance was set at the beginning of each experiment with a LICOR Model LI-2100 light meter. All mesocosms were slowly stirred by mechanically controlled paddles. After 5 days of stabilization, nutrients (20 μM nitrate, 20 μM silicate and 1.5 μM phosphate) were added to the tanks to initiate a phytoplankton bloom; the dominant species in the bloom were chain-forming diatoms such as *Skeletonema* spp. and *Chaetoceros* spp., and solitary diatoms like *Rhizosolenia* sp. and *Ditylum* sp. The bloom was monitored for 21 days to

study aggregation; during this period the tanks were sampled six times, and four roller tank experiments were conducted: pre-bloom (t1), bloom (t2 and t3), and post-bloom (t4) (see below).

A second mesocosm experiment (ME2) using 200-µm filtered coastal seawater from Stony Brook Harbor was conducted during August 2011in the same facility and under the same light regime. After one day of stabilization, nutrients (40 µM nitrate, 40 µM silicate and 2.5 µM phosphate) were added to the tanks to initiate a phytoplankton bloom. For this experiment one sets of triplicate mesocosms was manipulated to simulate future CO_2 (750 ppm) concentration and 16°C (acidified-cooler temperature, 2AC), and a second set of triplicate mesocosms was maintained as a control at present CO_2 concentration (390 ppm) and 16°C (present CO_2-cooler temperature, 2PC). After nutrient addition, the development and decline of the resulting phytoplankton bloom was monitored for 12 days. The tanks were sampled three times: pre-bloom (t1), bloom (t2), and post-bloom (t3), and three roller tank experiments were conducted at those times to study aggregation.

A third mesocosm experiment (ME3) using 200-µm filtered coastal seawater from Stony Brook Harbor took place during June 2012. This experiment was performed in the greenhouse facility of Flax Pond Laboratory at Stony Brook, where natural light was used and the air temperature was not controlled (i.e., it varied with outside temperature). Irradiance was measured in each tank at the beginning of the experiment with a LICOR Model LI-2100 light meter. Eight tanks (~1 m^3) were filled simultaneously, and mesocosms were slowly stirred by mechanically controlled paddles. Four different treatments were tested in duplicate: a) future CO_2 concentration (750 ppm) at ~21°C (acidified-cooler temperature, 3AC), b) future CO_2 concentration (750 ppm) at ~25°C (acidified-warmer temperature, 3AW), c) present CO_2 concentration (380 ppm) and ~25°C (present CO_2 -warmer temperature, 3PW) and d) a control

with present CO_2 concentration (380 ppm) and ~21°C (present CO_2-cooler temperature, 3PC). The temperature difference between the warm tanks and the cool tanks was not constant, but always around 2 degrees and the absolute values of temperature (measured twice daily) varied naturally with the outside air temperature. The desired future CO_2 (750 ppm) concentration was achieved by addition of high-CO_2 seawater as described above; pH was monitored twice a day, and the amount of high-CO_2 seawater required was larger than in the previous experiments (between 2 and 6L every 24 hours) because of the higher temperatures.

After 5 days of temperature and pH stabilization, nutrients were added for 4 consecutive days to obtain concentrations in the mesocosm of 40 µM nitrate, 40 µM silicate and 2.5 µM phosphate on day 6, and 20 µM nitrate, 20 µM silicate and 1.25 µM phosphate on days 7-9. The development and decline of the resulting natural phytoplankton bloom was monitored for 30 days; during this period the tanks were sampled six times, and roller tank experiments were conducted at 5 of these times: bloom (t1), and post-bloom (t2, t3, t4, t5) to study aggregation. Because of the lack of good temperature control, the use of natural light and the higher addition of nutrients in this experiment compared to ME1 and ME2, the phytoplankton bloom generated in ME3 is not comparable with ME1 and ME2. Moreover, the treatments and sampling times were different and further replication of this experiment is needed; therefore ME3 will be not be discussed here. Relevant data will be included as supplementary material.

2.2 *Roller tank experiments*

Aggregation under different CO_2 and temperature conditions was studied in roller tank experiments. Roller tank experiments were performed with water from the mesocosms during different stages of the phytoplankton bloom during each of the 3 mesocosm experiments

described above (Fig. 1). For each aggregation experiment, roller tanks were filled with water from each mesocosm, and incubated on a roller table to promote aggregate formation (Shanks and Edmonson, 1989). Each roller tank had a volume of 5 L; they were incubated in the dark and rotated at 0.8 rpm. After 24 to 48 h the roller tanks were sampled for two fractions: a) aggregates (AGG) removed with a serological pipet and b) surrounding seawater (SSW) as in Engel et al. (2009a). Briefly, on each sampling day, each rotating roller tank was filmed for 10 min; these videos were analyzed at a later time to determine physical parameters of the aggregates. Then, the roller tank was removed from the roller table, and the particles were allowed to settle for 20 min; the upper lid was removed and the temperature and pH of the roller tank water measured. After that the SSW was sampled with a Tygon tube by gravity into a 2-L Nalgene bottle. Then, visible aggregates (i.e., > 0.5 mm) were carefully removed with a 10-ml serological pipette using medium suction. The volume of several aggregates at a time was measured inside the pipette before the aggregates were transferred to a 1-L Nalgene bottle. This process was repeated until all the aggregates were removed. The volume of aggregates collected was between 5 and 160 mL. Then, 0.2-μm filtered seawater was added to the aggregates to a final volume of 300 mL so that there was enough sample to split for all the analyses. The sample was gently mixed before filtration of separate aliquots for the various analyses.

For calculation of different particulate parameters, such as chlorophyll *a* (Chl- *a*), particulate organic carbon (POC), transparent exopolymeric particles (TEP) and Coomassie stainable particles (CSP), it is important to consider that the AGG fraction also contains some SSW, and this mixture is called slurry (SL). To obtain a conservative value of the AGG fraction, the concentration of the particulate constituent in the SSW fraction was subtracted from that in the

slurry (Engel et al., 2009a); in this way the concentration of each parameter can be reported per liter of tank water.

2.3 Determination of aggregate size and settling velocity in the roller tanks

The size of aggregates and their settling velocity within the roller tanks were determined by video recording aggregates in a 5-L roller tank of 23-cm diameter and 13-cm height. The rotation speed was 0.8 rpm. After rotating for 24 to 48 h in the dark, aggregates were recorded for 10 min. The area captured by the video was a rectangle 4.2 cm wide x 3.1 cm high located about 5 to 6 cm from the center of the tank. Single pictures were captured from the video every second using the public domain software Free Studio, version 6.5 (Video to JPG converter v. 5.0.57) and analyzed according to Engel and Schartau (1999) and Engel et al. (2009b). Between 10 and 20 random aggregates from each roller tank were analyzed; several aggregate parameters such as area, length of the major axis, length of the minor axis, the x-feret diameter and position in the x-y plane, were measured semi-automatically using the public domain ImageJ software, and were used to estimate aggregate dimensions and settling velocity according to Engel and Schartau (1999). The equations used to determine the physical properties of aggregates are briefly described below.

2.3.1 Size determination

The visible volume (V) of aggregate was calculated as the volume of an equivalent ellipsoid $V = 4/3\pi abc$, where a is the major axis and b and c are the minor axes. The equivalent spherical diameter (ESD) was calculated as $ESD = 2(3V/4\pi)^{1/3}$ (Ploug et al., 2010). The area of the aggregate perpendicular to the fall direction (Ap) was calculated using $Ap = \pi (d_f)^2/4$, where d_f is the x-ferret diameter.

2.3.2 Sinking velocity determination

The aggregate sinking velocity (U_{AG}) was determined from its apparent velocity (U*), which can be estimated from the vertical displacement ($\Delta y_{1,2}$) of the aggregate with time (t), $U^{*}=\Delta y_{1,2}/\Delta t_{1,2}$. Then $U_{AG} = \omega\overline{x_{1,2}} + U^{*}$, where ω is the angular velocity of the fluid (s^{-1}), and $\overline{x_{1,2}}$ is the average position of the aggregate along the x-axis.

2.3.3 Excess density determination

The excess density of individual aggregates ($\Delta\rho_{AG}$) was calculated from their sinking velocity (U_{AG}, cms^{-1}). The theoretical sinking velocity of an aggregate in fluids reflects the balance between the drag force and gravity (Alldredge and Gotschalk, 1988) following the equation $U_{AG} = (2g(\rho_{AG} - \rho_{fl})V/(C_D\rho_{fl}A_P))^{0.5}$, where g is gravity ($981cm\ s^{-2}$), ρ_{AG} is the density of the aggregate, ρ_{fl} is the density of the fluid, V is the visible aggregate volume, Ap is the area perpendicular to the fall direction, and C_D is the drag coefficient calculated at higher (>0.5) Reynolds numbers (Re) as $C_D = 95(\mathrm{Re})^{-1.85}$. Here Re = dU_{AG}/v, where d is the particle diameter and v is the kinematic viscosity. The kinematic viscosity is the quotient of the dynamic viscosity (ζ), which depends on the salinity and temperature, and the density of the fluid (ρ_{fl}). The excess density ($\Delta\rho_{AG}$) of the aggregate is ρ_{AG}-ρ_{fl}, and its value for marine snow ranges between 10^{-2} and 10^{-5} gcm^{-3}. Aggregates are four times less dense than a single phytoplankton cells due to their higher porosity (Alldredge and Gotschalk, 1988).

2.4 Biological and chemical analysis

2.4.1 Total alkalinity (TA) and dissolved inorganic carbon (DIC)

During mesocosm experiment 3, samples for TA and DIC were collected every other day and analyzed the same day. TA and DIC samples from mesocosm experiments 1 and 2 were stored too long before analysis. TA was measured by titration (Gran, 1952) with 0.1N HCl solution using a Gilmont micrometer burette and an Orion model 370 pH meter. DIC was measured by the flow injection analysis method (Hall and Aller, 1992). Other CO_2 system variables ($CO_2; HCO_3^-$) were calculated using the CO2SYS program (http://cdiac.ornl.gov/ftp/co2sys/) (Lewis and Wallace, 1998).

2.4.2 pH and temperature (T)

pH and T values were measured at least once a day using YSI Pro 1030 waterproof handheld meters and standard DIN/NBS buffers (PL 4, PL 7 and PL 9) recalibrated using Tris-based reference material provided by A. Dickson (http://andrew.ucsd.edu/co2qc/).

2.4.3 Chlorophyll a (Chl- a) and particulate organic carbon (POC)

Concentrations of chlorophyll *a* (Chl- *a*) were determined by ion-pairing reverse-phase high-performance liquid chromatography (HPLC) (Mantoura and Llewellyn, 1983; Bidigare et al., 1985; Sun et al., 1991). Briefly, between 20 and 50-mL samples were filtered onto combusted GF/F filters in duplicate and frozen until analysis. Chl- *a* was extracted from filters by sonication in HPLC-grade 100% acetone; two successive 5-mL extracts were combined and filtered through a 0.2-µm Zetapor membrane. Samples were covered with aluminum foil to protect them from light during handling and analysis. Chl- *a* was separated from other chloropigments by HPLC on a 5-µm Adsorbosphere C-18 column (Sun et al., 1991). Chl- *a* was detected by fluorescence (excitation λ=440 nm, emission λ=660 nm) and was identified and quantified using an authentic standard (Sigma-Aldrich).

Particulate organic carbon (POC) contents were quantified using a Carlo Erba EA-1112 CNS analyzer (uncertainty ±2% for C and ±5% for N analysis). Samples of 20-50 mL were filtered onto combusted GF/F filters in duplicate. PIC was not removed because preliminary analysis showed negligible differences in POC between HCl-treated and non-treated samples. The mesocosm experiment was dominated by diatoms, with a minimum presence of PIC.

2.4.4 Transparent gel particles: TEP and CSP

TEP and CSP were analyzed spectrophotometrically after staining with a solution of 0.02% AB (Alcian Blue 8X, Sigma Aldrich) at pH 2.5 and a solution of 0.04% CBB (Coomassie Brilliant Blue G-250, SERVA electrophoresis) at pH 7.4, according to Passow and Alldredge (1995) and Cisternas-Novoa et al. (2014), respectively. Briefly, 20-50 mL samples were filtered using low, constant vacuum (< 200 mbar) onto 0.4-μm Nucleopore filters (25 mm). Parallel samples were stained for TEP and CSP determination. TEP filters were stained with 1 mL AB for 5 seconds and CSP filters with 1 mL of CBB for 30 seconds. Excess dye was removed by rinsing with Milli-Q water. All filters were prepared in duplicate and stored frozen at -20 °C until analysis. For TEP determination, stained filters were placed in 15-mL polypropylene tubes and 6 mL of extraction solution (80% H_2SO_4) added; tubes were incubated with gentle shaking for two hours. Absorbance of the AB in solution was measured spectrophotometrically at 787 nm in a 1-cm cell. Blanks were prepared from Milli-Q water or 0.2−μm filtered seawater for each set of samples. Concentrations of TEP are reported relative to a xanthan gum standard and expressed in micrograms of xanthan gum equivalents per liter (μg XG eq. L^{-1}) after Passow and Alldredge (1995).

For CSP measurements, stained filters were transferred to 15-mL polypropylene tubes, and 4 mL of extraction solution (3% SDS in 50% isopropyl alcohol; Ball 1986) added. Tubes

were sonicated in a water bath (50-60 kHz) for 2 hours at 37°C. After the incubation, the absorbance of the extraction solution was determined spectrophotometrically. The absorption maximum of the eluted CBB is 615 nm. Blanks were treated in the same way as for TEP determination. Concentrations of CSP are reported relative to a bovine serum albumin standard and expressed in micrograms of bovine serum albumin equivalents per liter (μg BSA eq L^{-1}) after Cisternas-Novoa et al. (2014).

2.4.5 Nutrients

Samples were filtered through 0.2-μm syringe filters and frozen at -20ºC until analysis. Measurements of nitrate, phosphate and silicate were made spectrophotometrically using an autoanalyzer. Detection limits were 3 μM for nitrate, 5μM for phosphate and 5μM for silicate.

2.5 Statistical Analysis

The Wilcoxon rank sum test was used to determine whether the medians of aggregate sinking velocity (U), aggregate size (as equivalent spherical diameter ESD) and aggregate sinking velocity of any two treatments were statistically different (Table 4-5). The Wilcoxon rank sum test is a nonparametric test for two populations; we used this test because it was suitable for data that that did not always have a normal distribution and for data where each treatment had different sample sizes. The null hypothesis is that data in any two treatments are samples from continuous distributions with equal medians, or, the alternative, that they are not. The test assumes that the two samples are independent.

3. Results

3.1 Mesocosm experiment 1 (ME1)

3.1.1 Temperature and pH

The pH corresponding to 750 ppm (AC and AW) was calculated using the initial values of T, pH, and TA (Table 4-1). The temperature and pH were monitored throughout the experiment (Fig. 4-2). After 5 days of stabilization the average pH and temperature in each treatment during the experiment were AC: pH 7.79±0.10 and 16.2 ±0.4 ºC; AW: pH 7.8±0.10 and 20.1 ±0.4 ºC, and PC: pH 8.1±0.1 and 16.1 ±0.5 ºC.

3.1.2 Biological and chemical parameters

The ME1 phytoplankton bloom started approximately 24 hours after nutrient addition (day 6). Maximum Chl-*a* concentrations were reached between day 12 and day 16 (Fig. 3), which coincided with the decline in nutrients (Fig. 4-4). The bloom peak values varied between 7.4 and 32.5 μg Chl-*a* L^{-1}. In two PC mesocosms, PC-A and PC-C, and one AC mesocosm, AC-A, the bloom was very small; while one AW mesocosm, AW-C, did not bloom at all and had low Chl-*a* and high nutrient values throughout the experiment (Fig. 4-2; Table 4-2). The differences in Chl-*a* and nutrient uptake between mesocosms with the same treatment were as great as the differences between those with different CO_2 and temperature treatments.

TEP concentrations in mesocosm seawater were higher during the decline of the bloom in all the treatments, with highest values that varied between 346 ± 23 and 1175 ± 117 μg X.G. eq L^{-1} in post-bloom samples (t4) (Fig. 4-5A). In general the lowest TEP concentration was found in the mesocosms that had the lowest Chl-*a* concentrations (PC-A, AC-A and AW-C), with the exception of PC-C, where TEP concentration increased gradually until the end of the experiment. The highest abundance of CSP (Fig. 4-5B) generally coincided with the Chl-*a* maximum. Highest values between 219 ± 49 and 808 μg BSA eq L^{-1} in bloom samples (t2 and t3). Mesocosms with low Chl-*a* also had low CSP, except for PC-C. POC concentrations increased

gradually during the experiment, most mesocosms reaching their highest values between 88 and 191 μM at the Chl-a peak and then staying high until the post-bloom sampling (t4); unfortunately we do not have data for POC at the Chl-*a* max for all the mesocsosm during t2 (Fig. 4-5C).

3.1.3 Roller tank aggregation experiments

Four aggregation experiments were conducted with seawater from the mesocosm at pre-bloom (t1), bloom (t2 and t3), and post-bloom (t4) times (Fig. 4-3). Aggregates were not always formed in the roller tank experiments (Table 4-3).

Aggregate size as equivalent spherical diameter (ESD), sinking velocity (U) and excess density (Fig. 4-6) were determined from video pictures. Before the bloom (t1), excess density showed a significant relationship with U with a Pearson product-moment correlation coefficient of r= 0.83 (n=70, p-value < 0.0001; Fig. 4-6B, pre-bloom), while the correlation between ESD and U was lower, r= 0.34 (n=70, p-value < 0.01; Fig. 4-6A, pre-bloom). This suggests that the major factor controlling U pre-bloom was the excess density (Fig. 4-6B, pre-bloom). However in the late stage of the bloom (t3) the strongest relation was between ESD and U with a Pearson product-moment correlation coefficient of r= 0.57 (n=67, p-value < 0.0001; Fig. 4-6A, pre-bloom), while the correlation between excess density and U was lower, r= 0.26 (n=67, p-value < 0.1; Fig. 4-6B). This suggests that the major factor controlling the sinking velocity changed from excess density to aggregate size as the bloom progressed. Excess density showed a large variation (0-0.05 g cm^{-3}) before the bloom (t1, Fig. 4-6C), but at the end of the bloom it was less than 0.02 g cm^{-3} in all treatments. Pre-bloom ESD showed a small range (0. 15 to 0.25 cm), and did not vary between treatments. However, by the end of the bloom (t3 and t4) the size of aggregates increased and ESD range was between 0-1 cm.

The aggregates produced were enriched in gel particles in all treatments (Fig. 4-7). As in the mesocosm seawater (Fig.4- 5), CSP was relatively more abundant in the aggregate fraction during the bloom (t2 and t3) than in pre-bloom (t1), while TEP concentration in the aggregates was high during pre-bloom (t1), decreased during t2 (peak of the bloom for most tanks; Fig. 4-3), and reached the highest values at the late stage of the bloom t3 (Fig. 4-7). Not all the roller tanks formed aggregates (Table 4-3); during the last roller tank experiment (t4, post-bloom) only one tank formed aggregates; thus conclusions about post-bloom aggregate formation could not be made from this experiment. In general the Chl *a* and gel particle concentrations were relatively low in the tanks that did not form aggregates (PC-A, AW-C) (Table 4-4), so that there may have been insufficient material available for aggregate formation.

Sinking velocity of aggregates (Fig. 4-8A) was relatively constant during the bloom in PC mesocosms, decreased with time in AC mesocosms and increased from t2 to t4 in AW mesocosms. The ESD (Fig. 4-8B) increased with time in PC and AW, but was relatively constant in AC. Opposite to TEP and ESD, excess density of aggregates (Fig.4- 8C) decreased initially in all treatments and then stayed fairly constant.

At cooler temperature the aggregates formed in water from the high CO_2 treatment (AC, blue) were smaller than aggregates formed in water from the present CO_2 treatment (PC, green) at t1 and t3 (Fig. 4-8 and Table 4-5). Pre-bloom sinking velocity of aggregates formed in water from the mesocosm with water at present CO_2 (PC, green) was lower than for aggregates formed from high CO_2 (AC, blue). On the contrary, during the bloom peak (t2 and t3), the sinking velocity of aggregates formed in water from the mesocosm with high CO_2 (AC, blue) was lower than for aggregates formed from water at present CO_2 (PC, green). Unfortunately, only two tanks from the high CO_2, high temperature treatment (AW, red) formed aggregates, and they had an

intermediate sinking velocity. There were no significant differences in the medians of excess density between treatments. The p-values and the decision for the Wilcoxon rank sum test comparing the medians of the treatments are presented in Table 4-5.

3.2 Mesocosm experiment 2 (ME2)

3.2.1 Temperature and pH

Temperature and pH were monitored throughout the experiment (Fig. 4-9). After 1.5 days of stabilization the average pH and temperature between day 2 and day 8 in each treatment were AC: pH 7.8±0.1 and 16.4 ±0.5 ºC, and PC: pH 8.4±0.2 and 16.3 ±0.5 ºC. On day 9 of the experiment, Hurricane Irene arrived in Stony Brook causing a loss of power in the mesocosm facility and prevented our access to the experiment for 2 days. Because the mesocosms were without light, temperature control, and stirring for an undetermined amount of time, we terminated the experiment; the last sampling point was thus collected on day 11.

3.2.2 Biological and chemical parameters

The phytoplankton bloom started quickly after nutrient addition. Maximum Chl-*a* concentrations were reached between day 4 and day 6 (Fig. 4-10); however, due to our sampling resolution and the impact of Hurricane Irene, we cannot be certain that we sampled the mesocosm during the bloom peak. Nutrients declined to almost zero on the last day of sampling (Fig. 11), which was on day 11 after the hurricane for the biological and chemical parameters. Mesocosm AC-B had the highest Chl-*a* concentration at t1 (122 ± 17 μg Chl-*a* L^{-1}); all other mesocosms had the highest Chl-*a* values at t2, varying between 45.6 ± 7.2 and 101.6 ± 2 μg Chl-*a* L^{-1}. A bloom occurred in all mesocosms during ME2. Chl-*a* and nutrient uptake in the PC treatment showed relatively small variability while the AC treatment showed a large variability.

TEP concentrations increased with time in all mesocosms until day 6 (t2); at this point TEP concentration varied between 1145 ± 6 and 1235 ± 20 μg X.G. eq L^{-1} (Fig. 4-12A). Post-bloom samples (t3) were more variable, probably due to the changes in temperature and light caused by Hurricane Irene; no significant effect of CO_2 was observed on TEP concentration. In general the highest abundance of CSP was measured at t2 (663 ± 37 to 992 ± 81μg BSA eq. L^{-1}), and it coincided with the Chl-*a* maximum (Fig. 4-12B); however in two mesocosms (different treatments), the highest concentration of CSP was measured at t3, reaching 1221±211 μg BSA eq. L^{-1}. POC concentration, similar to TEP, increased gradually until t2 in all mesocosms, but differently to TEP, the POC concentration decreased drastically in all mesocosms at t3. (Fig. 4-12C)

3.2.3 Roller Tank aggregation experiments

Triplicate aggregation experiments were conducted with seawater from the ME2 at pre-bloom (t1), bloom (t2), and post-bloom (t3) times (Fig. 4-11). Unlike ME1, aggregates formed in all roller tanks. Aggregate size as equivalent spherical diameter (ESD), sinking velocity (U) and excess density were determined from video pictures. Similar to ME1, before the bloom (t1), there was a positive relationship between the sinking velocity (U) and the excess density (Fig. 4-13B, pre-bloom). There was no relationship between ESD and U (Fig. 4-13A) or between ESD and excess density at any time during the bloom. Excess density showed a large variation (0-0.2 g cm^{-3}) before the bloom (t1, Fig. 4-13C); the spherical equivalent diameter (ESD) was less variable (0. 15 to 0.20 cm), and did not vary between treatments. However, post-bloom (t3) ESD increased considerably, reaching 1 cm (Fig. 4-13).

The aggregates produced were enriched in gel particles in both treatments (Fig. 4-14). CSP was similar in the aggregate fraction during the pre-bloom (t1) and bloom (t2) periods, and was

somewhat lower post-bloom (t3) except for two roller tanks (AC-A, PC-B and PC-C). TEP was more abundant in aggregates during the post-bloom (t3). In general the Chl-*a* concentration in the aggregate fraction was higher and similar between the treatments at pre-bloom (t1) and bloom (t2) times (Fig. 4-14C).

Sinking velocity of aggregates was relatively constant during the pre-bloom (t1) and bloom (t2) in PC and lower post-bloom (t3); sinking velocity in AC decreased from t1 to t3 (Fig. 4-15A). The ESD (Fig. 4-15B) increased with time in PC and AC. In agreement with results from ME1, TEP content and ESD of the aggregates increased and excess density of aggregates decreased with time in all treatments (Fig. 4-15C). Direct observation of aggregates formed in the roller tank during the different phases of the bloom (Fig. 4-16) confirmed the increase in the ESD and the decrease in excess density in both treatments. During pre-bloom (t1) sampling, aggregates were smaller and extremely delicate (most of them broke after collection); in contrast aggregates sampled post-bloom (t4) were larger, more flexible and did not break easily. The Chl-*a* content of the aggregate fraction decreased in almost all the roller tanks post-bloom (t3), which coincided with the decrease in excess density.

Aggregate settling velocity from the high CO_2 treatment (AC, blue) was lower than that from the present CO_2 treatment (PC-green) in t1 and t2 (Fig. 4-15A and Table 4-6). Aggregates from the high CO_2 treatment were smaller than aggregates from the present CO_2 treatment in t1, while the excess density of aggregates from the high CO_2 treatment were lower than aggregates formed in water from the present CO_2 treatment during the bloom peak (t2). During post-bloom (t3) there was no difference in U, ESD or excess density between aggregates from different CO_2 treatments. The p-values and Wilcoxon rank sum test data comparing the medians of the treatments are presented in Table 4-6.

4. Discussion

Previous mesocosm experiments showed that under elevated CO_2 concentrations (i.e., 750 to 1000 ppm) the consumption of DIC by phytoplankton increases, but the net production of POC and PON related to the consumption of DIC and nitrate decrease (Engel, 2005; Riebesell et al., 2007). It has been hypothesized that the exudation of DOC increases under elevated CO_2 conditions, and that a fraction of the DOC may be transformed into TEP (Riebesell *et al.*, 2007), and thus POC (Engel et al., 2004), increasing the amount of aggregates that can sink out of the surface layer (Engel, 2005; Riebesell *et al.*, 2007). Evidence related to this hypothesis is contradictory; recent studies found that TEP concentration increased at elevated CO_2 conditions in a nutrient-limited experiment with *Emiliania huxleyi* (Borchard and Engel 2012). A positive relationship of TEP and POC production with CO_2 concentration was also observed during a nutrient-induced phytoplankton bloom in an outdoor mesocosm experiment (Engel et al., 2014a). This increase in TEP concentration may be caused by an increase in dissolved exudates that act as TEP precursors; however this relationship is not well understood. For example, Kim *et al.* (2011) showed that warming and acidification enhance the production of DOC over POC, but such an increase in DOC is not necessarily translated into increased gel particle formation (Egge et al., 2009). In addition, an increase in TEP formation does not always lead to enhanced aggregation and carbon export (Seebah *et al.*, 2014). Our mesocosm studies were designed to measure gel particle production, aggregate formation, and carbon export in a single system, as well as to measure the effect of elevated CO_2 and temperature on these processes.

Our results from two indoor mesocosm experiments showed that there were no significant changes in Chl-*a*, POC, or gel particle concentration, nor in nutrient uptake at higher than ambient levels of CO_2 or temperature. These results agree with previous work that suggests

that further increases in atmospheric CO_2 may not lead to a higher conversion of DIC to TEP, as the rate of TEP production might to be at its maximum under present atmospheric CO_2 concentrations (Engel, 2002), and that abiotic formation of TEP is not altered by high CO_2 concentrations and low pH (Passow, 2012).

During the mesocosm experiments described here, the phytoplankton blooms were dominated by diatoms. It has previously been shown that not all phytoplankton species respond similarly to high CO_2, and diatoms seem to be less sensitive than other phytoplankton to different CO_2 levels (Engel *et al.*, 2008). Our finding of no significant effect of CO_2 on gel particle production agrees with results from a previous mesocosm experiment with natural phytoplankton assemblages dominated by diatoms and dinoflagellates in which there was no increase of TEP concentration at elevated CO_2 (Egge et al., 2009); Engel et al (2008) suggested that the lack of an apparent increase in TEP concentration with elevated CO_2 concentration might be explained by loss processes like faster sinking of TEP in aggregates. However, our measurements of gel particle concentrations in aggregates formed in seawater from mesocosms with elevated, and present CO_2 levels showed no differences in the TEP content of the aggregates; this suggests that CO_2 may not be directly affecting TEP production or that the effect may be species and/or environment-specific. We used coastal seawater from Stony Brook Harbor, a narrow inlet of Long Island Sound, in our experiments. In coastal areas pH and temperature vary widely and organisms may be adapted to this variation; therefore the effects of anthropogenic increases of CO_2 may be less clear than in the open ocean (Hendriks et al., 2014). Nevertheless, a recent mesocosm study from the oligotrophic ocean also showed no effect of CO_2 on primary production and DOC production (Maugendre *et al*., 2015). In addition, a chemostat experiment

conducted with *Emiliania huxleyi* reported no changes in organic matter elemental stoichiometry related to elevated CO_2 (Engel et al., 2014b).

It is important to consider that ME1and ME2 had relatively high Chl-a and gel particle concentrations due to the added nutrients; these higher concentrations were needed to study aggregates in roller tank experiments. In the ME1 phytoplankton bloom, Chl-*a* concentrations were at least three times lower than in ME2 (Figs. 3 and 10); however, no effect of CO_2 on gel particle, Chl-*a* or POC concentration was observable in either experiment independent of the bloom magnitude. Chl-*a* concentration varied greatly between individual mesocosms during ME1; there was no obvious reason for these differences. Intuitively we tend to think that a larger bloom and higher Chl-*a* concentration should lead to more aggregate formation. However, the Chl-*a* concentration alone was not a good predictor of aggregate formation in the roller tanks. For instance, while AW-C and PC-A mesocosms had low Chl-*a* and gel particle concentrations, and did not form aggregates in the roller tank experiment, PC-C had relatively low Chl-*a* concentration (< 10 μg L^{-1}), but comparatively higher concentration of gel particles and did form aggregates (except at the last time point). These data support the idea that higher TEP concentrations may facilitate aggregation by increasing both particle abundance and particle stickiness, and also suggest that there is a threshold value of the ratio TEP: phytoplankton cell number for aggregate formation, similar to the idea that the ratio between TEP and solid particles determine the sinking or ascending velocity of aggregates (Azetsu-Scott and Passow, 2004).

In ME1 and ME2, TEP concentrations were greater during the bloom decline, while the highest abundance of CSP coincided with the chlorophyll maximum. Roller tank experiments using either ME1 or ME2 seawater indicated that the aggregates produced were enriched in gel particles, with no significant differences between CO_2 or temperature treatments. Even though,

our aggregation experiments for did not produce sufficient aggregates to make definitive conclusions about the post-bloom situation, our results suggest that as in the mesocosm seawater itself, the highest abundance of CSP in the roller tank aggregates was during the bloom, while the highest abundance of TEP in the aggregate fraction was during the bloom decline, suggesting that the role of TEP and CSP in aggregation may change depending on the phase of phytoplankton growth. Further investigations of CSP stickiness are needed to elucidate whether CSP act as a binding matrix in earlier phases of the bloom in the same manner that TEP act at the end of the bloom as a glue binding together cells and detrital material to form aggregates (Alldredge et al., 1993, 1998). During ME1 not all the roller tanks formed aggregates. One possible explanation for this is that the chlorophyll and gel particle concentrations were relatively low in these tanks, and there may have been insufficient material available for aggregate formation. In general, during ME1 we observed that aggregates were more likely to form in roller tanks filled with seawater from mesocosms that had higher TEP concentrations during the bloom (t2 and t3) (Table 4-4). This observation is consistent with a positive relationship between TEP concentration during the bloom, and particle sedimentation was previously observed by Engel et al. (2014a).

Aggregate size, sinking velocity and excess density were determined by image analysis of pictures obtained from videos on the aggregates formed in the roller tanks. There were no significant differences in the concentrations of Chl-*a* and gel particles (Figs. 4-7 and 4-14) or visible differences in aggregates formed under different conditions (e.g., see Fig. 4-16). Aggregation depends on particle abundance, collision rate and particle stickiness. All roller tank experiments were conducted under the same physical conditions, so there was no difference in collision rate. Particle abundance and particle stickiness would be controlled by concentrations

of Chl-*a*, POC and gel particles; therefore, due to the lack of any significant differences in Chl-*a*, gel particle, or POC concentration between the different treatments in both ME1 and ME2, the fact that there were no significant differences in aggregate formation between treatments was expected.

Even though there were no changes in aggregate properties or appearance with different temperature and CO_2 treatments, there were observable changes in aggregate properties (Figs.4-8 and 4-15) and aggregate appearance (Fig. 4-16) with time. The major factor controlling the sinking velocity of the aggregates appeared to change over time, from excess density during the bloom development (t1) to aggregate size (ESD) by the end of the bloom. In both, ME1 and ME2 roller tank experiments, the particle ESD was smaller and less variable initially (t1) and increased in size and variability as the bloom progressed (Figs. 4-8B and 4-15B). Aggregate size is strongly controlled by the initial concentration of suspended particles (Engel *et al*., 2009a). For the roller tank experiments the initial concentration of suspended particles is likely to be related to the concentration of Chl-*a* and gel particles in the mesocosm. However, aggregate size seems to be independent of Chl-*a* and POC concentrations in the mesocosms, since particles with larger ESD were observed post-bloom (Figs. 4-8B and 4-15B) when TEP concentration was higher (Figs. 4-5B and 4-12B), but Chl-*a* (Figs. 4-3 and 4-10) and POC (Figs. 4-5C and 4-12C) were lower. The excess density (Figs.4- 8C and 4-15C) decreased inversely with TEP concentration and directly with CSP, Chl-*a* and POC.

Biogenic minerals and TEP have opposite effects on the size, excess density and sinking velocity of aggregates. Engel et al. (2009a) showed that aggregates with higher biogenic mineral content from calcified cocolithophores were smaller and had higher settling velocities and excess densities than aggregates with less biogenic minerals from non-calcified cocolithophores. The

sinking velocity they measured for non-calcified cell was comparable to the sinking velocity of diatom aggregates, suggesting that calcite may affect sinking velocity of aggregates more than opal does. Results presented here are from a natural assemblage of diatoms; we found at earlier stages in the bloom that diatom aggregates were smaller and had higher sinking velocity and excess density than at the end of the bloom (Fig. 4-8 and 4-15). This relation was observed in both experiments, but more clearly in ME2. In most studies, sinking velocity of diatom aggregates is measured at the end of the bloom when the concentration of gel particles, especially TEP, is comparatively higher than that of Chl-*a*. Our results indicate that diatom aggregates formed at earlier stages of the bloom or during the bloom have higher sinking velocity, and suggest that the stage of the bloom at which aggregates are measured can affect conclusions about the ballast potential of opal compared with other biogenic minerals (e.g. Klaas and Archer, 2002).

At the same temperature, aggregates formed in roller tanks from mesocosm water with higher CO_2 were smaller and had lower sinking velocity than aggregates formed under present CO_2 conditions during the bloom in both experiments (ME1, t2 and t3, Fig. 8; and ME2, t2, Fig.15), but those differences were not as clear at the end of the bloom. These results are consistent with previous studies that indicate lower sinking velocities under higher CO_2 conditions for aggregates dominated by calcareous material (Bierman and Engel 2010; de Jesus Mendes and Thomsen, 2012). However, recent laboratory studies with diatoms showed no effect of CO_2 concentration on aggregate size or composition (Passow *et al.*, 2014).

A recent aggregation experiment with *Thalassiosira weissflogii* showed higher concentrations of TEP at elevated temperatures; however this higher TEP did not translate to higher sinking velocity of aggregates; elevated CO_2 conditions reduced the aggregate sinking

velocity even more (Seebah et al., 2014). During our ME1 experiment, aggregates formed in water from the higher temperature mesocosm had relatively higher ESD, lower excess density and intermediate sinking velocity over time. Unfortunately, from the three mesocosms with the high CO_2, warmer temperature treatment (AW) only one formed aggregates in roller tanks during pre-bloom, bloom and post bloom; this mesocosm also had higher gel particle concentrations during the experiment; but, the lack of replication does not allow us to make clear conclusions about the synergistic effects of temperature and CO_2 in our experiment.

It is expected that increasing CO_2 concentrations will have different regional- and ecosystem-specific effects on the biological pump. Our results suggest that coastal environments dominated by diatoms have low sensitivity to high CO_2 and temperature, probably because the system is naturally highly variable. Findings from the aggregation experiments highlight the importance of studying the effects of multiple stressors at different stages of a phytoplankton bloom, since the intensity of the impact can vary with aggregate composition. The few measurements available regarding effects of warming and acidification on gel particles and the consequences for aggregation and carbon export come from small scale, usually single species, and laboratory experiments that have focused only on TEP. Large indoor mesocosm experiments like the ones presented here are more difficult to control and frequently the replicability is not optimum; however, they are an intermediate step to studying more complex systems.

References

Alldredge, A., Passow, U. and Haddock, H.D., 1998. The characteristics and transparent exopolymer particle (TEP) content of marine snow formed from thecate dinoflagellates. J. Plankton Res, 20(3).

Alldredge, A.L., Passow, U., Logan, B.E., 1993. The abundance and significance of a class of large, transparent organic particles in the ocean. Deep-Sea Res. Part I, 40(6): 1131-1140.

Alldredge, A.L. and Jackson, G.A., 1995. Preface: Aggregation in marine system. Deep-Sea Res. Part II, 42(1): 1-7.

Alldredge, A.L. and Gotschalk, C., 1988. In situ settling behavior of marine snow. Limnol. Oceanogr., 33(3): 339-351.

Armstrong, R., Lee, C., Hedges, J., Honjo, S. and Wakeham, S., 2002. A new, mechanistic model for organic carbon fluxes in the ocean based on the quantitative association of POC with ballast minerals. Deep-Sea Res. Part II, 49: 219.

Arrigo, K.R., 2007. Carbon cycle: Marine manipulations. Nature, 450(7169): 491-492.

Azetsu-Scott, K. and Passow, U., 2004. Ascending Marine Particles: Significance of Transparent Exopolymer Particles (TEP) in the Upper Ocean. Limnol. Oceanogr., 49(3): 741-748.

Bidigare, R.R., Kennicutt II, M.C.a. and Brooks, J.M., 1985. Rapid determination of chlorophylls and their degradation products by high-performance liquid chromatography. Limnol. Oceanogr., 30: 432-435.

Biermann, A. and Engel, A., 2010. Effect of CO_2 on the properties and sinking velocity of aggregates of the coccolithophore *Emiliania huxleyi*. Biogeosciences, 7(3): 1017-1029.

Borchard, C., Borges, A.V., Händel, N. and Engel, A., 2011. Biogeochemical response of *Emiliania huxleyi* (PML B92/11) to elevated CO_2 and temperature under phosphorous limitation: A chemostat study. J. Exp. Mar. Biol. Ecol., 410(0): 61-71.

Borchard, C. and Engel, A., 2012. Organic matter exudation by *Emiliania huxleyi* under simulated future ocean conditions. Biogeosciences, 9(8): 3405-3423.

Caldeira, K. and Wickett, M., 2003. Anthropogenic carbon and ocean pH. Nature, 425: 365.

Chen, C.-S., Anaya, J.M., Chen, E.Y.T., Farr, E. and Chin, W.-C., 2015. Ocean warming–acidification synergism undermines dissolved organic matter assembly. PLoS ONE, 10(2): e0118300.

Claquin, P., Probert, I., Lefebvre, S. and Veron, B., 2008. Effects of temperature on photosynthetic parameters and TEP production in eight species of marine microalgae. Aquat. Microb. Ecol., 51(1): 1-11.

Cisternas-Novoa, C., Lee, C. and Engel, A., 2014. A semi-quantitative spectrophotometric, dye-binding assay for determination of Coomassie Blue stainable particles. Limnol. Oceanogr. Meth., 12: 604-616.

Delille, B., Harlay, J., Zondervan, I., Jacquet, S., Chou, L., Wollast, R., Bellerby, R. G. J., Frankignoulle, M., Borges, A. V., Riebesell, U., and J.P. Gattuso., 2005. Response of primary production and calcification to changes of pCO_2 during experimental blooms of the coccolithophorid *Emiliania huxleyi*. Glob. Biogeochem. Cycles, 19(2): GB2023.

Doney, S.C., Fabry, V.J., Feely, R.A. and Kleypas, J.A., 2009. Ocean acidification: The other CO_2 problem. Ann. Rev. Mar. Sci., 1(1): 169-192.

Engel, A., Piontek, J., Grossart, H., Riebesell, U., Schulz, KG., and M. Sperling., 2014a. Impact of CO_2 enrichment on organic matter dynamics during nutrient induced coastal phytoplankton blooms. J. Plankton Res., 36(3): 641-657.

Engel, A., Cisternas- Novoa, C., Wurst, M., Endres, S., Tang, T., Schartau, M and C. Lee. 2014b. No detectable effect of CO_2 on elemental stoichiometry of Emiliania huxleyi in nutrient-limited, acclimated continuous cultures. Mar. Ecol. Progr. Ser., 507: 15-30.

Engel, A., Abramson, L., Szlosek, J., Liu, Z., Stewart, G., Hirschberg, D., and C. Lee., 2009a. Investigating the effect of ballasting by $CaCO_3$ in *Emiliania huxleyi*, II: Decomposition of particulate organic matter. Deep-Sea Res. Part II, 56(18): 1408-1419.

Engel, A., Szlosek, J., Abramson, L., Liu, Z. and Lee, C., 2009b. Investigating the effect of ballasting by $CaCO_3$ in *Emiliania huxleyi*: I. Formation, settling velocities and physical properties of aggregates. Deep-Sea Res. Part II, 56(18): 1396-1407.

Engel, A., Schulz, K. G., Riebesell, U., Bellerby, R., Delille, B., and M. Schartau. 2008. Effects of CO2 on particle size distribution and phytoplankton abundance during a mesocosm bloom experiment (PeECE II). Biogeosciences, 5(2): 509-521.

Engel, A., 2005. Testing the direct effect of CO_2 concentration on a bloom of the coccolithophorid *Emiliania huxleyi* in mesocosm experiments. Limnol. Oceanogr., 50: 493-504.

Engel, A. Delille, B., Jacquet, S., Riebesell, U., Rochelle-Newall, E., Terbrüggen, A., and I. Zondervan. 2004. Transparent exopolymer particles and dissolved organic carbon production by

Emiliania huxleyi exposed to different CO_2 concentrations: a mesocosm experiment. Aquat. Microb. Ecol., 34(1): 93-104.

Engel, A., 2002. Direct relationship between CO_2 uptake and transparent exoploymer particles production in natural phytoplankton. J. Plankton Res., 24: 49-53.

Engel, A. and Schartau, M., 1999. Influence of transparent exopolymer particles (TEP) on sinking velocity of *Nitzschia closterium* aggregates. Mar. Ecol. Progr. Ser., 182: 69-76.

Egge, J.K.,Thingstad, T.F., Larsen, A., Engel, A., Wohlers, J., Bellerby, R.G.J., and U. Riebesell., 2009. Primary production during nutrient-induced blooms at elevated CO_2 concentrations. Biogeosciences, 6(5): 877-885.

Feng, Y., Warner, M. E., Zhang, Y., Sun, J., Fu, F.X., Rose, J. M., and D.A. Hutchins., 2008. Interactive effects of increased pCO_2, temperature and irradiance on the marine coccolithophore *Emiliania huxleyi* (Prymnesiophyceae). Eur. J. Phycol., 43(1): 87-98.

Gattuso, J.P., Frankignoulle, M., Bourge, I., Romaine, S. and Buddemeier, R.W., 1998. Effect of calcium carbonate saturation of seawater on coral calcification. Glob. Planet. Change, 18: 37-46.

Gran, G., 1952. Determination of the equivalence point in potentiometric titrations of seawater with hydrochloric acid. Oceanol. Acta, 5: 209-218.

Hall, P.O.J. and Aller, R.C., 1992. Rapid, small-volume, flow injection analysis for $\sum CO_2$ and NH_4^+ in marine and freshwaters. Limnol. Oceanogr., 37(5): 1113-1119.

Honjo, S., Manganini, S., Krishfield, R. and Francois, R., 2008. Particulate organic carbon fluxes to the ocean interior and factors controlling the biological pump: a synthesis of global sediment trap programs since 1983. Prog. Oceanogr., 76: 217.

Kim, J.-M., Lee, K., Shin, K., Yang, E. J., Engel, A., Karl, D. M., Kim, H-Cl., 2011. Shifts in biogenic carbon flow from particulate to dissolved forms under high carbon dioxide and warm ocean conditions. Geophys. Res. Lett., 38(8): L08612.

Klaas, C. and Archer, D.E., 2002. Association of sinking organic matter with various types of mineral ballast in the deep sea: Implications for the rain ratio. Global Biogeochem. Cy., 16(4): 1116.

Mantoura, R.F.C. and Llewellyn, C.A., 1983. The rapid determination of algal chlorophyll and carotenoid pigments and their breakdown products in natural waters by reverse-phase high-performance liquid chromatography. Anal. Chim. Acta, 151(0): 297-314

Mari, X., 2008. Does ocean acidification induce an upward flux of marine aggregates? Biogeosciences, 5(4): 1023-1031.

Maugendre, L., Gattuso, J. P., Poulton, A. J., Dellisanti, W., Gaubert, M., Guieu, C. and F. Gazeau. No detectable effect of ocean acidification on plankton metabolism in the NW oligotrophic Mediterranean Sea: Results from two mesocosm studies. Estuar. Coast. Shelf S. http://dx.doi.org/10.1016/j.ecss.2015.03.009

Morán, X.A.G., Sebastián, M., Pedrós-Alió, C. and Estrada, M., 2006. Response of Southern Ocean phytoplankton and bacterioplankton production to short-term experimental warming. Limnol. Oceanogr., 51(4): 1791-1800.

Lewis, E. and Wallace, D., 1998. Program developed for CO_2 system calculations. ORNL/CDIAC-105, Carbon Dioxide Information Analysis Center, Oak Ridge National Laboratory, US Department of Energy, Oak Ridge, Tennessee.

Langdon, C., 2003. Effect of elevated CO_2 on the community metabolism of an experimental coral reef. Glob. Biogeochem. Cycles, 17: 1011.

Long, R., Azam, F., 1996. Abundant protein-containing particles in the sea. Aquat. Microb. Ecol., 10(3): 213-221.

Passow, U., De La Rocha, C., Fairfield, C. and Schmidt, K., Aggregation as a function of and mineral particles. Limnol. Oceanogr., 59(2): 532-547.

Passow, U., 2012. The abiotic formation of TEP under different ocean acidification scenarios. Mar. Chem., 128–129(0): 72-80.

Passow, U. and Alldredge, A.L., 1995. A dye-binding assay for the spectrophotometric measurement of transparent exopolymer particles (TEP). Limnol. Oceanogr. 40(7): 1326-1335

Ploug, H., Terbrüggen, A., Kaufmann, A., Wolf-Gladrow, D. and Passow, U., 2010. A novel method to measure particle sinking velocity in vitro, and its comparison to three other in vitro methods. Limnol. Oceanogr. Meth., 8: 386-393.

Piontek, J. et al., 2009. Effects of rising temperature on the formation and microbial degradation of marine diatom aggregates. Aquat. Microb. Ecol., 54(3): 305-318.

Riebesell, U., Schulz, K. G., Bellerby, R. G. J., Botros, M., Fritsche, P., Meyerhofer, M., Neill, C., Nondal, G., Oschlies, A., Wohlers, J., and E. Zollner., 2007. Enhanced biological carbon consumption in a high CO_2 ocean. Nature, 450(7169): 545-548.

Riebesell, U., Zondervan, I., Rost, B., Tortell, P. D., Zeebe, R. E., and F.M. M. Morel., 2000. Reduced calcification of marine plankton in response to increased atmospheric CO_2. Nature, 407(6802): 364-367.

Rost, B., Zondervan, I. and Wolf-Gladrow, D., 2008. Sensitivity of phytoplankton to future changes in ocean carbonate chemistry: current knowledge, contradictions and research directions. Mar. Ecol. Prog. Ser., 373: 227-237.

Seebah, S., Fairfield, C., Ullrich, M.S. and Passow, U., 2014. Aggregation and sedimentation of *Thalassiosira weissflogii* (diatom) in a warmer and more acidified future ocean. PLoS ONE, 9(11): e112379.

Solomon, S., Qin, D., Manning, M., Chen, Z. and Marquis, M., 2007. Climate Change 2007: The Physical Science Basis: Contribution of Working Group I to the Fourth Assessment Report of the Intergovernmental Panel on Climate Change. Cambridge University Press. Cambridge, United Kingdom and New York, NY, USA.

Sun, M., Aller, R.C. and Lee, C., 1991. Early diagenesis of chlorophyll-a in Long Island Sound sediments: A measure of carbon flux and particle reworking. J. Mar. Res., 49: 1-23.

Turner, J.T., 2015. Zooplankton fecal pellets, marine snow, phytodetritus and the ocean's biological pump. Prog. Oceanogr., 130: 205-248.

Turner, J.T., 2002. Zooplankton fecal pellets, marine snow and sinking phytoplankton blooms. Aquat. Microb. Ecol., 27(1): 57-102.

Wohlers, J., Engel, A., Zöllner, E., Breithaupt, P., Jürgens, K., Hoppe, H.G., Sommer, U., and U. Riebesell., 2009. Changes in biogenic carbon flow in response to sea surface warming. PNAS, 106(17): 7067-7072.

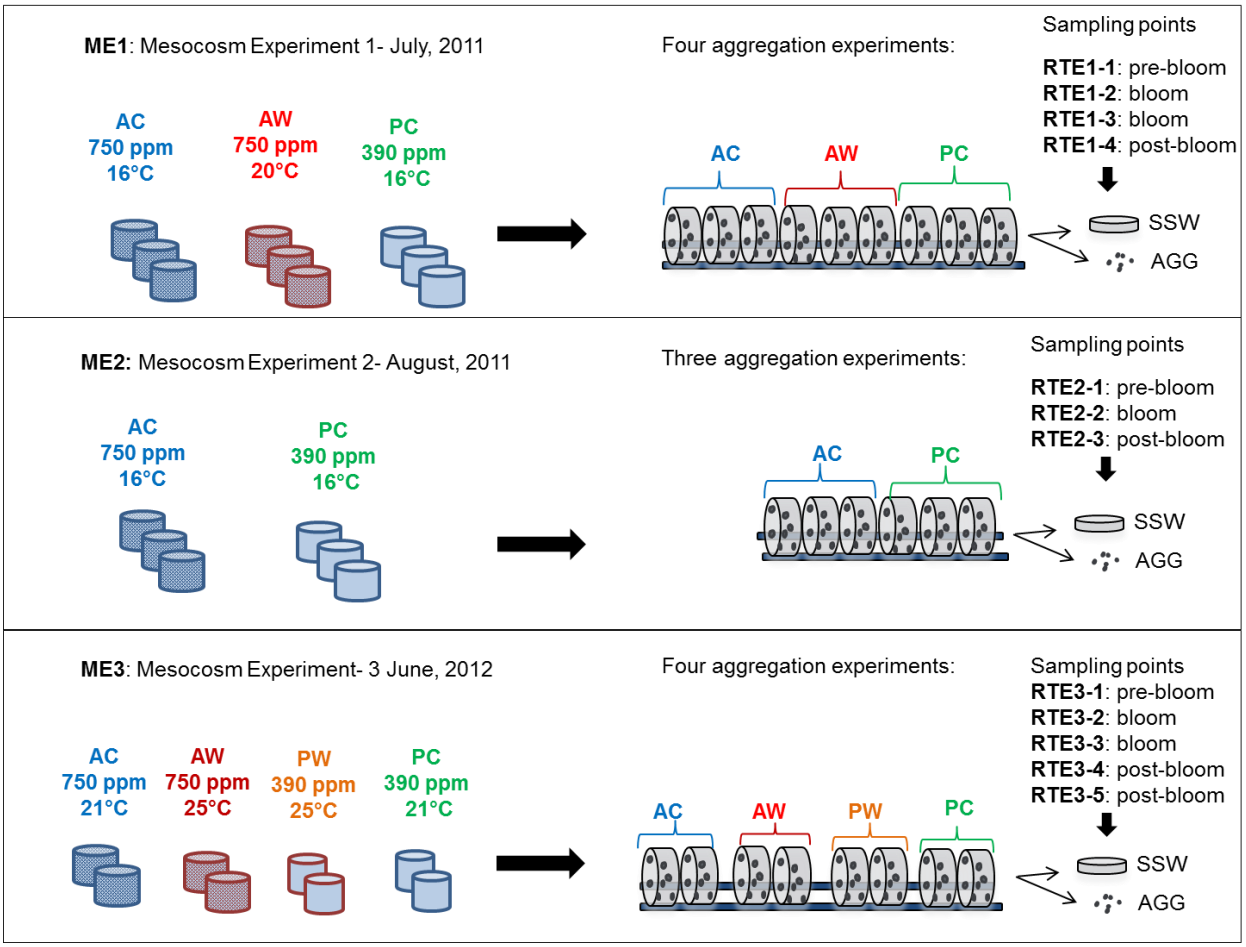

Figure 4-1. Experimental setup for the mesocosm (ME) and aggregation (RTE) experiments. AC: acidified-cooler; AW: acidified-warmer; PW: present CO_2-warmer, C-PC: control, present CO_2-cooler; AGG: aggregates, SSW surrounding seawater. See "methods" section for details.

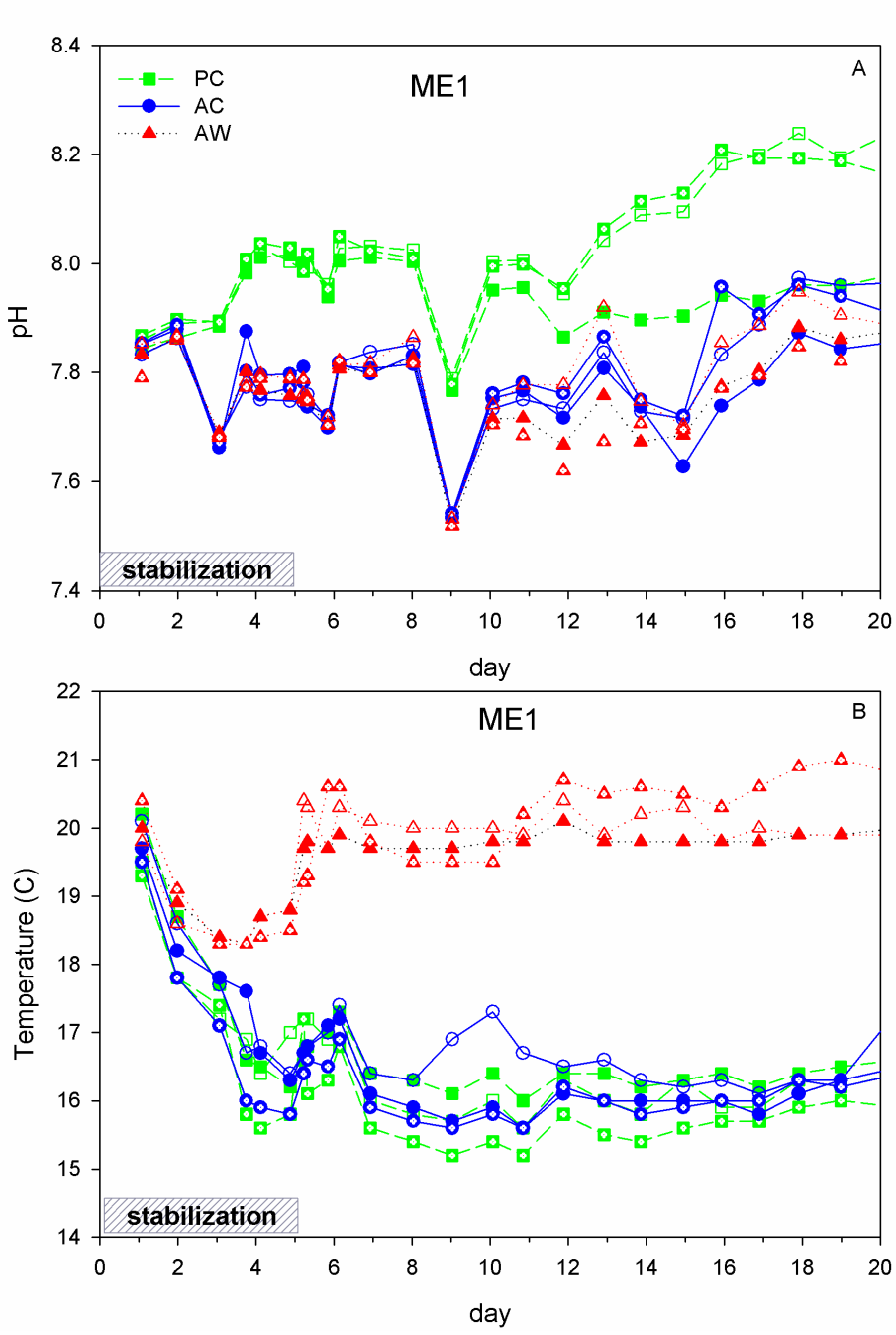

Figure 4-2. pH and temperature variations for the three treatments during ME1. Triplicate mesocosms were run for each treatment: AC (blue-circle): acidified-cooler; AW (red-triangle): acidified-warmer, and PC (green-square): present CO_2-cooler.

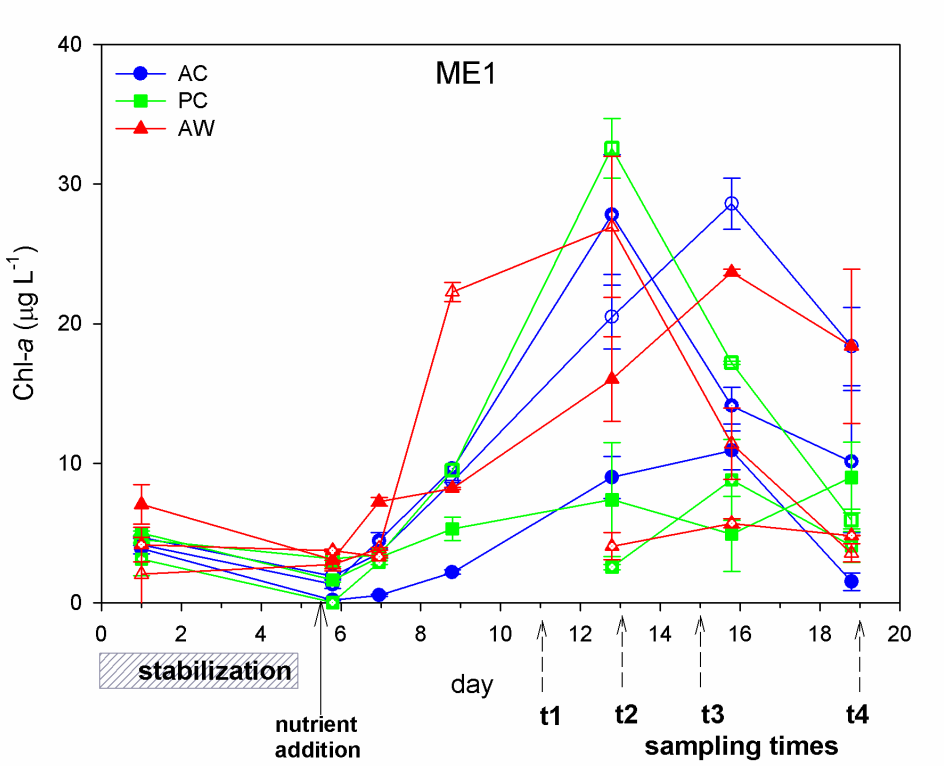

Figure 4-3. Chl-*a* over time during ME1 showing stabilization, nutrient addition and sampling times when roller tank aggregation experiments were performed. Triplicate mesocosms were run for each treatment: AC (blue-circle): acidified-cooler; AW (red-triangle): acidified-warmer and PC (green-square): present CO_2-cooler.

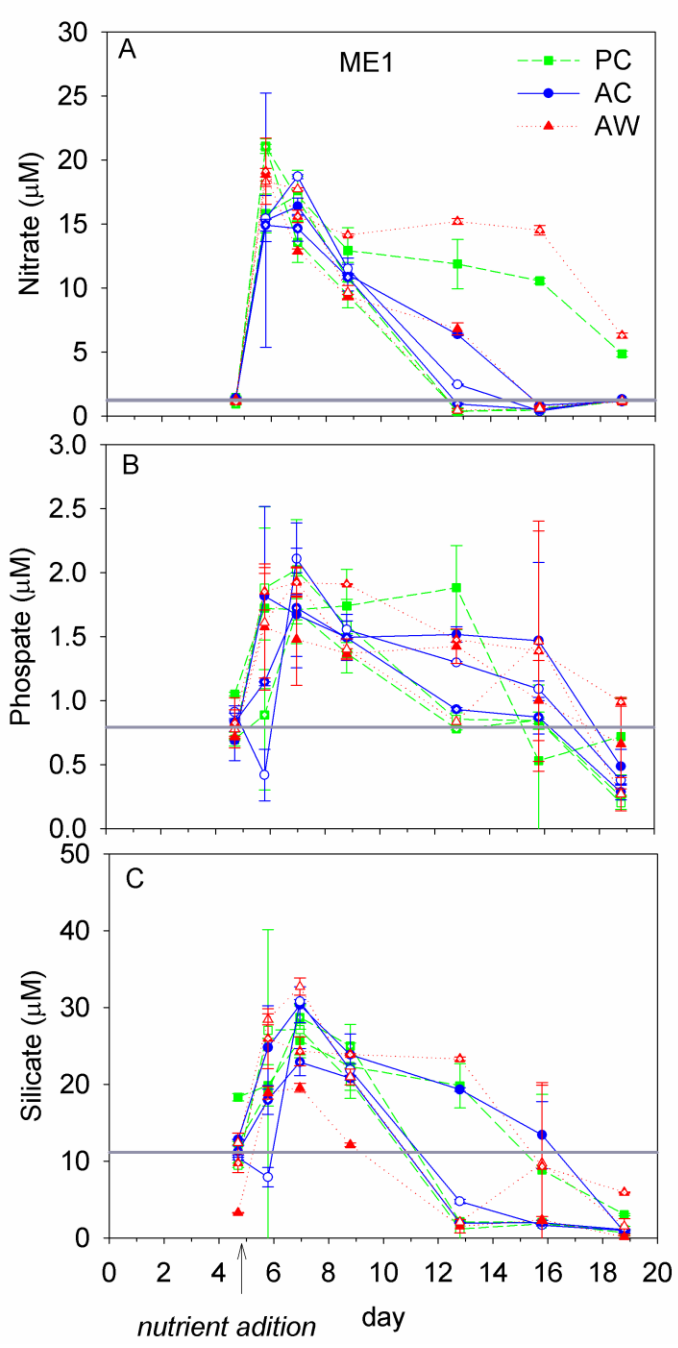

Figure 4-4. Nutrient concentration over time during ME1. Nitrate (A), Phosphate (B) and Silicate (C). The grey line represents the initial nutrient concentration (before nutrient addition). AC (blue-circle); AW (red-triangle), and PC (green-square). No significant differences were found in nutrient uptake among the three different treatments.

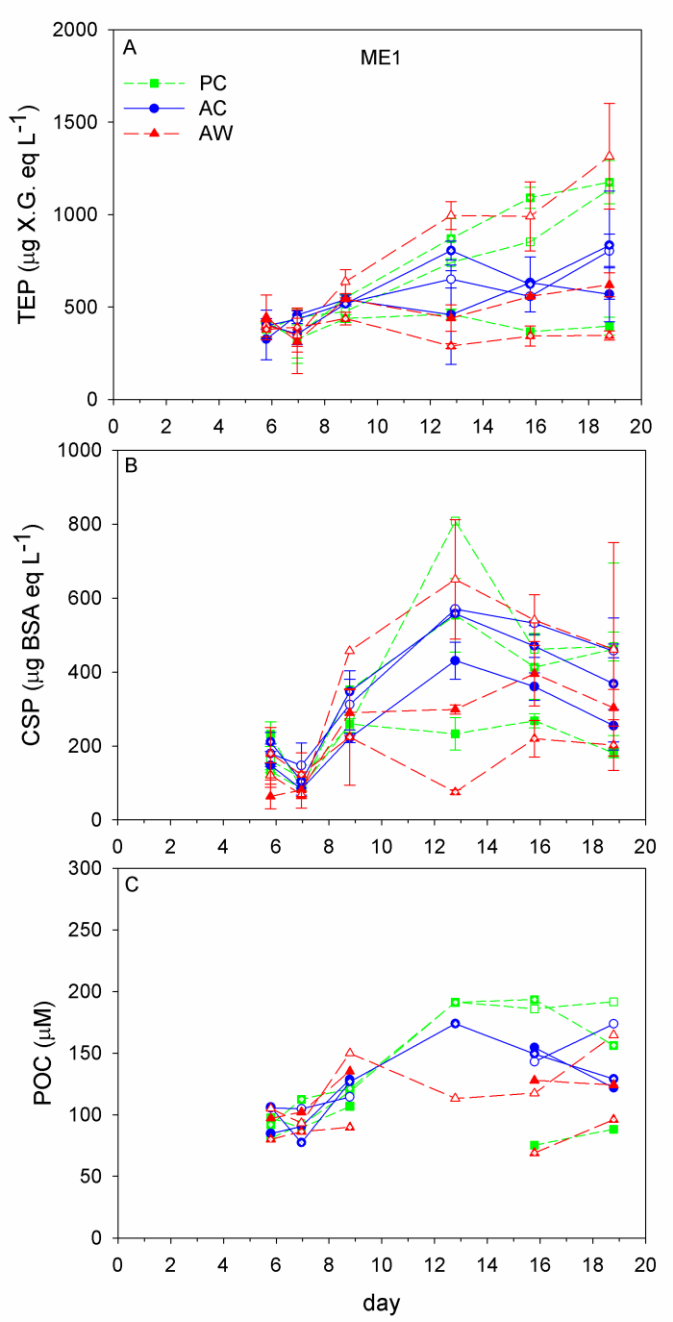

Figure 4-5.TEP (A), CSP (B) and POC (C) concentrations during the development of the bloom in ME1. AC (blue-circle); AW (red-triangle) and PC (green-square). No significant differences were found in gel particle or POC concentrations among the three different treatments.

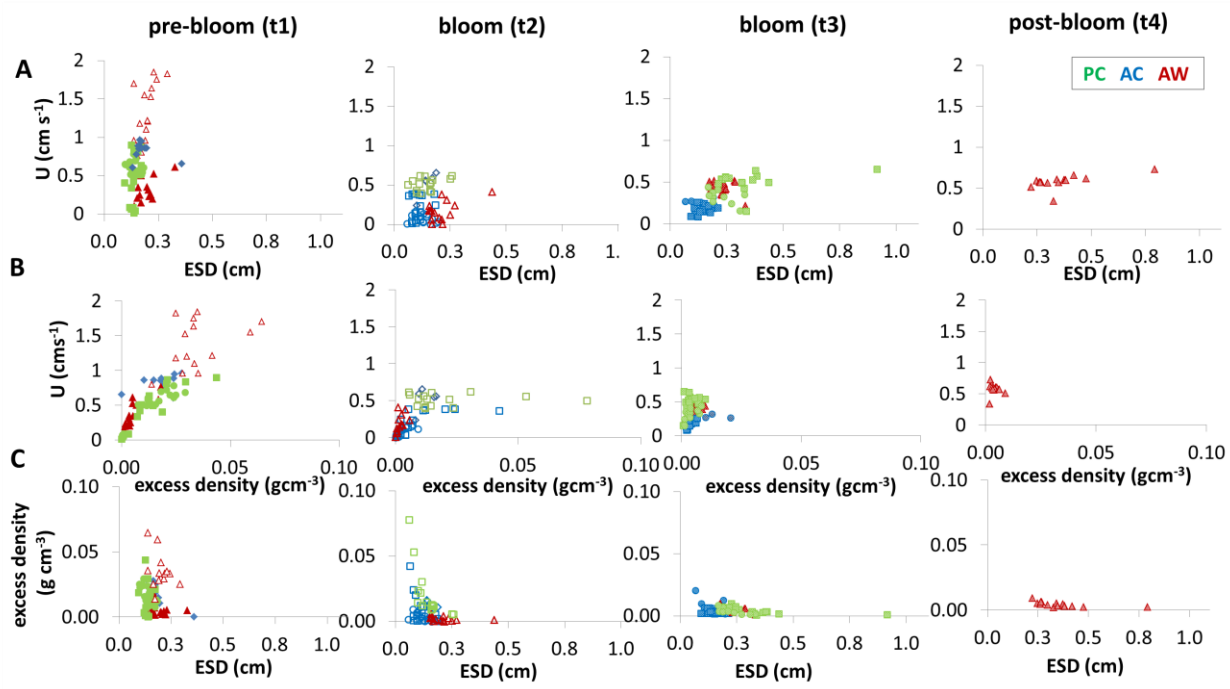

Figure 4-6. Equivalent spherical diameter (ESD, cm) versus sinking velocity (U, cm s^{-1}) (A). Excess density (g cm^{-3}) versus sinking velocity (B). ESD versus excess density (C) of aggregates formed during the aggregation experiments with seawater from ME1. AC (blue-circle; AW (red-triangle), and PC (green- square).

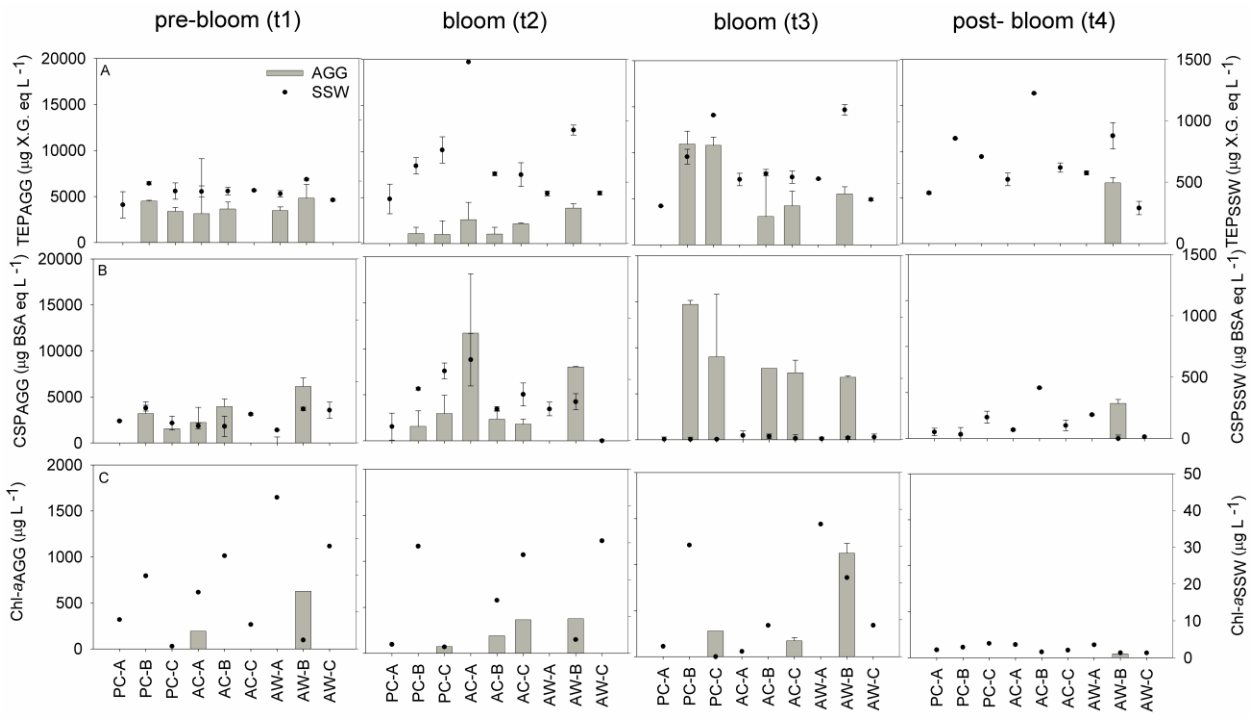

Figure 4-7. Concentrations of gel particles in aggregates formed in ME1 roller tank experiments conducted at the 4 different growth phases. Aggregates (grey bars) and smaller particles in the surrounding seawater (black dots) were analyzed separately to study the distribution of TEP (upper panel), CSP (middle panel) and Chl-*a* (lower panel) in both fractions in all of the roller tanks: AC (blue) AW (red), and PC (green). There is several missing data for the Chl-a set.

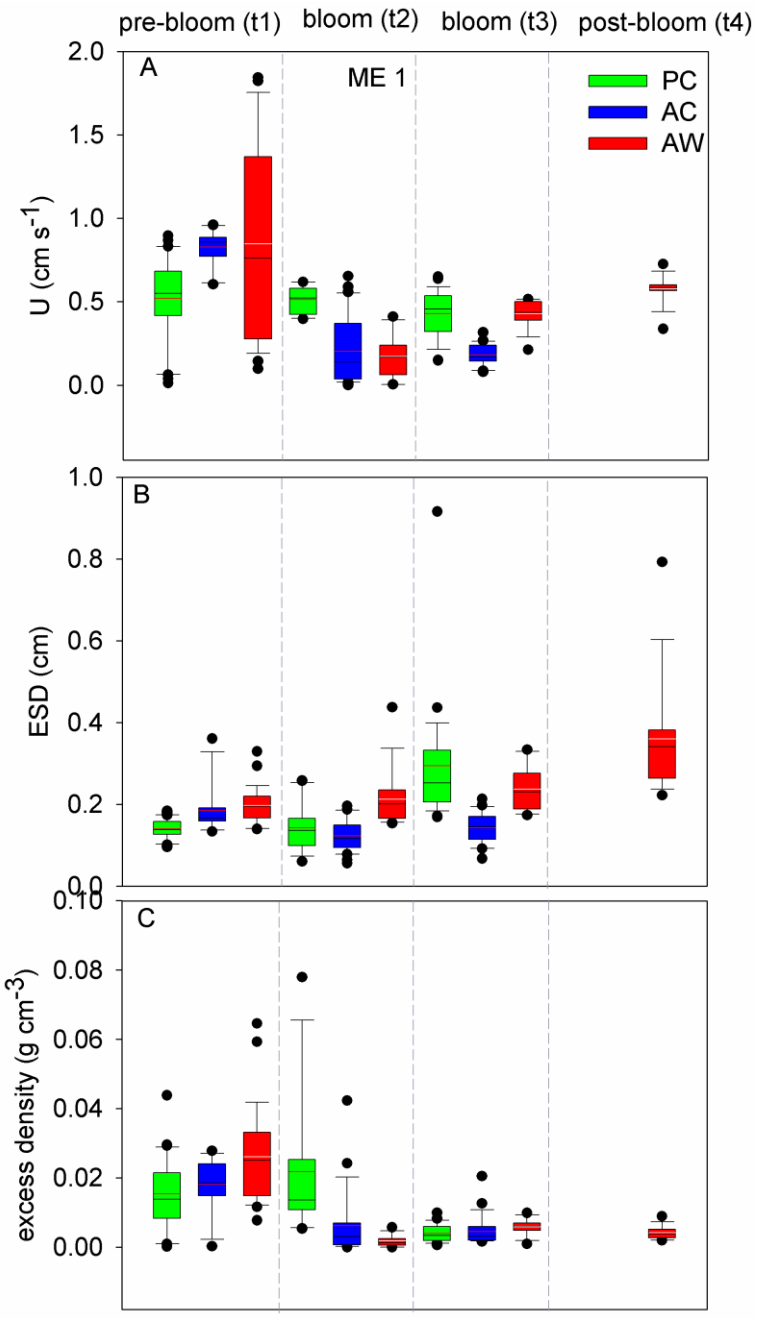

Figure 4-8. Properties of aggregates formed in four roller tank experiments conducted at different growth phases: pre-bloom (t1), bloom (t2 and t3), and post-bloom (t4) during ME1. (A) aggregate sinking velocity; (B) ESD and (C) excess density. Box plots include all the individually-measured aggregates in each roller tank in the different treatments: AC (blue), AW

(red), and PC (green). For pre-bloom, AC (blue) represents roller tank AC-A (n=11); AW (red) represents roller tank AW-A (n=14) and AW-B (n=15); and PC (green) represents roller tank PC-B (n=15) and PC-C (n=15). For bloom (t2), AC (blue) represents roller tank AC-A (n=3), AC-B (n=13), and AC-C (n=16); AW (red) represents roller tank AW-B (n=15); and PC (green) represents roller tanks PC-B (n=2) and PC-C (n=15). For bloom (t3), AC (blue) represents roller tank AC-B (n=10), and AC-C (n=16); AW (red) represents roller tank AW-B (n=16); and PC (green) represents roller tanks PC-B (n=15) and PC-C (n=10). For post-bloom, AW (red) represents roller tank AW-C (n=15). The boundary of the box closest to zero indicates the 25th percentile, the black line within the box is the median and the red line is the mean; the boundary of the box farthest from zero indicates the 75th percentile. Error bars above and below the box indicate the 90th and 10th percentiles, and black dots are the outlying points.

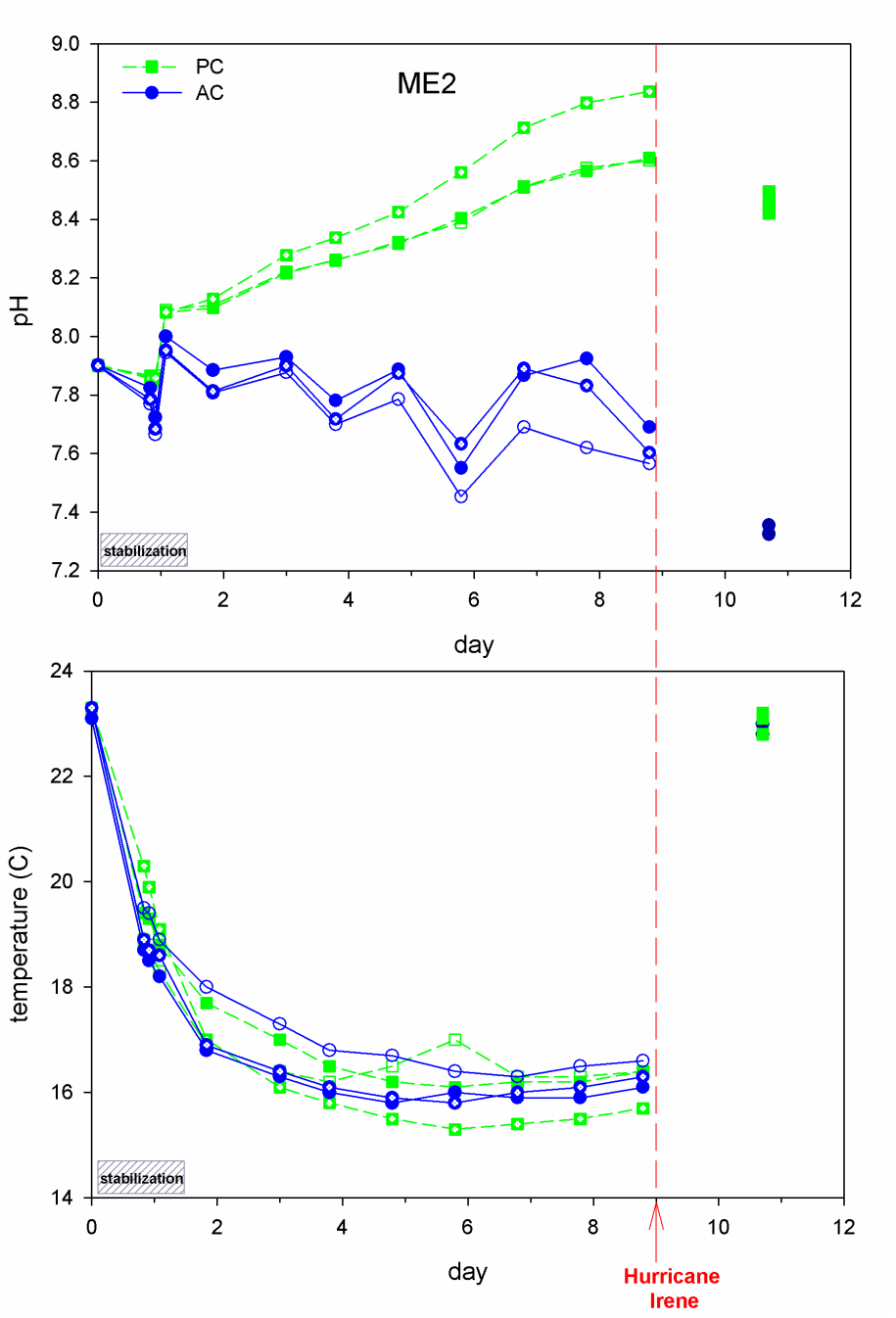

Figure 4-9. pH and temperature variations for the two sets of treatments during ME2. Triplicate mesocosms were run for each treatment: AC (blue-circle): acidified-cooler and PC (green-square): present CO_2-cooler.

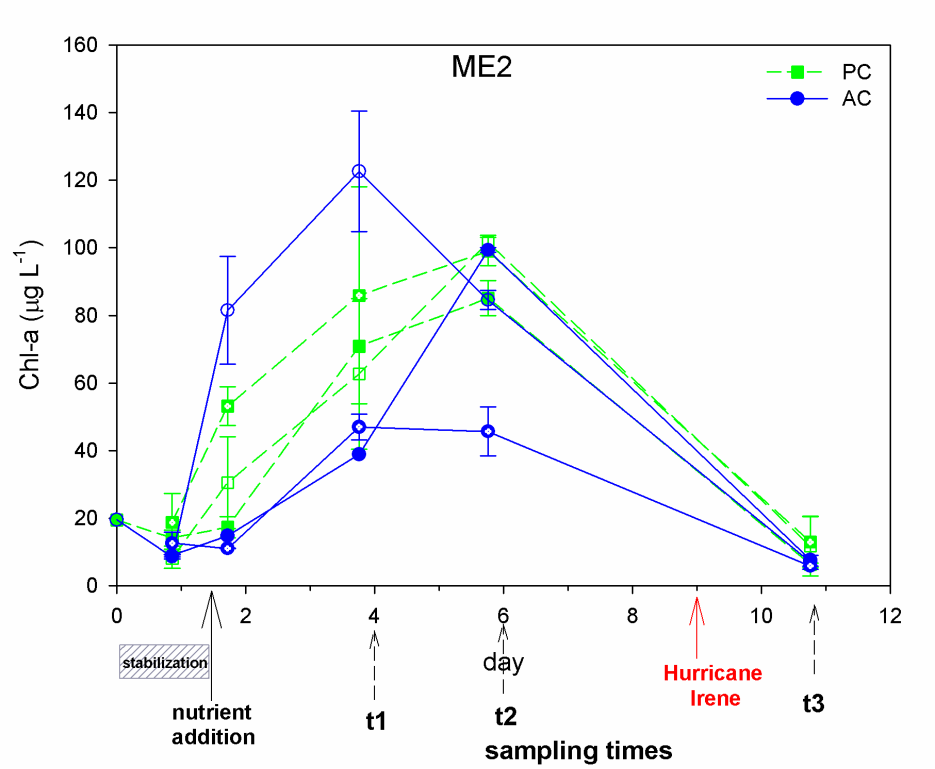

Figure 4-10. Chl-*a* over time during ME2 showing stabilization, nutrient addition, Hurricane Irene, and sampling times when roller tank aggregation experiments were performed. Triplicate mesocosms were run for each treatment: AC (blue-circle): acidified-cooler and PC (green-square): present CO2-cooler.

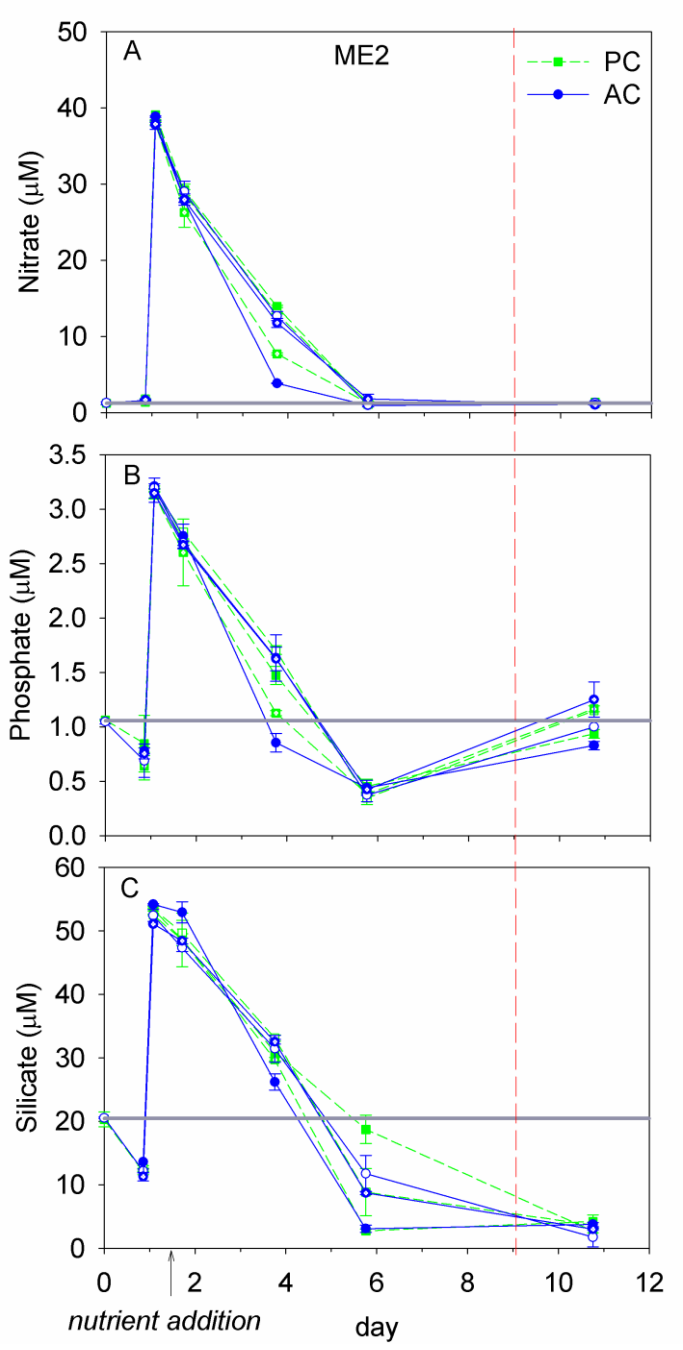

Figure 4-11. Nutrient concentration over time during ME2. Nitrate (A), Phosphate (B) and Silicate (C). The grey line represents the initial nutrient concentration (before nutrient addition). AC (blue-circle, and PC (green-square). No significant differences were found in nutrient uptake between the two different treatments.

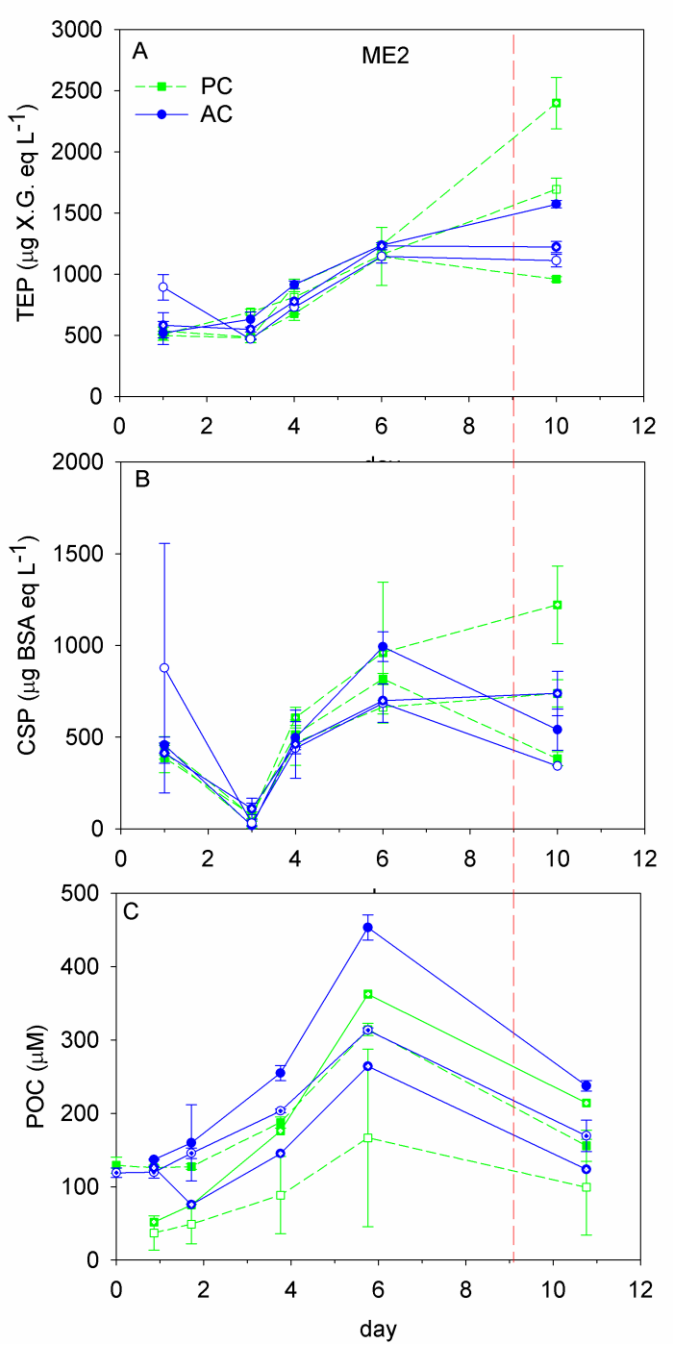

Figure 4-12. ME2 TEP (A), CSP (B) and POC (C) concentrations during the development of the bloom. AC (blue-circle) and PC (green- square). No significant differences were found in gel particle or POC concentrations between the two different treatments. The red line indicates Hurricane Irene.

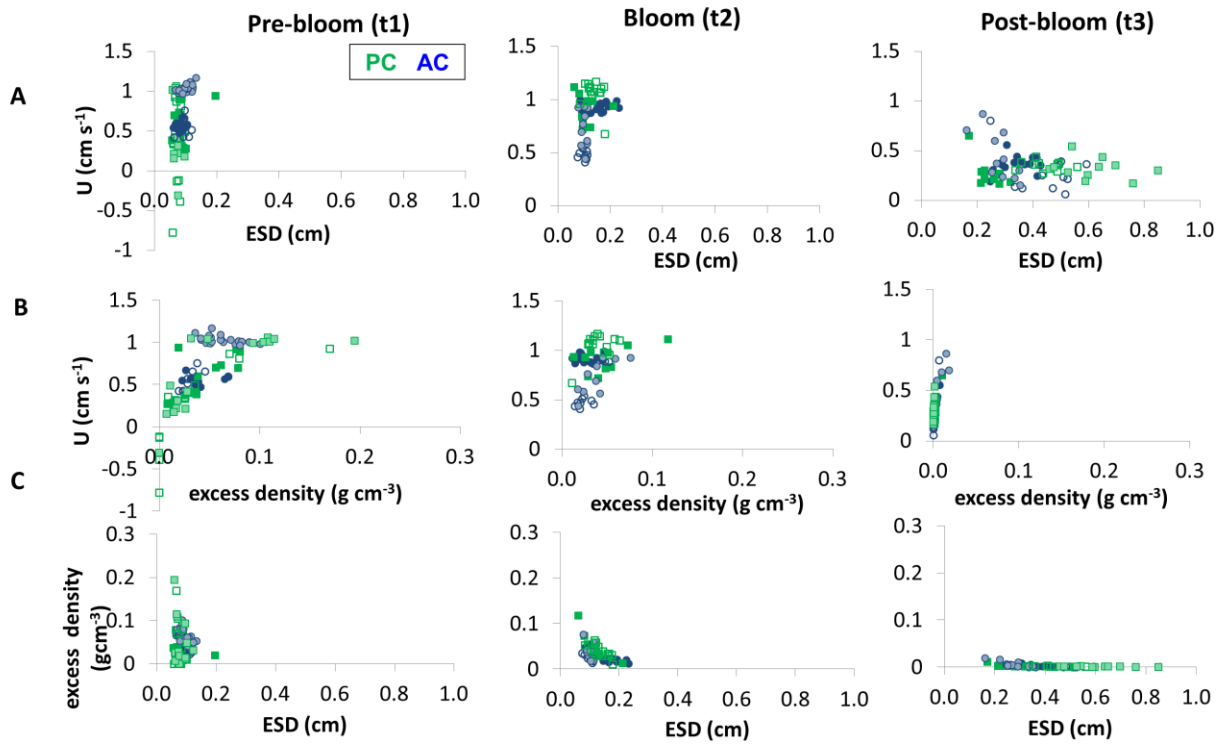

Figure 4-13. Equivalent spherical diameter (ESD cm) versus sinking velocity (U cm s^{-1}) (A); excess density (g cm^{-3}) versus sinking velocity (B); ESD versus excess density (C) of aggregates formed during the aggregation experiments with seawater from ME 2;.AC (blue circles) and PC(green squares).

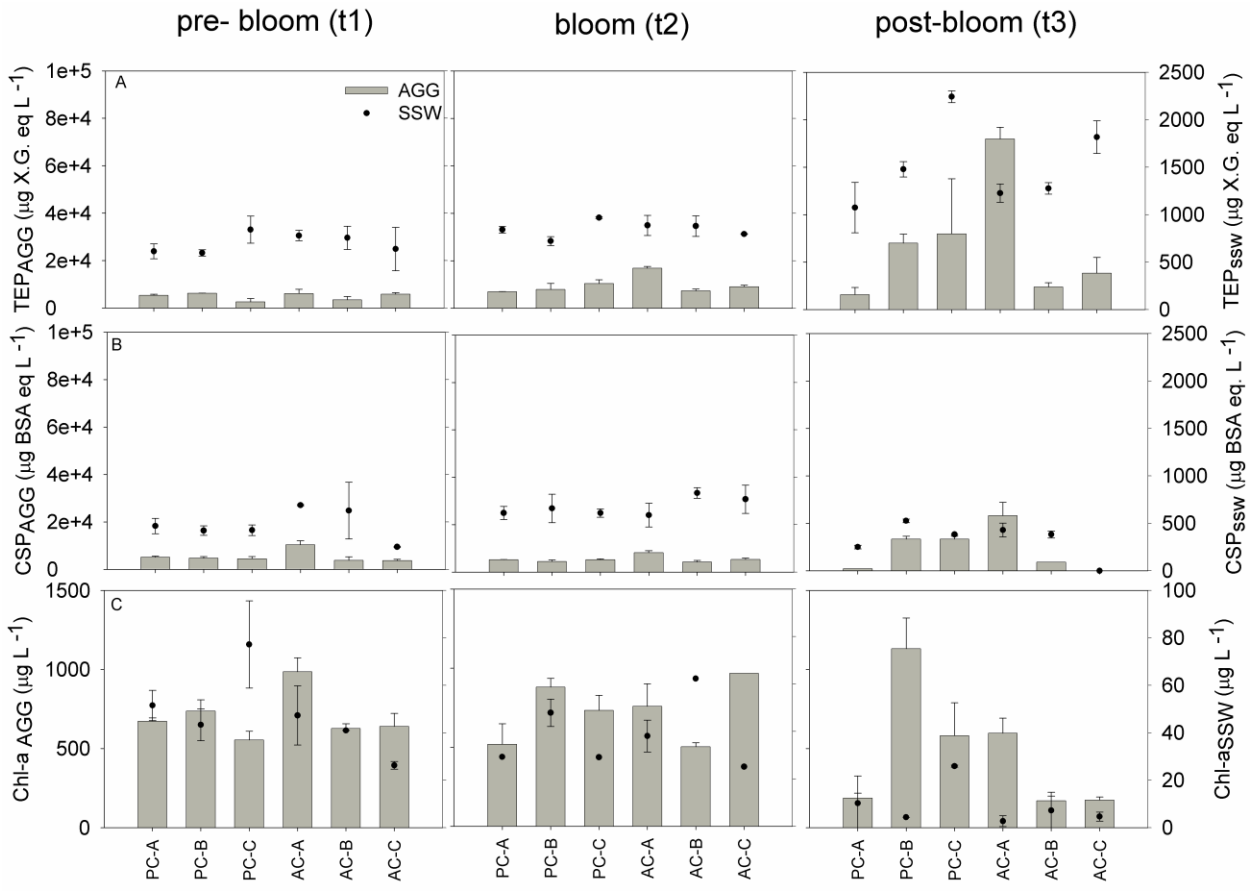

Figure 4-14. Concentrations of gel particles in aggregates formed in three ME2 roller tank experiments conducted at different growth phases; pre-bloom (t1), bloom (t2) and port-bloom (t3). Aggregates (grey bars) and surrounding seawater (black dots) were analyzed separately to study the distribution of TEP (upper panel), CSP (middle panel) and Chl-a (lower panel) in both fractions during the aggregation experiments: AC (blue) and PC (green). There is no data available for CSP in roller tank AC-C during t3.

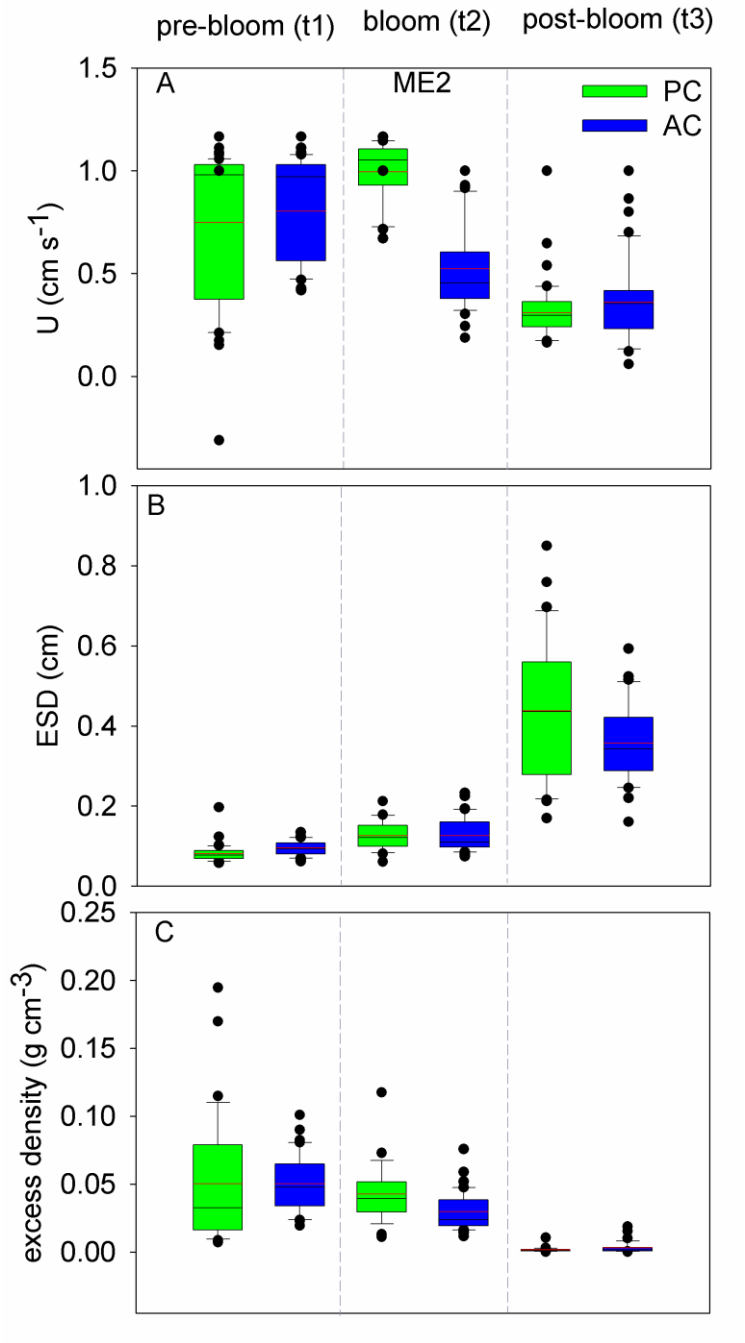

Figure 4-15. Properties of aggregates formed in three roller tank experiments conducted at different growth phases: pre-bloom (t1), bloom (t2), and post-bloom (t3) during ME2. (A) aggregate sinking velocity; (B) ESD and (C) excess density. Box plots included all the individually measure aggregates in each roller tank in the different treatments: AC (blue) and PC

(green). For pre-bloom AC (blue) represents 3 roller tanks (n=40); PC (green) represents 3 roller tanks (n=34). For bloom (t2) AC (blue) represents 3 roller tanks (n=40) and PC (green) represents 2 roller tanks (n=25). For bloom (t3) AC (blue) represents 3 roller tanks (n=31), and PC (green) represents 2 roller tanks (n=22). The boundary of the box closest to zero indicates the 25th percentile, the black line within the box is the median and the red line is the mean; the boundary of the box farthest from zero indicates the 75th percentile. Error bars above and below the box indicate the 90th and 10th percentiles, black dots are the outlying points.

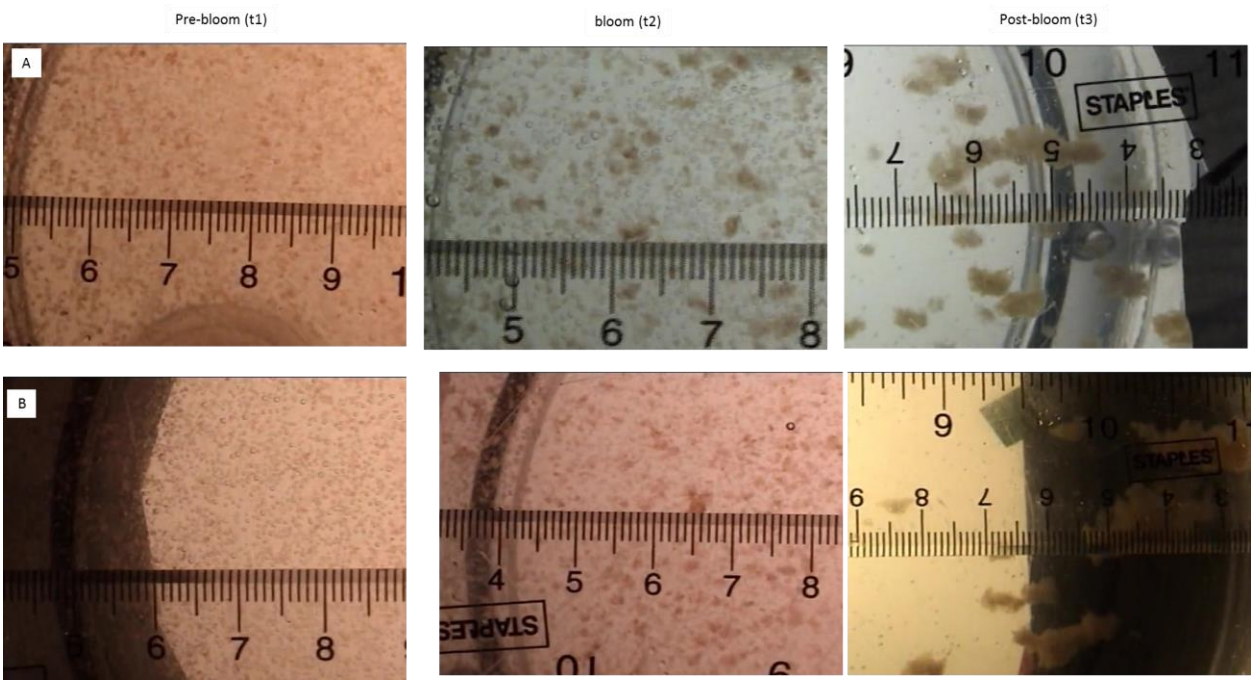

Figure 4-16. Pictures from two roller tanks AC-A (above) and PC-A (below), during ME2, showing aggregates formed in roller tank experiments conducted at three different growth phases; pre-bloom (t1), bloom (t2) and post-bloom (t3).

Table 4-1: Initial carbonate chemistry in ME1

Mesocosm treatment	T °C	TA (µmol kg^{-1})	Target pH_T at 750 ppm CO_2
AC-A	17.6	1840	7.7
AC-B	16.7	1760	7.7
AC-C	16	1760	7.7
AW-A	18.3	1800	7.7
AW-B	18.3	1880	7.8
AW-C	18.3	1840	7.7

Table 4-2: Chl-a (μg L^{-1}) concentrations during the bloom peak in each mesocosm tank during ME1

	Chla (μg L^{-1})		
	(t2)	(t3)	bloom
PC-A	7.4	4.9	small
PC-B	32.5	17.1	yes
PC-C	2.5	8.8	small
AC-A	8.9	10.9	small
AC-B	20.4	28.5	yes
AC-C	27.8	14.1	yes
AW-A	16	23.6	yes
AW-B	22.2	26.9	yes
AW-C	4.0	5.6	no

Table 4-3: Aggregate inventory during roller tank experiments performed with seawater from ME1. RTexp = roller tank experiment; yes, few and no indicate the number of aggregates in each roller tank.

	RTexp1 pre-bloom (t1)	RTexp2 bloom (t2)	RTexp3 bloom (t3)	RTexp4 post-bloom (t4)
PC-A: RT2	no	No	no	no
PC-B: RT8	yes	few (2)	yes	no
PC-C: RT9	yes	Yes	yes	no
AC-A: RT1	yes	few (3)	no	no
AC-B: RT3	no	Yes	yes	no
AC-C: RT5	no	Yes	yes	no
AW-A: RT4	yes	No	no	no
AW-B: RT6	yes	Yes	yes	yes
AW-C: RT7	no	No	no	no

Table 4-4. TEP (μg X.G. eq L^{-1}), Chl-*a* (μg L^{-1}) and TEP/ Chl-*a* ratio related to aggregate formation during roller tank experiments performed with seawater from ME1

	bloom (t2)				bloom (t3)			
	TEP (μg X.G. eq L^{-1})	Chl-a (μg L^{-1})	TEP/Chla	AGG	TEP (μg X.G. eq L^{-1})	Chl-a (μg L^{-1})	TEP/ Chl-a	AGG
PC-A	461.4	7.4	62.5	no	367.7	4.9	74.5	no
PC-B	740.2	32.6	22.7	few	853.1	17.2	49.6	yes
PC-C	870.0	2.1	410.7	yes	1091.1	17.2	63.5	yes
AC-A	459.0	9.0	51.1	few	632.0	10.9	57.9	no
AC-B	649.8	20.5	31.7	yes	557.5	28.6	19.5	yes
AC-C	805.1	27.8	29.0	yes	622.4	14.1	44.1	yes
AW-A	439.8	16.0	27.4	no	557.5	23.7	23.5	no
AW-B	994.9	26.9	36.9	yes	990.1	11.4	86.9	yes
AW-C	288.4	4.0	71.2	no	343.7	4.8	71.3	no

Table 4-5: Results from the Wilcoxon rank sum test for ME1. U is the aggregate sinking velocity and ESD is the equivalent spherical diameter and represents aggregate size. PC = present CO_2 cooler temperature, AC= high CO_2 and cooler temperature, and AW = high CO_2 and warmer temperature. In this test the null hypothesis is that the medians for two independent unequal-sized samples are equal. p is the p-value of the test; h determines the decision of the test, the result h = 1 indicates a rejection of the null hypothesis (i.e., the medians for two samples are different), and h = 0 indicates a failure to reject the null hypothesis (i.e., there is not enough evidence to say that the medians for two samples are different) at the 5% significance level.

		U (cm s^{-1})		ESD (cm)		Excess density (g cm^{-3})	
time	treatments	p	h	p	h	p	h
t1	PC-AC	p<0.0001	1	p<0.01	1	p<1	0
	PC-AW	p<0.1	0	p<1	0	p<1	0
	AC-AW	p<1	0	p<0.0001	1	p<1	0
t2	PC-AC	p<0.0001	1	p<1	0	p<0.0001	1
	PC-AW	p<0.0001	1	p<0.01	1	p<0.0001	1
	AC-AW	p<1	0	p<0.0001	1	p<0.1	1
t3	PC-AC	p<0.0001	1	p<0.0001	1	p<1	0
	PC-AW	p<1	0	p<1	0	p<0.1	1
	AC-AW	p<0.0001	1	p<0.0001	1	p<0.1	1

Table 4-6: Results from the Wilcoxon rank sum test for ME2; in this test the null hypothesis is that the medians for two independent unequal-sized samples are equal. p is the p-value of the test; h determines the decision of the test, the result h = 1 indicates a rejection of the null hypothesis, and h = 0 indicates a failure to reject the null hypothesis at the 5% significance level.

time	treatment	U (cm s^{-1})		ESD (cm)		Excess density (g cm^{-3})	
		p	h	p	h	p	h
t1	PC-AC	p<0.0001	1	p<0.0001	1	p<0.5	0
t2	PC-AC	p<0.0001	1	p<0.1	0	p<0.01	1
t3	PC-AC	p<1	0	p<0.1	0	p<0.5	0

Supplementary figures

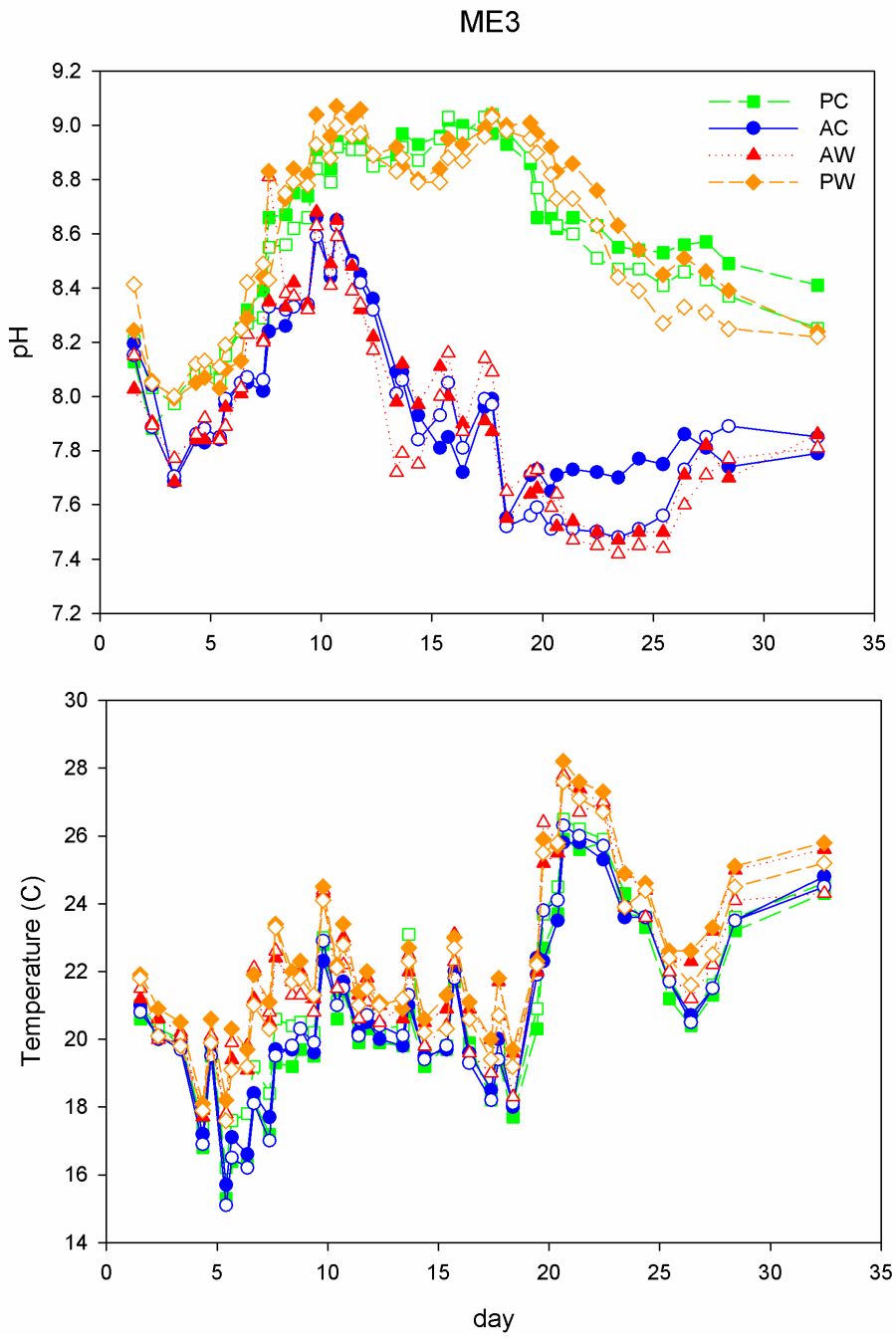

Figure 4-17. pH and temperature variations for the four sets of treatment during ME3. Triplicate mesocosms were run for each treatment: AC (blue-circle): acidified-cooler, PC

(green- square): present CO_2-cooler, AW (red-triangle): acidified- warmer, and PC (orange-diamond): present CO_2- warmer.

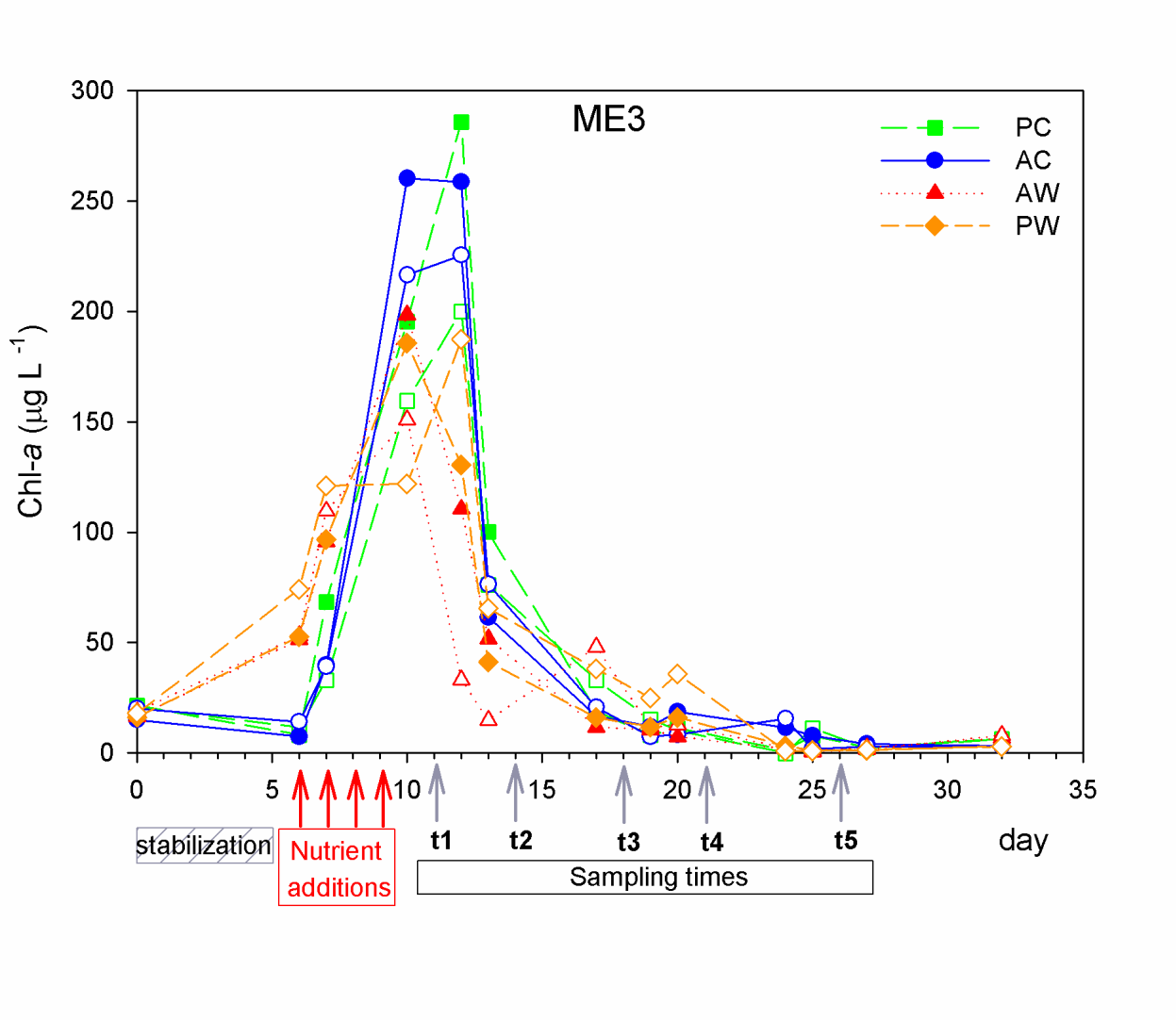

Figure 4-18. Chl-*a* over time during ME3 showing stabilization, nutrient additions, and sampling times when roller tank aggregation experiments were performed. Triplicate mesocosms were run for each treatment: AC (blue-circle), PC (green- square), AW (red-triangle), and PC (orange-diamond).

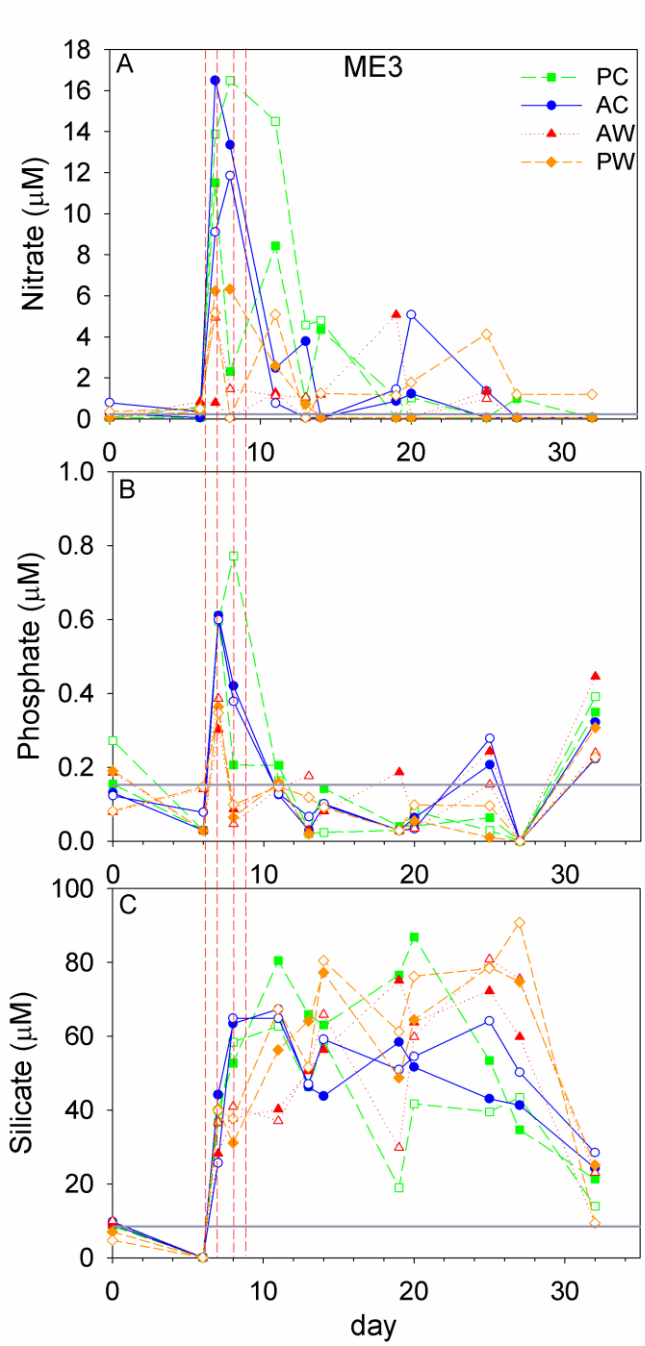

Figure 4-19. Nutrient concentration over time during ME3. Nitrate (A), Phosphate (B) and Silicate (C). The grey line represents the initial average nutrient concentration (before nutrient addition). AC (blue-circle); AW (red-triangle), PW (orange-diamond), and PC (green-square).

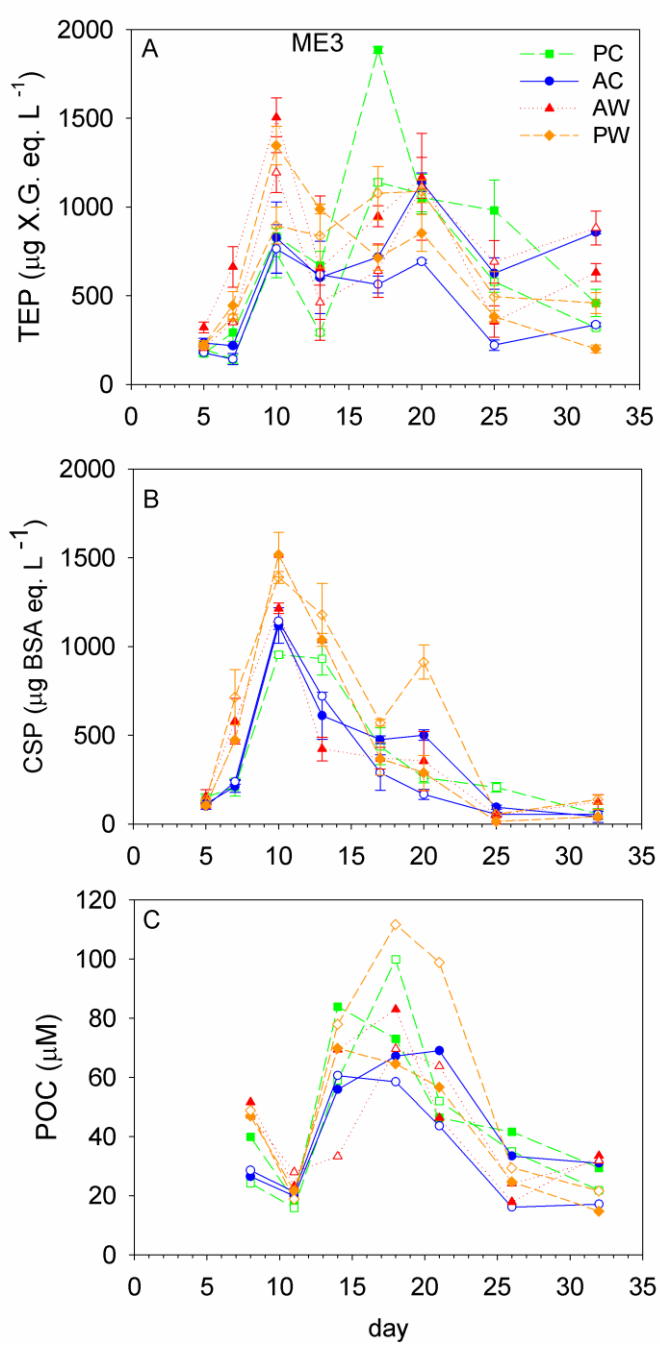

Figure 4-20. TEP (A), CSP (B) and POC (C) concentrations during the development of the bloom in ME3. AC (blue-circle); AW (red-triangle); PW (orange-diamond), and PC (green-square).

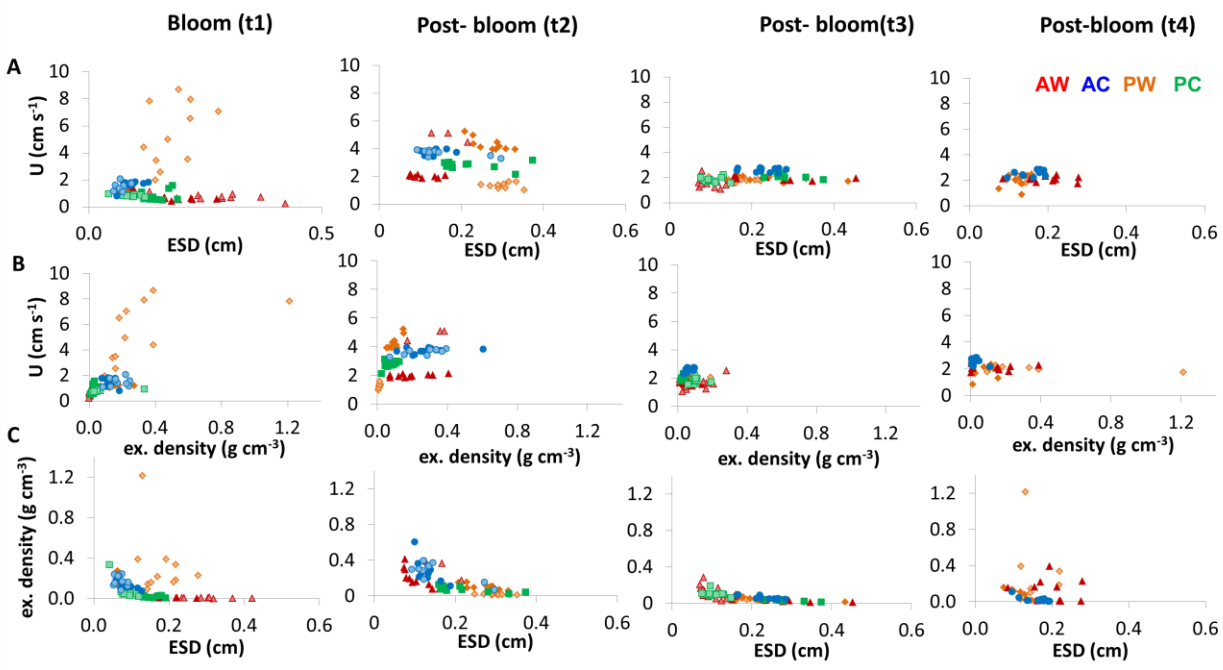

Figure 4-21. Equivalent spherical diameter (ESD, cm) versus sinking velocity (U, cm s^{-1}) (A). Excess density (g cm^{-3}) versus sinking velocity (B). ESD versus excess density (C) of aggregates formed during the aggregation experiments with seawater from ME3. AC (blue-circle; AW (red-triangle); PW (orange-diamond),, and PC (green- square).

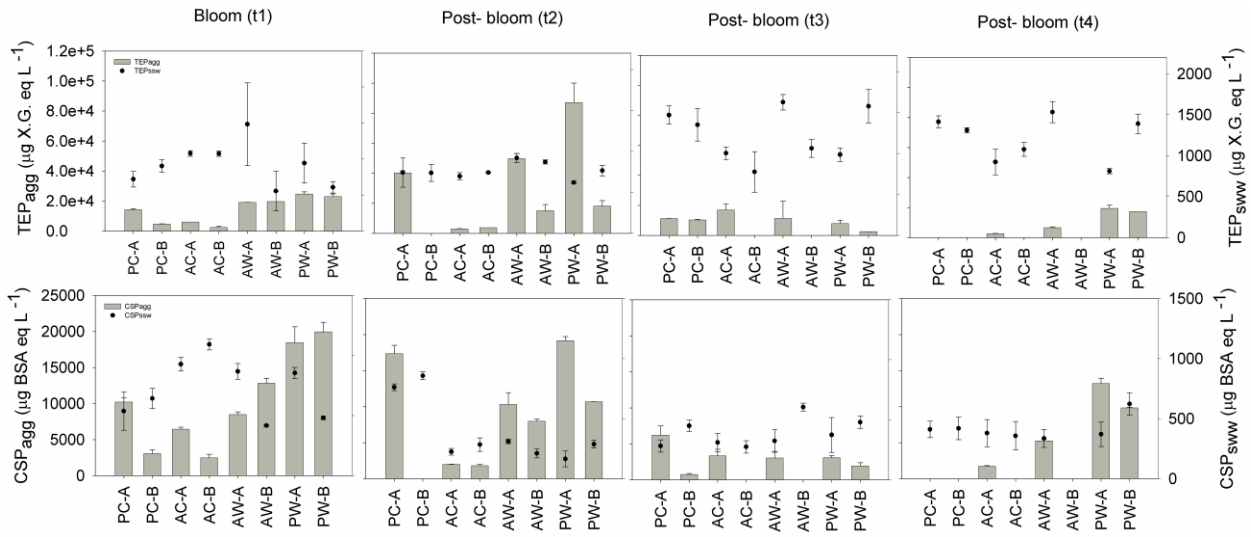

Figure 4-22. Concentrations of gel particles in aggregates formed in three ME2 roller tank experiments conducted at different growth phases; pre-bloom (t1), bloom (t2) and port-bloom (t3). Aggregates (grey bars) and surrounding seawater (black dots) were analyzed separately to study the distribution of TEP (upper panel), CSP (middle panel) and Chl-a (lower panel) in both fractions during the aggregation experiments: AC (blue) and PC (green).

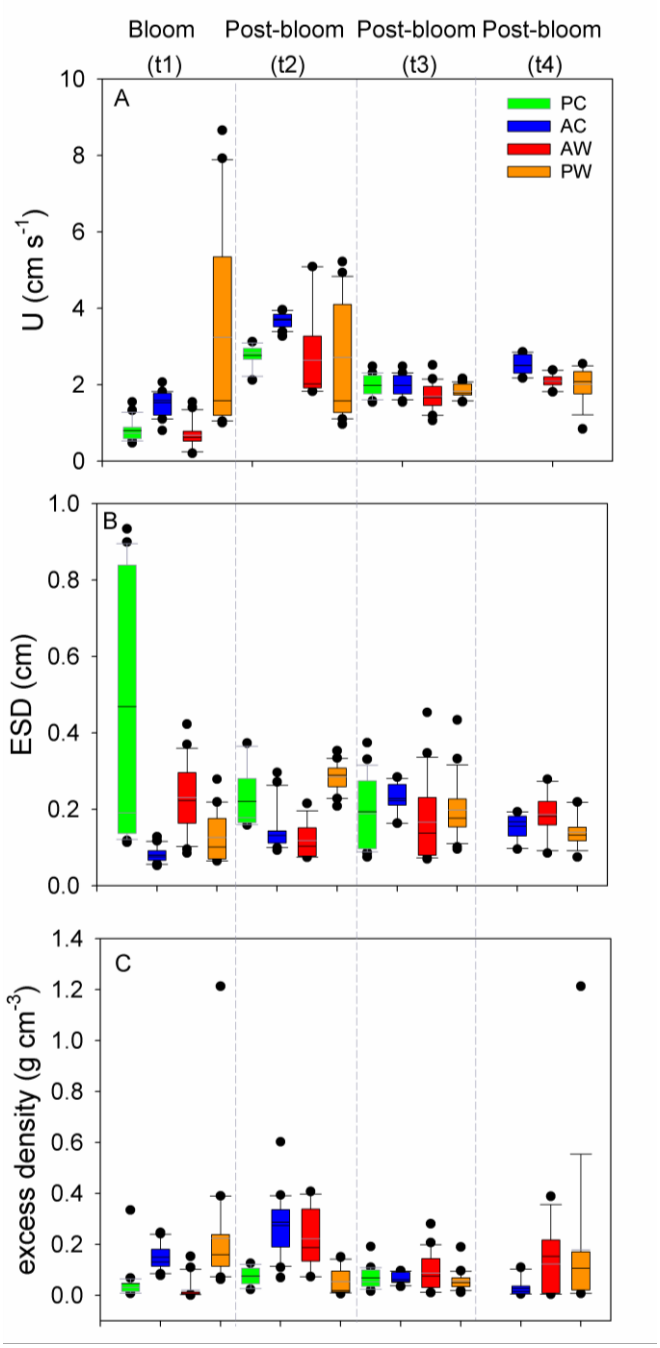

Figure 4-23. Properties of aggregates formed in four roller tank experiments conducted at different growth phases: bloom (t1), post- bloom (t2, t3, and t4), during ME3. (A) aggregate sinking velocity; (B) ESD and (C) excess density. Box plots include all the individually-measured aggregates in each roller tank in the different treatments: AC (blue), AW (red), PC

(orange), and PC (green). For bloom (t1), AC (blue) represents two roller tanks AC-A (n=11) and AC-B (n=10); AW (red) represents two roller tanks AW-A (n=10) and AW-B (n=10); PW (orange) represents two roller tanks PW-A (n=11) and PW-B (n=10); and PC (green) represents two roller tank PC-A (n=11) and PC-B (n=11). For post-bloom (t2), AC (blue) represents two roller tank AC-A (n=10) and AC-B (n=10); AW (red) represents two roller tanks AW-A (n=10) and AW-B (n=3); PW (orange) represents two roller tanks PW-A (n=11) and PW-B (n=10); and PC (green) represents one roller tanks PC-A (n=11. For post-bloom (t3), AC (blue) represents one roller tank AC-A (n=11; AW (red) represents two roller tanks AW-A (n=11) and AW-B (n=10); PW (orange) represents two roller tanks PW-A (n=11) and PW-B (n=11); and PC (green) represents two roller tank PC-A (n=11) and PC-B (n=11). For post-bloom (t4), AC (blue) represents one roller tank AC-A (n=10); AW (red) represents one roller tank AW-A (n=10); PW (orange) represents two roller tanks PW-A (n=6) and PW-B (n=11); there were no aggregates in PC (green). The boundary of the box closest to zero indicates the 25th percentile, the black line within the box is the median and the grey line is the mean; the boundary of the box farthest from zero indicates the 75th percentile. Error bars above and below the box indicate the 90th and 10th percentiles, and black dots are the outlying points.

Chapter 5

Conclusions and Implications

1. Summary of major findings

In Chapter 1, what gel particles are and how they have been analyzed in the past is explained. Then our present knowledge about how gel particles form in seawater is summarized. Because marine gel particles are involved in the formation of the particles that play such a large role in the ocean's biological pump, I next discussed the role of gel particles in particle aggregation and transport. Lastly, some of the recent literature on how future ocean conditions might affect the physical processes was presented. From the revision of relevant literature, the research questions were identified and the objectives for this work were defined, it was clear that insufficient research have been conducted to understand the role of CSP. This research focused on three major objectives; first to develop a new technique for the quantitative analysis of protein-rich particles, second to understand differences between origin and vertical distribution of TEP and CSP in the ocean, and third, to examine the effect of higher temperature and CO_2 expected in the future ocean on gel particles, aggregation and POC flux.

The development of a semi-quantitative spectrophotometric method for determination of CSP described in Chapter 2 provided a tool for measuring CSP spectrophotometrically using BSA as standard in the same way that the TEP spectrophotometric method uses Xanthan Gum. This efficient and effective method facilitated considerably the study of CSP in laboratory experiments and field samples as described in Chapters 2, 3 and 4 of this dissertation.

Chapter 3 described results that improve our understanding of CSP and better distinguish the origins and describe the distributions of TEP and CSP in the ocean. This research was mainly oriented toward studying CSP since there was only limited information about them compared to TEP. CSP abundances were directly related to Chl-*a* concentration in samples from diatom and

cyanobacteria cultures in the lab, as well as in field samples from the oligotrophic Sargasso Sea, this suggested that CSP are either exuded directly by phytoplankton, or can be formed from dissolved precursors in the same manner as TEP. Preliminary experiments showed that CSP can be formed from dissolved precursors; however the concentrations of CSP were not high enough to firmly conclude this and further experiments are required. In addition, CSP were bound together by cationic linkages in the same manner as TEP. Experiments showed that the size and abundance of CSP decreases after the addition of the chelating agent EDTA.

TEP and CSP were produced in phytoplankton cultures and in mesocosm experiments with a natural coastal phytoplankton bloom induced by nutrient addition. However, the maximum abundance of those gel particles occurred at different times in the phytoplankton bloom. CSP highest abundance corresponded to the Chl-*a* maximum while TEP highest abundance was always at the end of the bloom and after nutrient depletion. In field samples from the Sargasso Sea, both types of gel particles were more abundant in the upper 100 m of the water column, but while highest TEP concentrations were always in the shallowest sample collected (< 70 m); highest CSP concentrations always coincided with the fluorescence maximum (between 70 and 100 m). These differences suggest that even though TEP and CSP are both produced by phytoplankton, they could be produced by different species, or TEP could be released free into the seawater while CSP remains associated with the phytoplankton cells.

The development of a FlowCAM method to visualize stained gel particles directly in seawater allowed the qualitative analysis of particle association behaviors of TEP and CSP. Samples in which the dominant phytoplankton species was diatoms were always more enriched in TEP compared with CSP; on the contrary, samples from cyanobacteria cultures were enriched in CSP and depleted in TEP. The same pattern was observed with aggregates naturally formed

from these two species in culture. Diatom aggregates were covered by TEP, and in some cases a TEP matrix was observed with cells embedded in it, forming larger conglomerates of TEP, detrital material and cells. Cyanobacteria aggregates were enriched in CSP, consistent with the possibility that CSP might be in close association with cyanobacteria cells in the Sargasso Sea. Overall, results for Chapter 3 indicated that even though TEP and CSP are produced by phytoplankton, these gel particles are different discrete particles that were produced at different times in a phytoplankton bloom, had different vertical distributions in the open ocean, had different particle association behaviors, and probably have different roles in aggregation depending on the dominant phytoplankton species. Even though these results showed that TEP and CSP are different particles; we cannot discard the possibility that there are particles that have both polysaccharide and protein components.

Chapter 4 examined the effects of elevated CO_2 and temperature conditions expected in the future ocean on the total concentration of gel particles, on the gel particle content of aggregates, and the implications for marine carbon flux. Mesocosm experiments were conducted with natural coastal phytoplankton assemblages. Results from those experiments indicated no effect of elevated CO_2 or temperature on concentrations of Chl-*a*, gel particle or POC concentrations, as well as no effect on nutrient uptake or aggregate formation. Nevertheless, roller tank experiments showed that during the phytoplankton bloom, aggregates generated under higher CO_2 at present temperature were smaller and had lower sinking velocity that those formed under present CO_2 and present temperature conditions. These findings indicate that elevated temperature and CO_2 in the future ocean might affect aggregate sinking and POC flux differently during different phases of the phytoplankton bloom. There is a very limited number of studies that have investigated the combined effects of ocean acidification and warming on natural

phytoplankton assemblages. In addition, this is the first study that addresses effects of elevated CO_2 and temperature on TEP and CSP production simultaneously as well as changes in TEP and CSP content of aggregates. Similar to what was observed in phytoplankton cultures and mesocosm experiments, the higher content of CSP in aggregates was found during the phytoplankton bloom, while the highest content of TEP in aggregates was found post-bloom. Changes in TEP concentration were more related than CSP concentration to changes in aggregate properties such as sinking velocity and excess density in the roller tank experiments. This agrees with our previous observations in Chapter 3 using the FlowCAM that indicated that diatom aggregates are enriched in TEP.

2. Directions and Future Work

This research has led to a better understanding of CSP using a combination of standard techniques and newly developed methods. New knowledge always generates new questions, and the new spectrophotometric method for studying CSP will allow a more efficient way to measure these particles in diverse aquatic environments under different conditions.

There are still open questions regarding CSP formation mechanisms. For instance, further experiments are required to clarify whether CSP can be abiotically formed from dissolved precursors produced by phytoplankton and bacteria like TEP can be. Also, the possibility that TEP and CSP are held together by hydrophobic interactions as well as cation bridges needs to be addressed. EPS released by phytoplankton can bind together by hydrophobic interactions; however there is no direct evidence for this for gel particles.

In addition, the composition of CSP as well as properties like stickiness remain poorly known; this information is fundamental to a better understanding of the role these particles play

in aggregation. The fact that the concentration of CSP decreased after the phytoplankton bloom in the mesocosm experiments might indicate that those particles are more labile than TEP and can be used as a source of nitrogen by bacteria; however degradation experiments are needed to test this speculation.

In terms of effects of ocean acidification and warming on gel particle production and aggregate formation and sedimentation, future work should be oriented towards investigation of the synergistic effect of environmental stressors in more natural conditions. So far, there is contradictory evidence about the effect of elevated CO_2 and temperature on gel particle production and aggregate formation and sinking. Most of the information available comes from laboratory experiments usually using only single species cultures. Large scale experiments are difficult to control and replicate; however the next step should be to study gel particle formation and sedimentation in large scale mesocosm experiments.